

AFRL-VA-WP-TR-1998-3043



**INNOVATIVE CONTROL EFFECTORS
(CONFIGURATION 101)
DYNAMIC WIND TUNNEL TEST REPORT
ROTARY BALANCE AND FORCED OSCILLATION TESTS**

William J. Gillard

*Air Force Research Laboratory (AFRL/VAAD)
2210 Eighth St., Suite 21
Wright-Patterson AFB OH 45433-7531*

JULY 1998

FINAL REPORT FOR PERIOD 11 MARCH 1998 – 24 APRIL 1998

APPROVED FOR PUBLIC RELEASE; DISTRIBUTION IS UNLIMITED

**AIR VEHICLES DIRECTORATE
AIR FORCE RESEARCH LABORATORY
AIR FORCE MATERIEL COMMAND
WRIGHT-PATTERSON AIR FORCE BASE, OHIO 45433-7562**

19990511 107

NOTICE

WHEN GOVERNMENT DRAWINGS, SPECIFICATIONS, OR OTHER DATA ARE USED FOR ANY PURPOSE OTHER THAN IN CONNECTION WITH A DEFINITE GOVERNMENT-RELATED PROCUREMENT, THE UNITED STATES GOVERNMENT INCURS NO RESPONSIBILITY OR ANY OBLIGATION WHATSOEVER. THE FACT THAT THE GOVERNMENT MAY HAVE FORMULATED OR IN ANY WAY SUPPLIED THE SAID DRAWINGS, SPECIFICATIONS, OR OTHER DATA, IS NOT TO BE REGARDED BY IMPLICATION, OR OTHERWISE IN ANY MANNER CONSTRUED, AS LICENSING THE HOLDER, OR ANY OTHER PERSON OR CORPORATION; OR AS CONVEYING ANY RIGHTS OR PERMISSION TO MANUFACTURE, USE, OR SELL ANY PATENTED INVENTION THAT MAY IN ANY WAY BE RELATED THERETO.

This technical report has been reviewed and is accepted for publication.

William J. Gillard

WILLIAM J. GILLARD
Project Engineer
Flight Dynamics & Control Branch

James J. Rudd

JAMES RUDD, Chief
Aeronautical Sciences Division
Air Vehicles Directorate

Stanley F. Lash

STANLEY F. LASH., Chief
Flight Dynamics & Control Branch
Aeronautical Sciences Division

If your address has changed, if you wish to be removed from our mailing list, or if the addressee is no longer employed by your organization, please notify AFRL/VAAD, 2210 Eighth St. Suite 11, WPAFB OH 45433-7521 to help maintain a current mailing list.

Copies of this report should not be returned unless return is required by security considerations, contractual obligations, or notice on a specific document.

REPORT DOCUMENTATION PAGE			Form Approved OMB No. 0704-0188
<p>Public reporting burden for this collection of information is estimated to average 1 hour per response, including the time for reviewing instructions, searching existing data sources, gathering and maintaining the data needed, and completing and reviewing the collection of information. Send comments regarding this burden estimate or any other aspect of this collection of information, including suggestions for reducing this burden, to Washington Headquarters Services, Directorate for Information Operations and Reports, 1215 Jefferson Davis Highway, Suite 1204, Arlington, VA 22202-4302, and to the Office of Management and Budget, Paperwork Reduction Project (0704-0188), Washington, DC 20503.</p>			
1. AGENCY USE ONLY (Leave blank)	2. REPORT DATE	3. REPORT TYPE AND DATES COVERED	
	July 1998	FINAL 03/11/98 - 04/24/98	
4. TITLE AND SUBTITLE		5. FUNDING NUMBERS	
INNOVATIVE CONTROL EFFECTORS (CONFIGURATION 101) DYNAMIC WIND TUNNEL TEST REPORT Rotary Balance and Forced Oscillation Tests		C PE 62201F PR 2403 TA 05 WU 9L	
6. AUTHOR(S)			
William J. Gillard			
7. PERFORMING ORGANIZATION NAME(S) AND ADDRESS(ES)		8. PERFORMING ORGANIZATION REPORT NUMBER	
AFRL/VAAD 2210 Eighth Street, Suite 11 Wright-Patterson AFB OH 45433-7521			
9. SPONSORING/MONITORING AGENCY NAME(S) AND ADDRESS(ES)		10. SPONSORING/MONITORING AGENCY REPORT NUMBER	
Air Vehicles Directorate Air Force Research Laboratory Air Force Materiel Command Wright-Patterson AFB OH 45433-7562 POC: William J. Gillard, AFRL/VAAD, 937-255-8490		AFRL-VA-WP-TR-1998-3043	
11. SUPPLEMENTARY NOTES			
12a. DISTRIBUTION AVAILABILITY STATEMENT		12b. DISTRIBUTION CODE	
Approved for public released; Distribution is unlimited.			
13. ABSTRACT (Maximum 200 words)			
<p>This report describes the technical effort investigating the dynamic characteristics of the Innovative Control Effectors Configuration 101 tailless aircraft concept. A series of static, rotary balance, and forced oscillation tests were conducted to acquire more information on the aerodynamic properties associated with this 65 degree, delta wing concept. Results show the vehicle to be well damped in pitch and roll motions and neutrally damped in yaw motions. Significant oscillating frequency effects were identified during forced oscillation testing with the impact most notable in the 15 < AOA < 45 degree region.</p>			
14. SUBJECT TERMS		15. NUMBER OF PAGES	
Tailless aircraft, rotary balance, forced oscillation, wind tunnel testing, dynamic stability & control.		204	
16. PRICE CODE			
17. SECURITY CLASSIFICATION OF REPORT	18. SECURITY CLASSIFICATION OF THIS PAGE	19. SECURITY CLASSIFICATION OF ABSTRACT	20. LIMITATION OF ABSTRACT
UNCLASSIFIED	UNCLASSIFIED	UNCLASSIFIED	SAR

TABLE OF CONTENTS

LIST OF FIGURES	iv
LIST OF TABLES	vi
NOMENCLATURE	vii
FOREWORD	viii
1. INTRODUCTION	1
2. DESCRIPTION OF MODEL	4
3. TEST FACILITIES	7
4. TEST PROCEDURES	10
4.1 Rotary Balance	10
4.2 Forced Oscillation	11
5. TEST CONDITIONS	14
6. DATA CORRECTIONS	20
7. STATIC CHARACTERISTICS	21
7.1 Neutral Control	21
7.2 Full Nose-Down Control	23
8. ROTARY BALANCE CHARACTERISTICS	27
8.1 Neutral Control	27
8.2 LEF = 30/30	33
8.3 AMT = 0/60	41
9. FORCED OSCILLATION CHARACTERISTICS	48
9.1 Pitch Axis	48
9.2 Roll Axis	55
9.3 Yaw Axis	62
10. SUMMARY & CONCLUSIONS	69
11. REFERENCES	70
APPENDIX A: ROTARY BALANCE, NEUTRAL CONTROLS, LEF =0/0 DATA	71
APPENDIX B: ROTARY BALANCE, NEUTRAL CONTROLS, LEF = 30/30 DATA ...	92
APPENDIX C: ROTARY BALANCE, AMT = 0/60 DATA	113
APPENDIX D: PITCH FORCED OSCILLATION DATA	134
APPENDIX E: ROLL FORCED OSCILLATION DATA	155
APPENDIX F: YAW FORCED OSCILLATION DATA	176

LIST OF FIGURES

Figure 1: Tailless Aircraft Concept	1
Figure 2: ICE 101 Configuration 3-View	2
Figure 3: Model Force and Moment Sign Convention	5
Figure 4: Model Mounted On MAT Rig	6
Figure 5: Close Up View Of Model	6
Figure 6: AFRL Vertical Wind Tunnel Layout	8
Figure 7: Model Enclosed In Tare Bag	11
Figure 8: Roll Forced Oscillation Mounting	12
Figure 9: Yaw Forced Oscillation Mounting	12
Figure 10: Pitch Forced Oscillation Mounting	13
Figure 11: CN vs AOA, Neutral Controls	22
Figure 12: Cm vs AOA, Neutral Controls	22
Figure 13: Cll vs AOA, Neutral Controls	22
Figure 14: Cln vs AOA, Neutral Controls	22
Figure 15: Full Nose-Down Control Configuration	24
Figure 16: CN vs AOA, Full Nose-Down Control, Beta = 0	25
Figure 17: Cm vs AOA, Full Nose-Down Control, Beta = 0	25
Figure 18: Cll vs AOA, Full Nose-Down Control, Beta = 0	25
Figure 19: Cln vs AOA, Full Nose-Down Control, Beta = 0	25
Figure 20: CN vs AOA, Full Nose-Down Control, Beta = 10	26
Figure 21: Cm vs AOA, Full Nose-Down Control, Beta = 10	26
Figure 22: Cll vs AOA, Full Nose-Down Control, Beta = 10	26
Figure 23: Cln vs AOA, Full Nose-Down Control, Beta = 10	26
Figure 24: CN vs $\Omega_b/2V$, Neutral Controls, AOA = 0	28
Figure 25: CN vs $\Omega_b/2V$, Neutral Controls, AOA = 10	28
Figure 26: CN vs $\Omega_b/2V$, Neutral Controls, AOA = 20	28
Figure 27: CN vs $\Omega_b/2V$, Neutral Controls, AOA = 40	28
Figure 28: Cm vs $\Omega_b/2V$, Neutral Controls, AOA = 0	29
Figure 29: Cm vs $\Omega_b/2V$, Neutral Controls, AOA = 10	29
Figure 30: Cm vs $\Omega_b/2V$, Neutral Controls, AOA = 20	29
Figure 31: Cm vs $\Omega_b/2V$, Neutral Controls, AOA = 40	29
Figure 32: Cll vs $\Omega_b/2V$, Neutral Controls, AOA = 0	31
Figure 33: Cll vs $\Omega_b/2V$, Neutral Controls, AOA = 10	31
Figure 34: Cll vs $\Omega_b/2V$, Neutral Controls, AOA = 20	31
Figure 35: Cll vs $\Omega_b/2V$, Neutral Controls, AOA = 40	31
Figure 36: Cln vs $\Omega_b/2V$, Neutral Controls, AOA = 0	32
Figure 37: Cln vs $\Omega_b/2V$, Neutral Controls, AOA = 10	32
Figure 38: Cln vs $\Omega_b/2V$, Neutral Controls, AOA = 20	32
Figure 39: Cln vs $\Omega_b/2V$, Neutral Controls, AOA = 40	32
Figure 40: LEF = 30/30 Deg. Configuration	35
Figure 41: CN vs $\Omega_b/2V$, LEF = 30/30 Deg., AOA = 0	36
Figure 42: CN vs $\Omega_b/2V$, LEF = 30/30 Deg., AOA = 10	36
Figure 43: CN vs $\Omega_b/2V$, LEF = 30/30 Deg., AOA = 20	36
Figure 44: CN vs $\Omega_b/2V$, LEF = 30/30 Deg., AOA = 40	36
Figure 45: Cm vs $\Omega_b/2V$, LEF = 30/30 Deg., AOA = 0	37

Figure 46: C_m vs $\Omega_b/2V$, LEF = 30/30 Deg., AOA = 10	37
Figure 47: C_m vs $\Omega_b/2V$, LEF = 30/30 Deg., AOA = 20	37
Figure 48: C_m vs $\Omega_b/2V$, LEF = 30/30 Deg., AOA = 40	37
Figure 49: C_{II} vs $\Omega_b/2V$, LEF = 30/30 Deg., AOA = 0	39
Figure 50: C_{II} vs $\Omega_b/2V$, LEF = 30/30 Deg., AOA = 10	39
Figure 51: C_{II} vs $\Omega_b/2V$, LEF = 30/30 Deg., AOA = 20	39
Figure 52: C_{II} vs $\Omega_b/2V$, LEF = 30/30 Deg., AOA = 40	39
Figure 53: C_{In} vs $\Omega_b/2V$, LEF = 30/30 Deg., AOA = 0	40
Figure 54: C_{In} vs $\Omega_b/2V$, LEF = 30/30 Deg., AOA = 10	40
Figure 55: C_{In} vs $\Omega_b/2V$, LEF = 30/30 Deg., AOA = 20	40
Figure 56: C_{In} vs $\Omega_b/2V$, LEF = 30/30 Deg., AOA = 40	40
Figure 57: AMT = 0/60 Deg. Configuration	42
Figure 58: ΔC_N vs $\Omega_b/2V$, AMT = 0/60 Deg., AOA = 0	43
Figure 59: ΔC_N vs $\Omega_b/2V$, AMT = 0/60 Deg., AOA = 10	43
Figure 60: ΔC_N vs $\Omega_b/2V$, AMT = 0/60 Deg., AOA = 20	43
Figure 61: ΔC_N vs $\Omega_b/2V$, AMT = 0/60 Deg., AOA = 40	43
Figure 62: ΔC_m vs $\Omega_b/2V$, AMT = 0/60 Deg., AOA = 0	44
Figure 63: ΔC_m vs $\Omega_b/2V$, AMT = 0/60 Deg., AOA = 10	44
Figure 64: ΔC_m vs $\Omega_b/2V$, AMT = 0/60 Deg., AOA = 20	44
Figure 65: ΔC_m vs $\Omega_b/2V$, AMT = 0/60 Deg., AOA = 40	44
Figure 66: ΔC_{II} vs $\Omega_b/2V$, AMT = 0/60 Deg., AOA = 0	46
Figure 67: ΔC_{II} vs $\Omega_b/2V$, AMT = 0/60 Deg., AOA = 10	46
Figure 68: ΔC_{II} vs $\Omega_b/2V$, AMT = 0/60 Deg., AOA = 20	46
Figure 69: ΔC_{II} vs $\Omega_b/2V$, AMT = 0/60 Deg., AOA = 40	46
Figure 70: ΔC_{In} vs $\Omega_b/2V$, AMT = 0/60 Deg., AOA = 0	47
Figure 71: ΔC_{In} vs $\Omega_b/2V$, AMT = 0/60 Deg., AOA = 10	47
Figure 72: ΔC_{In} vs $\Omega_b/2V$, AMT = 0/60 Deg., AOA = 20	47
Figure 73: ΔC_{In} vs $\Omega_b/2V$, AMT = 0/60 Deg., AOA = 40	47
Figure 74: Pitch Oscillation Test Points	49
Figure 75: ΔC_m vs $qc/2V$, Freq. Variation, AOA = 0	50
Figure 76: ΔC_m vs $qc/2V$, Freq. Variation, AOA = 10	50
Figure 77: ΔC_m vs $qc/2V$, Freq. Variation, AOA = 20	50
Figure 78: ΔC_m vs $qc/2V$, Freq. Variation, AOA = 40	50
Figure 79: ΔC_m vs $qc/2V$, Controls Variation, AOA = 0	52
Figure 80: ΔC_m vs $qc/2V$, Controls Variation, AOA = 10	52
Figure 81: ΔC_m vs $qc/2V$, Controls Variation, AOA = 20	52
Figure 82: ΔC_m vs $qc/2V$, Controls Variation, AOA = 40	52
Figure 83: ΔC_N vs $qc/2V$, Freq. Variation, AOA = 0	53
Figure 84: ΔC_N vs $qc/2V$, Freq. Variation, AOA = 10	53
Figure 85: ΔC_N vs $qc/2V$, Freq. Variation, AOA = 20	53
Figure 86: ΔC_N vs $qc/2V$, Freq. Variation, AOA = 40	53
Figure 87: ΔC_N vs $qc/2V$, Controls Variation, AOA = 0	54
Figure 88: ΔC_N vs $qc/2V$, Controls Variation, AOA = 10	54
Figure 89: ΔC_N vs $qc/2V$, Controls Variation, AOA = 20	54
Figure 90: ΔC_N vs $qc/2V$, Controls Variation, AOA = 40	54
Figure 91: Roll Oscillation Test Points	56
Figure 92: ΔC_{II} vs $pb/2V$, Freq. Variation, AOA = 0	57

Figure 93: ΔC_{l2} vs pb/2V, Freq. Variation, AOA = 20	57
Figure 94: ΔC_{l2} vs pb/2V, Freq. Variation, AOA = 30	57
Figure 95: ΔC_{l2} vs pb/2V, Freq. Variation, AOA = 40	57
Figure 96: ΔC_{l2} vs pb/2V, LEF Variation, AOA = 0	58
Figure 97: ΔC_{l2} vs pb/2V, LEF Variation, AOA = 20	58
Figure 98: ΔC_{l2} vs pb/2V, LEF Variation, AOA = 30	58
Figure 99: ΔC_{l2} vs pb/2V, LEF Variation, AOA = 40	58
Figure 100: ΔC_{ln} vs pb/2V, Freq. Variation, AOA = 0	60
Figure 101: ΔC_{ln} vs pb/2V, Freq. Variation, AOA = 20	60
Figure 102: ΔC_{ln} vs pb/2V, Freq. Variation, AOA = 30	60
Figure 103: ΔC_{ln} vs pb/2V, Freq. Variation, AOA = 40	60
Figure 104: ΔC_{ln} vs pb/2V, LEF Variation, AOA = 0	61
Figure 105: ΔC_{ln} vs pb/2V, LEF Variation, AOA = 20	61
Figure 106: ΔC_{ln} vs pb/2V, LEF Variation, AOA = 30	61
Figure 107: ΔC_{ln} vs pb/2V, LEF Variation, AOA = 40	61
Figure 108: Yaw Oscillation Test Points	63
Figure 109: ΔC_{ln} vs rb/2V, Freq. Variation, AOA = 0	64
Figure 110: ΔC_{ln} vs rb/2V, Freq. Variation, AOA = 20	64
Figure 111: ΔC_{ln} vs rb/2V, Freq. Variation, AOA = 30	64
Figure 112: ΔC_{ln} vs rb/2V, Freq. Variation, AOA = 40	64
Figure 113: ΔC_{ln} vs rb/2V, LEF Variation, AOA = 0	65
Figure 114: ΔC_{ln} vs rb/2V, LEF Variation, AOA = 20	65
Figure 115: ΔC_{ln} vs rb/2V, LEF Variation, AOA = 30	65
Figure 116: ΔC_{ln} vs rb/2V, LEF Variation, AOA = 40	65
Figure 117: ΔC_{ll} vs rb/2V, Freq. Variation, AOA = 0	67
Figure 118: ΔC_{ll} vs rb/2V, Freq. Variation, AOA = 20	67
Figure 119: ΔC_{ll} vs rb/2V, Freq. Variation, AOA = 30	67
Figure 120: ΔC_{ll} vs rb/2V, Freq. Variation, AOA = 40	67
Figure 121: ΔC_{ll} vs rb/2V, LEF Variation, AOA = 0	68
Figure 122: ΔC_{ll} vs rb/2V, LEF Variation, AOA = 20	68
Figure 123: ΔC_{ll} vs rb/2V, LEF Variation, AOA = 30	68
Figure 124: ΔC_{ll} vs rb/2V, LEF Variation, AOA = 40	68

LIST OF TABLES

Table 1: Dimensional Characteristics Of Full Scale ICE 101 Vehicle	4
Table 2: Strain Gauge Balance Accuracy	9
Table 3: Static And Rotary Balance Run Log	15
Table 4: Forced Oscillation Run Log	17
Table 5: Data Corrections	20

NOMENCLATURE

The units for physical quantities used herein are presented in U.S. Customary Units. All aerodynamic data are referenced to the body system of axes.

AFRL	Air Force Research Laboratory, Air Force Materiel Command
AOA, α	Angle of Attack, (deg)
b	Wing span, (ft)
BAR	Behrle Applied Research, Inc.; Jericho, NY
c	Mean aerodynamic chord, (ft)
CN	Normal Force Coefficient, (Normal Force / qS)
Cll	Rolling Moment Coefficient, (Rolling Moment / qSb)
Cm	Pitching Moment Coefficient, (Pitching Moment / qSc)
Cln	Yawing Moment Coefficient, (Yawing Moment / qSb)
DOD	Department of Defense
k	Reduced Frequency, ($\omega c/2V$ or $\omega b/2V$ depending on axis)
LAMP	Large Amplitude Multi-Purpose facility, Behrle Applied Research's Vertical Wind Tunnel with rotary balance rig, located in Neuberg a.d. Donau, Germany.
MAT	Multi-Axis Test Rig
NASA	National Aeronautics and Space Administration
$pb/2V$	Nondimensional Body Axis Roll Rate
$qc/2V$	Nondimensional Body Axis Pitch Rate
$rb/2V$	Nondimensional Body Axis Yaw Rate
S	Wing area, (ft ²)
SBIR	Small Business Innovation Research Program
VWT	Vertical Wind Tunnel
β	Sideslip Angle, (deg)
$\Omega b/2V$	Rotation Coefficient, positive for clockwise rotation
δ_{amt}	Skewed All Moving Tip deflection, (deg)
δ_{elevon}	Elevon deflection, (deg)
δ_{LEF}	Leading Edge Flap deflection, (deg)
δ_{pf}	Pitch Flap deflection, (deg)

FOREWORD

The wind tunnel model used during this test was constructed and delivered under the Innovative Control Effectors program that was jointly sponsored by the Air Force Research Laboratory (AFRL/VAAD) at Wright-Patterson AFB, Ohio and the Naval Air Warfare Center Aircraft Division (NAWCAD) located at Patuxent River, Maryland. Many people contributed their time and talents towards completion of this wind tunnel test and analysis. A few of the major contributors are listed below. This effort would not have been possible without their help.

- Test Support: Joe Martin, Tom Norris, Dwight Gering, Jon Tinapple, Tom Tighe (AFRL/VAAA), Jim Simon (AFRL/VAAD)
- Test Planning: Ken Dorsett (Lockheed Martin Tactical Aircraft Systems)

1. INTRODUCTION

Next generation fighter aircraft will require a combination of low radar cross section and high agility characteristics in order to remain survivable and lethal over future battlefields. Often, these two requirements are at odds with one another. Aggressive low signature requirements drive the configuration to have no vertical stabilization or control surfaces. Advanced control concepts are required to replace the function of the vertical tail and rudder on such aircraft. Highly agile fighter aircraft require large directional control moments to coordinate rolls, trim during crosswind landing, and counter asymmetric store loadings. Tailless aircraft, such as the one shown in Figure 1, place additional demands on yaw control power with the need to augment relaxed directional stability characteristics and provide adequate flying qualities throughout the flight envelope. Yaw thrust vectoring provides one means to generate yawing moments; however, while vectoring control power is very large at low speeds, its effectiveness falls off at higher speeds where aerodynamic surfaces provide a more efficient means of generating control moments.

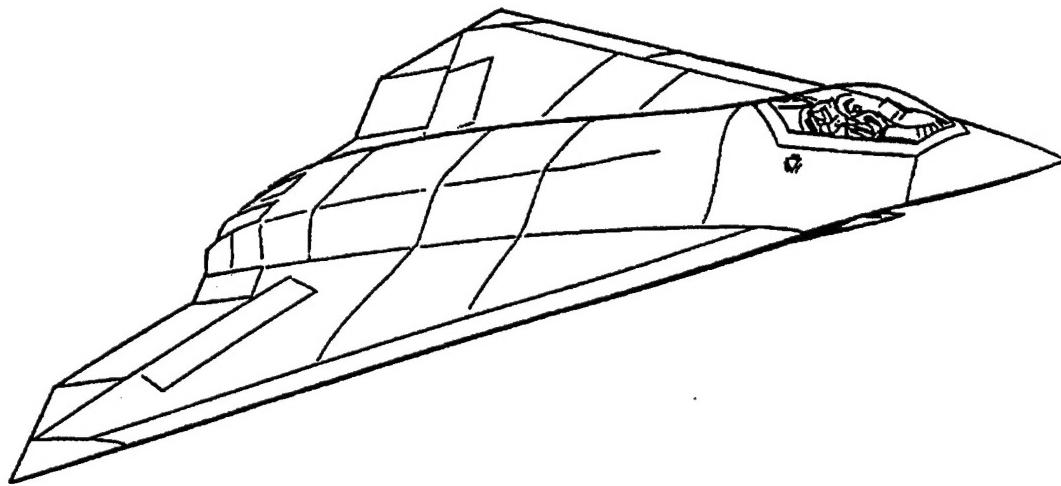


FIGURE 1 - Tailless Aircraft Concept

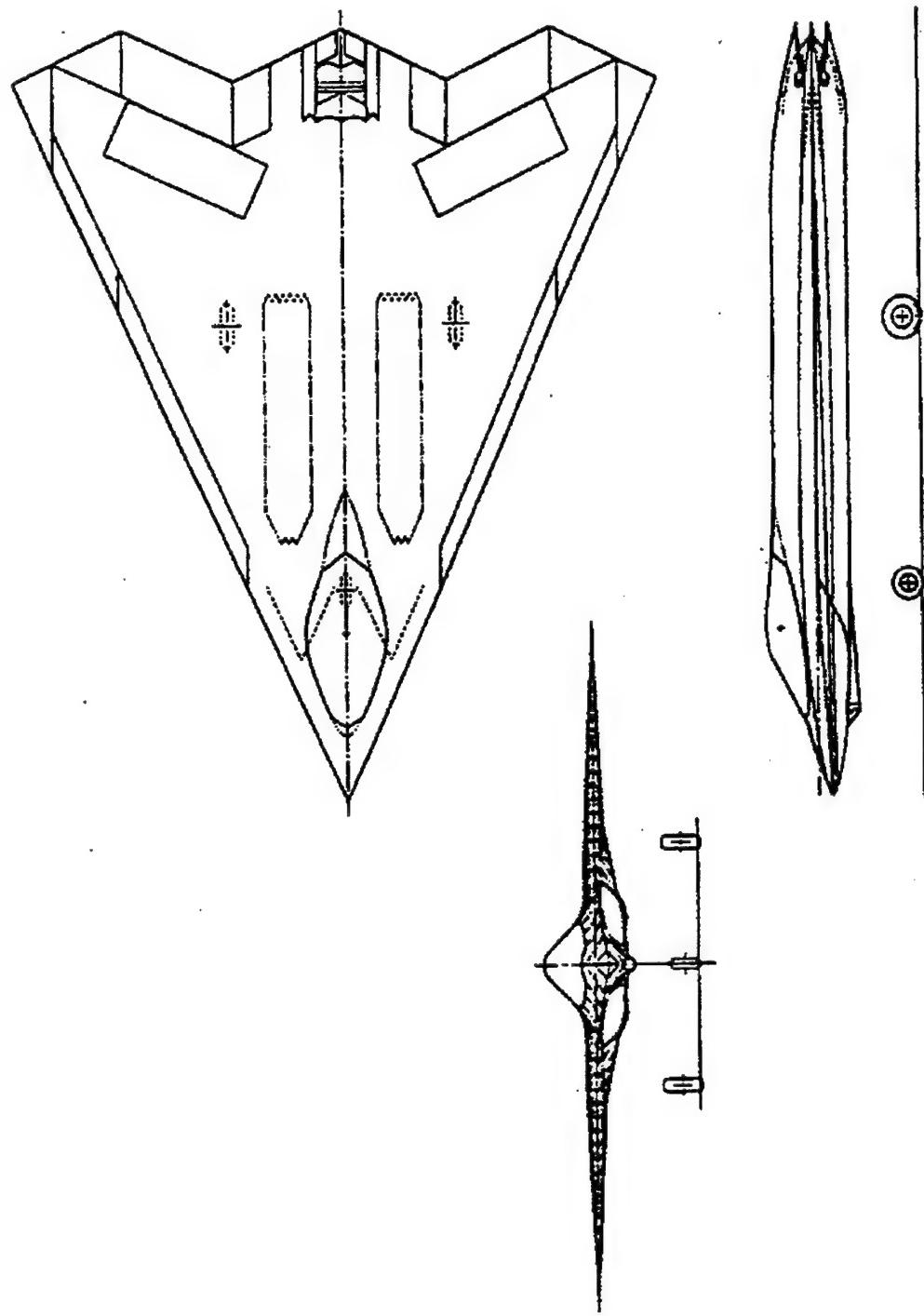


FIGURE 2 - ICE 101 Configuration 3-View

The Innovative Control Effectors (ICE) program was a jointly funded research effort between the Air Force Research Laboratory (AFRL) and the Naval Air Warfare Center that investigated innovative aerodynamic control concepts for highly maneuverable, tailless fighters and addressed the above stated issues.^{1,2} Lockheed Martin Tactical Aircraft Systems was awarded one of the contracts under the ICE effort and utilized two, corporately developed, configuration concepts in their control effector studies: ICE 101 for land-based operation and ICE 201 for carrier based operation. The ICE 101 concept was more suited to fulfilling Air Force needs and AFRL personnel focused a majority of their ICE efforts on the 101 concept configuration. A three view of this configuration is shown in Figure 2. One of the objectives of the ICE study was to see if tailless fighters could exhibit "F-16 class" maneuverability without the assistance of vertical stabilization or control surfaces. The elevated maneuvering requirements dictated the increased use of dynamic, high angle-of-attack flight, and therefore stability and control analysis of the ICE 101 concentrated on this flight regime.

A new, dual rotary balance / forced oscillation test capability has recently been added to the Air Force Research Laboratory Vertical Wind Tunnel (VWT) at Wright-Patterson AFB, Ohio, permitting both test types to be conducted in the same facility using a single model. A test program was conducted in the VWT to acquire additional data on the dynamic characteristics of the ICE 101 concept and to determine how well the innovative control devices perform under dynamic flight conditions. Rotary balance and forced oscillation tests were conducted through a wide angle-of-attack and sideslip range to study full envelope capabilities. This report documents the rotary balance and forced oscillation data taken during this test program and presents analysis of the acquired data.

2. DESCRIPTION OF MODEL

A 1/13th scale model, representing the ICE 101 configuration was constructed of fiberglass, balsa, and plywood under the ICE Phase II contract with Lockheed Martin. The materials were selected in order to keep the weight and inertia of the model as low as possible, but still provide the necessary strength to withstand aerodynamic loads. These requirements combined to produce relatively high aerodynamic to inertia load ratios which are critical for accurate, consistent data acquisition during dynamic wind tunnel testing.

The dimensional and control surface characteristics of the ICE 101 vehicle concept are given in Table 1. A diagram displaying the control surface deflection sign convention is shown in Figure 3. Photographs of model installed on the MAT rig are shown in Figures 4 and 5.

TABLE 1
DIMENSIONAL CHARACTERISTICS OF FULL SCALE ICE 101 VEHICLE

Model Scale	1/13
Overall Length, in	517.49
Fuselage Station @ Nose Tip, in	0.00
Reference Area, ft ²	808.60
Reference Span, ft	37.50
Mean Aerodynamic Chord, in	345.0
Aspect Ratio	1.74
FS LEMAC, in	160.84
LE Sweep, deg	65.00
TE Chevron Sweep, deg	25.00
Elevon Area (each side), ft ²	22.77
Pitch Flap Area (each side), ft ²	7.77
Skewed All Moving Tip Area (each side), ft ²	19.89

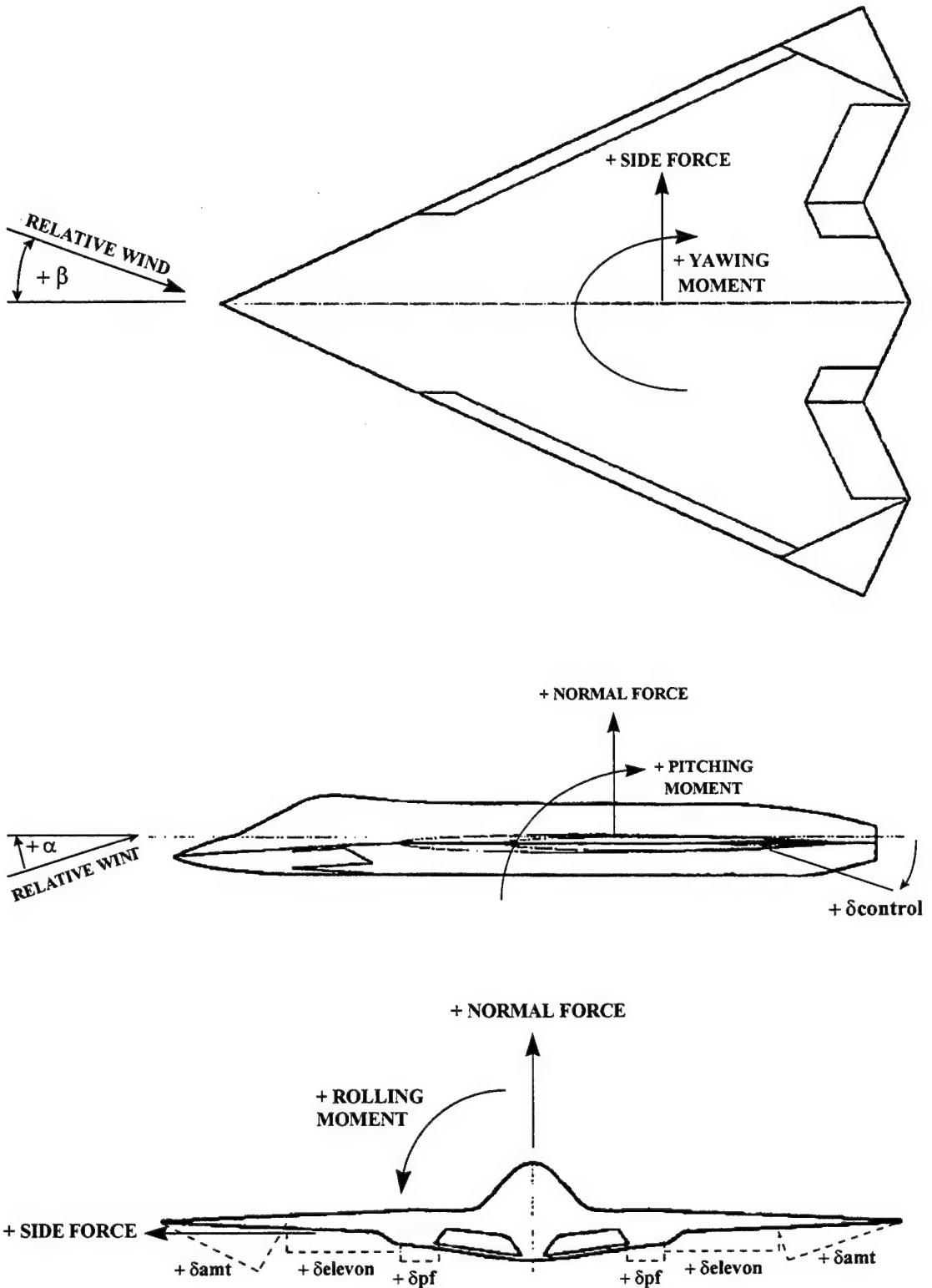


FIGURE 3 - Model Force and Moment Sign Convention

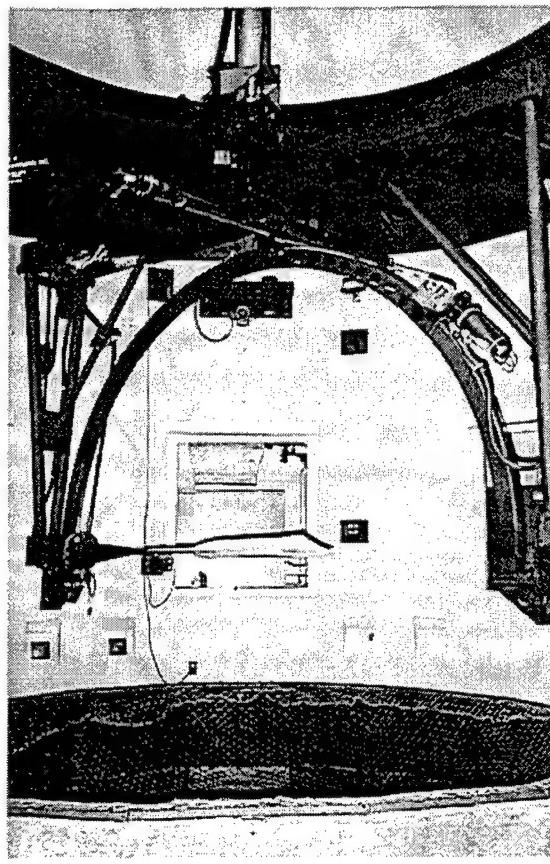


FIGURE 4 - Model Mounted on the MAT Rig

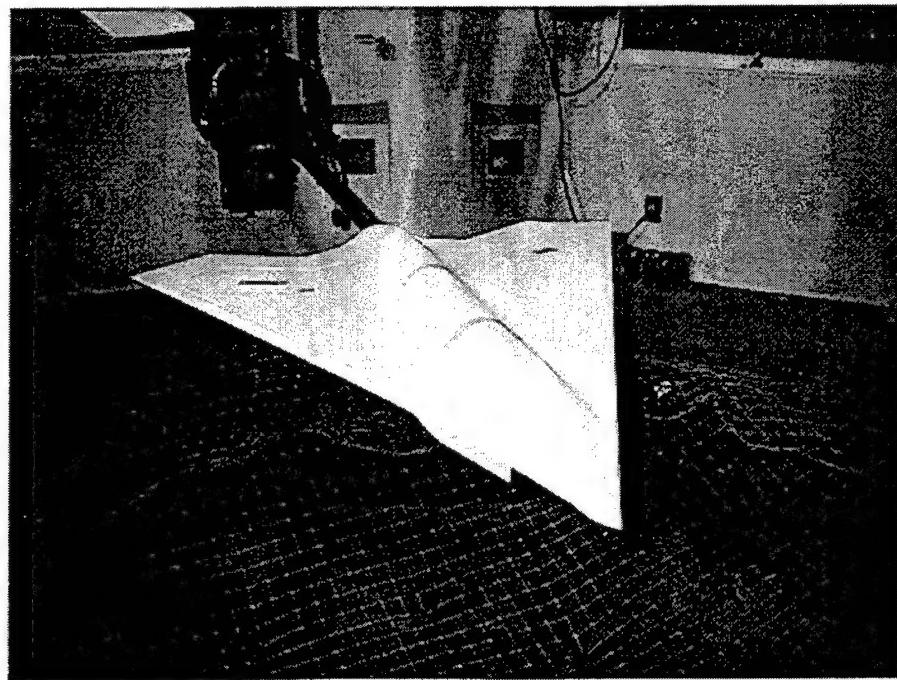


FIGURE 5 - Close Up View of the Model

3. TEST FACILITIES

The Air Force Research Laboratory's Vertical Wind Tunnel was built in the 1940's to conduct aircraft free flight spin testing to define spin modes and recovery techniques. It possesses an atmospheric pressure, annular return, closed circuit with an open test section, oriented vertically. This design permits year around, all weather operation and quick, easy access to wind tunnel models. A layout of the facility is shown in Figure 6. The 1000 horsepower, variable speed motor drives a four bladed fan propelling the air flow vertically up to 102 mph. The 12 ft diameter test section has a very uniform flow distribution as documented in a October 1993 flow survey³ making this facility highly suitable for aircraft dynamic motion testing.

The Multi-Axis Test (MAT) rig was recently designed, built, and installed under DOD SBIR Phase II contract F33615-94-C-3608 by Bihrlle Applied Research, Inc. and Production Service & Technology, Inc.⁴ This contracted effort added rotary balance and forced oscillation test capabilities to the AFRL Vertical Wind Tunnel facility. The C-sector sting support system was shaped to minimize support system aerodynamic interference and is capable of providing continuous angle of attack sweeps from 0 deg. to +90 deg. with sideslip angles out to \pm 30 deg. With the capability of aft or top mounting, the full angle-of-attack envelope is \pm 180 deg. The test rig is capable of rotating up to 130 rpm in either the clockwise or counter-clockwise direction and a wide range of $\Omega b/2V$ values can be attained by adjusting the rotational speed of the rig and/or the tunnel flow velocity. Forced oscillation capability is added by removing the rotary balance sting from the angle-of-attack carriage and attaching the appropriate pitch, roll, or yaw drive motor and corresponding sting assembly. Rig control is provided by a purpose-built computer installed in the control console. The control console, located outside of the tunnel test section, is used to control the wind tunnel fan and activate motors on the rig, which position the model to the desired attitude.

With dynamic testing, several factors need attention in order to produce high quality test data. To match aircraft rotation rates in the wind tunnel with those typically experienced in flight, the nondimensional rotation rates, such as $\Omega b/2V$, need to be the same. By observation, it is clear that changes in rotation rate need to be matched with

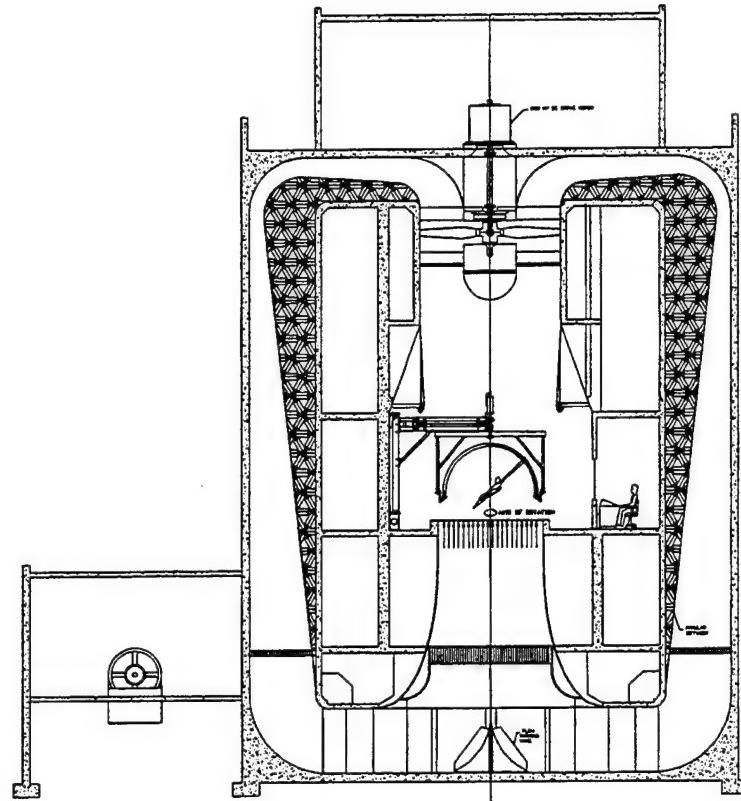


FIGURE 6 – AFRL Vertical Wind Tunnel Layout

corresponding changes in wind tunnel flow velocity. Low wind tunnel rotation rates are desired in order to keep the model weight and inertia from overstraining the balance during high rotation rates. This requirement dictates a low wind tunnel flow velocity to keep the nondimensional rotation rate consistent with flight. The low flow velocity lends itself to low aerodynamic forces and moments on the model so the balance must have a small range in order to maintain a high sensitivity to small changes in aerodynamic parameters. Therefore, the goal for dynamic testing is to test with the lightest weight model, the lowest rotation rate, and the lowest tunnel flow velocity as possible.

The six-component strain gauge balance used on the MAT rig (MAT1195A) was affixed to the end of the sting and mounted internally to the model. Listed in Table 2 are the accuracies of the ensemble-averaged coefficient values presented throughout this report.

TABLE 2
STRAIN GAUGE BALANCE ACCURACY

Coefficient	Full Scale Loads	2 σ Error of Full Scale	95% Confidence For Coefficient*
Normal Force	20.0	0.0972 lbs.	0.00371
Axial Force	20.0	0.0248 lbs.	0.00095
Pitching Moment	176.0	1.0102 in-lbs.	0.01744
Rolling Moment	81.6	0.235 in-lbs.	0.00310
Yawing Moment	80.0	0.4752 in-lbs.	0.00628
Side Force	15.0	0.0717 in-lbs.	0.00274

* Two standard deviations from the mean of 300 samples.

The data acquisition and analysis system consists of a 133 MHz Data Acquisition Computer, 166 MHz Data Analysis Computer, Keathley Signal Conditioners, and a laser printer. This PC-based system provides strong computing power, flexibility to perform other functions, and is easy and affordable to upgrade as PC technology advances. The data is viewed on screen, in real time, for quick assessment and then storage. A local area network connects the two computers for rapid transfer of data so comparisons against predictions or other wind tunnel data can be plotted and evaluated quickly. A CD-Writer device is also utilized for permanent storage of the data for future reference.

4. TEST PROCEDURES

4.1 Rotary Balance Testing

This testing technique consists of rotating the model at a fixed rate subjected to a uniform, steady aerodynamic flowfield with a strain gauge balance measuring the body axis forces and moments acting on a model. Historical background for this test technique is presented in References 5 & 6. Rotary aerodynamic data are obtained through a two step process. First, the inertial forces and moments acting on the model at different attitudes and steady state rotation rates are determined. Ideally these inertial terms would be measured by rotating the model in a vacuum. As a practical approach, the model is enclosed in a sealed spherical structure, known as a tare bag, that rotates with the model without touching it (Figure 7). In this manner, the surrounding air moves with the model, thus eliminating any aerodynamic force and moment that may be generated if the model were rotated in open, still air. As the model is rotated at the desired attitude and steady rate, the inertial forces and moments generated by the model are measured by acquiring 300 points of data taken over a 4.5 second time frame, then averaged to produce a single data point. From data acquired at different rotational rates for each geometric orientation (α , β), the data reduction system develops a mathematical relationship between model inertial values and rotation rate. This data is stored in computer memory for later retrieval. After all the tare files have been acquired, the tare bag is then removed from the rotary balance rig assembly and normal wind-on operation is started. The same process of setting the test condition angle-of-attack, sideslip and desired rotation rate as for the tare is conducted again except now the wind tunnel is running with the appropriate flow velocity. The wind-on data is taken, again acquiring 300 points of data taken over 4.5 seconds, then averaged to produce a data point for each (α , β , $\Omega_b/2V$) combination. Then the corresponding wind-off tare data that were recorded earlier are subtracted from these data, leaving only the aerodynamic forces and moments which are then converted into nondimensional coefficient form.

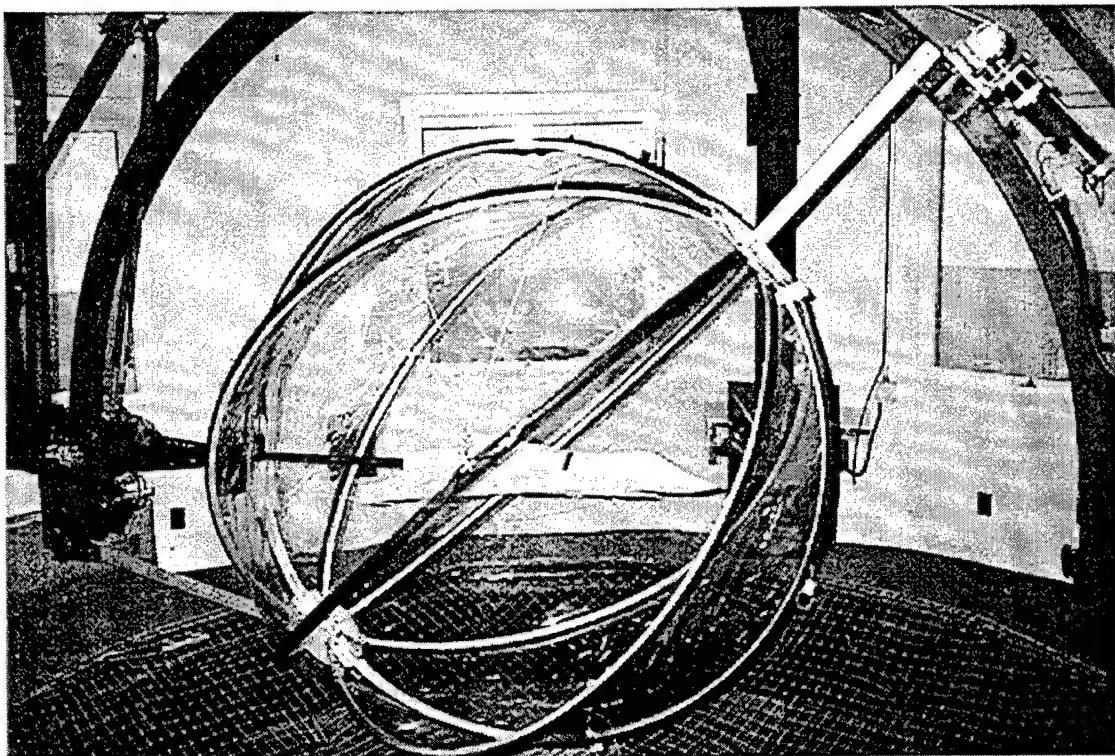


FIGURE 7 - Model Enclosed in the Tare Bag

4.2 Forced Oscillation Testing

To conduct forced oscillation testing, the rotary balance sting is removed and an oscillation motor is mounted to the sting carriage. For the roll and yaw oscillation setups, the motor oscillates the sting along the long axis which translates into one body axis, aft mounting for roll (Figure 8) and top mounting for yaw (Figure 9). For the pitch oscillation setup, a different motor, separate sting, and push rod are utilized (Figure 10). The internal balance measures the body axis forces and moments acting on a model as it oscillates. Forced oscillation aerodynamic data are also obtained through a two step process. First, with the wind tunnel air flow off, a time history of the inertial forces and moments acting on the model at each test attitude, frequency, and amplitude combination are recorded and stored in computer memory for later use. Once all the tare runs are completed, the next step is to acquire the time history force and moment data from normal wind-on operation at the same attitude, amplitude, and frequency combination as the tare data. The corresponding wind-off tares are then synchronized with the wind-on data and then subtracted, leaving only the aerodynamic forces and moment data. Data taken during the relatively constant velocity, non-accelerated points

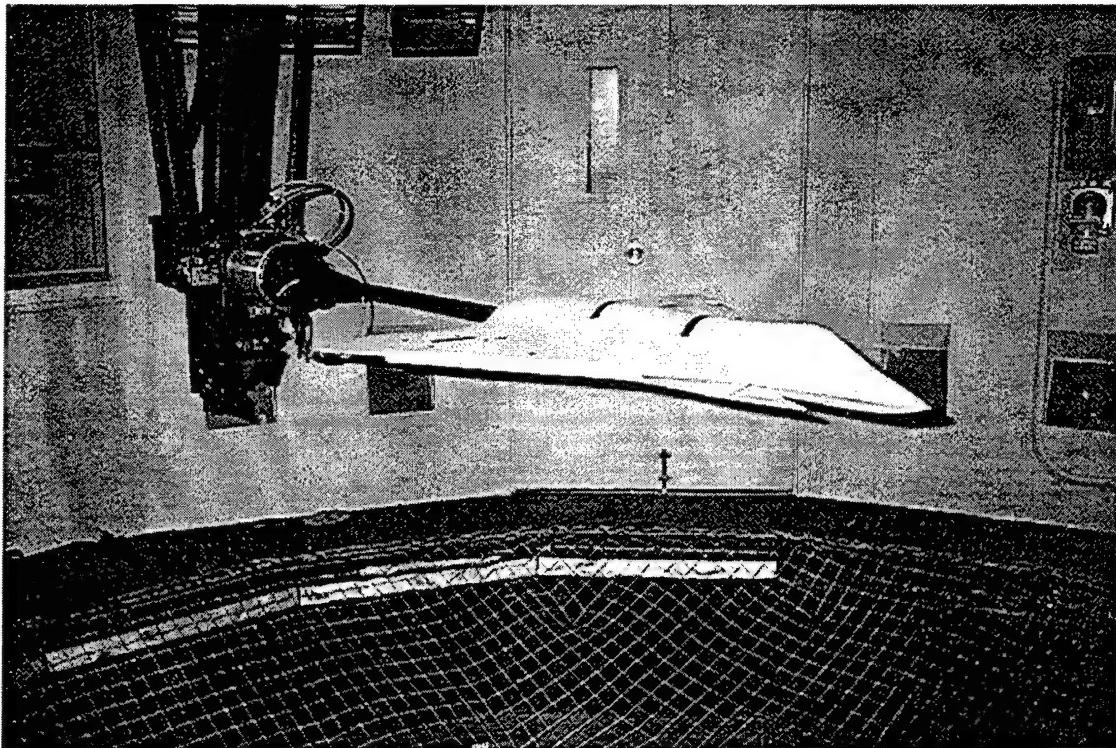


FIGURE 8 – Roll Forced Oscillation Mounting

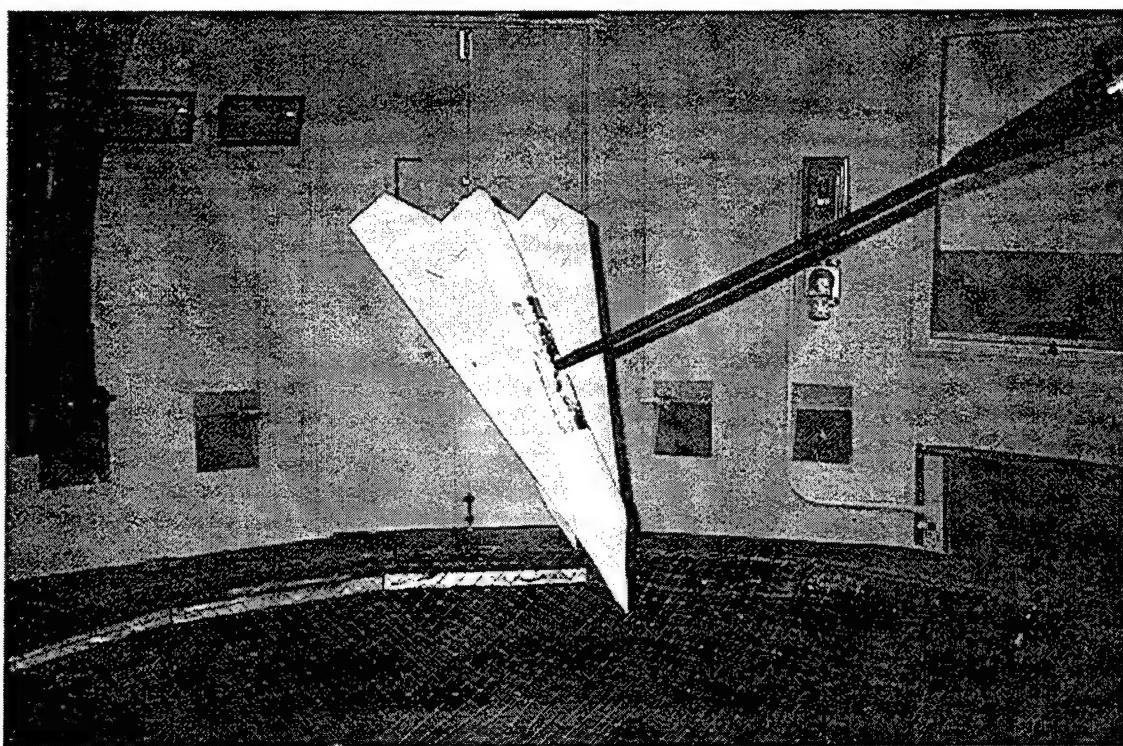


FIGURE 9 – Yaw Forced Oscillation Mounting

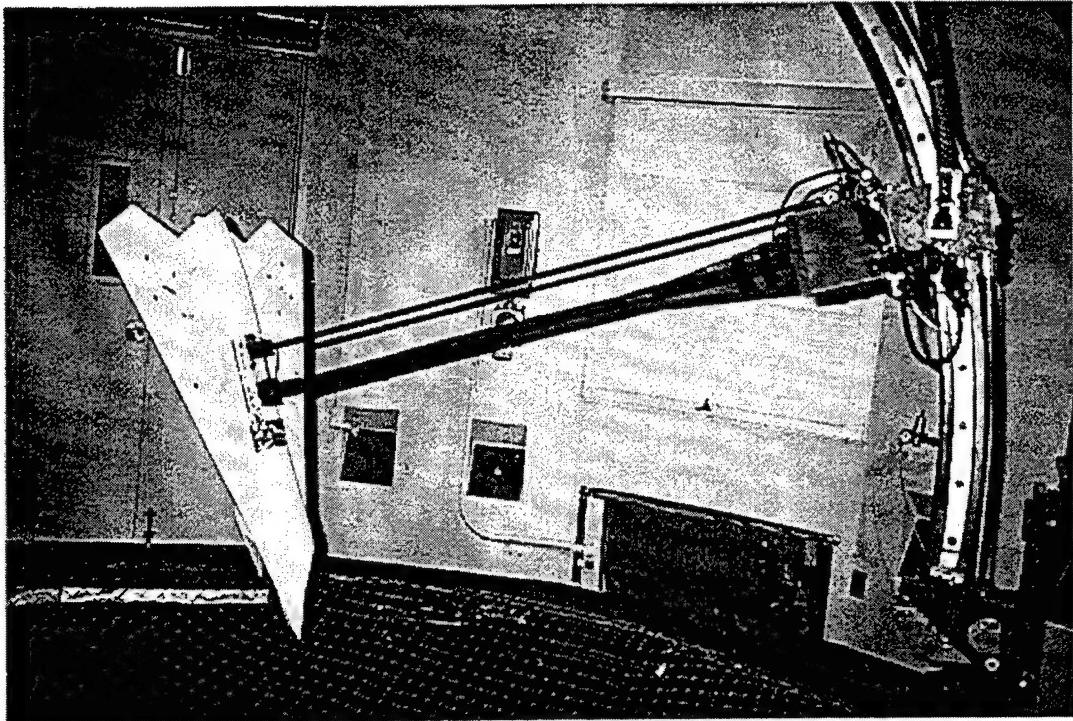


FIGURE 10 – Pitch Forced Oscillation Mounting

of the cycle are utilized and averaged over several cycles of data. This procedure is known as the Specific Point Method and produces both positive and negative rate data. Historical background for this test technique is presented in Reference 7.

5. TEST CONDITIONS

All testing was conducted in the AFRL Vertical Wind Tunnel utilizing the MAT rig with a freestream dynamic pressure of approximately 1.0 psf, corresponding to a freestream velocity of approximately 29.0 ft/sec and a Reynolds Number of approximately 0.175×10^6 per foot. The model was tested with the spin axis located at the model c.g. location of 0.38 cbar, but slightly below the waterline of the c.g. such that the balance moment center was located at FS 291.94, WL 95.06 (full scale). The vertical offset was accounted for when the overall forces and moments were computed. Therefore, all data presented in this report are referenced to FS 291.94, WL 100.0 (0.38 cbar).

For the rotary balance tests, all configurations were tested through an angle-of-attack range of 0 deg. to 90 deg. (upright) and sideslip angles of up to +/- 30 deg. Shown in Table 3 is the run log for all the rotary balance configurations tested. Unless otherwise noted in the table, data were obtained using increments in angle-of-attack of 5 deg. and $\Omega b/2V$ values of 0.0, 0.05, 0.10, 0.20, and 0.30 in both the clockwise (pilot's right) and counter-clockwise directions. For the forced oscillation tests, all configurations were tested through an angle-of-attack range of 0 deg. to 90 deg., at a sideslip angle of 0 deg. Shown in Table 4 is the run log for all the forced oscillation configurations tested.

TABLE 3 – STATIC AND ROTARY BALANCE RUN LOG

Full Scale Reference Values						
Sref = 808.6 ft ⁿ 2	A1 = AOA : 0 to 90, Δ 5					
MAC = 345.0 in	A3 = AOA : 0, 10, 20 to 40, Δ 1					
bref = 37.5 ft						
X MRC = 38% MAC						
WL MRC = 100 in						
FS LEMAC = 160.45 in						

A1 = AOA : 0 to 90, Δ 5
A3 = AOA : 0, 10, 20 to 40, Δ 1

Test conditions: Q = 1.0 psf, Velocity 29.0 ft/sec, Tunnel Fan = 167 RPM
Sign Convention: +LEF=LE Down, +Elevon=TE Down, +Pitch Flap=TE Down, +AMT=TE Down
S = Static, R = Rotary Balance, W0: LEF=0/0, W1: LEF=30/30

Air On Tunnel Data						
Configuration Name	AOA	Beta	LEF	Elevon	Pitch Flap	AMT
SICE1W0 p-30	A1	-30	0/0	0/0	0/0	0/0
SICE1W0 p-20	A1	-20	0/0	0/0	0/0	0/0
ICE1W0 p-10	A1	-10	0/0	0/0	0/0	0/0
SICE1W0 p-10	A1	-10	0/0	0/0	0/0	0/0
SICE1W0 p-10	A1	-10	0/0	0/0	0/0	0/0
ICE1W0	A1	0	0/0	0/0	0/0	0/0
ICE1W0 p+10	A1	10	0/0	0/0	0/0	0/0
SICE1W0 p+10	A3	10	0/0	0/0	0/0	0/0
SICE1W0 p+10	A3	10	0/0	0/0	0/0	0/0
ICE1W0 p+20	A1	20	0/0	0/0	0/0	0/0
ICE1W0 p+30	A1	30	0/0	0/0	0/0	0/0
 LEF Effectiveness						
AOA	Beta	LEF	Elevon	Pitch Flap	AMT	SSD
ICE1W1	A1	0	30/30	0/0	0/0	R
ICE1W1 p+10	A1	10	30/30	0/0	0/0	R
ICE1W1 p+20	A1	20	30/30	0/0	0/0	R
ICE1W1 p+30	A1	30	30/30	0/0	0/0	R

Data File						
Test	STICEJ	STICEG	TICEC	TICECX	TICEC	TICEA
SICE1W0 p-30	SICEJ	SICEG	R	S	S	S
SICE1W0 p-20	SICEG	SICEG	R	S	S	S
ICE1W0 p-10	ICEC	ICEC	R	S	S	S
SICE1W0 p-10	TICEC	TICEC	R	S	S	S
SICE1W0 p-10	TICECX	TICECX	R	S	S	S
ICE1W0	TICEC	TICEC	R	S	S	S
ICE1W0 p+10	TICEA	TICEA	R	S	S	S
ICE1W0 p+10	TICEB	TICEB	R	S	S	S
SICE1W0 p+10	STICEBX	STICEBX	R	S	S	S
SICE1W0 p+10	STICEBY	STICEBY	R	S	S	S
ICE1W0 p+20	TICEF	TICEF	R	S	S	S
ICE1W0 p+30	TICEH	TICEH	R	S	S	S

Comments						
AOA : 90 - 0	AOA : 0 - 90	AOA : 0 - 90	AOA : 90 - 0	AOA : 0 - 90	AOA : 0 - 90	AOA : 0 - 90
AOA : 0 - 90	AOA : 0 - 90	AOA : 0 - 90	AOA : 90 - 0			
AOA : 0 - 90	AOA : 0 - 90	AOA : 0 - 90	AOA : 90 - 0			
AOA : 0 - 90	AOA : 0 - 90	AOA : 0 - 90	AOA : 90 - 0			
AOA : 0 - 40	AOA : 0 - 40	AOA : 0 - 40	AOA : 40 - 0			
AOA : 40 - 0	AOA : 40 - 0	AOA : 40 - 0	AOA : 0 - 90			
AOA : 0 - 90						

TABLE 3 – STATIC AND ROTARY BALANCE RUN LOG (CONCLUDED)

AMT Effectiveness	AOA	Beta	LEF	Elevon	Pitch Flap	AMT	SSD	Test	Data File	Tare	COMMENTS
ICE1W0 p-10 AMT=60	A1	-10	0/0	0/0	0/0	0/+ 60	0/0	R	ICECT	TICEC	AOA : 0 - 90
ICE1W0 AMT=60	A1	0	0/0	0/0	0/0	0/+ 60	0/0	R	ICEAT	TICEA	AOA : 0 - 90
ICE1W0 p+10 AMT=60	A1	10	0/0	0/0	0/0	0/+ 60	0/0	R	ICEBT	TICEB	AOA : 0 - 90
Max Nose Down	AOA	Beta	LEF	Elevon	Pitch Flap	AMT	SSD	Test	Data File	Tare	COMMENTS
SICE1W0 Max N.D.	A1	0	0/0	30/30	30/30	(10/10)	0/0	S	SICEAN1	TICEA	AOA : 0 - 90
SICE1W0 p+10 Max N.D.	A1	10	0/0	30/30	30/30	(10/10)	0/0	S	SICEBN1	TICEB	AOA : 0 - 90
SICE1W0 p+20 Max N.D.	A1	20	0/0	30/30	30/30	(10/10)	0/0	S	SICEFN1	TICEF	AOA : 0 - 90
SICE1W0 p+30 Max N.D.	A1	30	0/0	30/30	30/30	(10/10)	0/0	S	SICEHN1	TICEH	AOA : 0 - 90
SICE1W0 Max N.D.	A1	0	0/0	30/30	30/30	(30/30)	0/0	S	SICEAN2	TICEA	AOA : 0 - 90
SICE1W0 p+10 Max N.D.	A1	10	0/0	30/30	30/30	(30/30)	0/0	S	SICEBN2	TICEB	AOA : 0 - 90
SICE1W0 p+20 Max N.D.	A1	20	0/0	30/30	30/30	(30/30)	0/0	S	SICEFN2	TICEF	AOA : 0 - 90
SICE1W0 p+30 Max N.D.	A1	30	0/0	30/30	30/30	(30/30)	0/0	S	SICEHN2	TICEH	AOA : 0 - 90

TABLE 4 – FORCED OSCILLATION RUN LOG

Full Scale Reference Values

Sref = 808.6 ft^2
MAC = 345.0 in
bref = 37.5 ft
X MRC = 38% MAC
WL MRC = 100 in
FS LEMAC = 160.45 in

A1 = AOA : 0 to 90, Δ 5

Test conditions: Q ~ 1.0 psf, Velocity = 29.0 ft/sec, Tunnel Fan = 167 RPM

Upright Sign Convention: +LEF=LE Down, +Elevon=TE Down, +Pitch Flap=TE Down,
+AMT=TE Down

Roll Oscillation

Configuration	AOA (Deg)	Beta (Deg)	LEF (Deg)	Elevon (Deg)	P. Flap (Deg)	AMT (Deg)	SSD	Red.Freq K	Amp. (Deg)	Rate pb/2V	Osc. Freq (rad/sec)	DataFile	Tare	
ICE1W0, Mid Freq														
	A1	0	0/0	0/0	0/0	0/0	0/0	0.1492	(+- 10)	0.026	3.0	R0A10	TRO0A10	
	A1	0	0/0	0/0	0/0	0/0	0/0	0.1492	(+- 20)	0.052	3.0	R0A20	TR0A20	
	A1	0	0/0	0/0	0/0	0/0	0/0	0.1492	(+- 30)	0.078	3.0	R0A30	TR0A30	
ICE1W0, Low Freq														
	A1	0	0/0	0/0	0/0	0/0	0/0	0.1194	(+- 12.5)	0.026	2.4	R0A10A	TR0A10A	
	A1	0	0/0	0/0	0/0	0/0	0/0	0.1194	(+- 25)	0.052	2.4	R0A20A	TR0A20A	
	A1	0	0/0	0/0	0/0	0/0	0/0	0.1194	(+- 37.5)	0.078	2.4	R0A30A	TR0A30A	
ICE1W0, High Freq														
	A1	0	0/0	0/0	0/0	0/0	0/0	0.1790	(+- 8.33)	0.026	3.6	R0A10B	TR0A10B	
	A1	0	0/0	0/0	0/0	0/0	0/0	0.1790	(+- 16.66)	0.052	3.6	R0A20B	TR0A20B	
	A1	0	0/0	0/0	0/0	0/0	0/0	0.1790	(+- 25)	0.078	3.6	R0A30B	TR0A30B	
Configuration	AOA (Deg)	Beta (Deg)	LEF (Deg)	Elevon (Deg)	P. Flap (Deg)	AMT (Deg)	SSD	Red.Freq K	Amp. (Deg)	Rate pb/2V	Osc. Freq (rad/sec)	DataFile	Tare	
ICE1W1														
	A1	0	30/30	0/0	0/0	0/0	0/0	0.1492	(+- 10)	0.026	3.0	R0A10F	TRO0A10	
	A1	0	30/30	0/0	0/0	0/0	0/0	0.1492	(+- 20)	0.052	3.0	R0A20F	TR0A20	
	A1	0	30/30	0/0	0/0	0/0	0/0	0.1492	(+- 30)	0.078	3.0	R0A30F	TR0A30	

TABLE 4 – FORCED OSCILLATION RUN LOG (CONTINUED)

Yaw Oscillation									
Configuration	AOA (Deg)	Beta (Deg)	LEF (Deg)	Elevon (Deg)	P. Flap (Deg)	AMT (Deg)	SSD (Deg)	Red Freq (Deg)	Amp. (rad/2V)
ICE1W0, Mid Freq	A1	0	0/0	0/0	0/0	0/0	0/0	0.1492 (+/- 10)	0.026
	A1	0	0/0	0/0	0/0	0/0	0/0	0.1492 (+/- 20)	0.052
	A1	0	0/0	0/0	0/0	0/0	0/0	0.1492 (+/- 30)	0.078
ICE1W0, Low Freq	A1	0	0/0	0/0	0/0	0/0	0/0	0.1194 (+/- 12.5)	0.026
	A1	0	0/0	0/0	0/0	0/0	0/0	0.1194 (+/- 25)	0.052
	A1	0	0/0	0/0	0/0	0/0	0/0	0.1194 (+/- 37.5)	0.078
ICE1W0, High Freq	A1	0	0/0	0/0	0/0	0/0	0/0	0.1790 (+/- 8.33)	0.026
	A1	0	0/0	0/0	0/0	0/0	0/0	0.1790 (+/- 16.66)	0.052
	A1	0	0/0	0/0	0/0	0/0	0/0	0.1790 (+/- 25)	0.078
Configuration	AOA (Deg)	Beta (Deg)	LEF (Deg)	Elevon (Deg)	P. Flap (Deg)	AMT (Deg)	SSD (Deg)	Red Freq (Deg)	Amp. (rad/sec)
ICE1W1	A1	0	30/30	0/0	0/0	0/0	0/0	0.1492 (+/- 10)	0.026
	A1	0	30/30	0/0	0/0	0/0	0/0	0.1492 (+/- 20)	0.052
	A1	0	30/30	0/0	0/0	0/0	0/0	0.1492 (+/- 30)	0.078

TABLE 4 – FORCED OSCILLATION RUN LOG (CONCLUDED)

<i>Pitch Oscillation</i>									
Configuration	AOA (Deg)	Beta (Deg)	LEF (Deg)	Elevon (Deg)	P. Flap (Deg)	AMT (Deg)	SSD (Deg)	Red.Freq (Deg)	Amp. qc/2V
ICE1W0, Mid Freq	A1	0	0/0	0/0	0/0	0/0	0/0	0.1036 (+/- 5.00)	0.009
	A1	0	0/0	0/0	0/0	0/0	0/0	0.1036 (+/- 10.00)	0.018
	A1	0	0/0	0/0	0/0	0/0	0/0	0.1036 (+/- 15.00)	0.027
	A1	0	0/0	0/0	0/0	0/0	0/0	0.0827 (+/- 6.25)	0.009
ICE1W0, Low Freq	A1	0	0/0	0/0	0/0	0/0	0/0	0.0827 (+/- 12.50)	0.018
	A1	0	0/0	0/0	0/0	0/0	0/0	0.0827 (+/- 18.75)	0.027
	A1	0	0/0	0/0	0/0	0/0	0/0	0.1242 (+/- 4.16)	0.009
	A1	0	0/0	0/0	0/0	0/0	0/0	0.1242 (+/- 8.33)	0.018
ICE1W0, High Freq	A1	0	0/0	0/0	0/0	0/0	0/0	0.1242 (+/- 12.50)	0.027
	A1	0	0/0	0/0	0/0	0/0	0/0		3.26
	A1	0	0/0	0/0	0/0	0/0	0/0		3.26
	A1	0	0/0	0/0	0/0	0/0	0/0		3.26
<i>Configurations</i>									
Configuration	AOA (Deg)	Beta (Deg)	LEF (Deg)	Elevon (Deg)	P. Flap (Deg)	AMT (Deg)	SSD (Deg)	Red.Freq (Deg)	Amp. qc/2V
ICE1W1	A1	0	30/30	0/0	0/0	0/0	0/0	0.1036 (+/- 5.00)	0.009
	A1	0	30/30	0/0	0/0	0/0	0/0	0.1036 (+/- 10.00)	0.018
	A1	0	30/30	0/0	0/0	0/0	0/0	0.1036 (+/- 15.00)	0.027
	A1	0	30/30	0/0	0/0	0/0	0/0		2.71

<i>Configuration</i>									
Configuration	AOA (Deg)	Beta (Deg)	LEF (Deg)	Elevon (Deg)	P. Flap (Deg)	AMT (Deg)	SSD (Deg)	Red.Freq (Deg)	Amp. qc/2V
ICE1W0 MAX N.D.	A1	0	0/0	30/30	30/30	0/0	0.1036 (+/- 5.00)	0.009	2.71
	A1	0	0/0	30/30	30/30	0/0	0.1036 (+/- 10.00)	0.018	2.71
	A1	0	0/0	30/30	30/30	0/0	0.1036 (+/- 15.00)	0.027	2.71
	A1	0	0/0	30/30	30/30	0/0			2.71

6. DATA CORRECTIONS

Development of the MAT rig data acquisition system relied significantly on software already developed for the NASA Langley Research Center Spin Tunnel and the Bihrlle Applied Research LAMP facility. The method for computing dynamic pressure was corrected for temperature variations on density but assumed atmospheric pressure would remain at 97% of sea level standard. The actual atmospheric pressure varied significantly enough that it could not be ignored. A more accurate computation method, including pressure variations on density, was developed and replaced the original version. This new method was incorporated into the rotary balance data acquisition system before the ICE 101 test started. However, it was not incorporated into the forced oscillation data acquisition system until after the roll and yaw forced oscillation tests were completed. The atmospheric pressure during the roll forced oscillation test was fortunately near 97% of sea level standard, so no correction was performed. However, during yaw forced oscillation, the pressure was significantly different and a post test correction was needed. Those correction values are listed below in Table 5.

TABLE 5
DATA CORRECTIONS

Date	Filename	Temp (F)	Press (in Hg)	Computer Q (psf)	Actual Q (psf)	Correction
9-Apr-98	Y0A10B	58.0	28.408	0.9737	0.9500	1.0249
9-Apr-98	Y0A30B	58.0	28.412	0.9737	0.9502	1.0247
10-Apr-98	Y0A10	54.6	28.798	0.9794	0.9687	1.0110
10-Apr-98	Y0A20	54.6	28.848	0.9794	0.9704	1.0093
10-Apr-98	Y0A30	54.6	28.842	0.9794	0.9702	1.0095
10-Apr-98	Y0A30A	54.6	28.856	0.9794	0.9706	1.0091
10-Apr-98	Y0A20A	54.6	28.878	0.9794	0.9714	1.0082
10-Apr-98	Y0A10A	54.6	28.879	0.9794	0.9714	1.0082
10-Apr-98	Y0A10F	54.6	28.910	0.9794	0.9724	1.0072
10-Apr-98	Y0A20F	54.6	28.910	0.9794	0.9724	1.0072
10-Apr-98	Y0A30F	55.0	28.950	0.9794	0.9738	1.0058

7. STATIC CHARACTERISTICS

7.1 Neutral Control

The baseline vehicle exhibits a traditional normal force curve, as shown in Figure 11, peaking at $\alpha = 35$ deg. before stalling and then moderating to a fully separated condition up to $\alpha = 90$ deg. The effect of sideslip significantly reduced the magnitude of normal force over the entire angle-of-attack range. For pitching moment, the vehicle was essentially trimmed with neutral controls up to $\alpha = 10$ deg, as shown in Figure 12. As angle-of-attack was increased, the vehicle became unstable and then broke stable for $\alpha > 30$ up to 90 deg. The effect of sideslip on pitching moment was isolated to the $20 < \alpha < 55$ deg. region where higher sideslip added more stable moments. For rolling moment, a small, positive asymmetry was identified at $\beta = 0$ deg., as shown in Figure 13. With sideslip, the vehicle exhibited strong lateral stability for the entire angle-of-attack range except in the $25 < \alpha < 35$ deg. region where a small instability was seen for small to moderate sideslip angles ($\beta < 15$ deg.) For yawing moment, the vehicle showed very little asymmetry for the $\beta = 0$ deg. case, as shown in Figure 14. With sideslip, the vehicle exhibited moderate directional instability throughout the entire angle-of-attack range. This instability was magnified as much as 500% in the $25 < \alpha < 50$ deg. region. Strong directional control effectors would be needed to augment stability in this area.

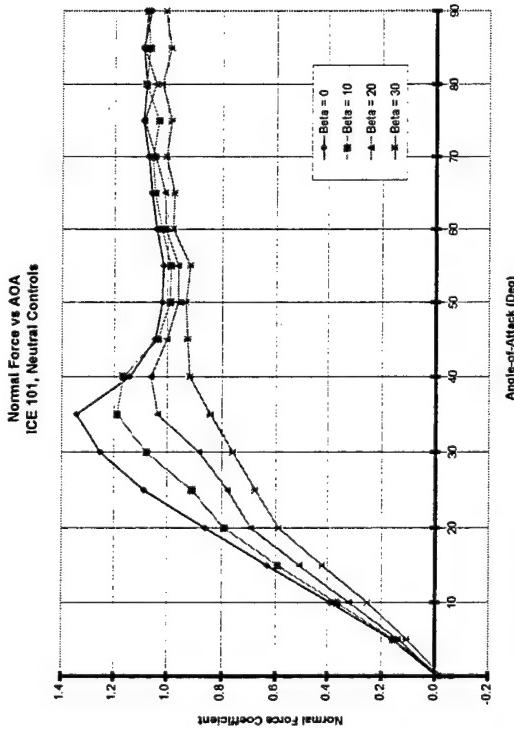


FIGURE 11

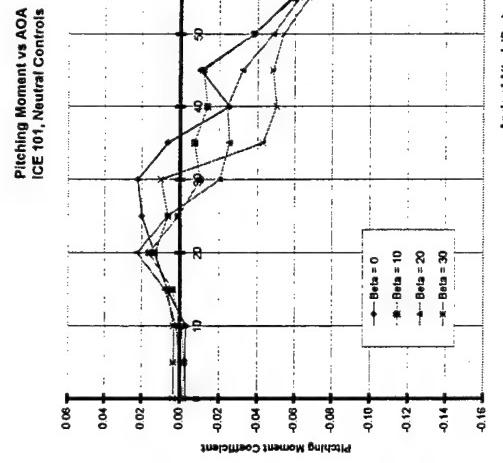


FIGURE 12

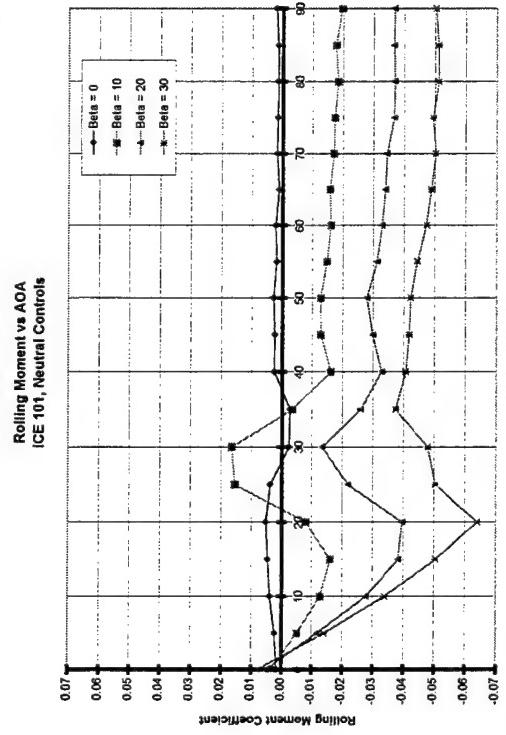


FIGURE 13

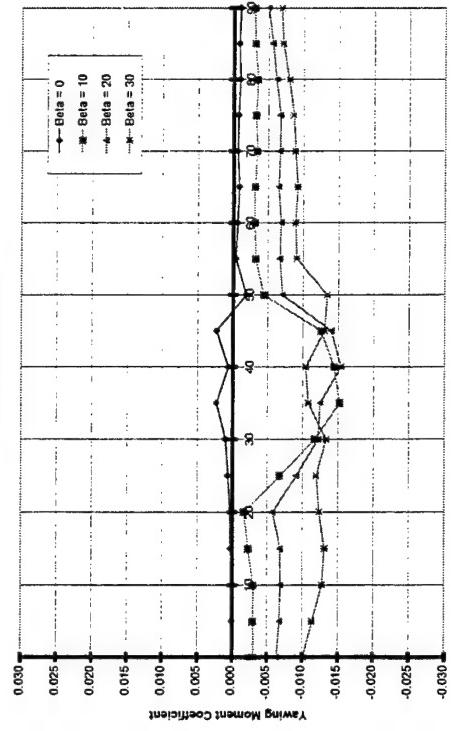


FIGURE 14

7.2 Full Nose-Down Control

As part of the investigation of the ICE 101 vehicle concept, full nose-down control was tested to acquire data for aircraft recovery from high AOA flight conditions and maximum nose-down pitch rate performance studies. This configuration consisted of the pitch flaps and elevons being set to 30 deg. trailing edge down. In addition, the AMTs were also deflected downward and set to $\text{AMT} = 10/10$ and $30/30$ deg. because it could not be determined beforehand how effective they would be when interacting with the other control surfaces. Graphical presentation of the $\beta = 0$ deg. data are shown in Figures 16 - 19 and $\beta = 10$ deg. data are shown in Figures 20 - 23.

There was little difference in normal force between the $\text{AMT} = 10/10$ and $\text{AMT} = 30/30$ datasets. Both demonstrated significant CN increases over the neutral controls case up to $\alpha = 70$ deg. where the three then merge. The pitching moment data shows $\alpha = 30$ deg. to be the minimum nose-down control point with a value of -0.02 for both $\text{AMT} = 10/10$ and $30/30$ cases. Again, there was little difference in C_m between the two AMT cases except at $\alpha = 0$ & 5 deg. where the $\text{AMT} = 30/30$ case produced slightly more negative moment. The data suggested no additional pitching moment comes from the AMTs when increasing deflection from $10/10$ to $30/30$ deg. The small roll asymmetry identified in the neutral controls case was also seen in the AMT cases with differences appearing only around $\alpha = 30$ deg. No asymmetries were identified for the yawing moment case.

The full nose-down controls configuration at $\beta = 10$ deg. contained very similar normal force characteristics as the $\beta = 0$ deg. situation. For pitching moment, the minimum nose-down control point had moved to $\alpha = 20$ deg., increasing in value to -0.04 for both the $\text{AMT} = 10/10$ and $30/30$ deg. cases. Lateral stability was significantly increased for $\alpha < 15$ deg. from full nose-down control. For $\alpha > 15$ deg., there was little to no effect on lateral stability. There was also no effect of full nose-down control on roll and yawing moments in the sideslip condition ($\beta = 10$ deg.).

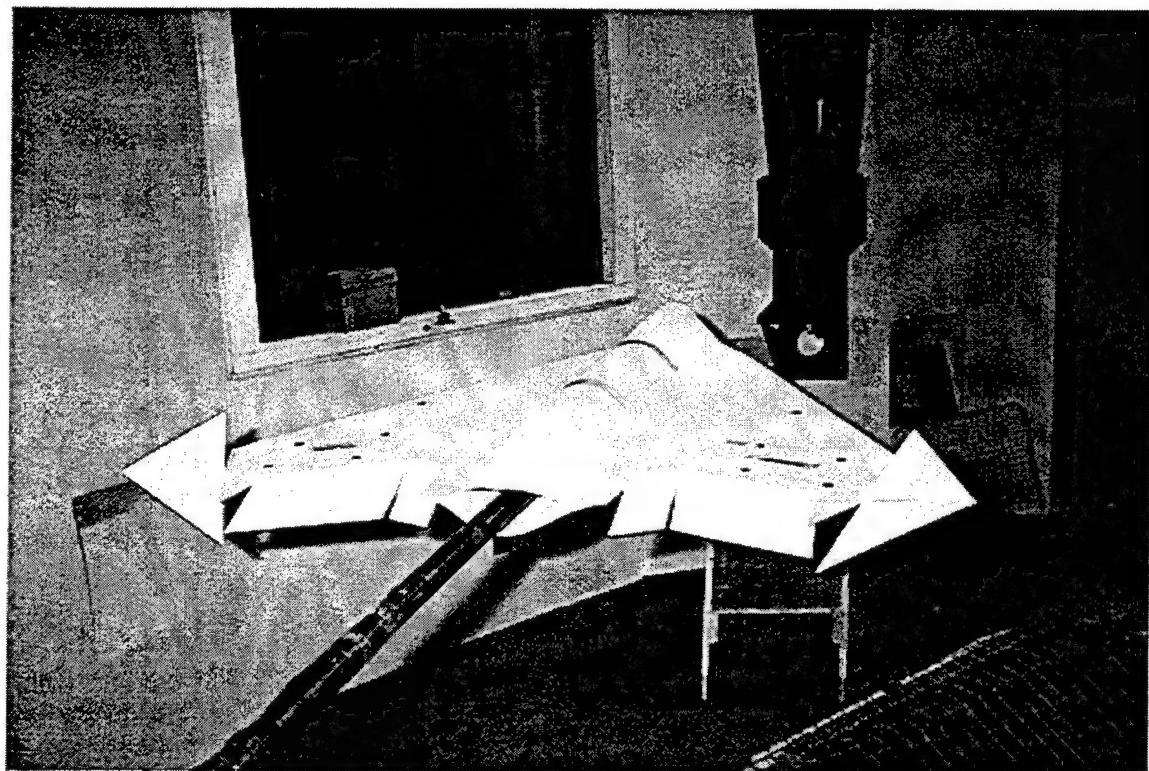
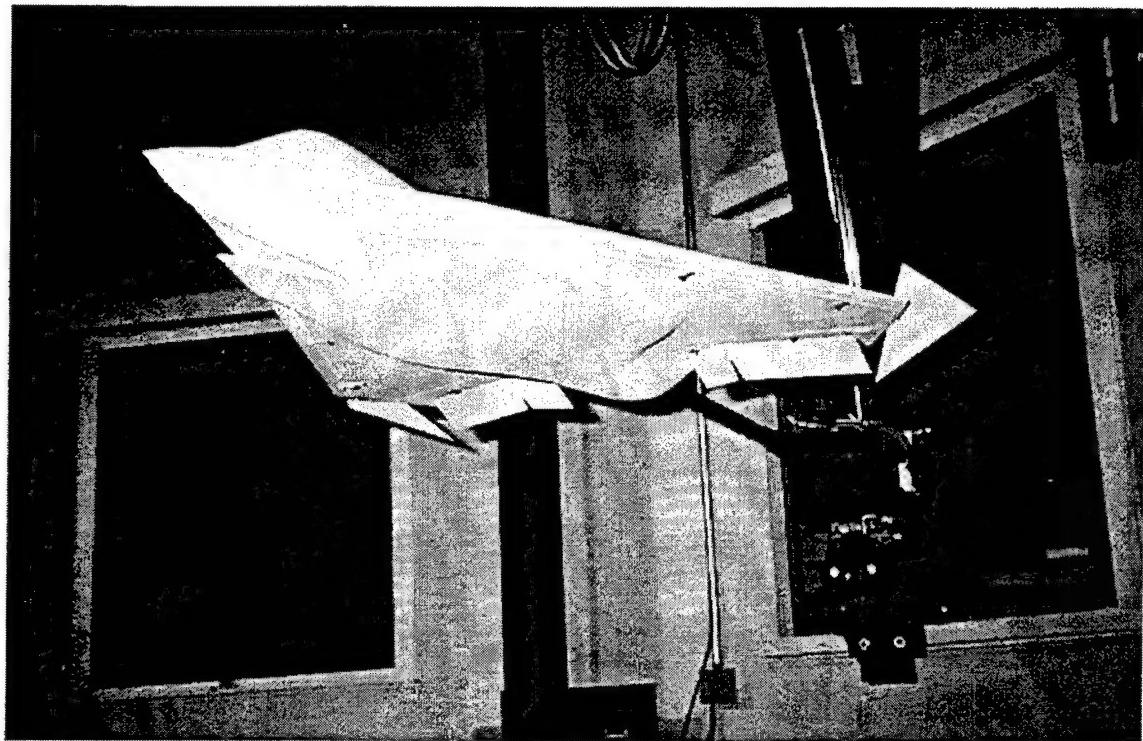


Figure 15 - Full Nose Down Control
AMT = 30 / 30, Elevon = 30 / 30, Pitch Flap = 30 / 30

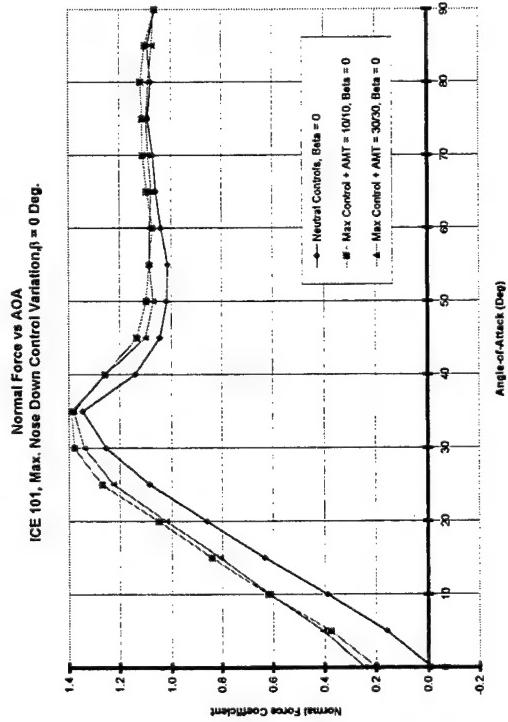


FIGURE 16

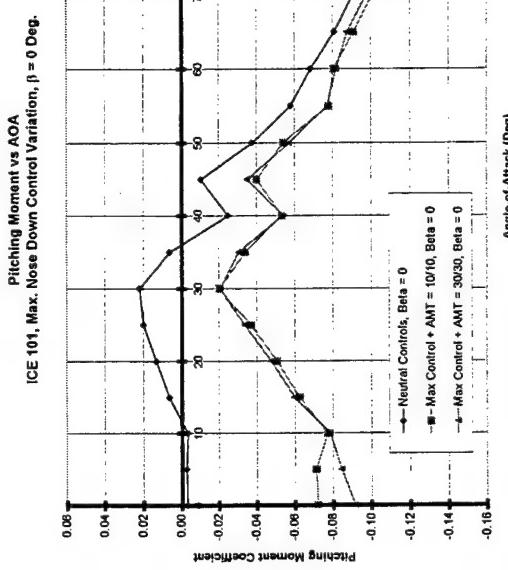


FIGURE 17

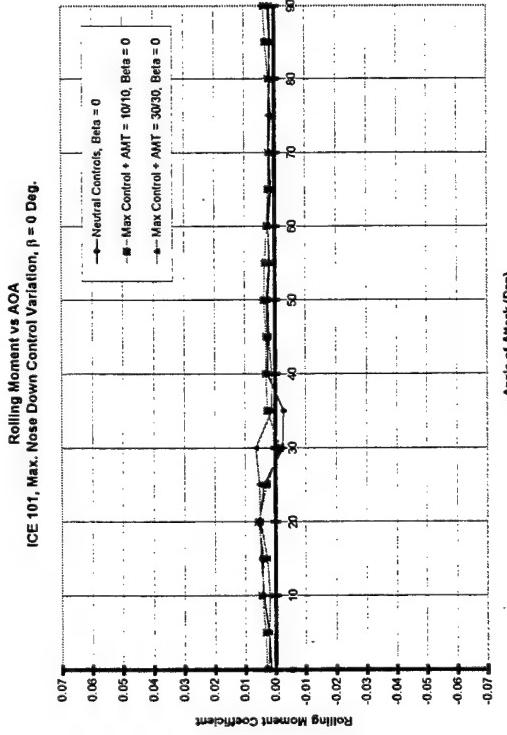


FIGURE 18

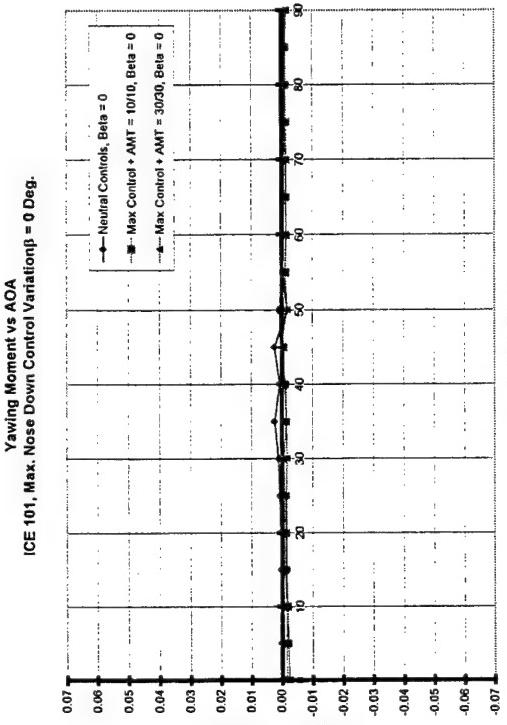


FIGURE 19

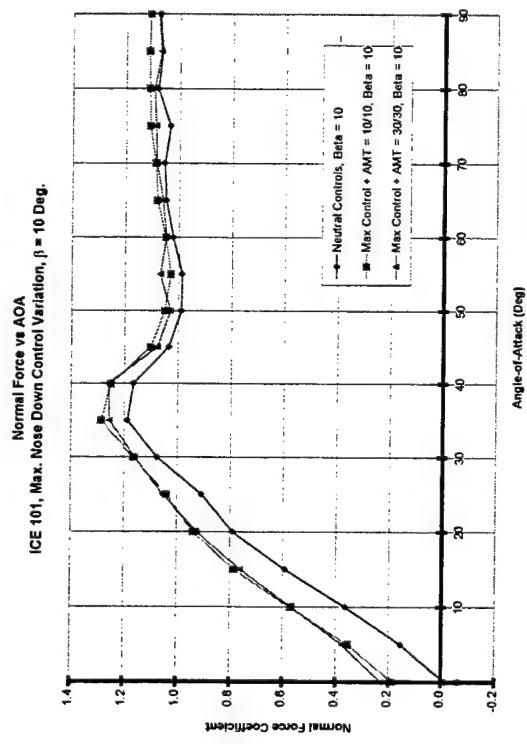


FIGURE 20

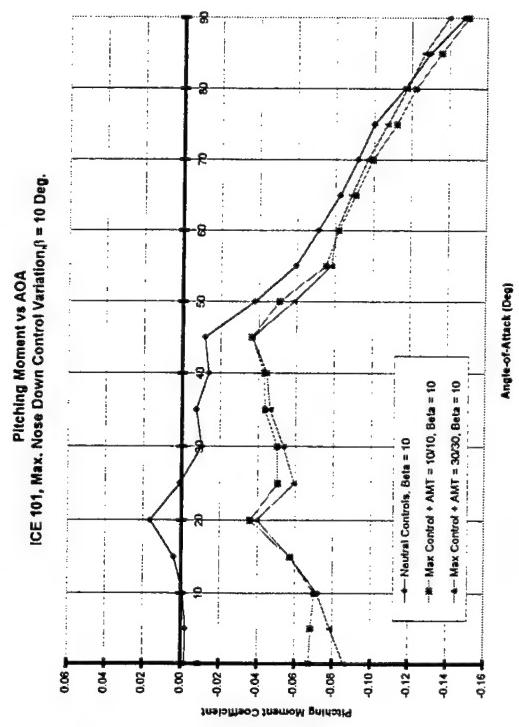
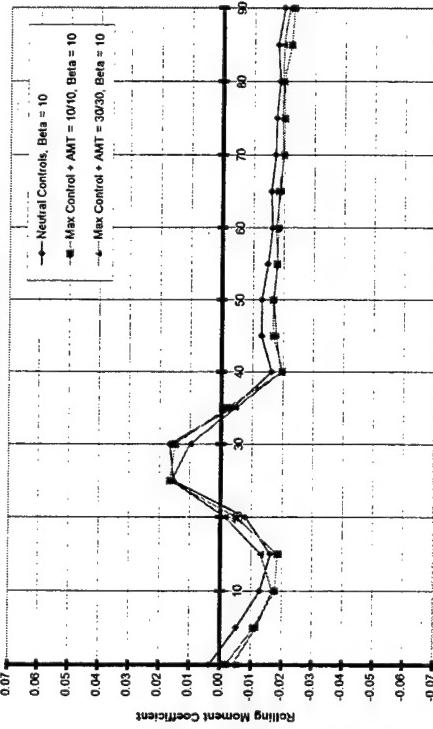


FIGURE 21



26

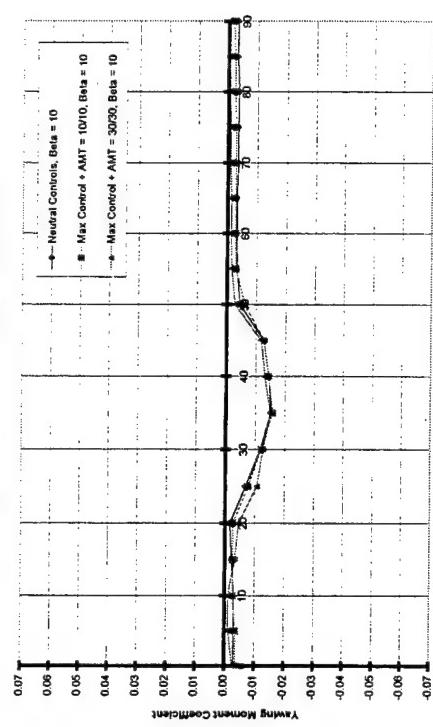


FIGURE 22

FIGURE 23

8. ROTARY BALANCE CHARACTERISTICS

8.1 Neutral Control

This vehicle configuration has all the control surfaces set to the zero deflection position. The testing established fundamental vehicle characteristics when subjected to steady, wind-axis rotation rate. The full set of data plots for this configuration can be found in Appendix A.

At $\beta = 0$ deg., no rotational effects on normal force (CN) were identified, up to $\alpha = 35$ deg. Above that, increasing rotation rate added a positive increment to CN, as much as 20 - 30 % for rates up to $\Omega b/2V = 0.3$. This effect was seen for both positive and negative rotation rates and angles-of-attack up to 90 deg. Nonzero sideslip did not change the rotational effects on CN except at low angles-of-attack. Below $\alpha = 15$ deg, positive β tended to increase CN with positive rate and decrease CN at negative rates. This effect became more notable as β increases in value. The normal force rotational data plots for $\alpha = 0, 10, 20, \& 40$ deg. are shown in Figures 24 – 27 to provide a representative sample of the data.

Rotational effects on pitching moment (Cm) were seen at $\beta = 0$ deg. showing a slight nose down moment with increasing rotation rate in either direction. This effect was small up to $\alpha = 55$ deg. where it then became more pronounced. The magnitude of this effect reached $\Delta C_m = -0.04$ for rates up to $\Omega b/2V = +/- 0.3$. Increasing sideslip angle produced a significant change in the rotational effects on Cm. Positive sideslip provides more nose down moment with positive rotation and more nose up moment with negative rotation. At high angles-of-attack ($\alpha > 45$), sideslip had little impact on positive rotation effects on pitching moment but inserted more nose up pitch moment during negative rotation that persisted through $\alpha = 90$ deg. The pitching moment rotational data plots for $\alpha = 0, 10, 20, \& 40$ deg. are shown in Figures 28 – 31 to provide a representative sample of the data.

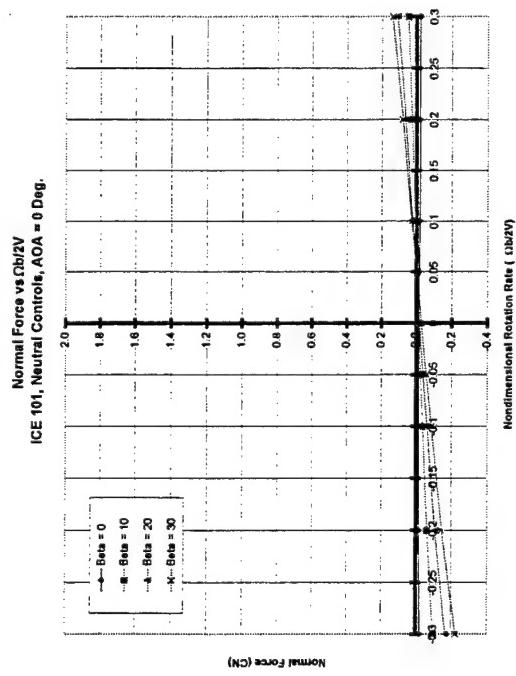


FIGURE 24

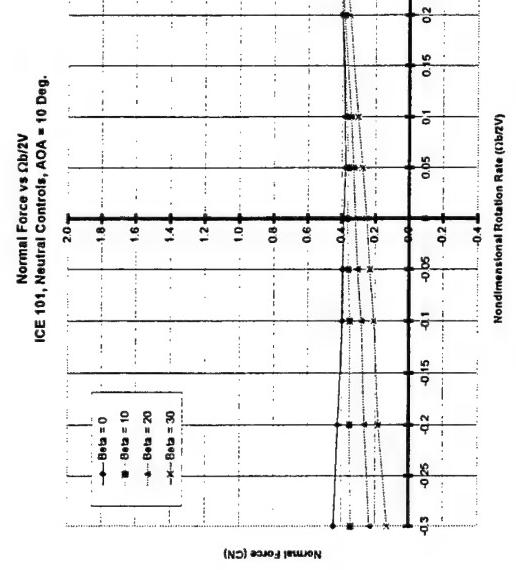


FIGURE 25

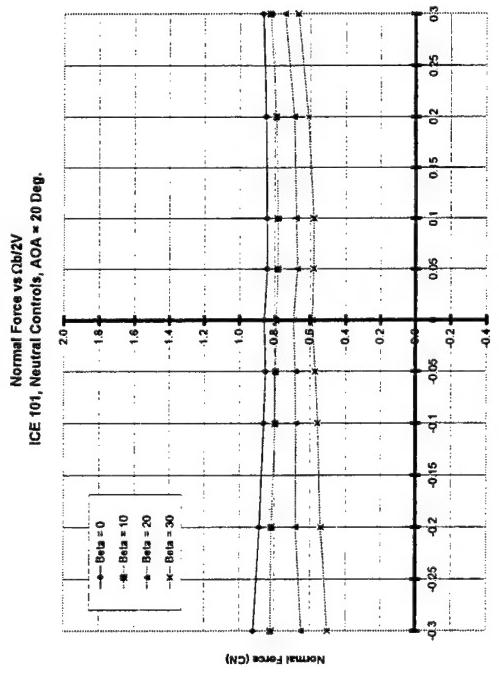


FIGURE 26

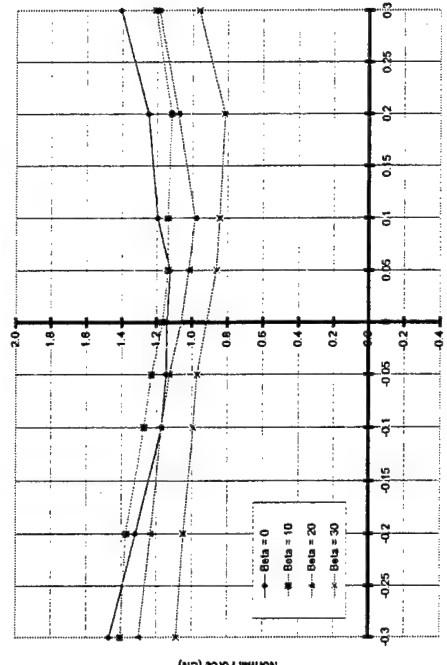


FIGURE 27

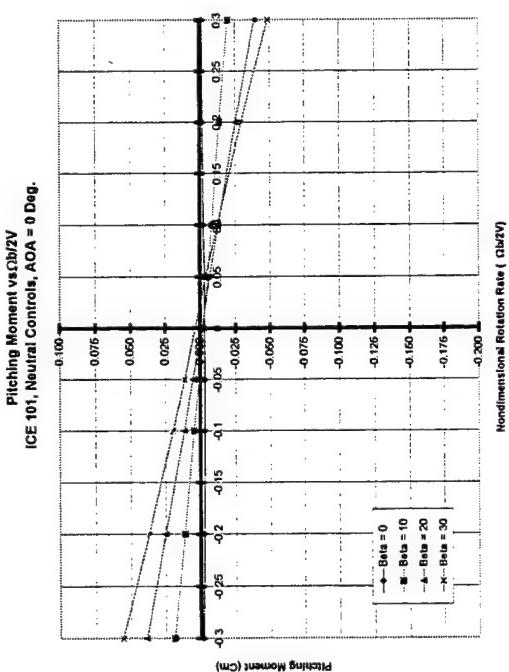


FIGURE 28

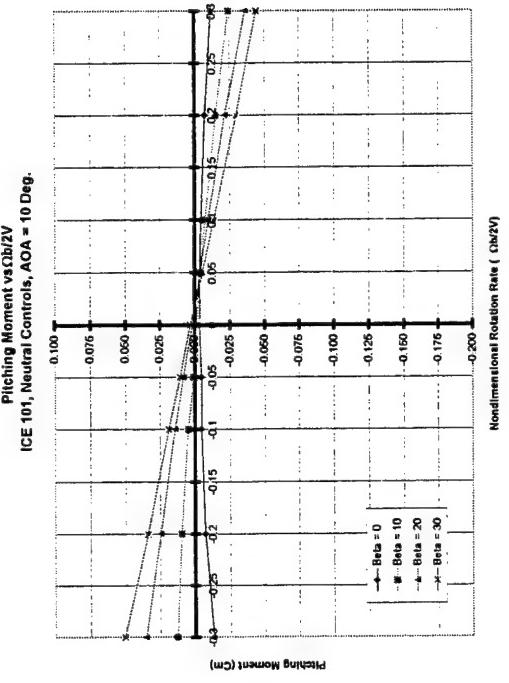


FIGURE 29

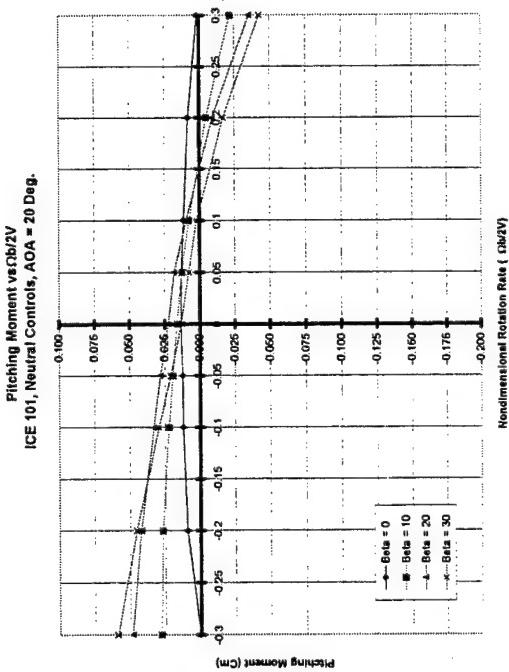


FIGURE 30

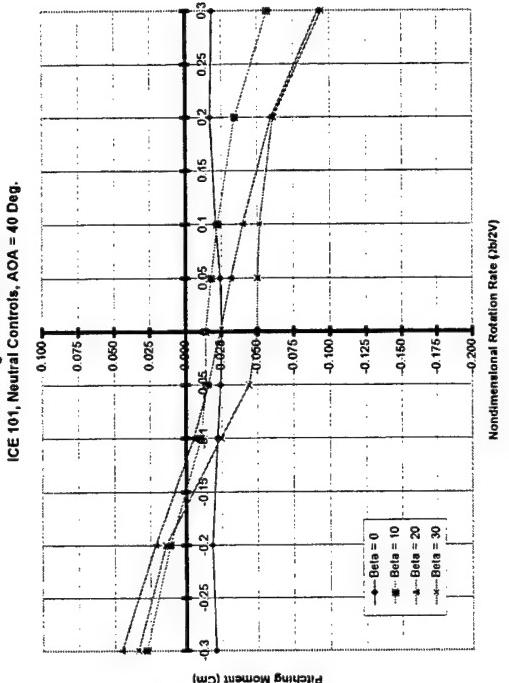


FIGURE 31

Wind axis rotational effects on body axis rolling moment ($C_{l\beta}$) were seen, at $\beta = 0$ deg. showing the vehicle is well damped in roll up to $\alpha = 35$ deg and then lightly damped up to $\alpha = 70$ deg. Above $\alpha = 70$ deg., rotation actually added a small propelling roll moment which increased in value as AOA approaches 90 deg. Nonzero sideslip had little influence on the rotational effects on rolling moment at low angles-of-attack ($\alpha < 20$). At higher AOA's, sideslip reduced roll damping to near neutral. Around $\alpha = 35$ deg, positive β showed no rolling moment effect with positive rotation rates but significant propelling roll moments at negative rotation rates. By $\alpha = 70$ deg., the strong propelling roll moment at negative rate dissipated and above $\alpha = 70$ deg., sideslip no longer influenced the rotational characteristics. The rolling moment rotational data plots for $\alpha = 0, 10, 20, \& 40$ deg. are shown in Figures 32 – 35 to provide a representative sample of the data.

The vehicle was neutrally damped for body axis yawing moment (C_{ln}) up to $\alpha = 30$ deg. when under the influence of wind axis rotation. At $\alpha = 35$ deg., low rate rotation in either direction produces a very nonlinear, propelling yawing moment. This effect then disappeared by $\alpha = 40$ deg. and above where the vehicle maintained a small amount of yaw damping. Adding positive sideslip provided little impact on rotational increments to yawing moment at low angles-of-attack ($\alpha < 20$ deg.). At higher angles-of-attack, increasing sideslip reduced yaw damping to the point of being neutrally damped. The yawing moment rotational data plots for $\alpha = 0, 10, 20, \& 40$ deg. are shown in Figures 36 – 39 to provide a representative sample of the data.

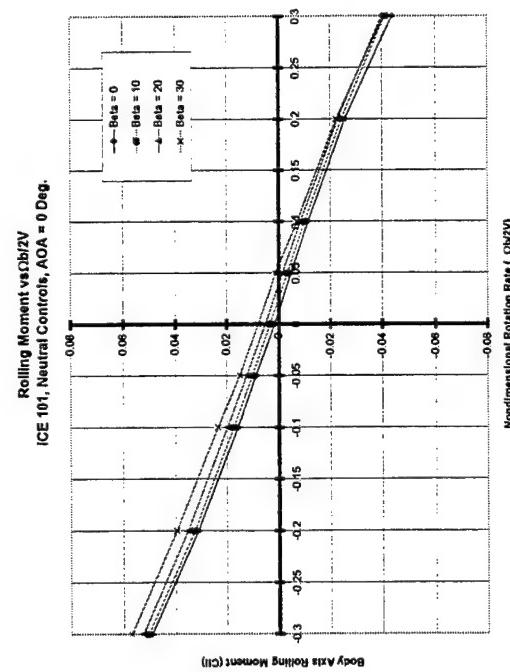


FIGURE 32

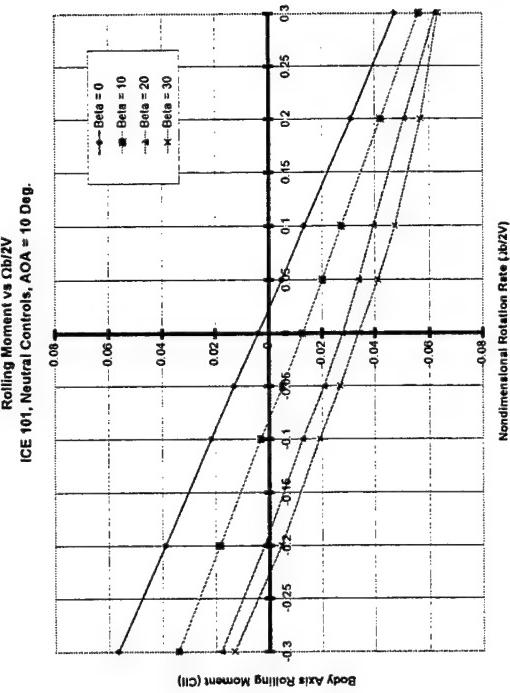


FIGURE 33

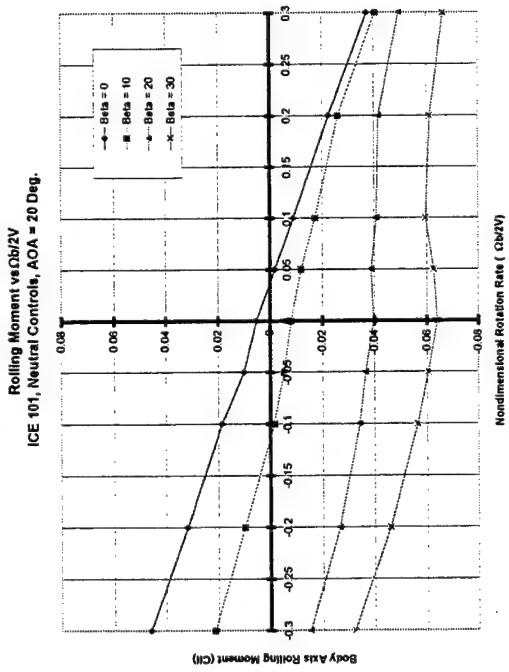


FIGURE 34

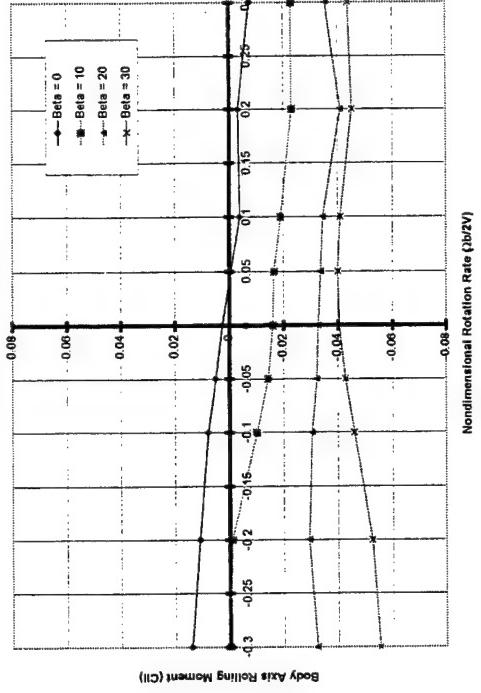


FIGURE 35

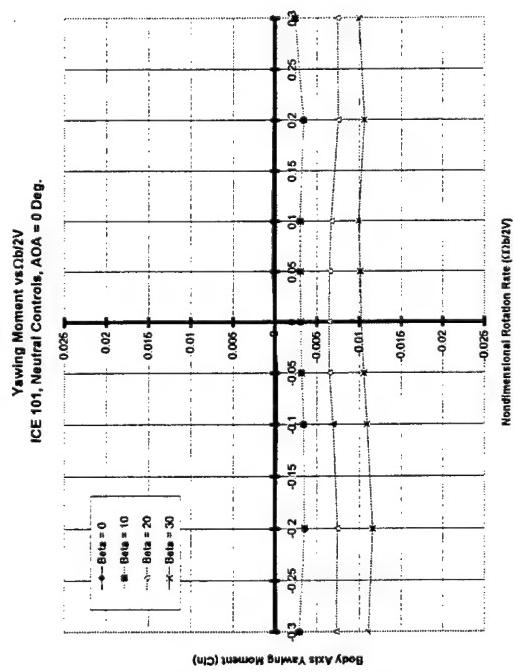


FIGURE 36

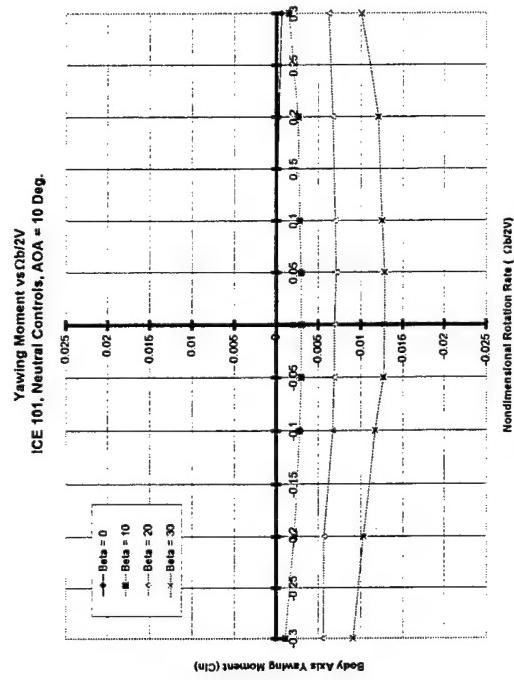


FIGURE 37

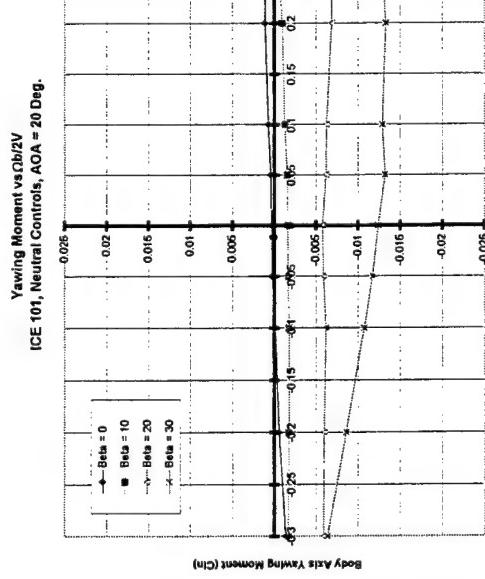


FIGURE 38

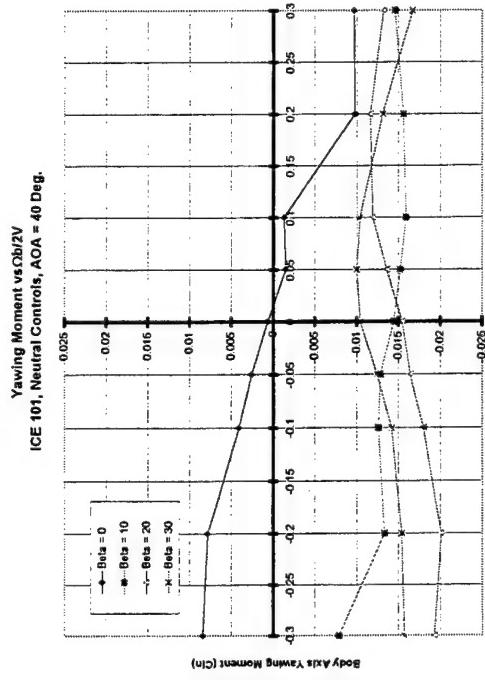


FIGURE 39

8.2 LEF = 30/30 Characteristics

For this vehicle configuration, all of the control surfaces were set to the zero deflection position except the leading edge flaps which were both set to 30 deg. (leading edge down). This testing established the effect of deflecting the leading edge flaps has on vehicle characteristics as a function of wind axis rotation rate. Photographs of the vehicle with the LEF = 30 / 30 deg. deflections are presented in Figure 40. The full set of data plots for this configuration can be found in Appendix B.

There were no rotational effects on normal force with LEF = 30/30 deg., at $\beta = 0$ deg., up to $\alpha = 35$ deg. Above $\alpha = 35$ deg., increasing rotation rate added a positive increment to CN, as much as 20 - 30 % for rates up to $\Omega b/2V = 0.3$. This effect was seen for both positive and negative rotation rates and angles-of-attack up to 90 deg. Nonzero sideslip did not change the rotational effects on CN except at low angles-of-attack. Below $\alpha = 15$ deg, positive β tended to increase CN at positive rates and decreases CN at negative rates. This effect became more notable as β increases in value. All these observations are the same as the neutral control case. This suggests that there was no change in normal force rotational characteristics with deflection of the leading edge flaps. The normal force rotational data plots for $\alpha = 0, 10, 20, \& 40$ deg. are shown in Figures 41 – 44 to provide a representative sample of the data.

There were no rotational effects on pitching moment with LEF = 30/30 deg., for $\beta = 0$ deg. up to $\alpha = 10$ deg. Above $\alpha = 10$ deg., a nose-down moment was developed for increasing rotation rate in either direction and becomes more pronounced as angle-of-attack increases. The magnitude of this effect reached $\Delta C_m = -0.03$ at AOA = 65 deg. for rates out to $\Omega b/2V = +/- 0.3$. Nonzero sideslip produced a significant change in the rotational effects on pitching moment. Positive sideslip provided more nose-down pitching moment with positive rotation and more nose-up pitching moment with negative rotation. At high angles-of-attack ($\alpha > 45$), sideslip had little impact on positive rotation effects on pitching moment but it did insert more nose-up pitching moment during negative rotation that persists through $\alpha = 90$ deg. These observations are very similar to the neutral control

case. Therefore, there was little to no effect on the pitching moment rotational characteristics with deflection of the leading edge flaps. The pitching moment rotational data plots for $\alpha = 0, 10, 20, \& 40$ deg. are shown in Figures 45 – 48 to provide a representative sample of the data.

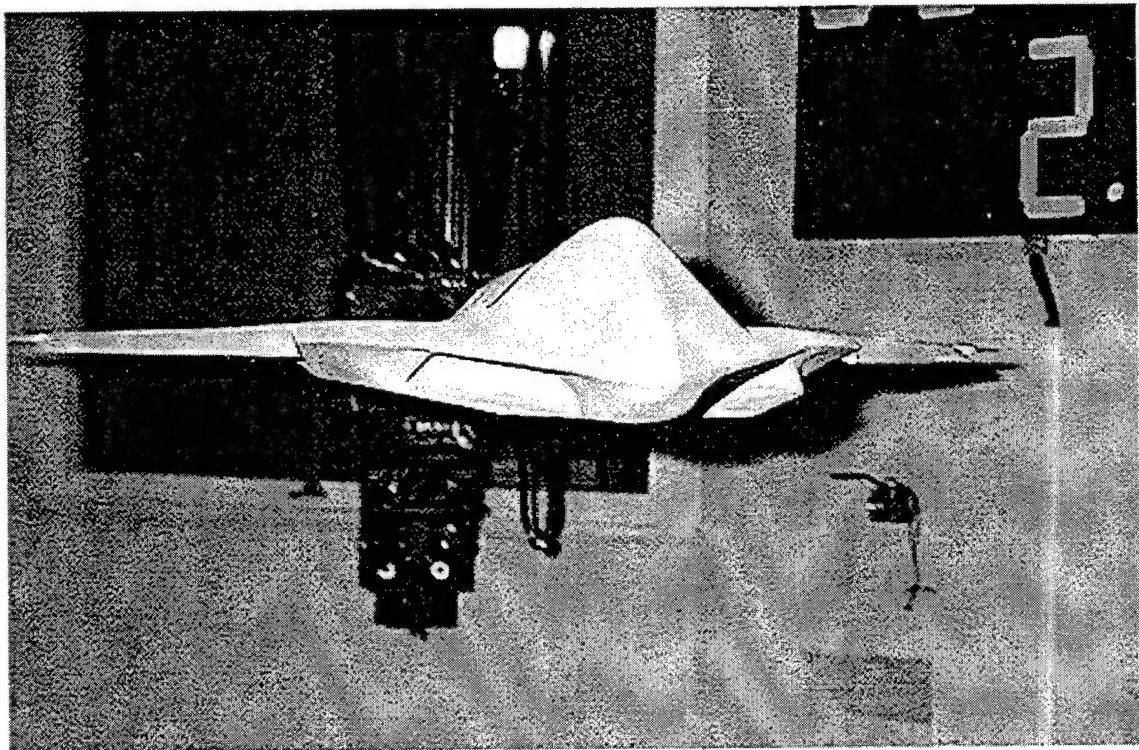
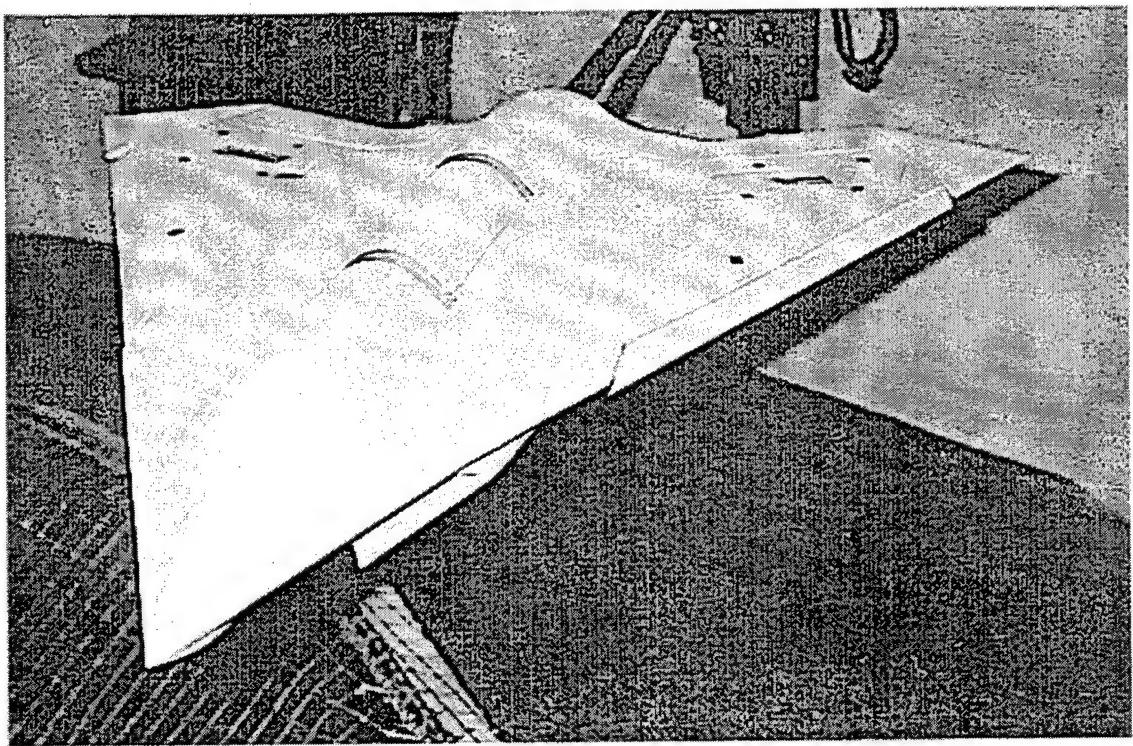


Figure 40 - LEF = 30 / 30 Configuration

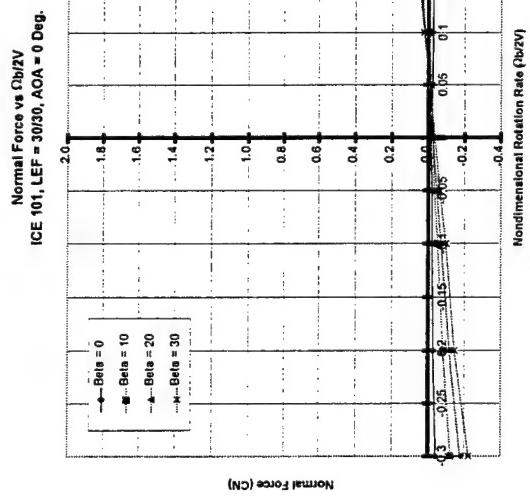


FIGURE 41

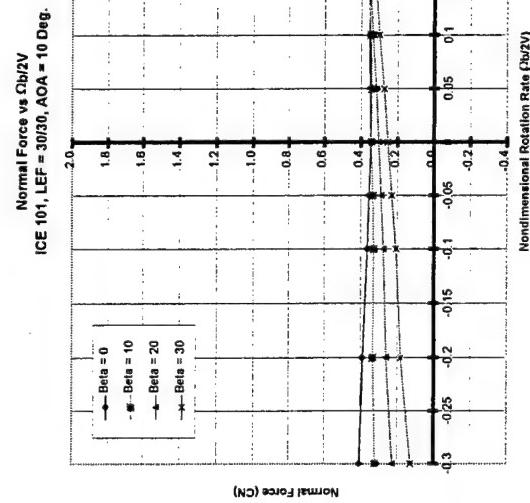


FIGURE 42

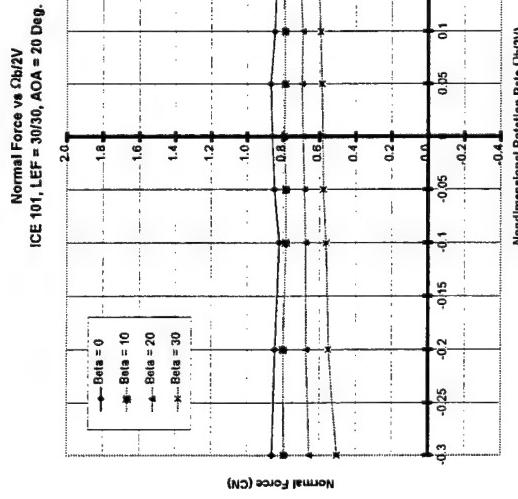


FIGURE 43

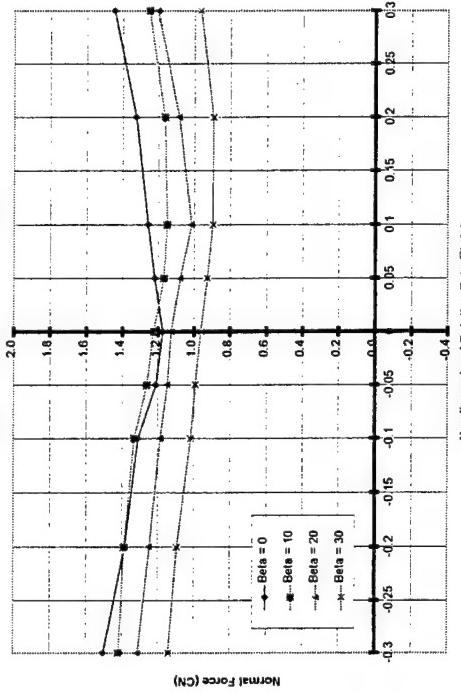


FIGURE 44

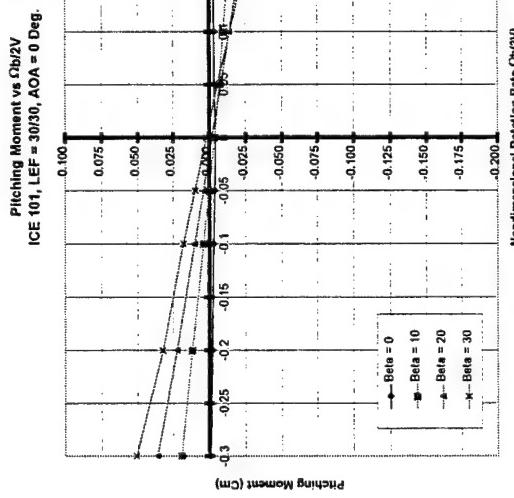


FIGURE 45

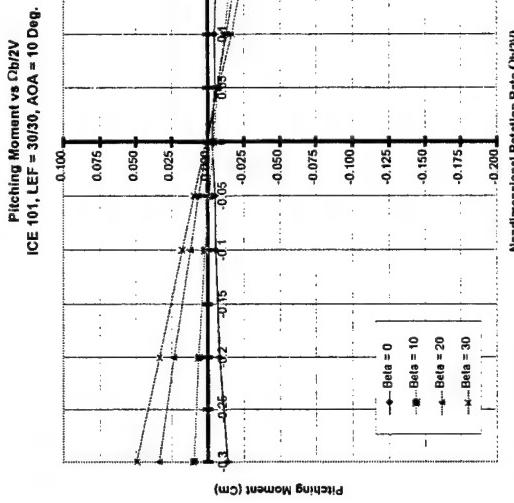


FIGURE 46

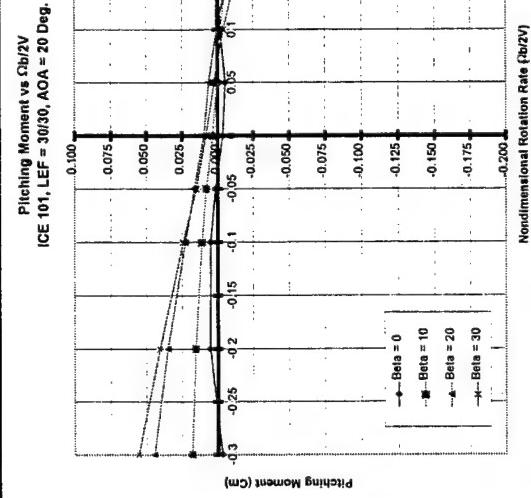


FIGURE 47

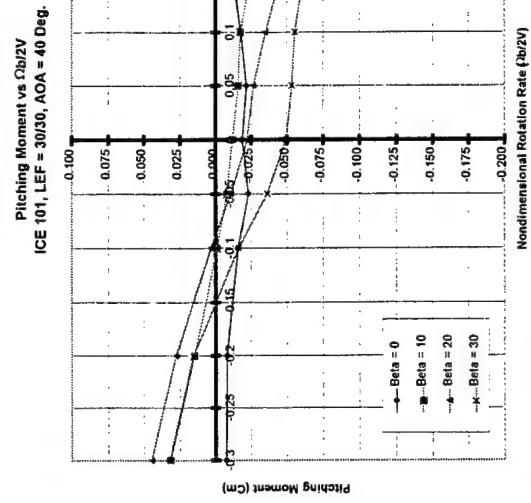


FIGURE 48

With wind axis rotation, body axis rolling moment for LEF = 30/30 deg., β = 0 deg., showed the vehicle to be well damped in roll up to α = 35 deg. In the α = 40 - 70 deg. region, most of its damping was lost becoming neutrally damped around α = 70 deg. Above α = 70 deg., rotation added a small propelling roll moment which increases in value as AOA approached 90 deg. Nonzero sideslip had little impact on rotational effects to rolling moment for low angles-of-attack ($\alpha < 20$). At higher AOA's, sideslip reduced roll damping to near neutral. At α = 35 deg., positive sideslip showed no rolling moment effect at positive rotation rates but significant propelling roll moments at negative rotation rates. At around α = 70 deg., the strong propelling roll moment at negative rate dissipated and above α = 70 deg., sideslip no longer influenced rotational effects on rolling moment. The rolling moment observations mentioned above are very similar to the neutral control case. Therefore, there was little to no effect on the rolling moment rotational characteristics with deflection of the leading edge flaps. The rolling moment rotational data plots for α = 0, 10, 20, & 40 deg. are shown in Figures 49 – 52 to provide a representative sample of the data.

With wind axis rotation, body axis yawing moment for LEF = 30/30 deg., β = 0 deg., showed the vehicle to be slightly damped in yaw up to α = 15 deg. At that point, low rate rotation in either direction produced a very small, propelling yaw moment. At α = 35 deg., a large, nonlinear, propelling yaw moment was seen at low rotation rates. By α = 40 deg., this effect disappeared and at higher angles-of-attack, the vehicle maintained a small amount of yaw damping. Adding positive sideslip provided little impact on rotational increments to yawing moment at low angles-of-attack ($\alpha < 20$ deg.). At moderate AOAs ($20 < \alpha < 30$ deg.), negative rotation provided some yaw damping with increasing positive β while positive rotation provides little, if any, damping with increasing β . For $\alpha > 65$ deg., increasing sideslip had no impact on rotational effects on yawing moment. These observations are very similar to the neutral control case. Therefore, deflection of the leading edge flaps had a small, stabilizing influence on yawing moment rotational characteristics for $\alpha < 15$ deg and no influence for $\alpha > 15$ deg. The yawing moment rotational data plots for α = 0, 10, 20, & 40 deg. are shown in Figures 53 – 56 to provide a representative sample of the data.

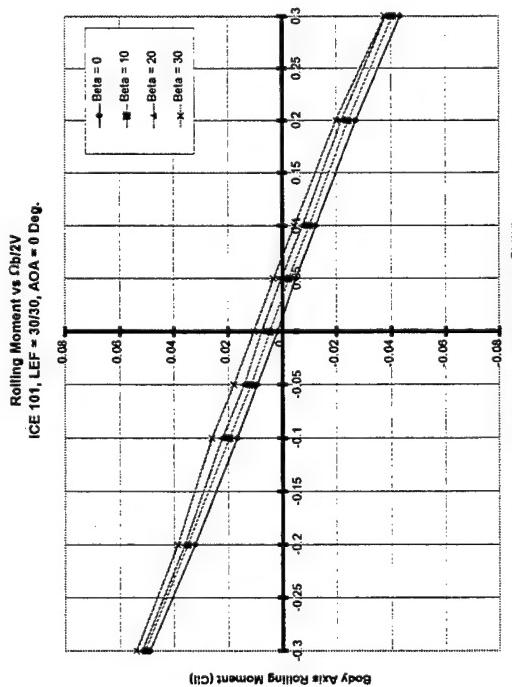


FIGURE 49

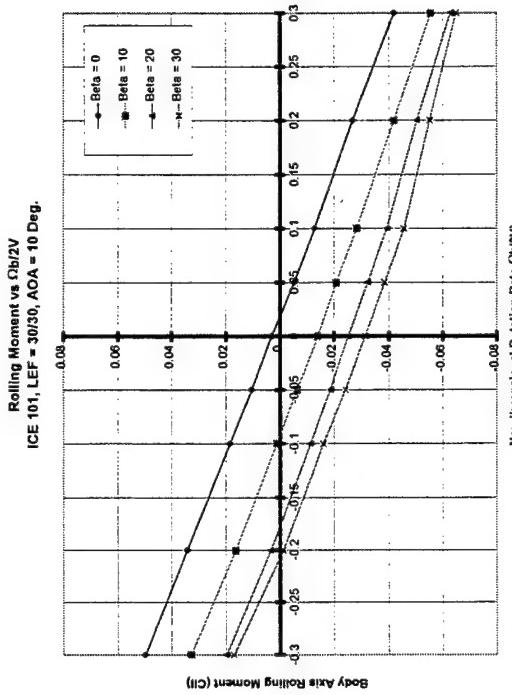


FIGURE 50

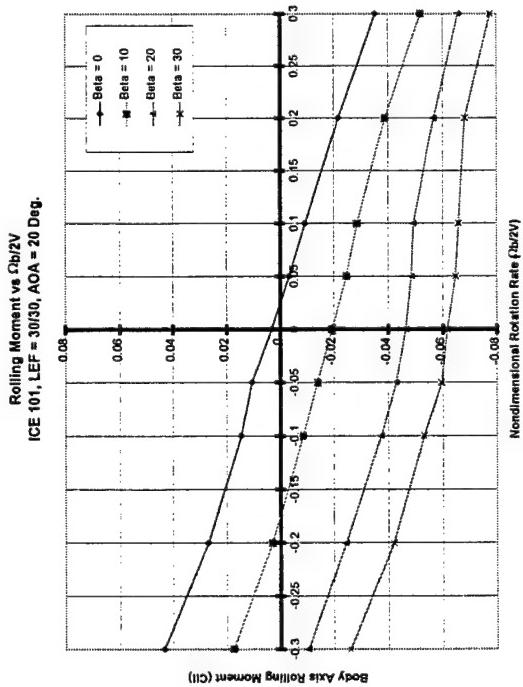


FIGURE 51

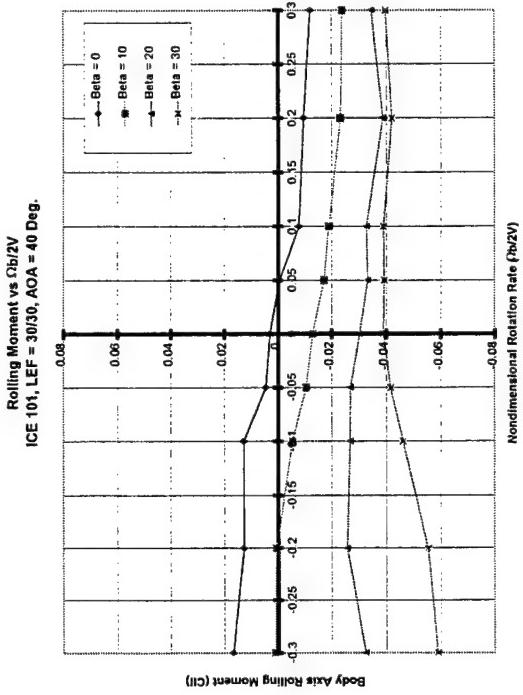


FIGURE 52

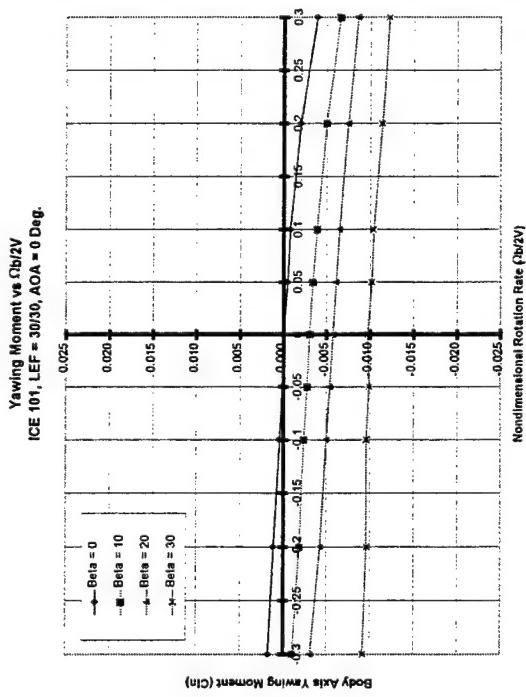


FIGURE 53

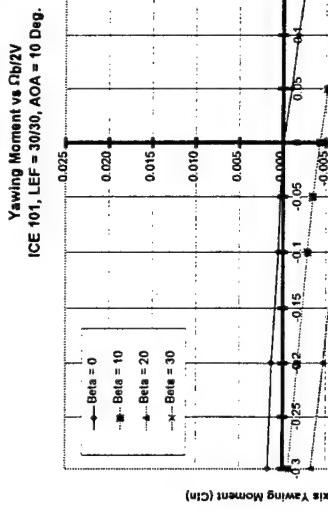


FIGURE 54

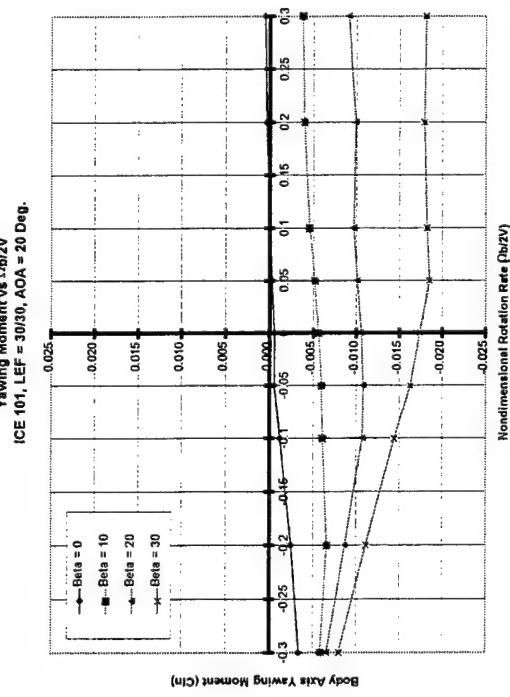


FIGURE 55

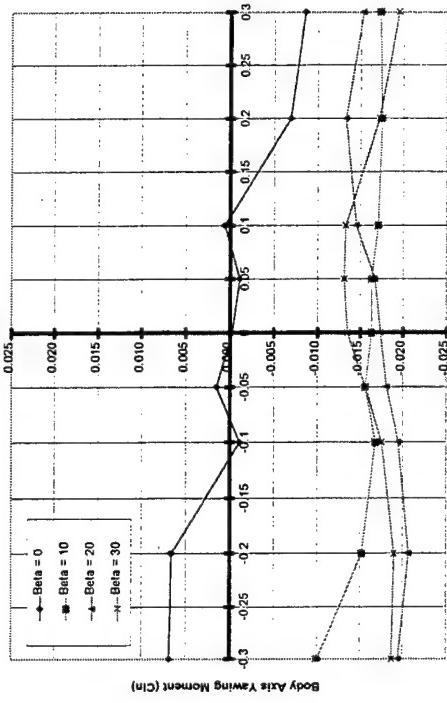


FIGURE 56

8.3 AMT = 0/60 - Control Power Increments

The All Moving Wing Tip (AMT) is a control effector concept that was investigated during the Innovative Control Effector program.^{1,2} During static wind tunnel testing, it showed considerable promise for providing yaw moment control for tailless aircraft. Hence, the impact of wind axis rotation on the effectiveness of the AMT warranted investigation. The right AMT, deflected to 60 deg. (trailing edge down), was tested by AFRL and is shown in Figure 57. Incremental data was developed by subtracting the AMT = 0/60 data from the neutral control data. The full set of data plots for this configuration can be found in Appendix C.

Small rotational effects on AMT-generated normal force were seen for $\beta = 0$ deg. Negative wind axis rotation slightly increased the ΔCN due to a right AMT deflection, whereas positive rotation slightly reduced ΔCN , for low angles-of-attack ($0 < \alpha < 15$ deg.). Above $\alpha = 15$ deg., there were nonlinearities with rotation rate, but small in magnitude, so the overall effect was small with respect to rotation on normal force due to the AMT deflection. Adding positive sideslip tended to have little impact whereas adding negative sideslip tended to add a small positive ΔCN to the right AMT deflection. The normal force rotational data plots for $\alpha = 0, 10, 20, \& 40$ deg. are shown in Figures 58 – 61 to provide a representative sample of the data.

Rotational effects on AMT-generated pitching moment were seen for $\beta = 0$ deg. Negative rotation produced more nose-down moment due to a right AMT deflection, whereas positive rotation provided the opposite, more nose-up moment, at low angles-of-attack ($0 < \alpha < 20$ deg.). Above $\alpha = 20$ deg., there was little impact due to rotation on AMT pitch effectiveness. Again, there were nonlinearities with rotation rate, but they were small in magnitude. Adding positive sideslip tended to produce more nose-down moment from a right AMT deflection. Aligning the vehicle with negative sideslip added a small, positive ΔCm due to the right AMT deflection for negative rotation and a small, negative ΔCm for positive rotation. The pitching moment rotational data plots for $\alpha = 0, 10, 20, \& 40$ deg. are shown in Figures 62 – 65 to provide a representative sample of the data.

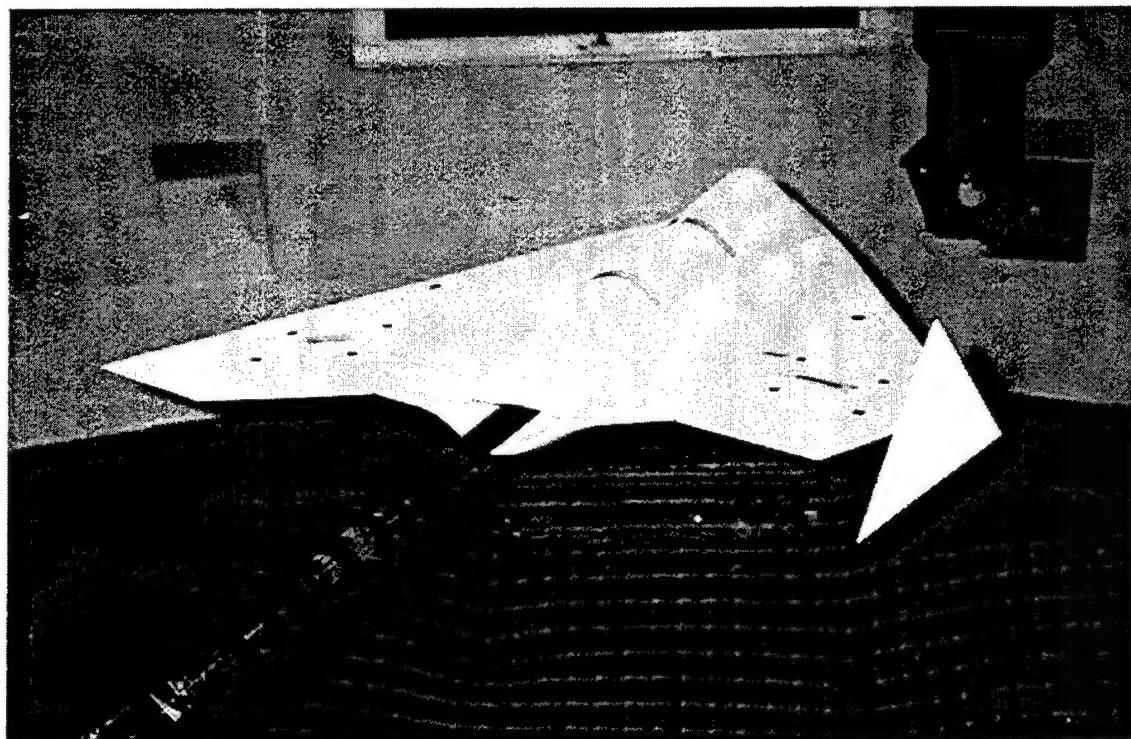
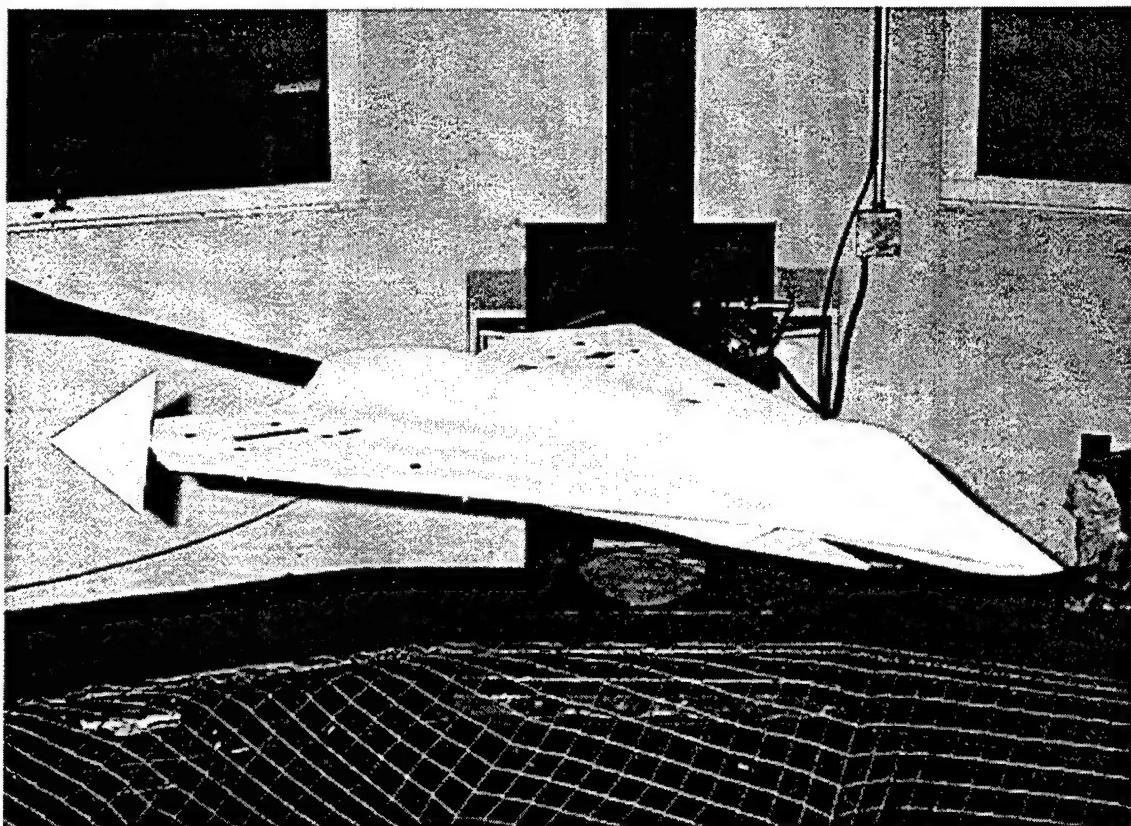


Figure 57 - Right All Moving Tip (AMT) Deflection = +60 Deg.

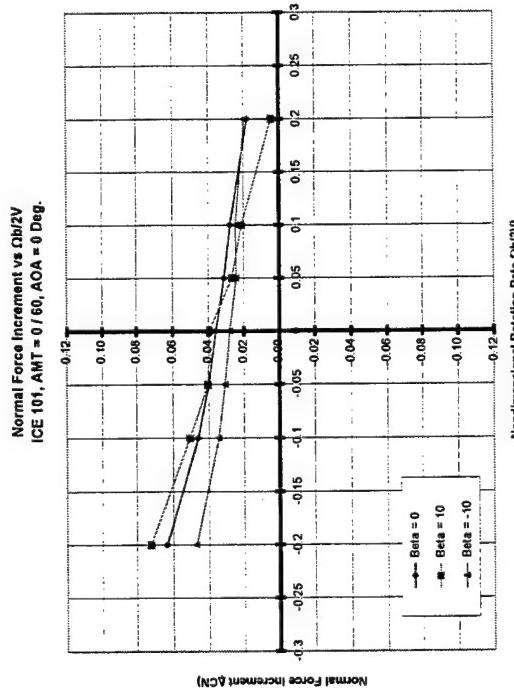


FIGURE 58

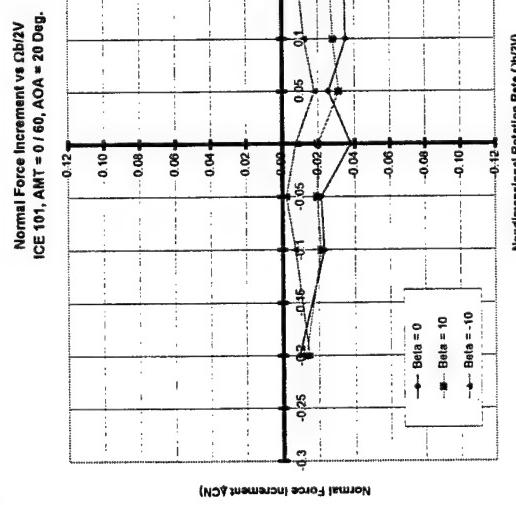


FIGURE 59

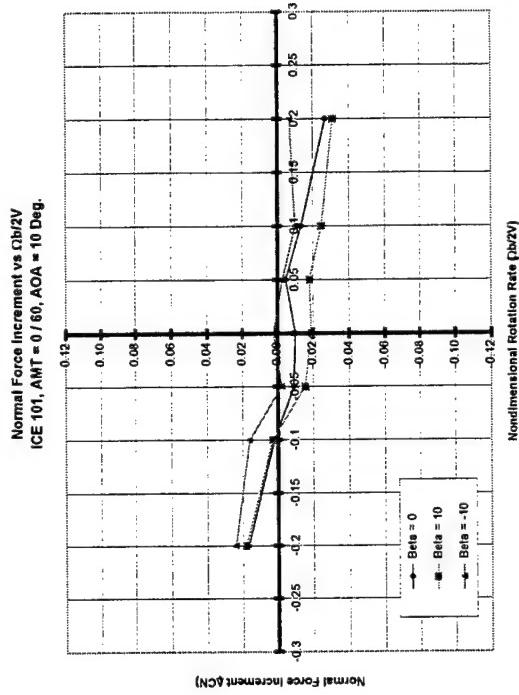


FIGURE 60

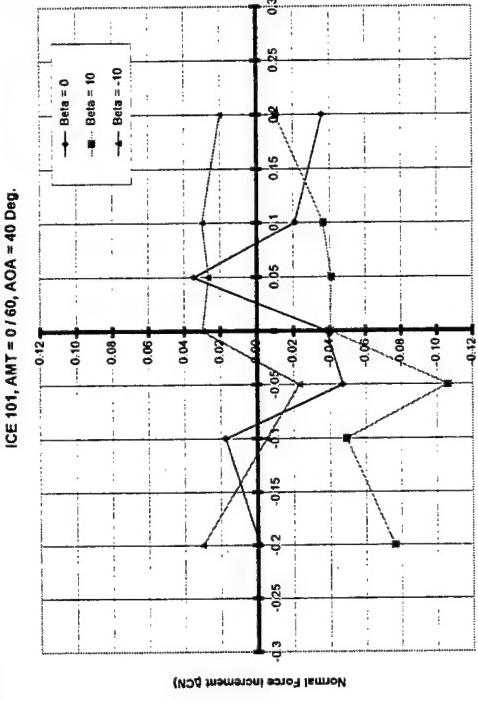


FIGURE 61

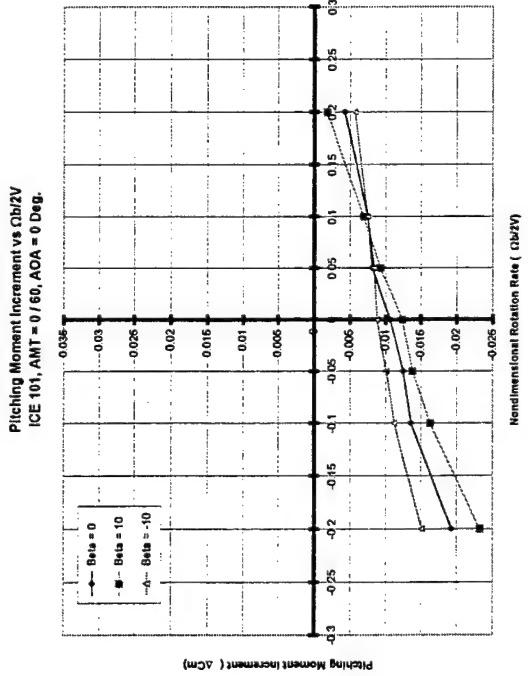


FIGURE 62

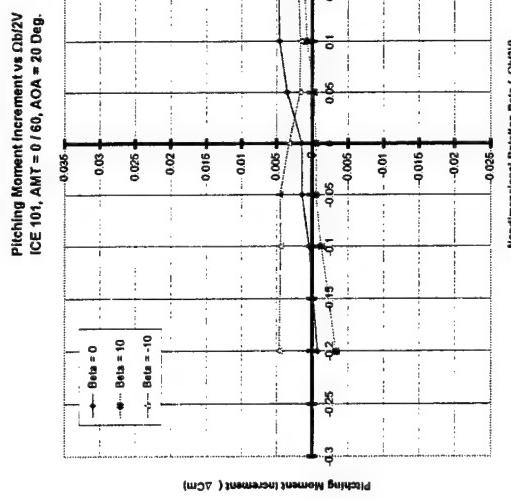


FIGURE 64

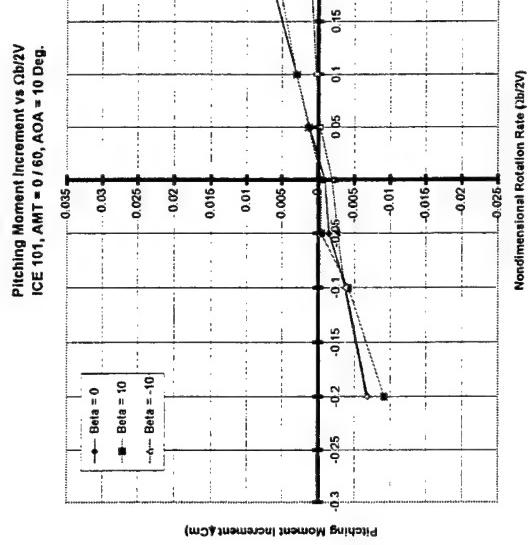


FIGURE 63

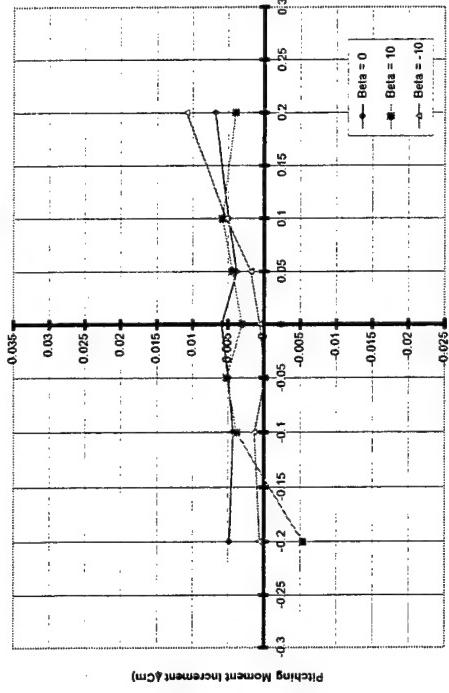


FIGURE 65

Rotational effects on AMT-generated rolling moment were observed for $\beta = 0$ deg. which indicated an increase in rolling moment when the AMT was deflected on the advancing wing and lost some rolling moment when the AMT is deflected on the retreating wing. This effect continued to $\alpha = 30$ deg. where AMT roll control power became invariant with rotation rate; this result continued to $\alpha = 90$ deg. In the $0 < \alpha < 20$ deg. region, positive sideslip produced more negative rolling moment with the right AMT deflected on the advancing wing and a less negative rolling moment when the right AMT is deflected on the retreating wing. The effects on rolling moment were predictably the opposite for negative sideslip. In the $20 < \alpha < 40$ deg range, positive sideslip with a right AMT deflection provided negative rolling moment for rotation in either direction. Negative sideslip produced more positive rolling moment with the AMT deflected on the advancing wing and no impact with the AMT deflected on the retreating wing. Above $\alpha = 40$ deg., sideslip had little to no impact on AMT roll control power effectiveness. The rolling moment rotational data plots for $\alpha = 0, 10, 20, \& 40$ deg. are shown in Figures 66 – 69 to provide a representative sample of the data.

AMT-generated yawing moment, under the influence of wind axis rotation, for $\beta = 0$ deg. indicates no variation in ΔC_{ln} due to AMT with rotation rate up to $\alpha = 30$ deg. There was some random variation in the $35 < \alpha < 50$ deg. range. Above $\alpha = 50$ deg., more yawing moment was developed from the AMT when it was deflected on the advancing wing (right AMT with negative rotation) than when the AMT was deflected on the receding wing. This characteristic demonstrated that the AMT is an effective control device for stabilizing a tailless vehicle during a developed spin condition. Windward sideslip (positive β in this case) did not change AMT rotational effects for the entire AOA range. The magnitude of the yawing moment control power did not change with windward sideslip in the $0 < \alpha < 25$ deg. range but then did add extra yawing moment control power at higher angles-of-attack. Leeward sideslip (negative β in this case) reduced yawing moment control power somewhat but did not significantly effect rotational characteristics. The yawing moment rotational data plots for $\alpha = 0, 10, 20, \& 40$ deg. are shown in Figures 70 – 73 to provide a representative sample of the data.

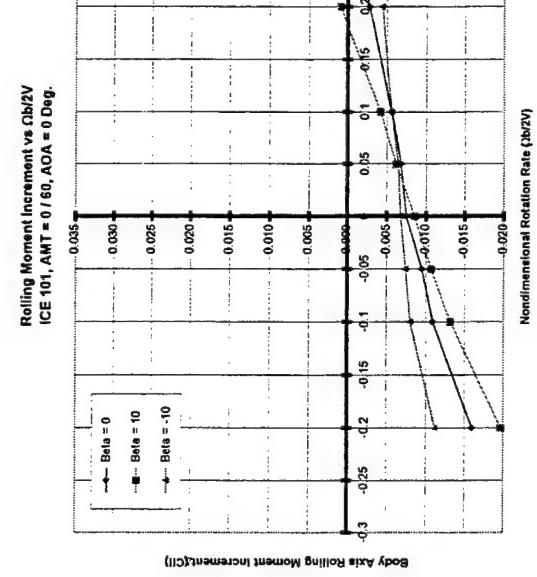


FIGURE 66

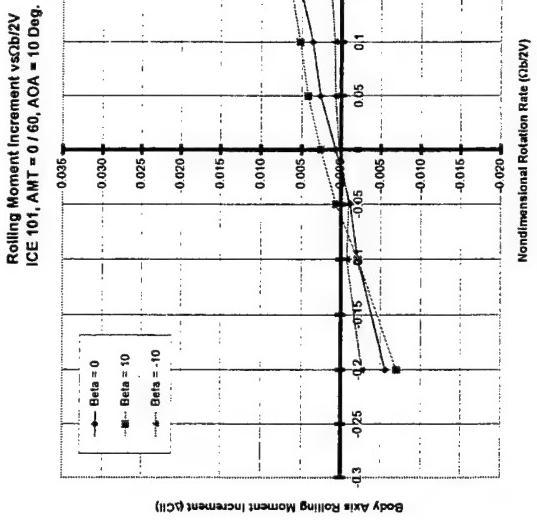
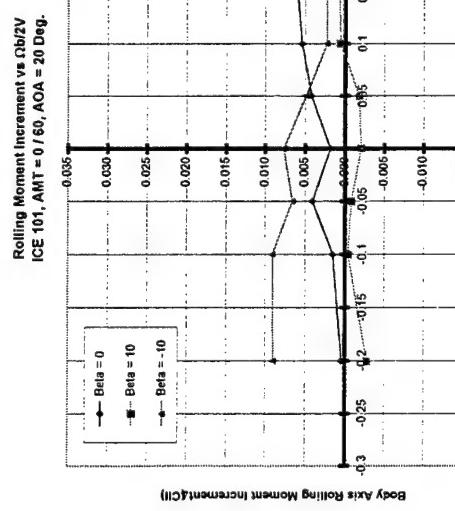


FIGURE 67



46



FIGURE 69



FIGURE 68



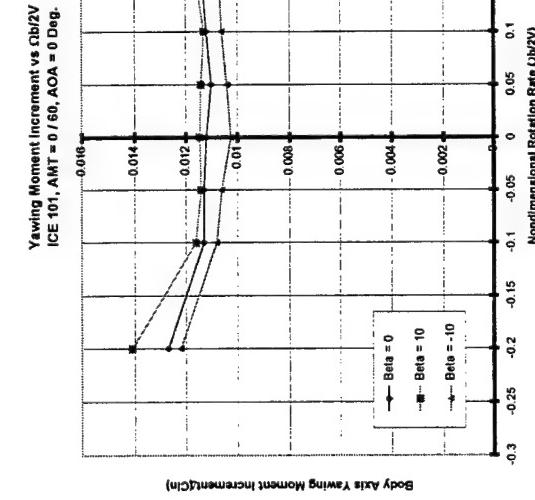


FIGURE 70

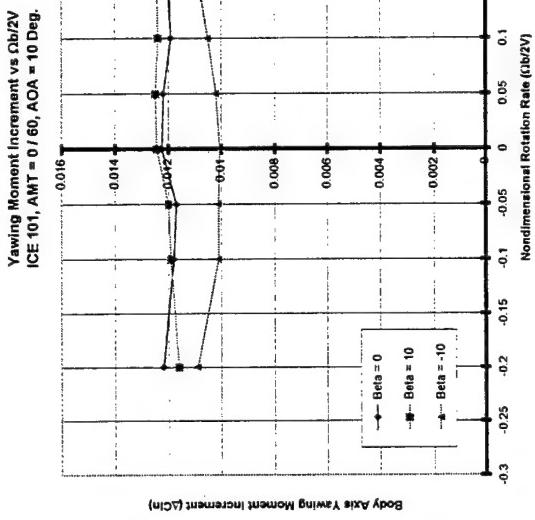


FIGURE 71

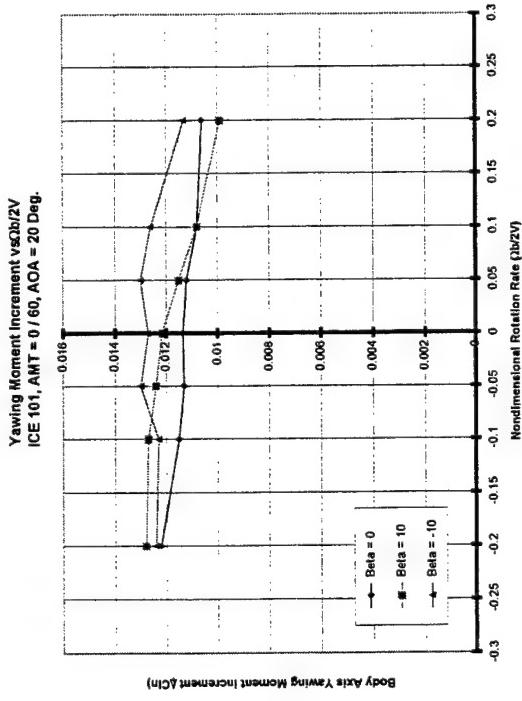


FIGURE 72

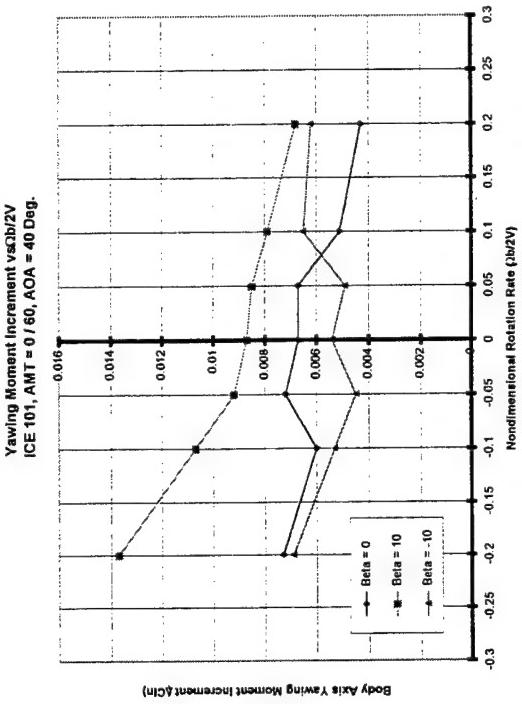


FIGURE 73

9. FORCED OSCILLATION CHARACTERISTICS

Forced oscillation tests were performed to acquire body axis force & moment data while the vehicle is being oscillated about one of the body axes (pitch, roll, or yaw). The test results indicated the data was a nonlinear function of rate in some angle-of-attack regions so linear dynamic stability derivatives would not work for full flight envelope aerodynamic math modeling. The data was therefore plotted as the force or moment coefficient due to rate versus nondimensional rate. All data were acquired at $\beta = 0$ deg. so no sideslip effects were addressed. The pitching moment data are broken out with both positive and negative rates presented. The presented rolling and yawing moment data were constituted from an average of the positive and negative rate data.

9.1 *Pitch Axis*

For pitch forced oscillation, the model was top mounted onto the pitch oscillation mechanism, as previously shown in Figure 10. This test focused on studying rate, frequency, and flight control effects on pitch forced oscillation data. Reduced frequency (k) values of 0.0827, 0.1036, and 0.1242 were tested to produce data at different oscillation frequencies. Amplitudes were varied from 4.16 to 18.75 deg. to match pitch rates ($qc/2V$) of 0.009, 0.018, and 0.027. A presentation of the amplitude / frequency combinations is shown in Figure 74. For pitch oscillation, only the pitching moment and normal force data were plotted. The full set of data plots for this configuration can be found in Appendix D.

In the $0 < \alpha < 20$ deg. region, pitch up (positive) rates tended to produce slightly more pitch damping than pitch down (negative) rates. In the $25 < \alpha < 40$ deg. region, the trend reversed where positive rates produced little if any damping, whereas negative rates provided strong damping. Above $\alpha = 40$ deg., damping in both directions was increasing and was about the same in magnitude. Again, oscillating frequency only effected the data in the $25 < \alpha < 50$ deg. region but the effects varied and were not consistent. The pitching moment data plots for $\alpha = 0, 10, 20, \& 40$ deg. are shown in Figures 75 – 78 to provide a representative sample of the data.

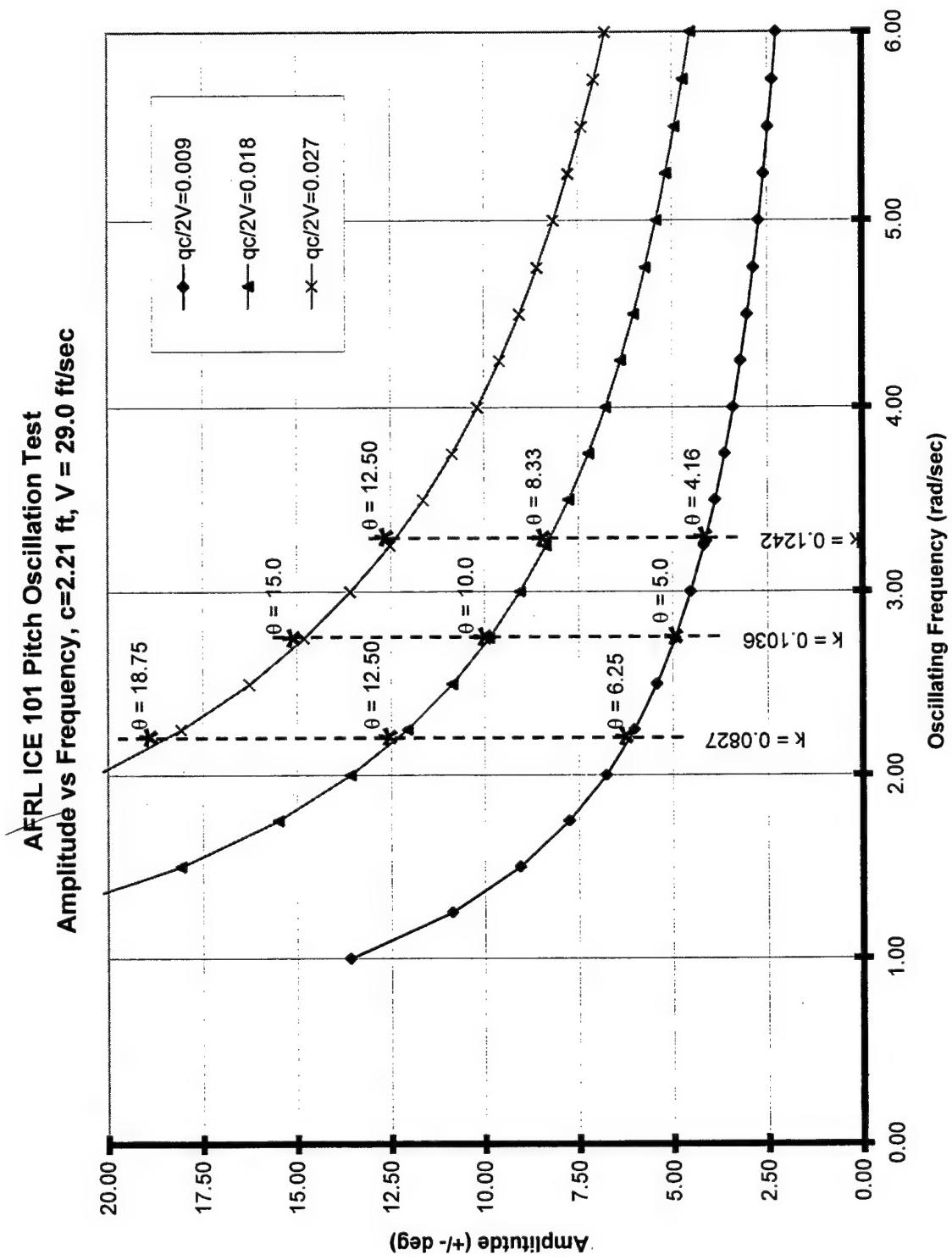


FIGURE 74 – PITCH FORCED OSCILLATION TEST POINTS

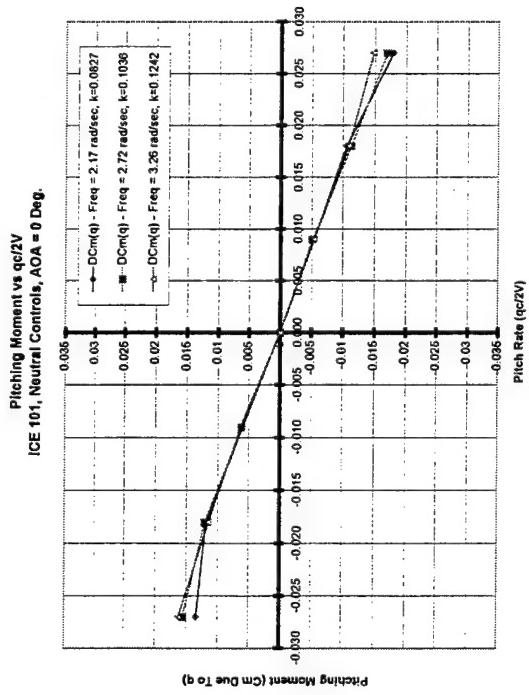


FIGURE 75

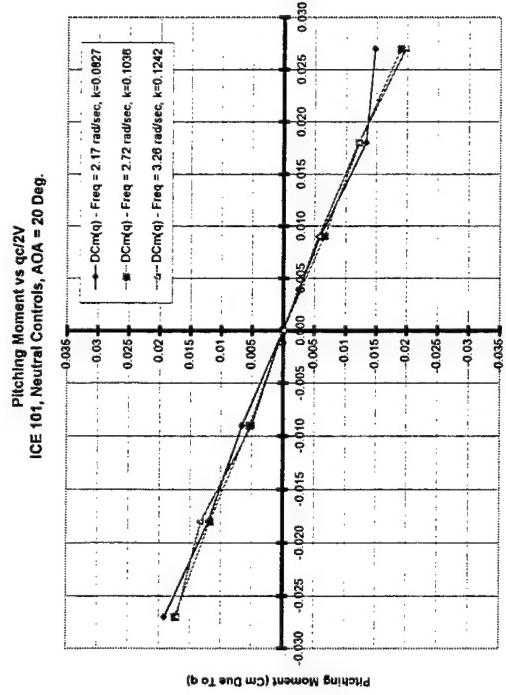


FIGURE 77

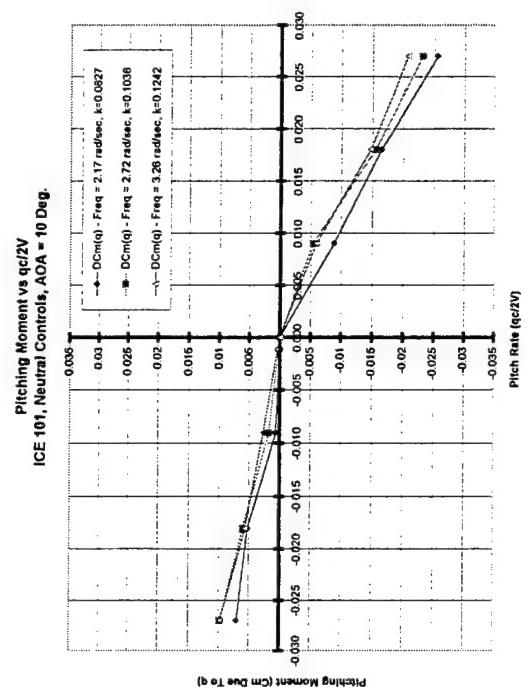


FIGURE 76

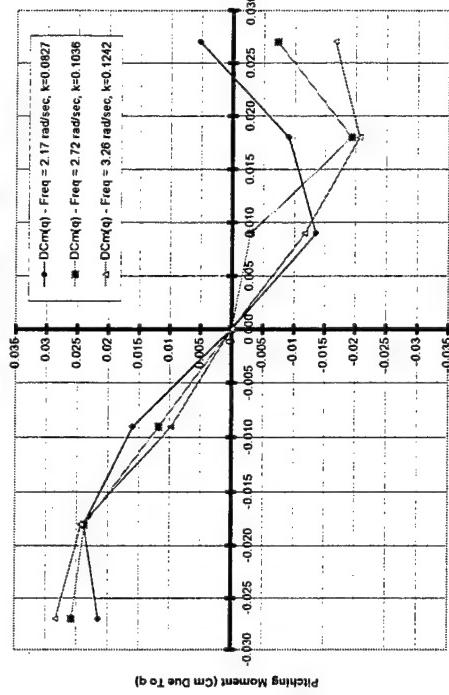


FIGURE 78

When looking at flight control deflection impacts on pitch damping, LEF = 30/30 provided only a small change to neutral control values, slightly more damping for both positive and negative rates. Full nose down control tended to reduce pitch damping for negative rates at low angles-of-attack ($0 < \alpha < 10$ deg.) and for both positive and negative rates at high AOA ($50 < \alpha < 90$). The pitching moment data plots for $\alpha = 0, 10, 20, & 40$ deg. are shown in Figures 79 – 82 to provide a representative sample of the data.

The normal force increment was almost linear with $qc/2V$ for the entire AOA range of 0 to 90 deg. The slope, or effect of rate on CN, steadily increases as AOA increases from 0 to 35 deg. and then the slope decreases to 0, or no effect of rate, as AOA approaches 90 deg. Oscillating frequency only effected the data in the $25 < \alpha < 50$ deg. region where higher frequencies tended to reduce the measured normal force increment due to rate. Setting LEF = 30/30 had no impact on rate effects and maximum nose down control produced a small reduction in normal force in the $35 < \alpha < 45$ deg. region. The normal force data plots for oscillating frequency and flight control surface variations at $\alpha = 0, 10, 20, & 40$ deg. are shown in Figures 83 – 90 to provide a representative sample of the data.

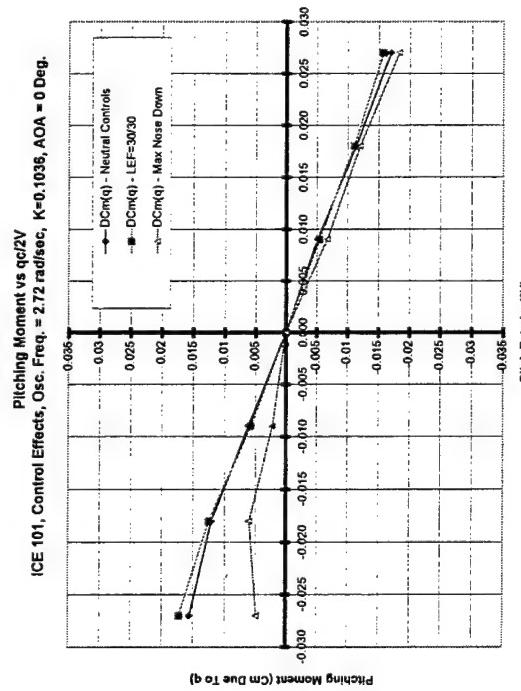


FIGURE 79

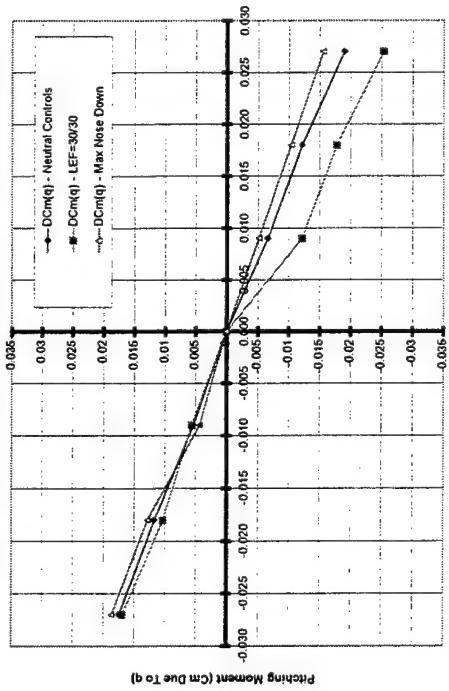


FIGURE 81

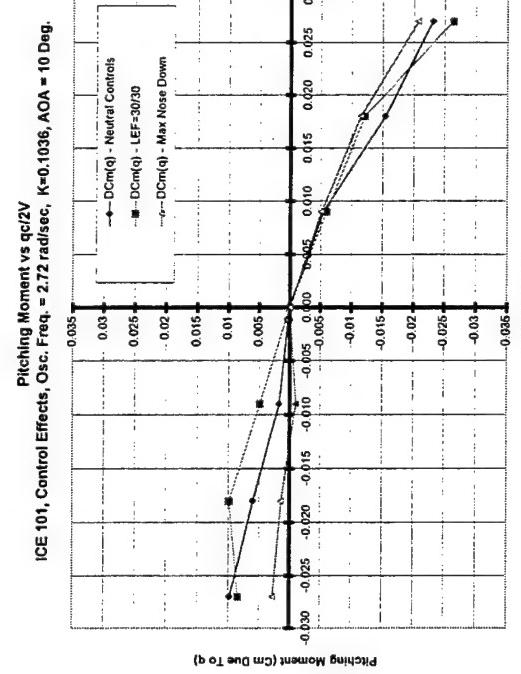


FIGURE 80

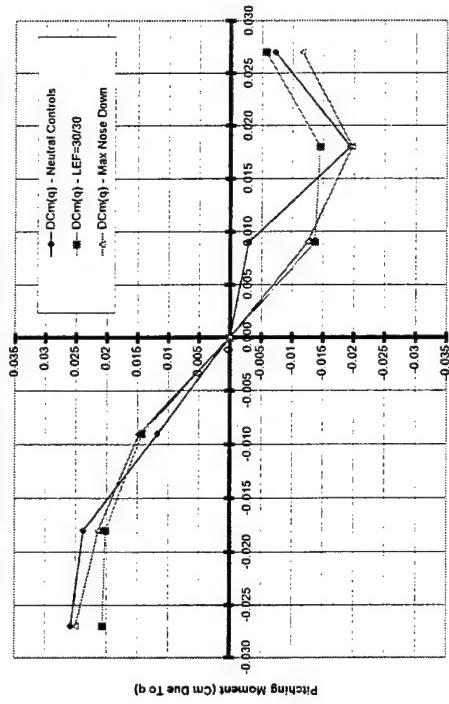


FIGURE 82

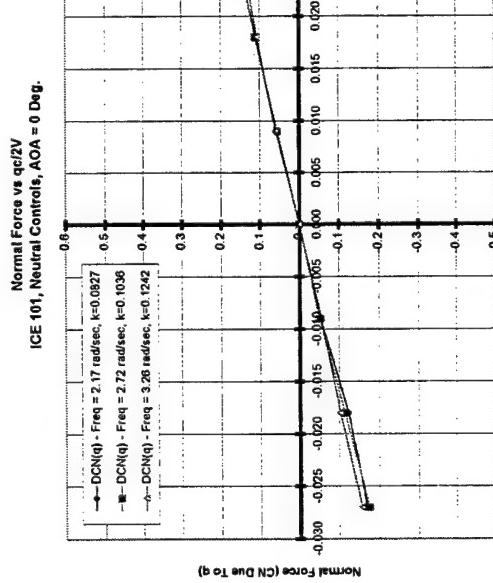


FIGURE 83

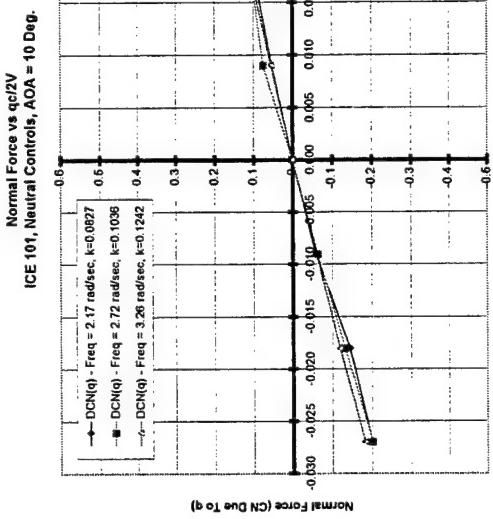


FIGURE 84

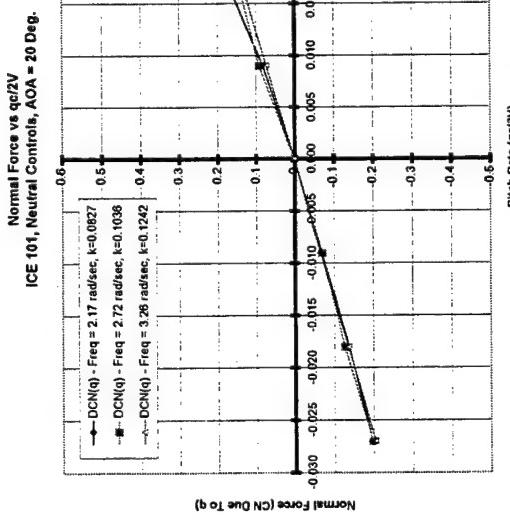


FIGURE 85

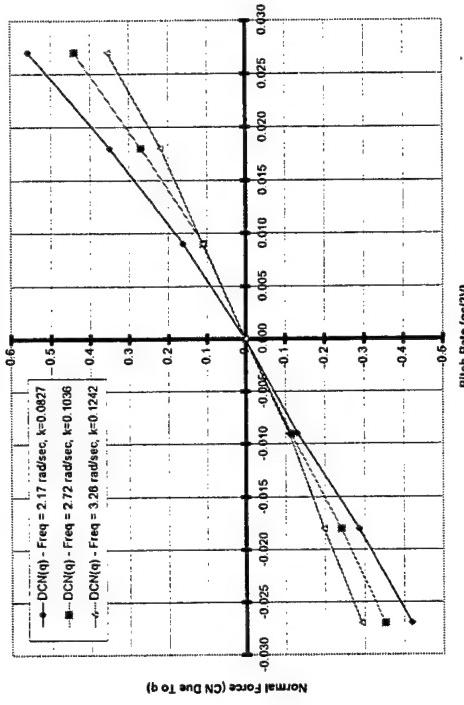


FIGURE 86

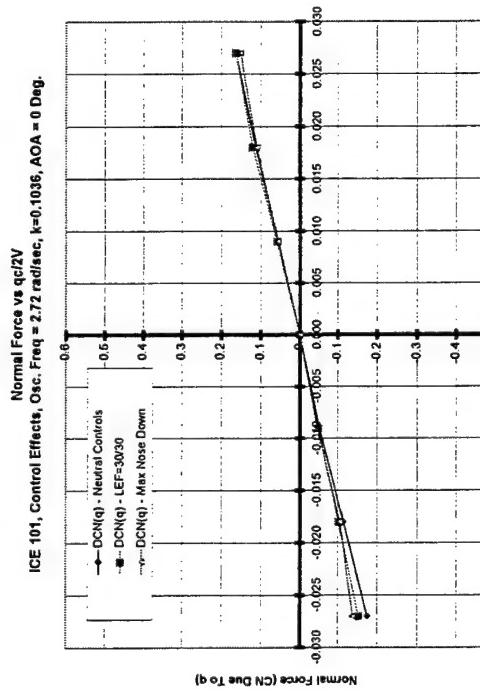


FIGURE 87

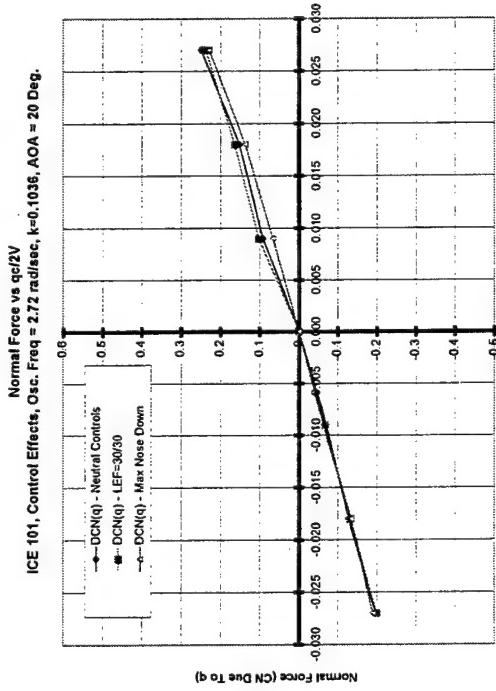


FIGURE 89

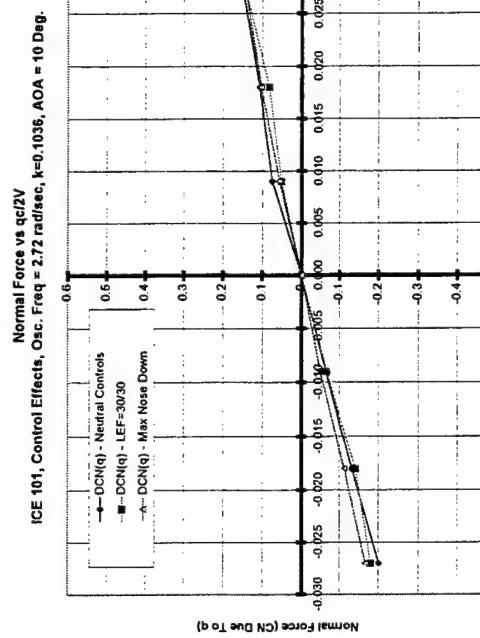


FIGURE 88

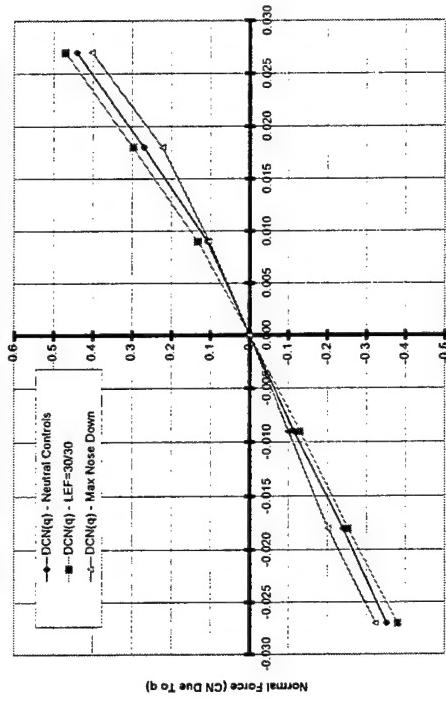


FIGURE 90

9.2 Roll Axis

For body axis roll forced oscillation, the model was aft mounted onto the roll oscillation mechanism, as previously shown in Figure 8. This test focused on studying rate, frequency, and LEF effects on roll forced oscillation data. Reduced frequency (k) values of 0.1194, 0.1492, and 0.1790 were tested to produce data at different oscillating frequencies. Amplitudes were varied from 8.33 to 37.50 deg. to match roll rates ($pb/2V$) of 0.026, 0.052, and 0.078. A presentation of the amplitude / frequency combinations is shown in Figure 91. For roll oscillation, only the rolling and yawing moment data were plotted. The full set of data plots for this configuration can be found in Appendix E.

The vehicle was well damped for a body axis roll. The slope of the ΔC_{lI} vs $pb/2V$, an indication of roll damping magnitude, steadily increased up to $\alpha = 35$ deg., at which point the trend reverses as AOA increased and roll damping eventually returned close to the $\alpha = 0$ deg. value by $\alpha = 90$ deg. Throughout most of the angle-of-attack range, there was no frequency effect on the data. However, in the $15 < \alpha < 40$ deg. range, significant differences due to testing at different frequencies became apparent. The differences, as much as 40% greater rolling moment with a frequency decrease of 1.2 rad/sec, maximized at $\alpha = 30$ deg. Further study on how frequency influences forced oscillation data acquisition and implementation needs to be performed. The rolling moment data plots for $\alpha = 0, 20, 30, \& 40$ deg. are shown in Figures 92 – 95 to provide a representative sample of the data.

A small impact of LEF deflection on roll damping was observed with the LEF = 30/30 case showing a slight reduction in damping in the $[0 < \alpha < 35]$ and $[70 < \alpha < 90]$ deg. regions. One variation that was not consistent with the rest of the data was the significant increase in roll damping with LEF = 30/30 at $\alpha = 40$ deg. More data taken around the $\alpha = 40$ deg. point and flow visualization will be needed to better understand this rapid change in damping characteristics. The rolling moment data plots for $\alpha = 0, 20, 30, \& 40$ deg. are shown in Figures 96 – 99 to provide a representative sample of the data.

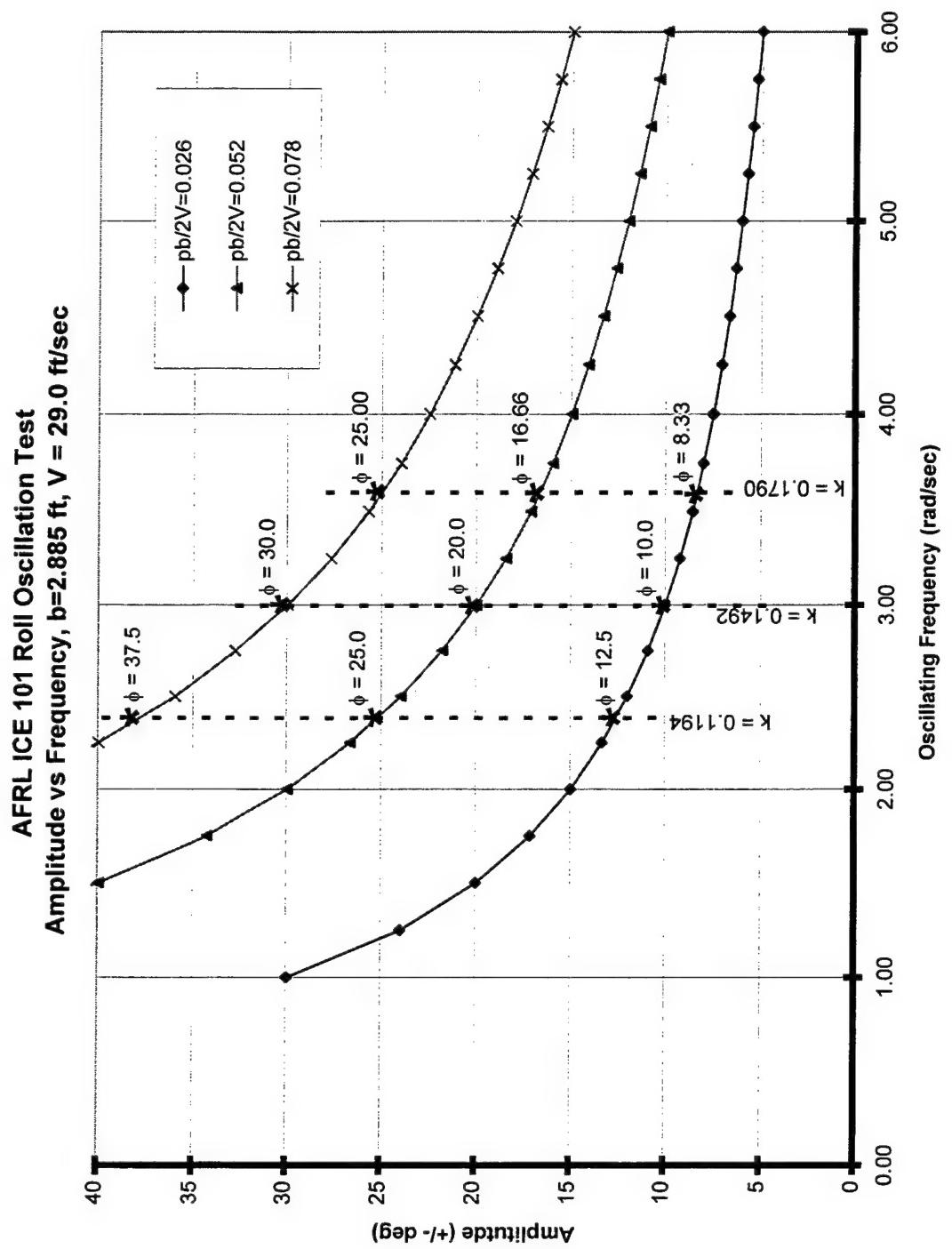


FIGURE 91 – ROLL FORCED OSCILLATION TEST POINTS

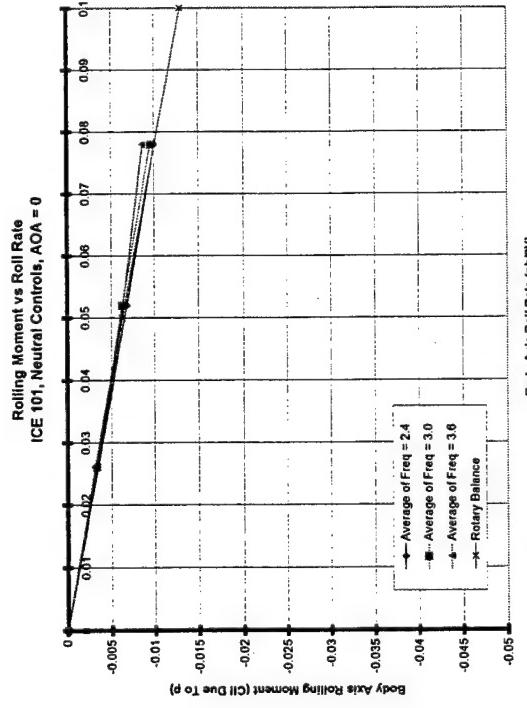


FIGURE 92

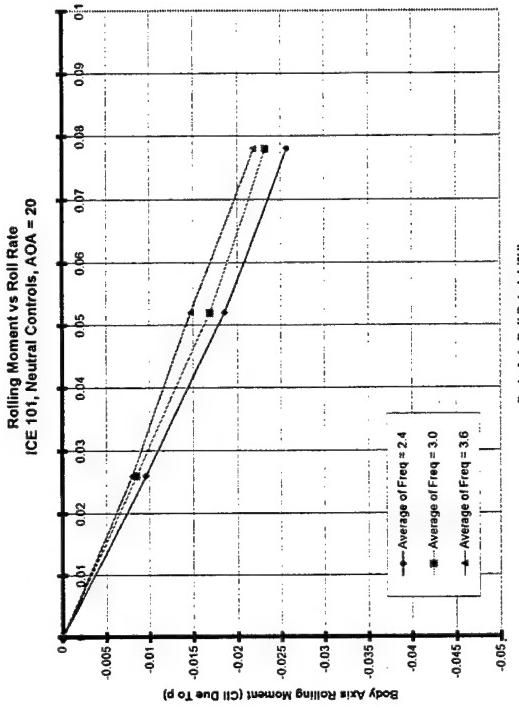


FIGURE 93

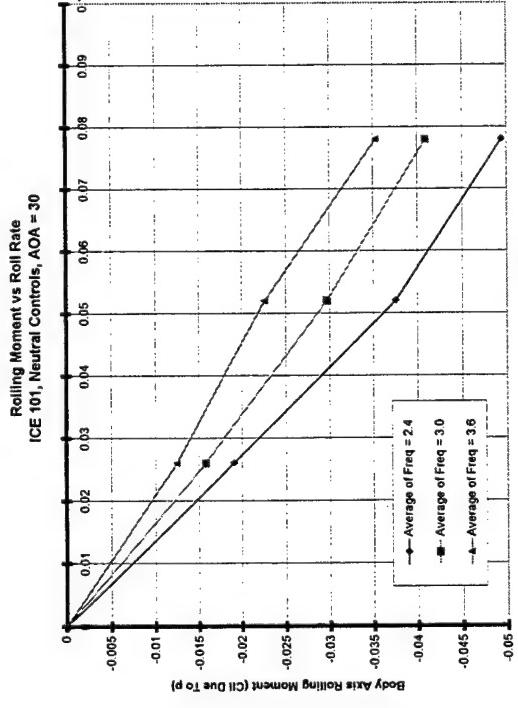


FIGURE 94



FIGURE 95

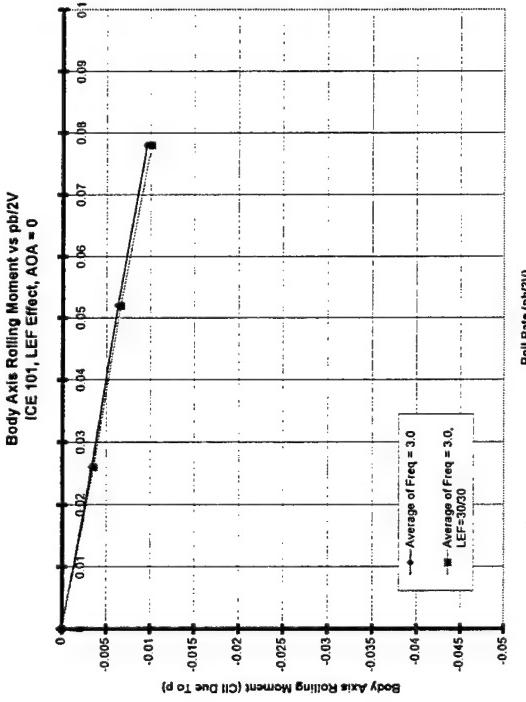


FIGURE 96

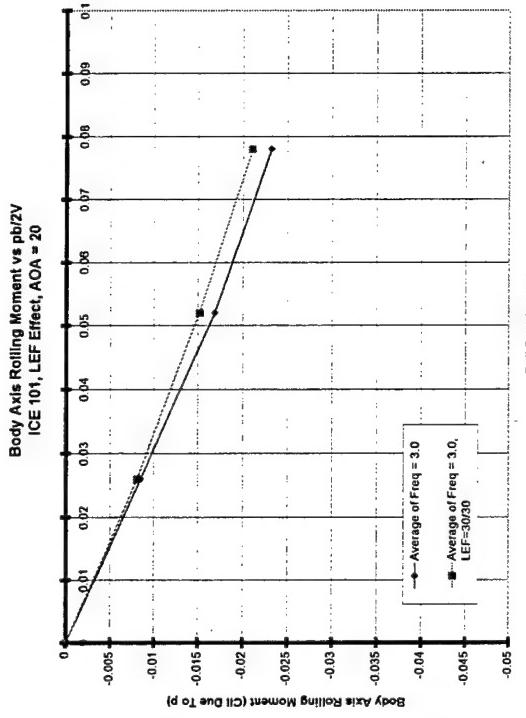


FIGURE 97

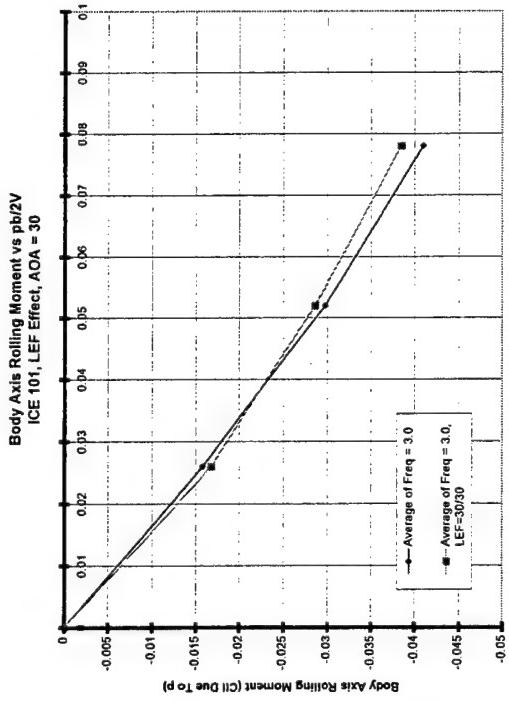


FIGURE 98

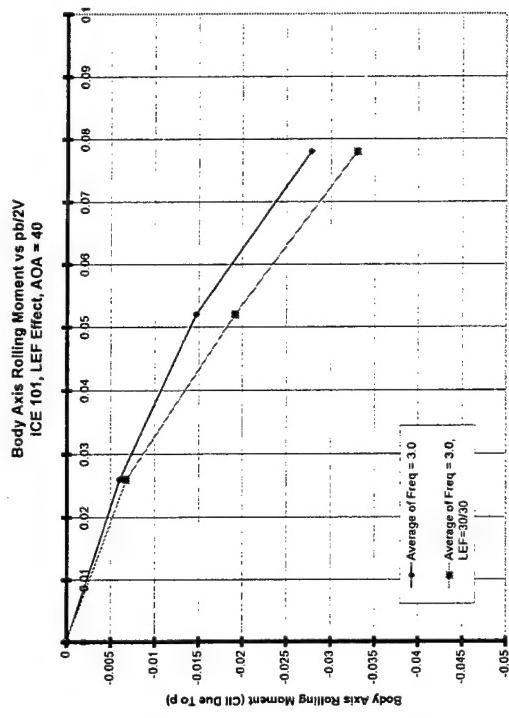


FIGURE 99

Cross axis coupling effects are important for lateral-directional control analysis and warranted analysis. It was observed that there was no effect on yawing moment due to roll rate at low angles-of-attack ($0 < \alpha < 25$ deg.). However, in the $30 < \alpha < 50$ deg. region, a positive roll rate provided significant coordinating yawing moment, after which, at higher angles-of-attack, the data illustrated that there was no effect on yawing moment due to roll rate. There were also no frequency effects on the data except in the $30 < \alpha < 50$ deg. region where differences again reached 40%. The yawing moment data plots for $\alpha = 0, 20, 30, \& 40$ deg. are shown in Figures 100 – 103 to provide a representative sample of the data.

A moderate impact of LEF deflection was observed on yawing moment for the LEF = 30/30 case showing an adverse yawing moment increment relative to the neutral controls case. This increment was small for most of the angle-of-attack range, but amplifies to significance in the $30 < \alpha < 50$ deg. region. The yawing moment data plots for $\alpha = 0, 20, 30, \& 40$ deg. are shown in Figures 104 – 107 to provide a representative sample of the data.

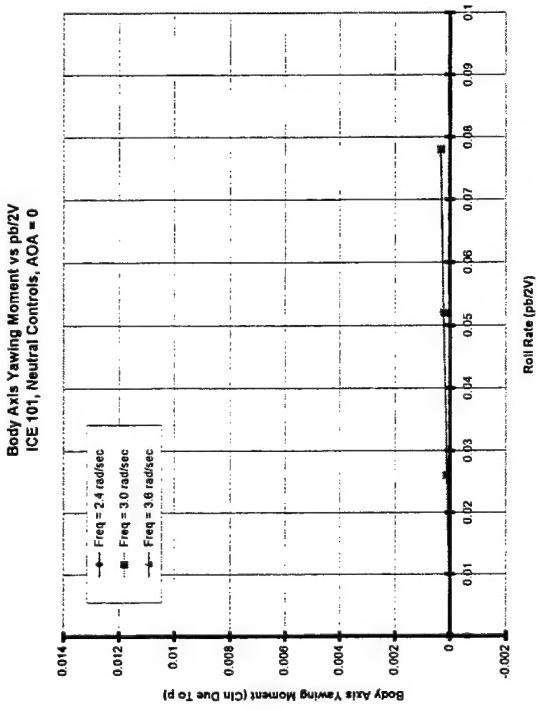


FIGURE 100

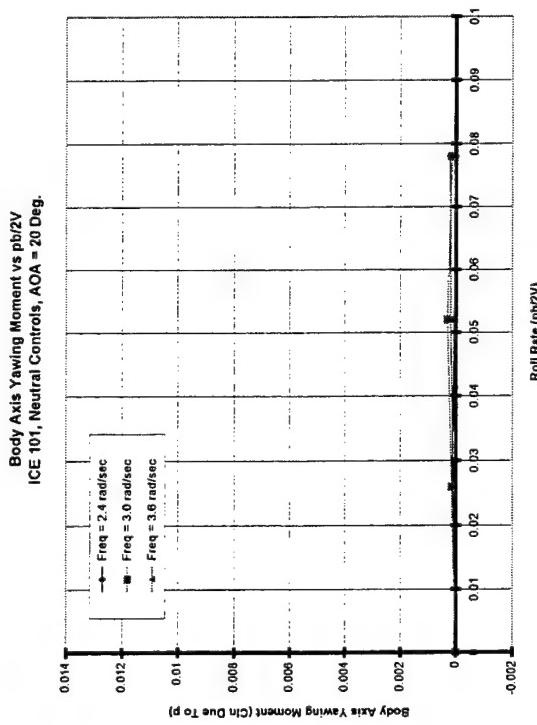


FIGURE 101

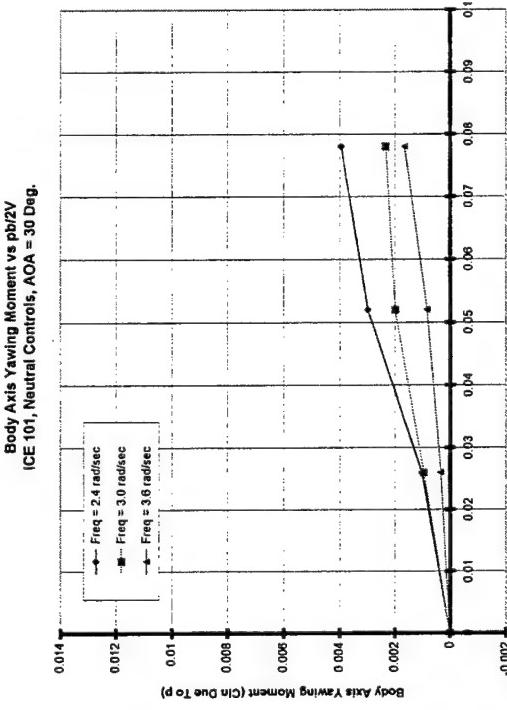


FIGURE 102

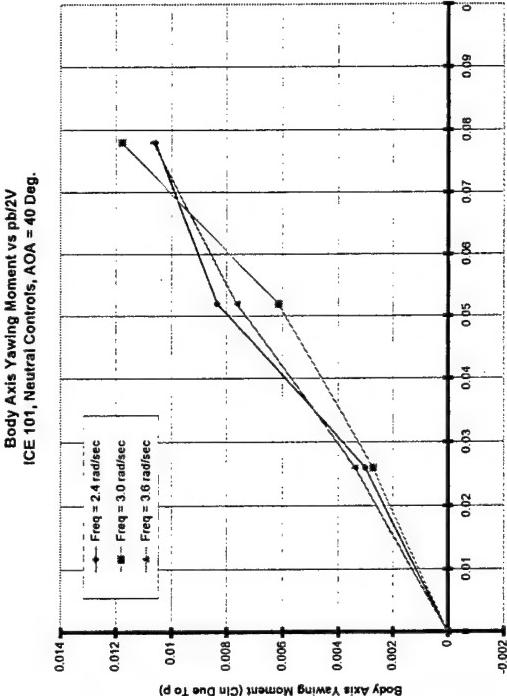


FIGURE 103

FIGURE 104

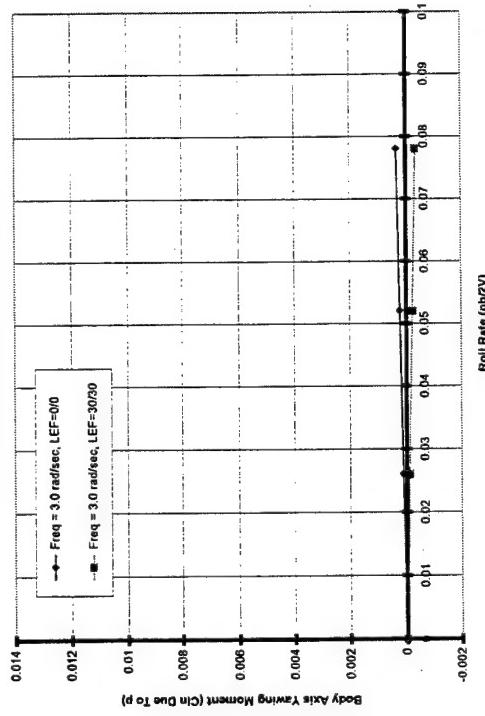


FIGURE 104

FIGURE 105

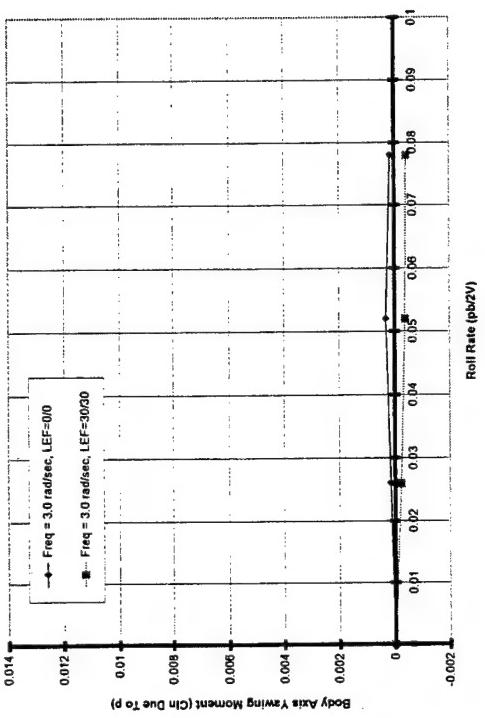


FIGURE 105

FIGURE 106

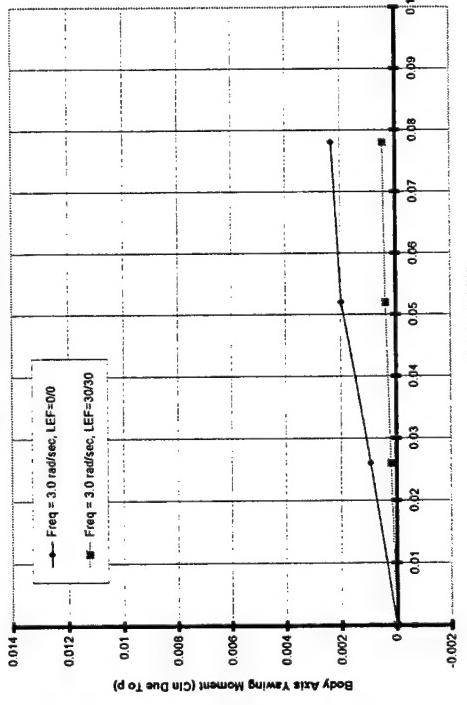
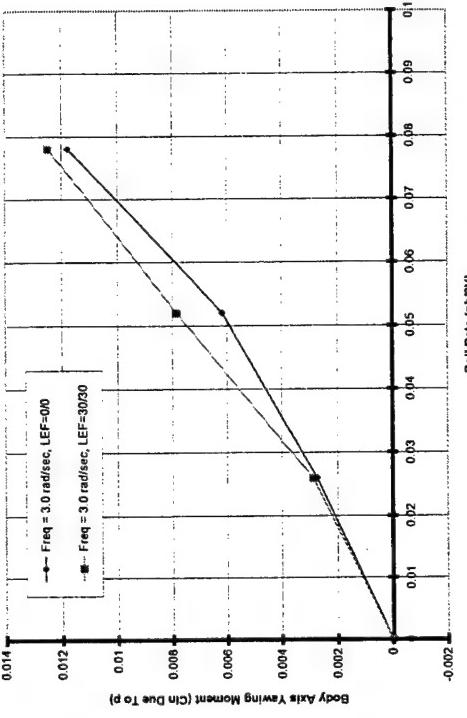


FIGURE 106

FIGURE 107



9.3 Yaw Axis

For body axis yaw forced oscillation, the model was top mounted onto the yaw oscillation mechanism, as previously shown in Figure 9. This test focused on studying rate, frequency, and LEF effects on yaw forced oscillation data. Reduced frequency (k) values of 0.1194, 0.1492, and 0.1790 were tested to produce data at different oscillation frequencies. Amplitudes were varied from 8.33 to 37.50 deg. to match yaw rates ($rb/2V$) of 0.026, 0.052, and 0.078. A presentation of the amplitude / frequency combinations is shown in Figure 108. For yaw oscillation, only the yawing and rolling moment data were plotted. The full set of data plots for this configuration can be found in Appendix F.

The body axis yawing moment due to yaw rate data had magnitudes that are much smaller than typical aircraft because there is little side surface on this tailless vehicle. Little to no yaw damping was observed in the $0 < \alpha < 20$ deg. region. Damping increased with yaw rate in a nonlinear fashion in the $25 < \alpha < 45$ deg. region. This was another condition for which linear dynamic stability derivatives would not work well in aerodynamic math models of this vehicle concept. Above $\alpha = 50$ deg., damping reduces to neutral all the way to $\alpha = 90$ deg. Significant frequency effects were observed in the $25 < \alpha < 45$ deg. region, but their impact was not consistent. For the $25 < \alpha < 35$ region, higher frequency reduced yaw damping, but for the $35 < \alpha < 45$ deg. region, higher frequency increased yaw damping. The yawing moment data plots for $\alpha = 0, 20, 30, \& 40$ deg. are shown in Figures 109 – 112 to provide a representative sample of the data.

A small impact of LEF deflection was observed on yawing moment with $LEF = 30/30$ deg. adding positive yawing moment increment, which was propelling for positive yaw rate. This effect was consistent for the entire AOA range, but the magnitude of the effect varied with a maximum difference around $\alpha = 25$ deg. The yawing moment data plots for $\alpha = 0, 20, 30, \& 40$ deg. are shown in Figures 113 – 116 to provide a representative sample of the data.

AFRL ICE 101 Yaw Oscillation Test
Amplitude vs Frequency, $b=2.885$ ft, $V = 29.0$ ft/sec

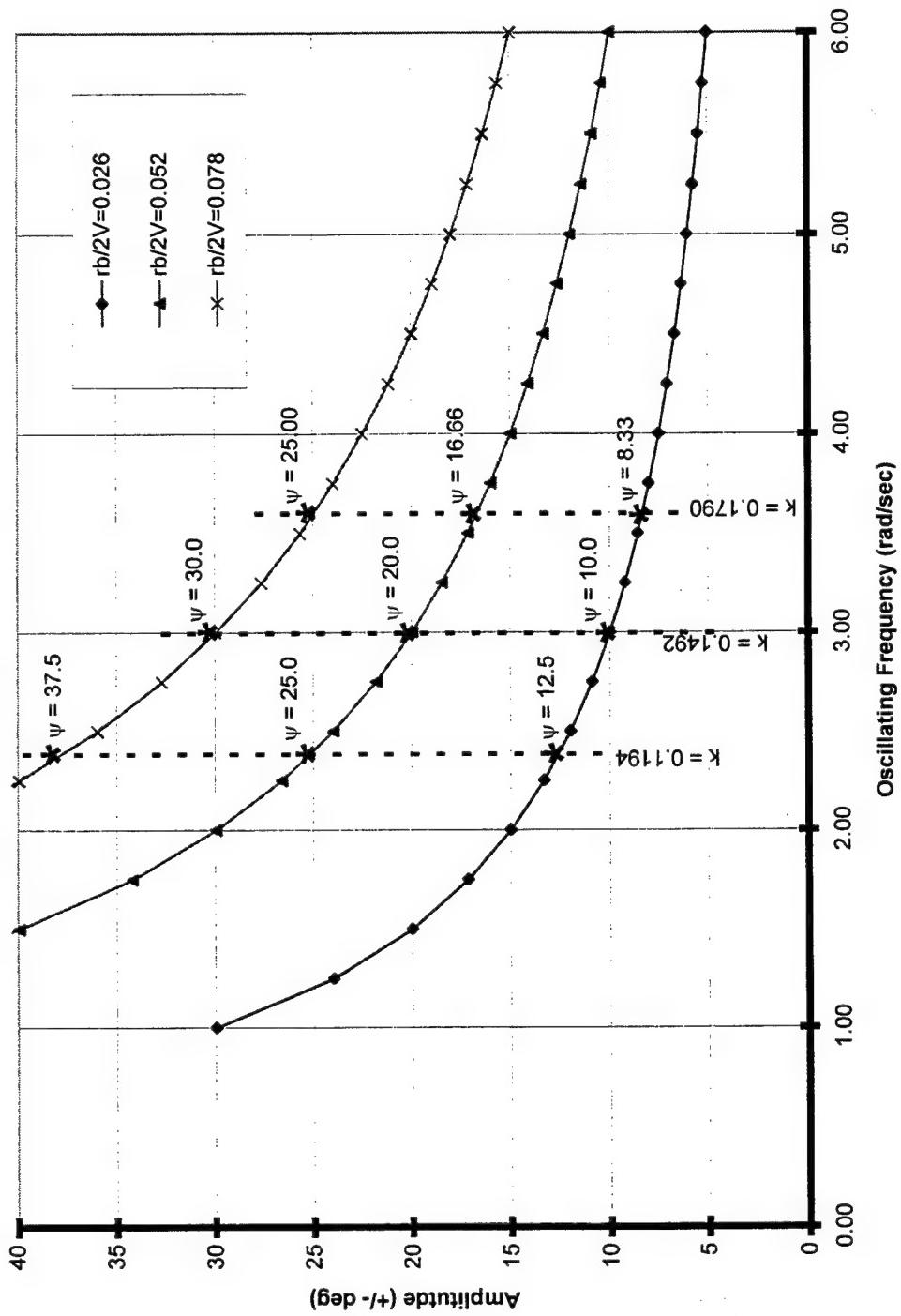


FIGURE 108 – YAW FORCED OSCILLATION TEST POINTS

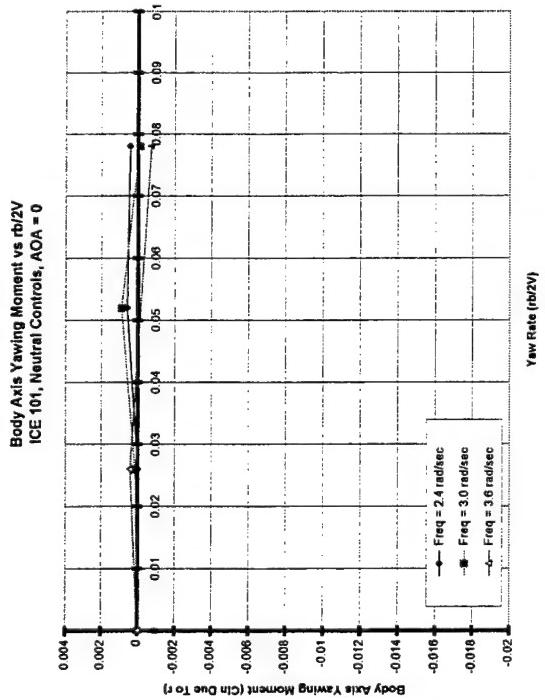


FIGURE 109

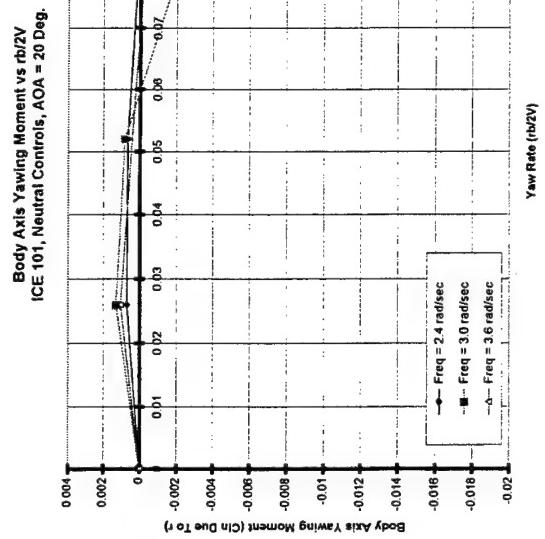


FIGURE 110

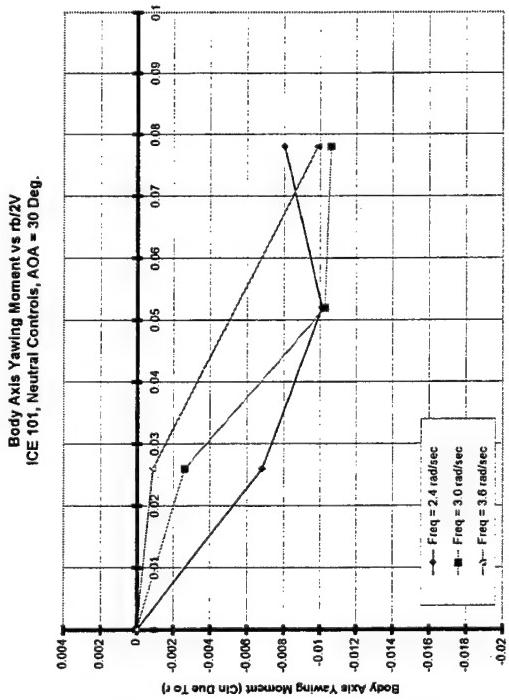


FIGURE 111

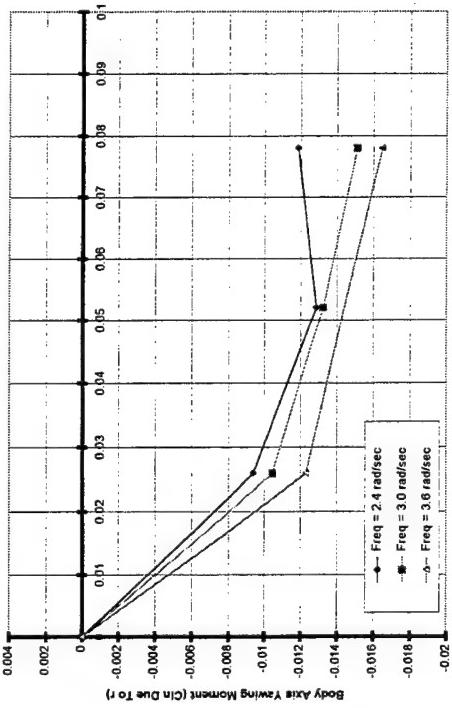


FIGURE 112

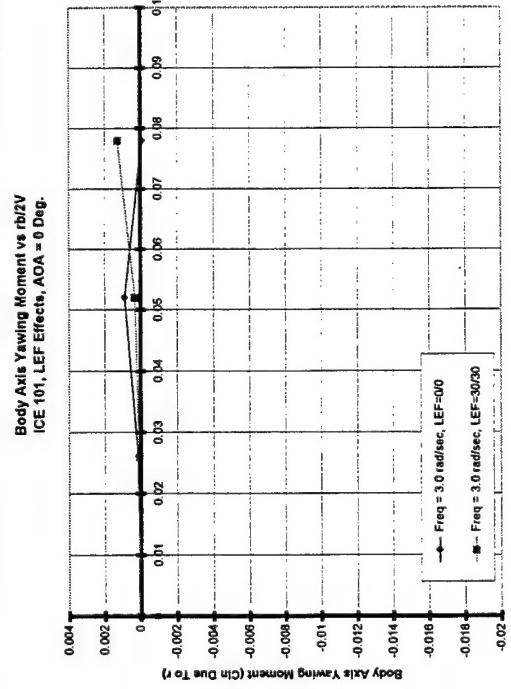


FIGURE 113

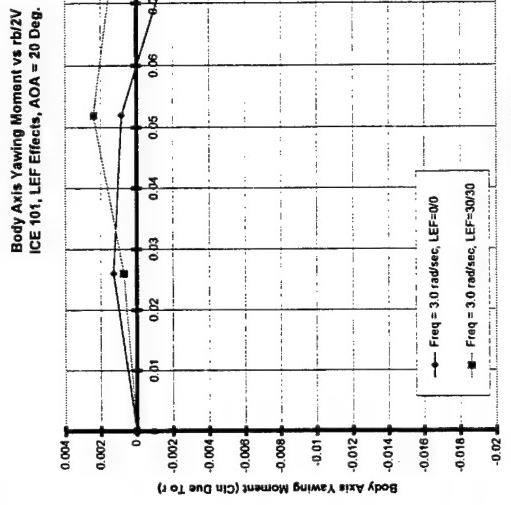


FIGURE 114

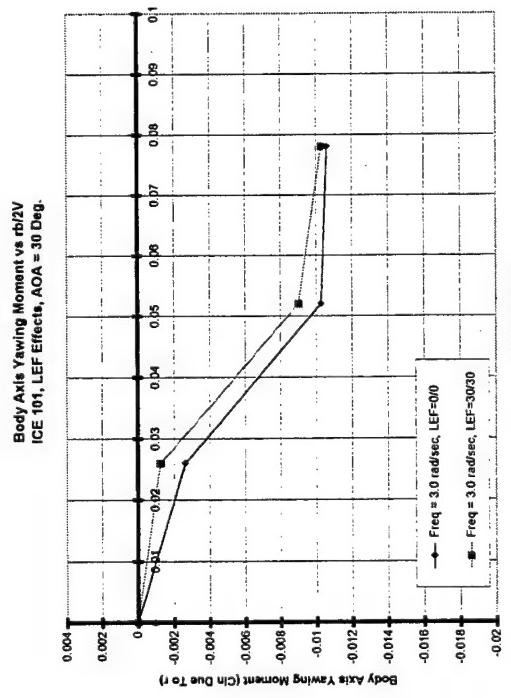


FIGURE 115

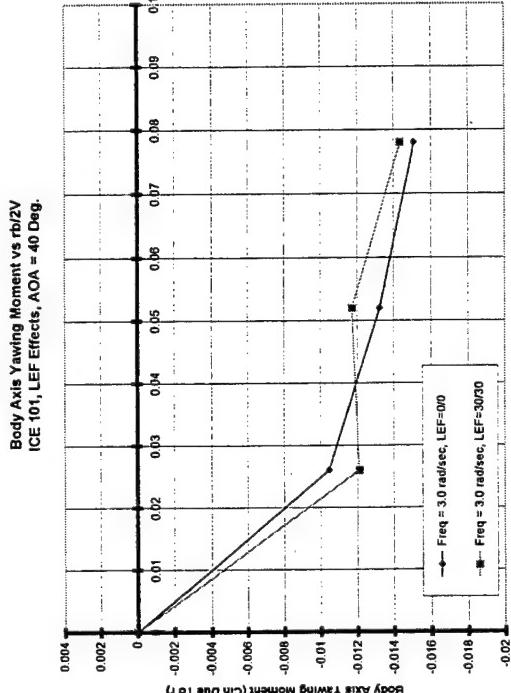


FIGURE 116

Significant cross axis coupling effects were observed for the incremental rolling moment data in the $5 < \alpha < 25$ deg. region. A positive yaw rate provided significant positive (coordinating) rolling moment, with a maximum effect seen at $\alpha = 25$ deg. Above $\alpha = 25$ deg., the ΔC_{II} decreased but remains positive for AOA up to 90 deg. There were no frequency effects on the data except in the $20 < \alpha < 35$ deg. region which was consistent with all the other forced oscillation data. The higher frequency testing produced lower rolling moment (less positive) increments due to rate. The rolling moment data plots for $\alpha = 0, 20, 30, \& 40$ deg. are shown in Figures 117 – 120 to provide a representative sample of the data.

A moderate impact of LEF deflection was observed on rolling moment for the LEF = 30/30 case, but only in the $10 < \alpha < 25$ deg. range. Lower rolling moment increments were produced by LEF = 30/30 when compared with the controls neutral case. The rolling moment data plots for $\alpha = 0, 20, 30, \& 40$ deg. are shown in Figures 121 – 124 to provide a representative sample of the data.

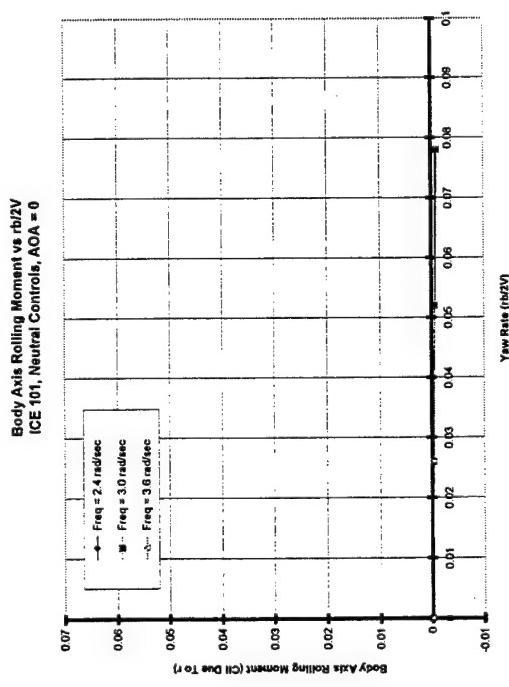


FIGURE 117

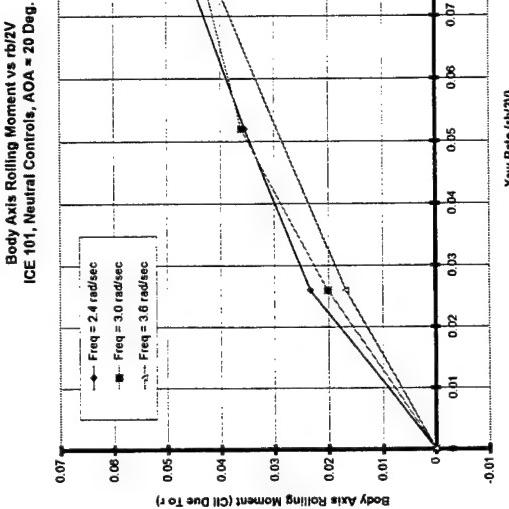


FIGURE 118

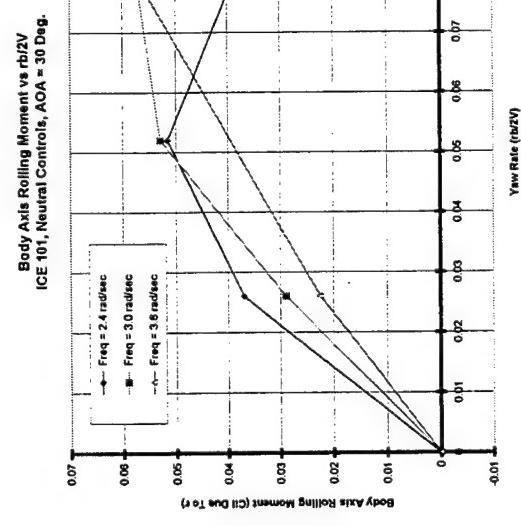


FIGURE 119

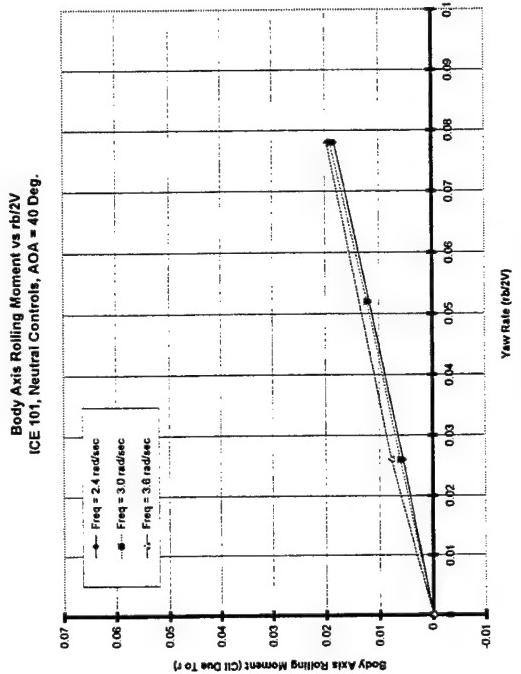


FIGURE 120

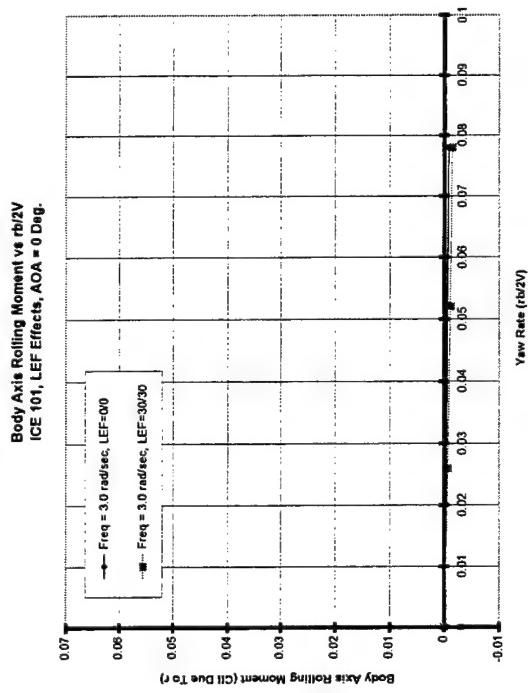


FIGURE 121

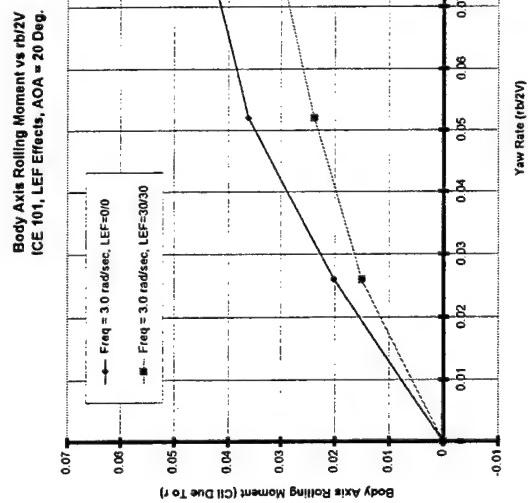


FIGURE 122

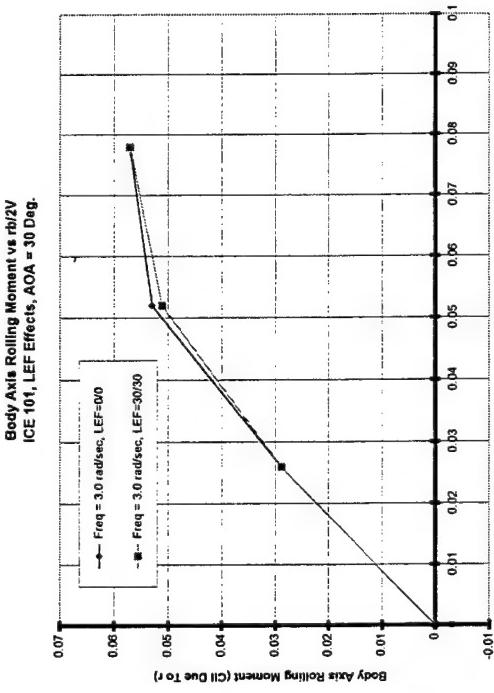


FIGURE 123

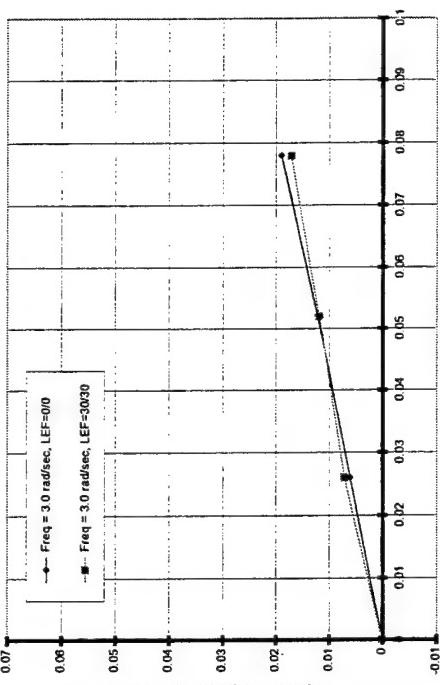


FIGURE 124

10. SUMMARY & CONCLUSIONS

The Innovative Control Effectors Configuration 101 dynamic wind tunnel model was tested in the AFRL Vertical Wind Tunnel to enhance the understanding of the dynamic characteristics of this vehicle concept. Analysis of the wind tunnel results show:

1. The baseline vehicle, with wind axis rotation and neutral controls, exhibited a small increase in normal force and a small nose-down pitching moment with increasing rotation rate. It was also well damped in roll and neutrally damped in yaw.
2. Rotational characteristics were altered with increasing vehicle sideslip angle.
3. Deflection of the leading edge flaps to 30 deg. did not significantly alter the normal force, pitching moment, and rolling moment rotational characteristics. However, a small, stabilizing yawing moment was identified for $\alpha < 15$ deg. and was attributable to the LEF deflection variation.
4. All Moving Tip control power was maintained during vehicle rotation.
5. Positive dynamic normal force was found at all AOA.
6. Pitch damping was exhibited at all AOA, sometimes nonlinear with rate.
7. Roll damping was strong at all AOA, sometimes nonlinear with rate.
8. Yaw damping was neutral at low AOA with nonlinear damping in the $25 < \alpha < 45$ deg. region.
9. Significant frequency effects were identified during the forced oscillation test. These effects were most notable in the $15 < \alpha < 45$ deg. region. Further study is necessary to better understand how oscillating frequency influences forced oscillation test results.

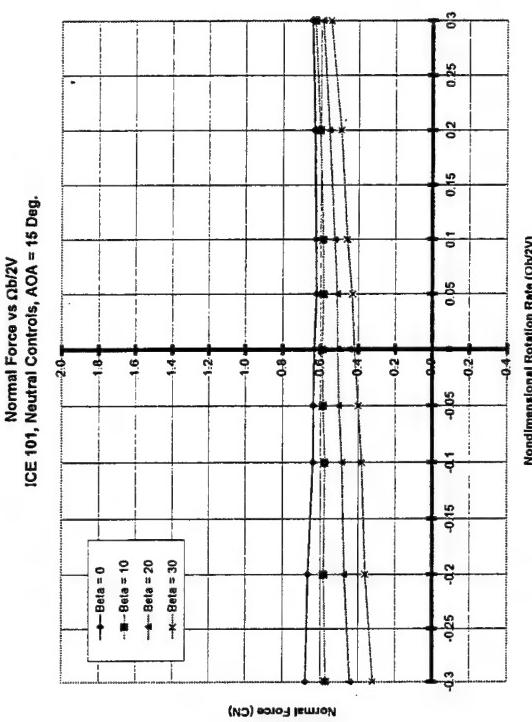
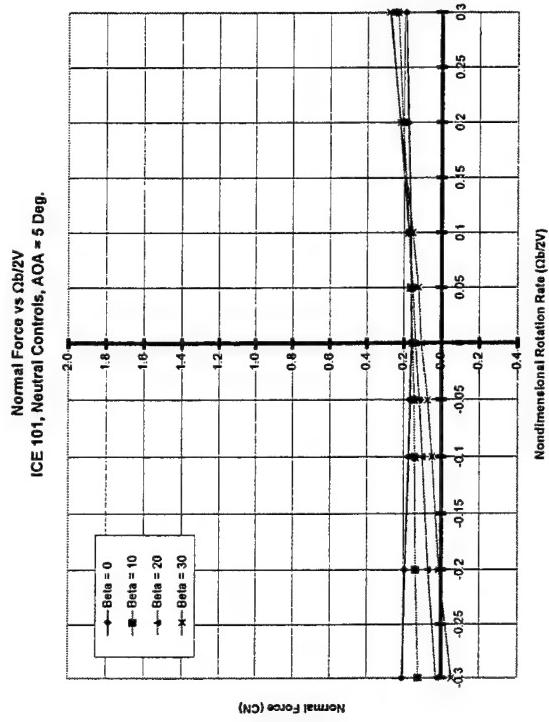
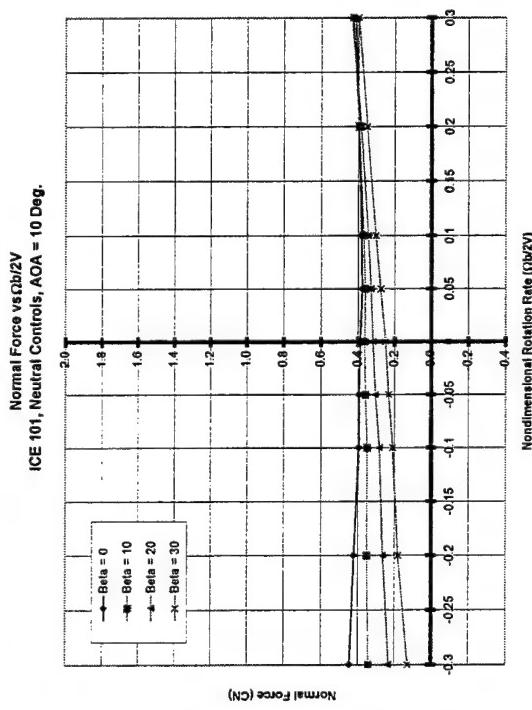
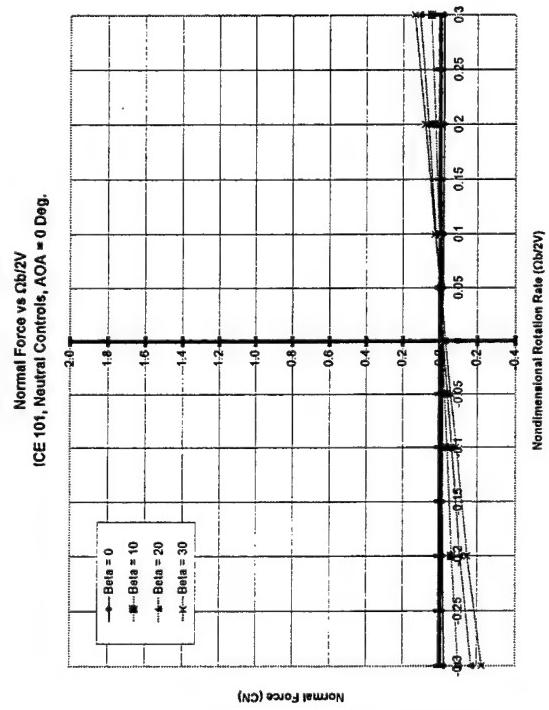
11. REFERENCES

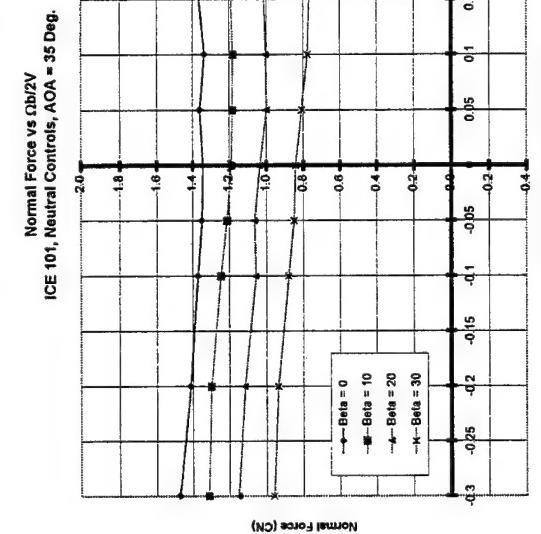
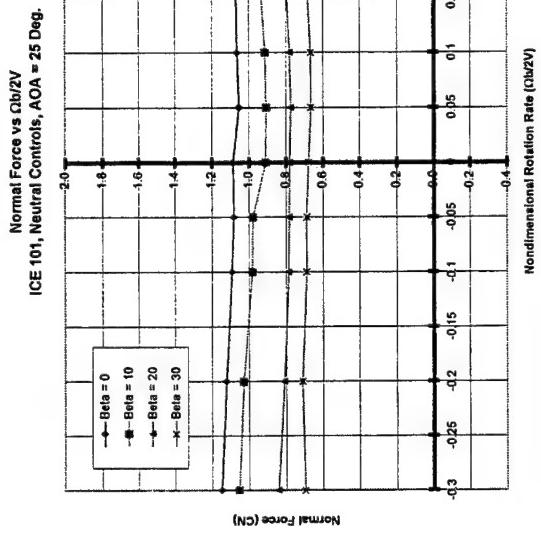
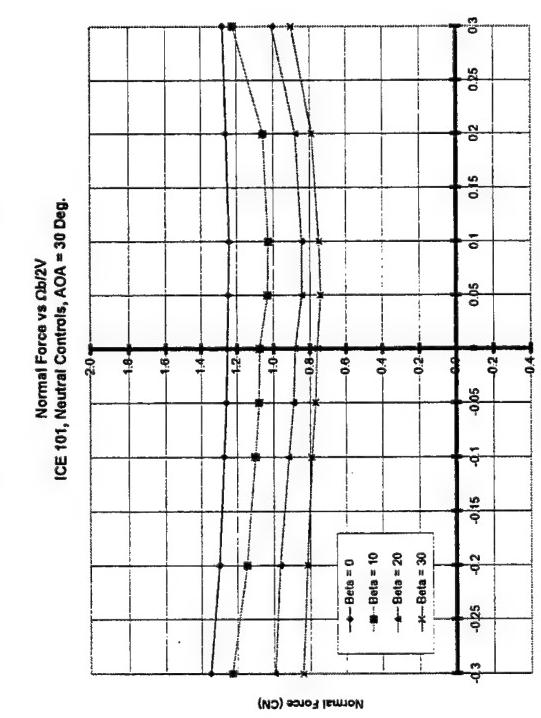
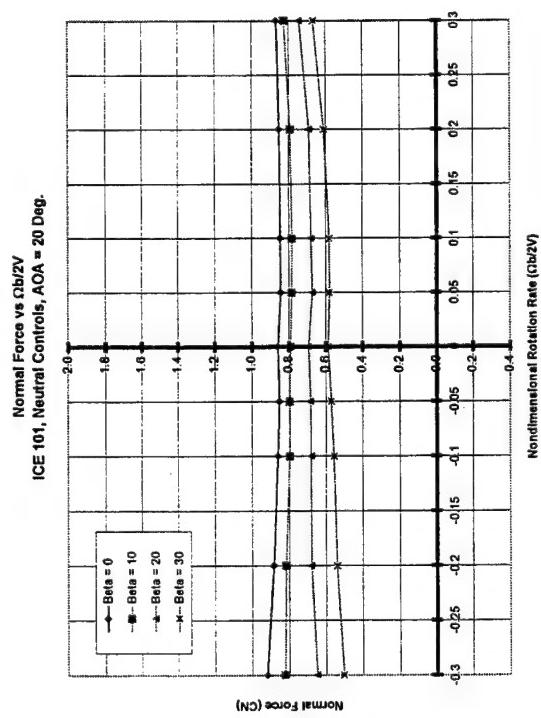
1. Dorsett, K. M., Mehl, D. R., "Innovative Control Effectors (ICE)", WL-TR-96-3043, January 1996.
2. Dorsett, K. M., Fears, S. P., Houlden, H. P., "Innovative Control Effectors (ICE) Phase II", WL-TR-97-3059, August 1997.
3. Dickes, E. G., "Preliminary Design Of A Test Rig For The Wright Laboratory Vertical Wind Tunnel", WL-TR-94-3153, Jan. 1994
4. Hultberg, R.S., "Multi-Axis Test Rig For The AFRL Vertical Wind Tunnel", AFRL-VA-WP-TR-1998-3036, June 98.
5. Bihrlle, W., Jr., "Prediction of High Alpha Flight Characteristics Utilizing Rotary Balance Data", 13th ICAS Congress/AIAA Aircraft Systems and Technology Conference Proceedings, Aug. 1981.
6. "Rotary-Balance Testing for Aircraft Dynamics", AGARD-AR-265, Dec 1990
7. Campbell, J.P., Johnson, J.L., & Hewes, D.E., "Low-Speed Study Of The Effect Of Frequency On The Stability Derivatives Of Wings Oscillating In Yaw With Particular Reference To High Angle-Of-Attack Conditions", NACA RM L55H05, November 1955

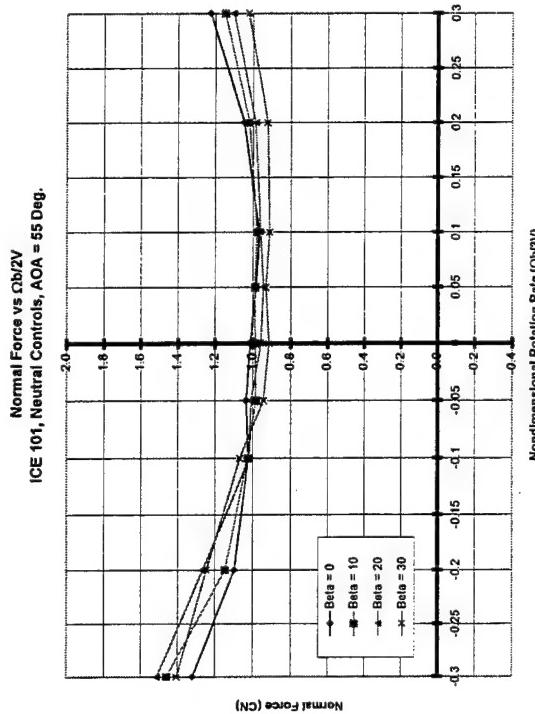
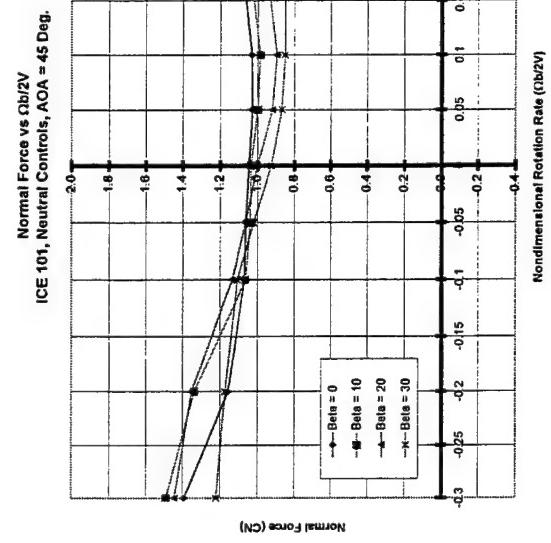
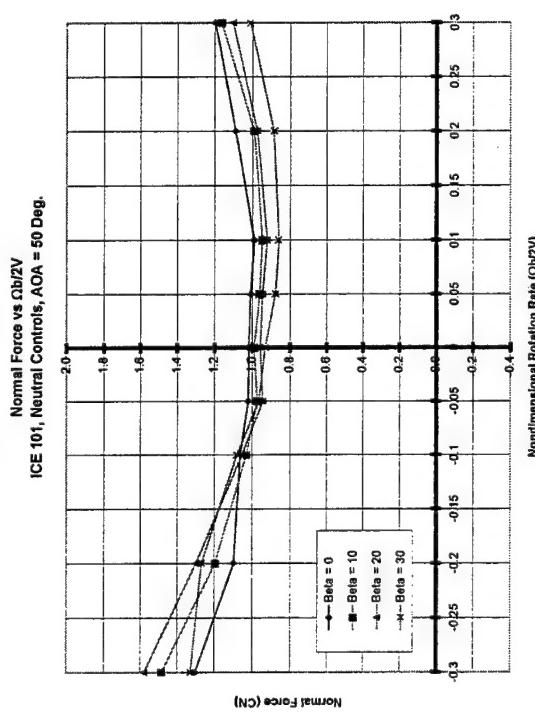
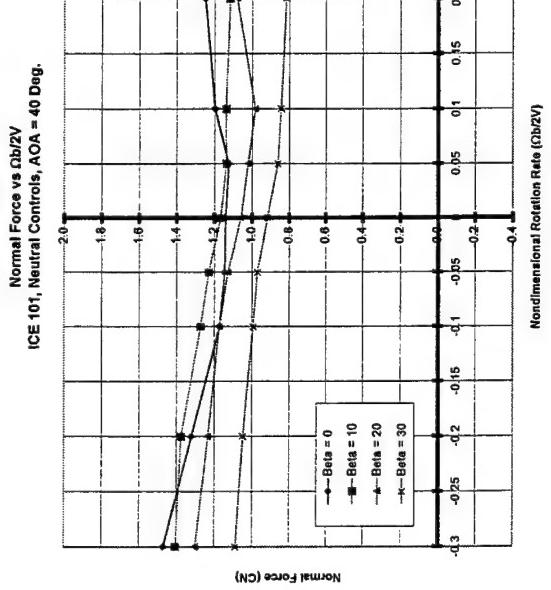
Appendix A

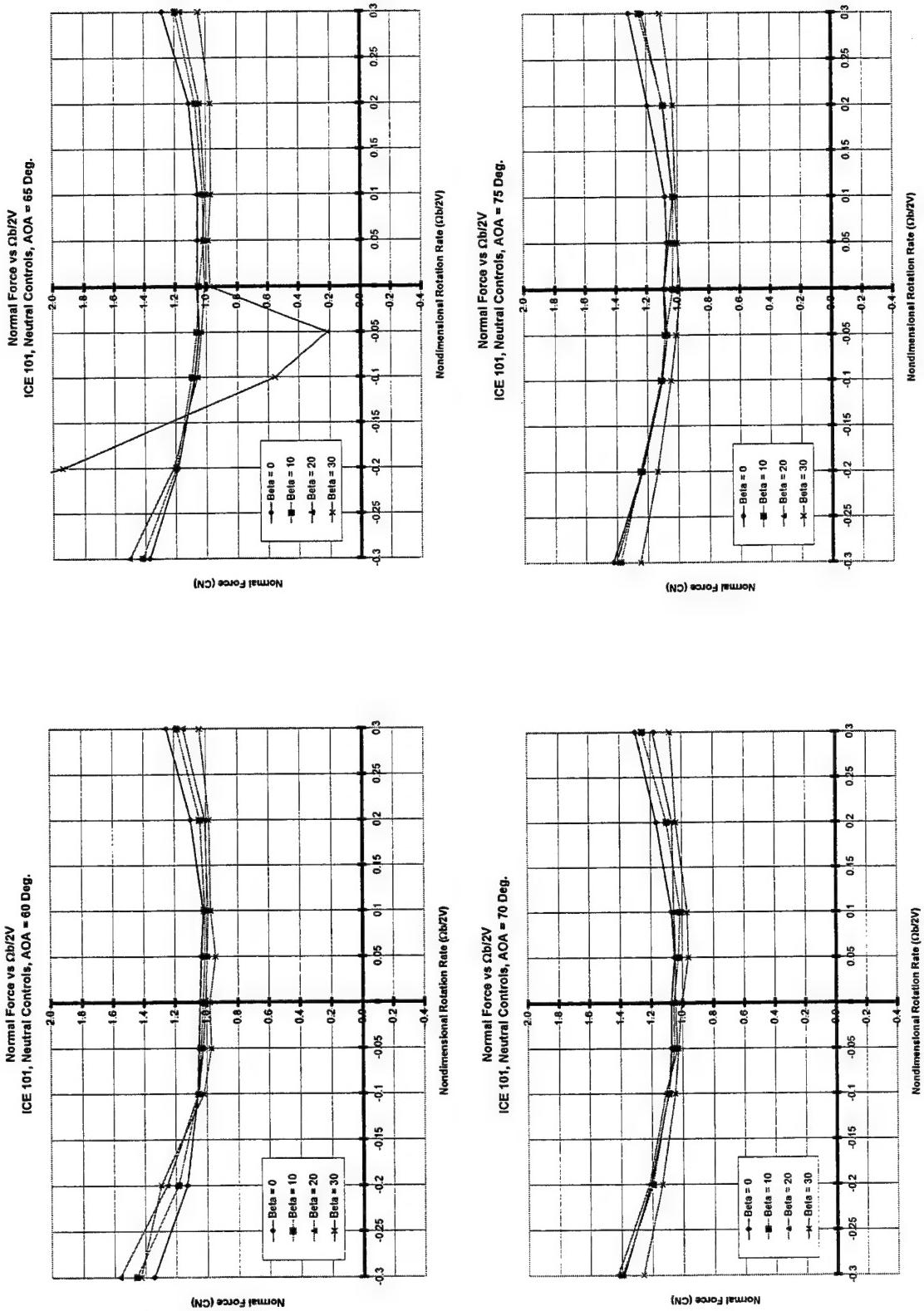
Rotary Balance Data Plots

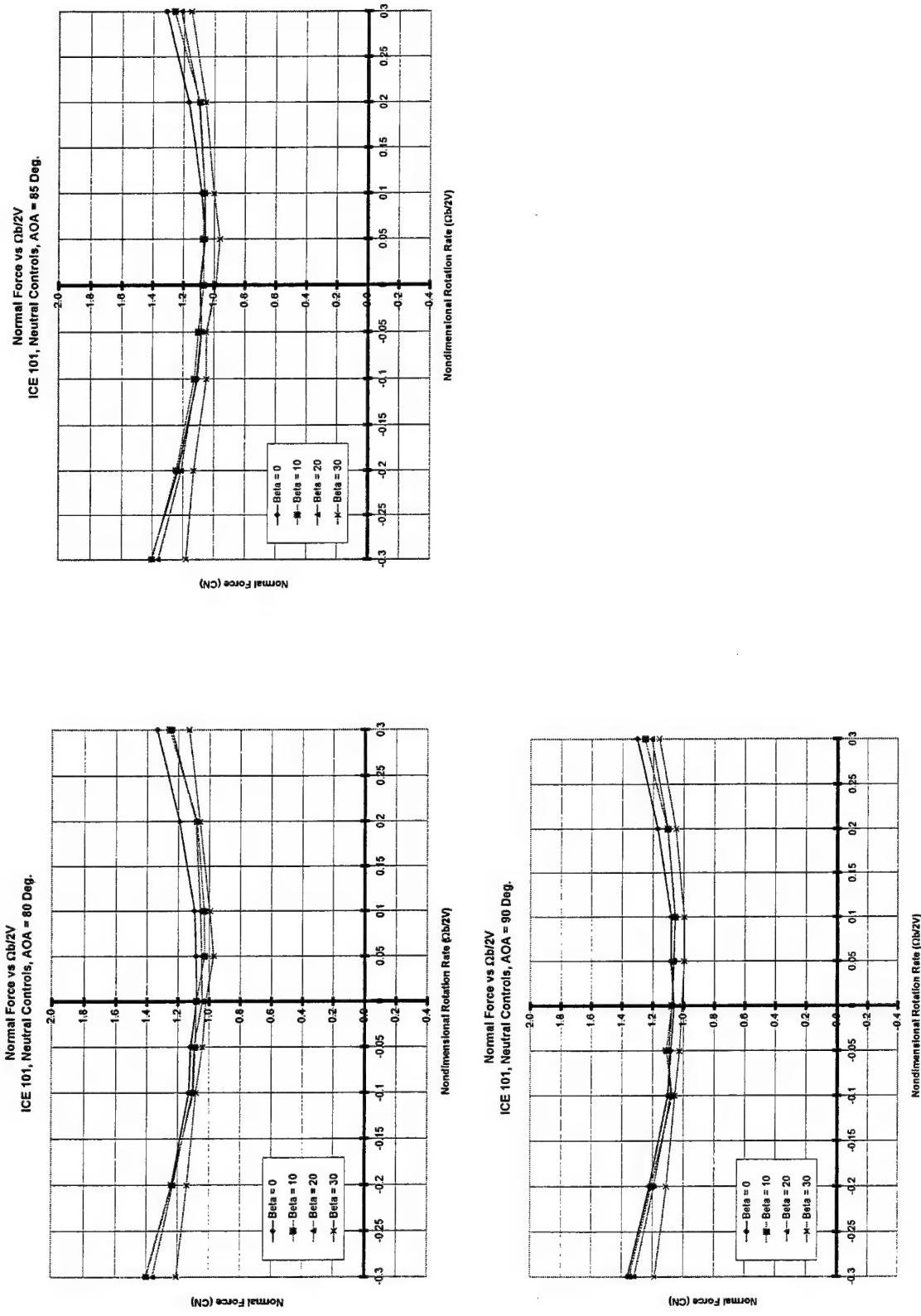
Neutral Controls, LEF = 0/0

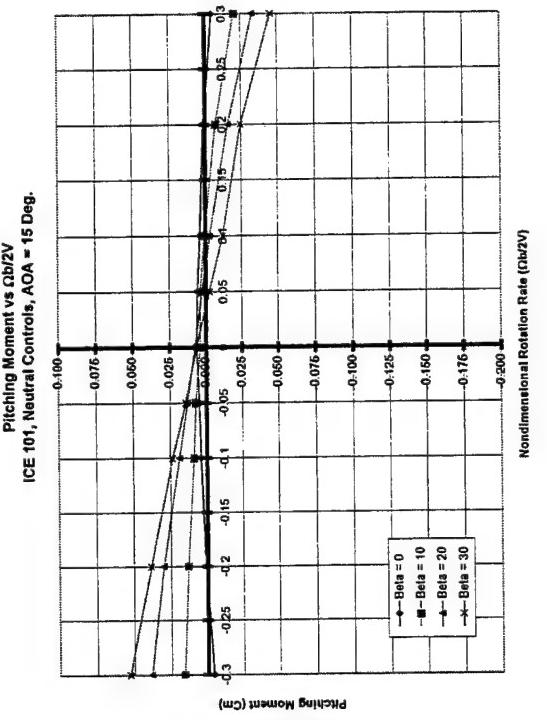
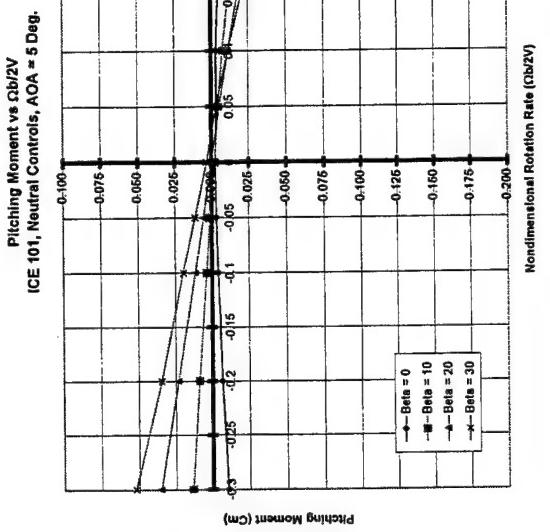
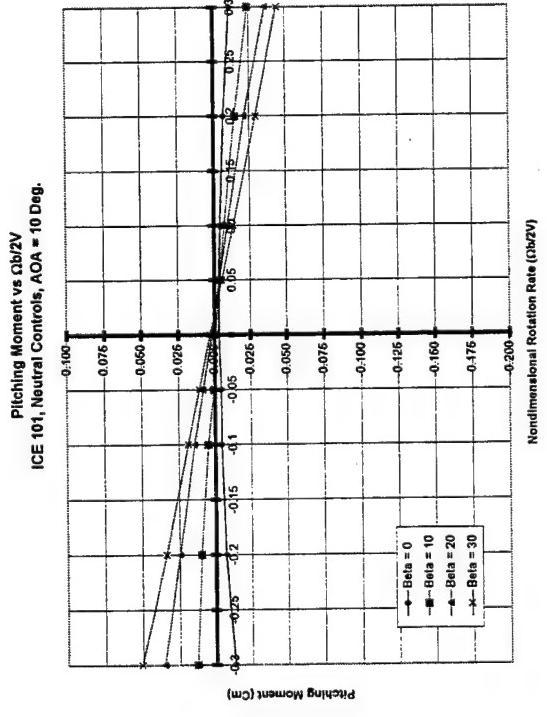
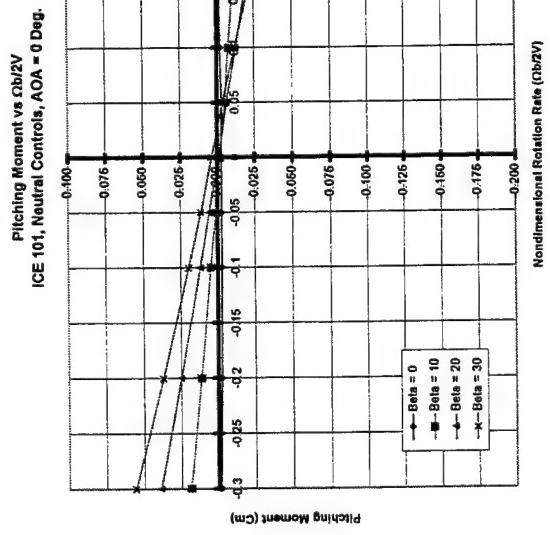


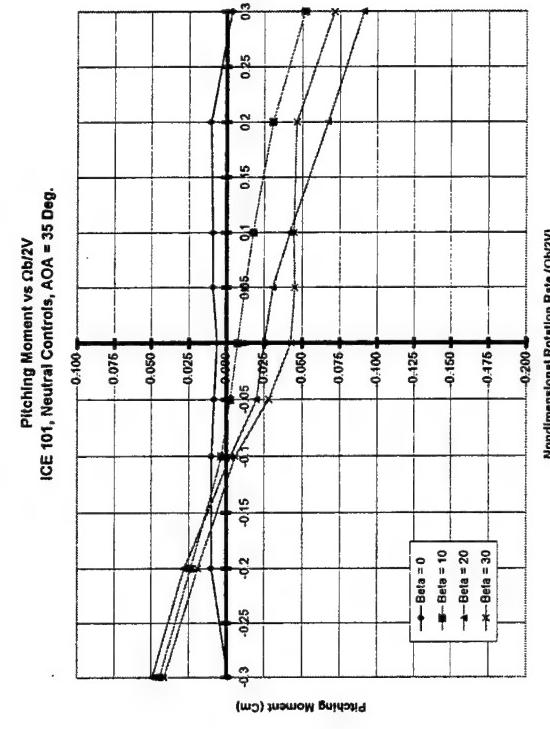
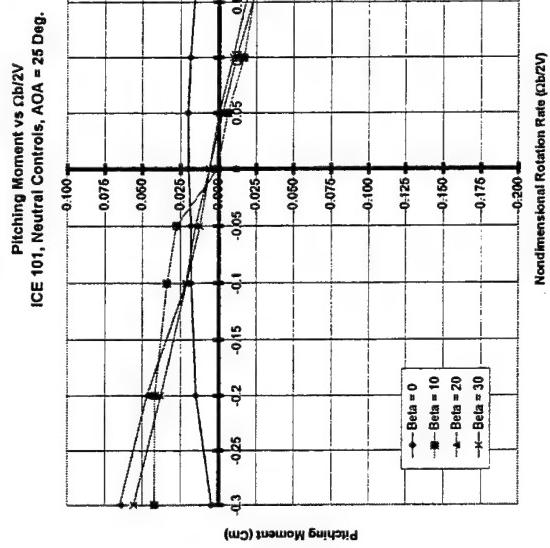
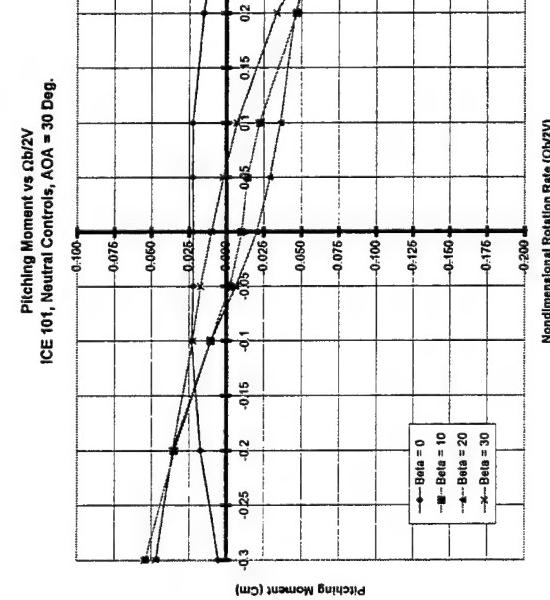
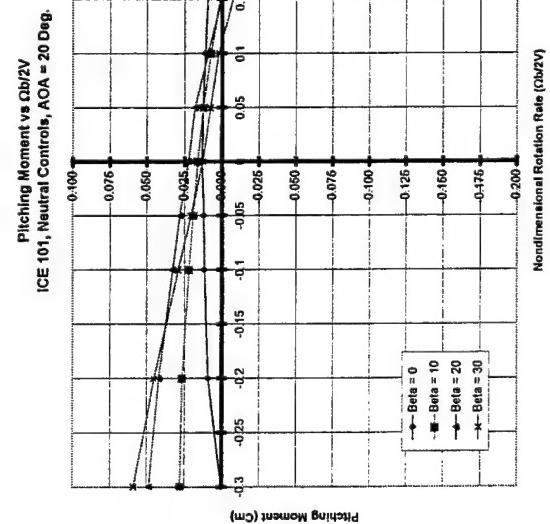


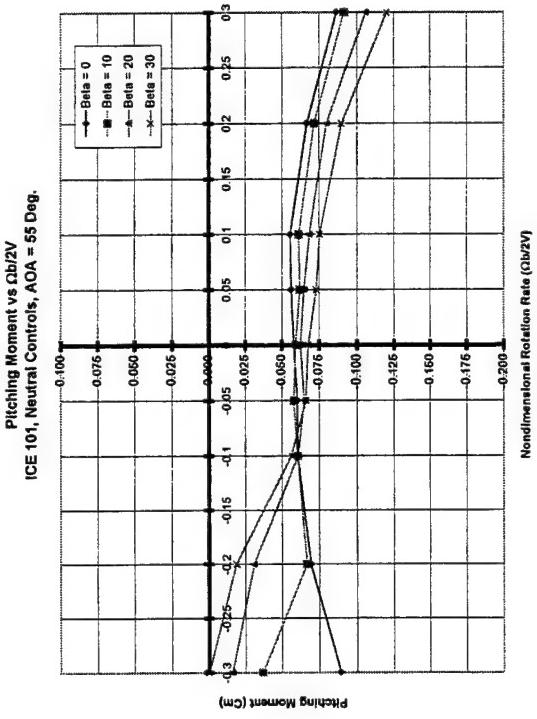
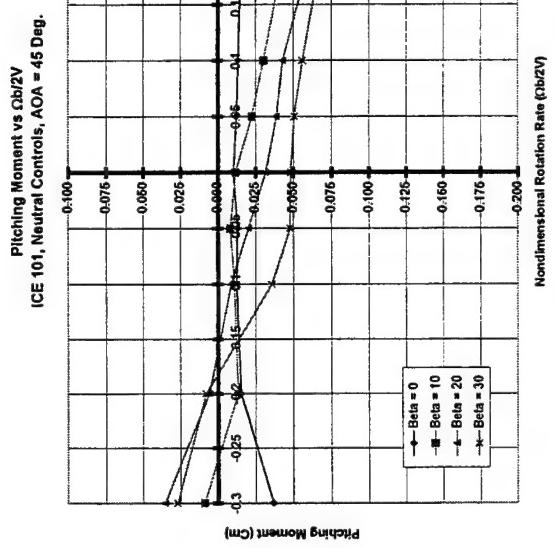
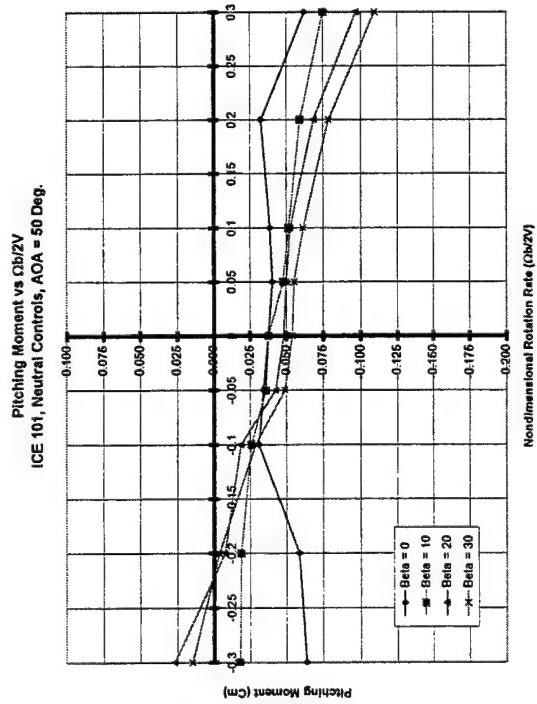
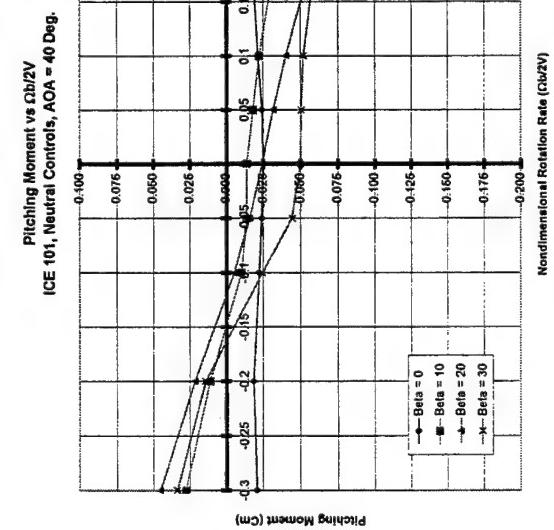


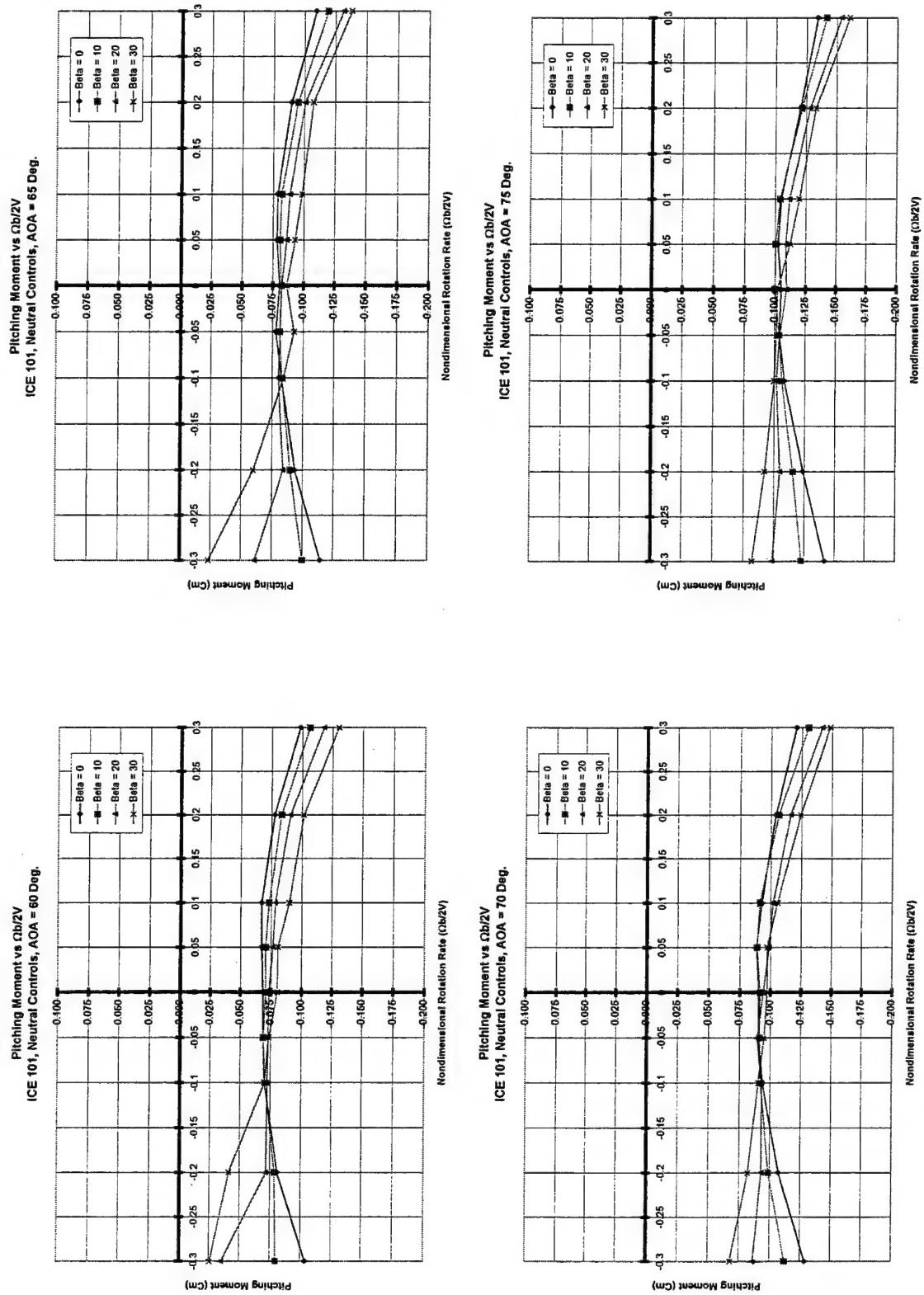




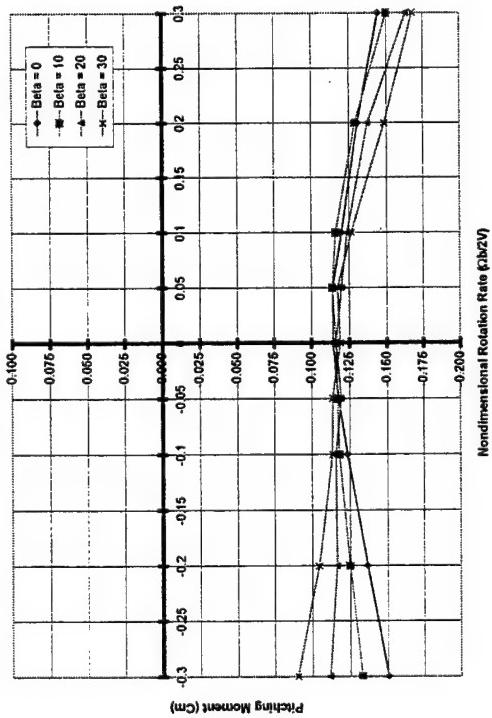




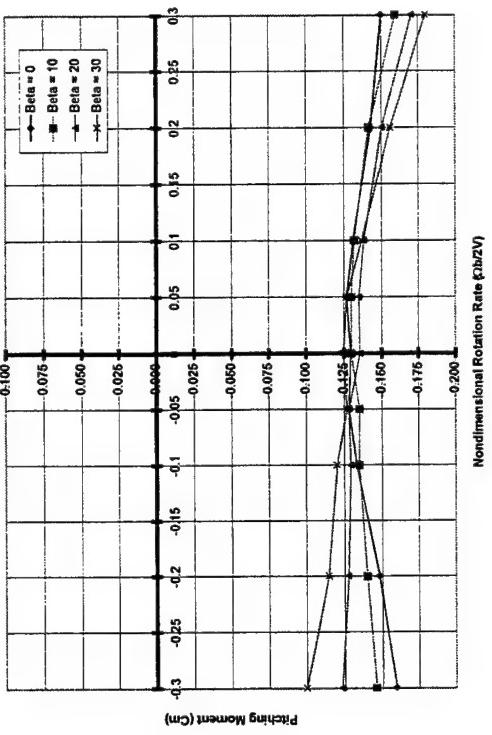




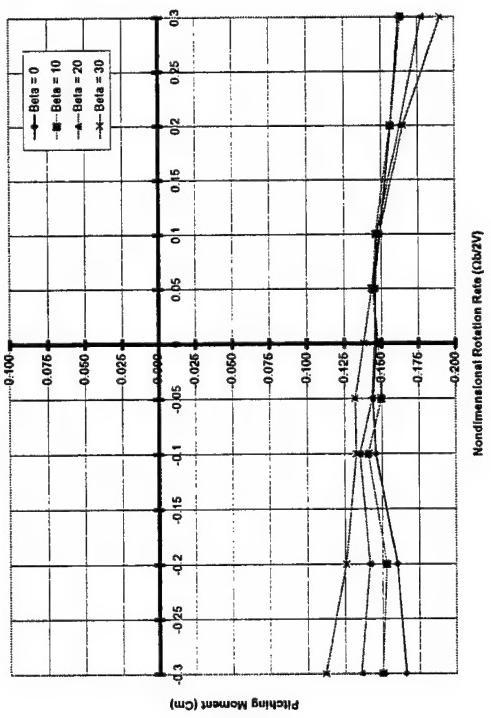
Pitching Moment vs $\Omega b/2V$
ICE 101, Neutral Controls, AOA = 80 Deg.

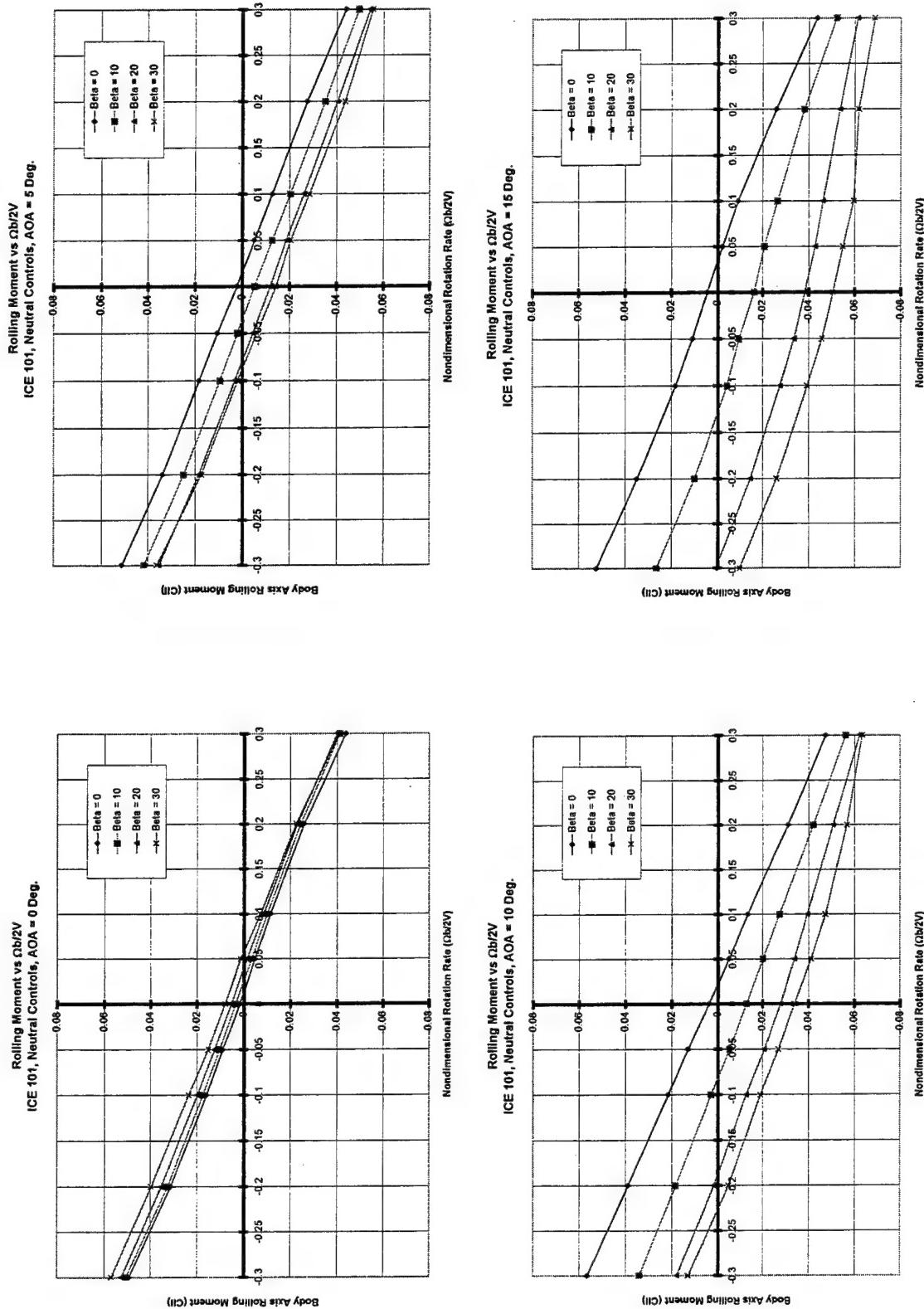


Pitching Moment vs $\Omega b/2V$
ICE 101, Neutral Controls, AOA = 85 Deg.

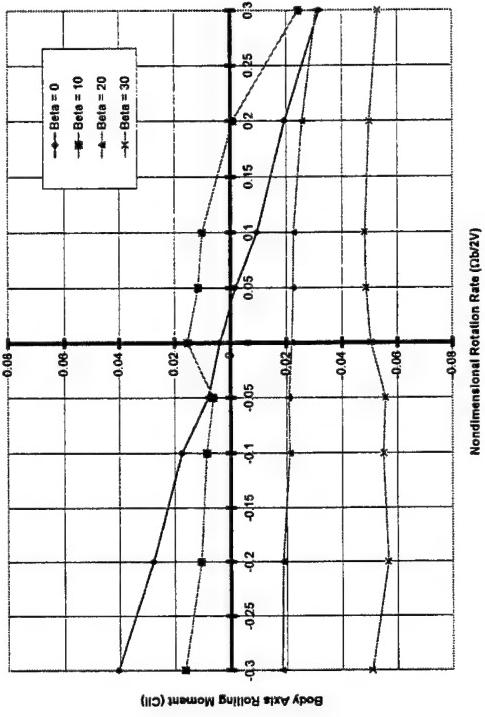


Pitching Moment vs $\Omega b/2V$
ICE 101, Neutral Controls, AOA = 80 Deg.

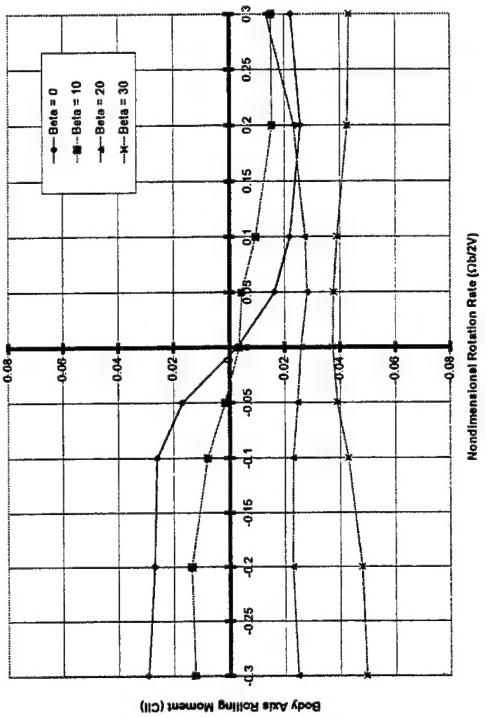




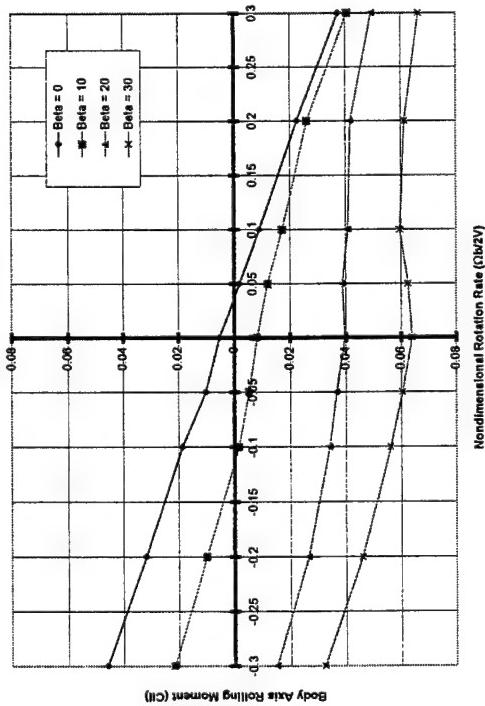
ICE 101, Neutral Controls, AOA = 25 Deg.



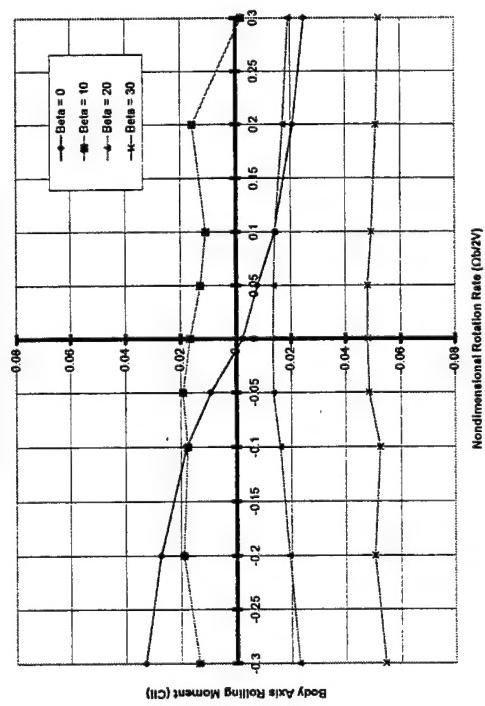
ICE 101, Neutral Controls, AOA = 35 Deg.

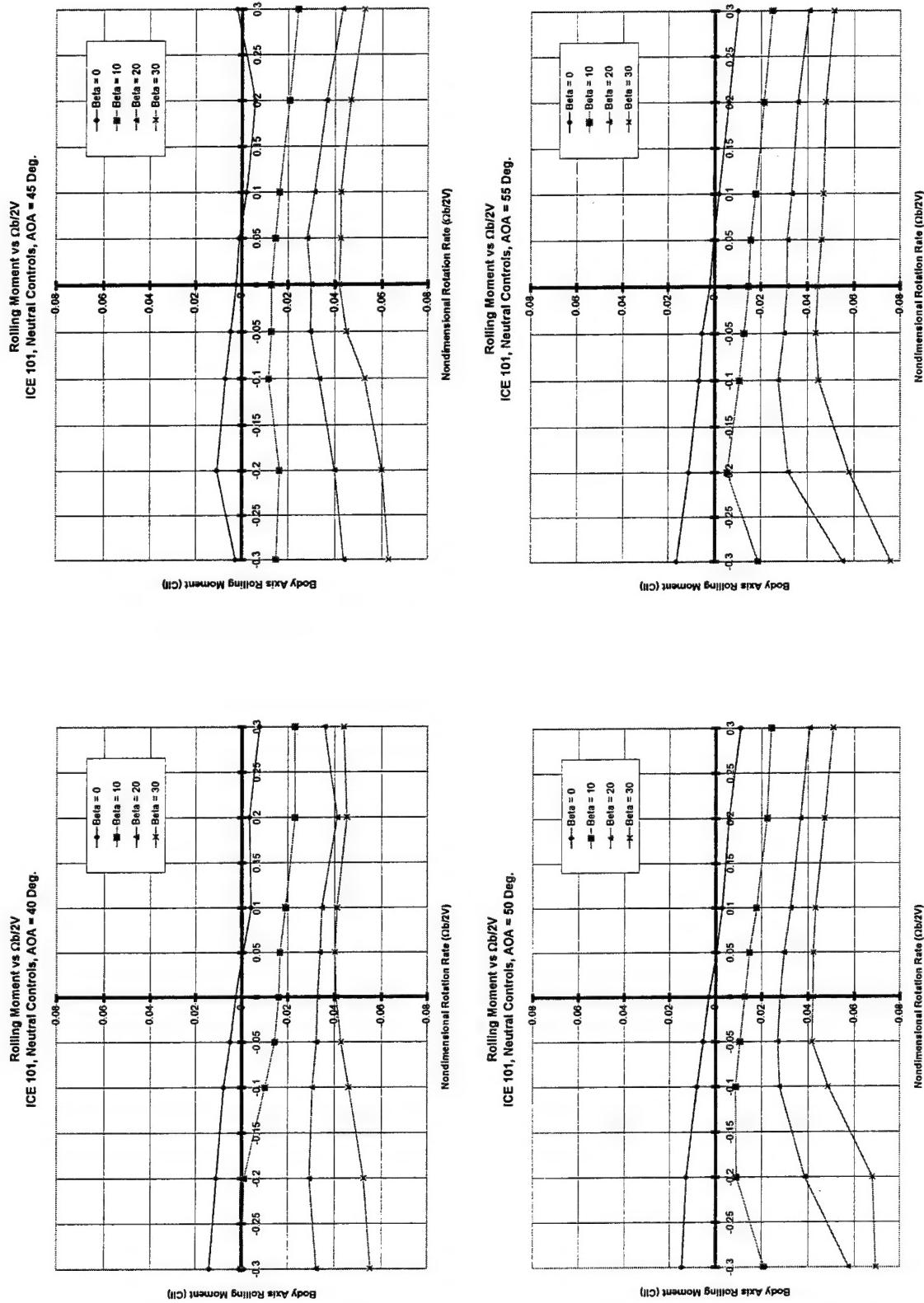


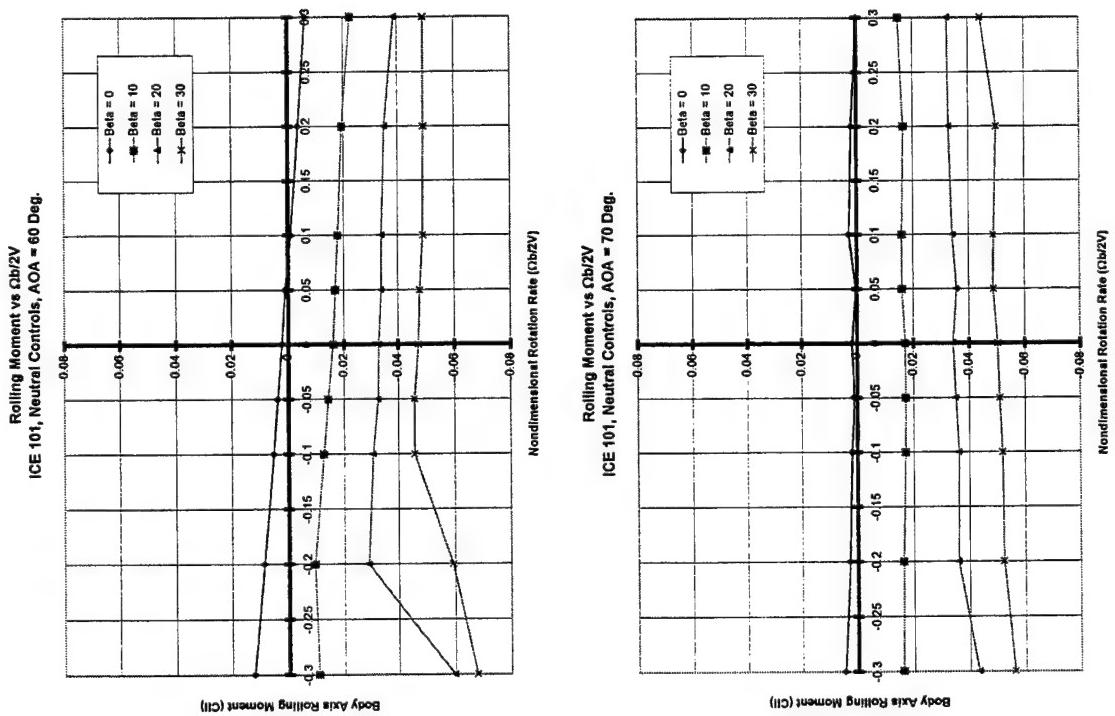
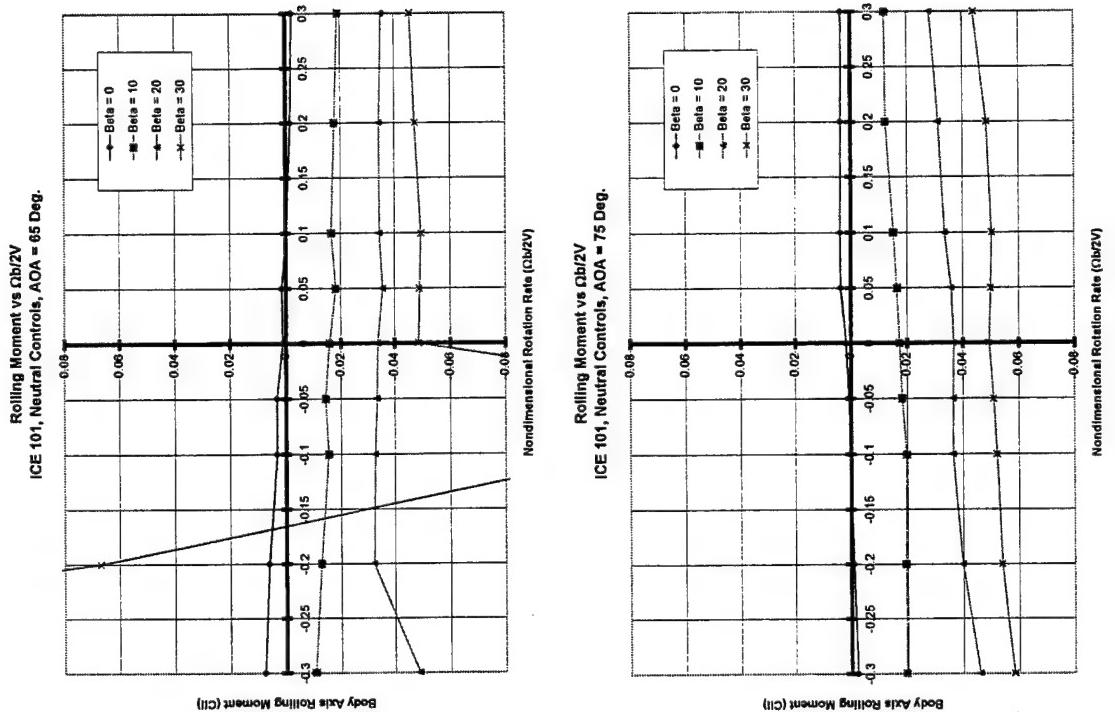
ICE 101, Neutral Controls, AOA = 20 Deg.

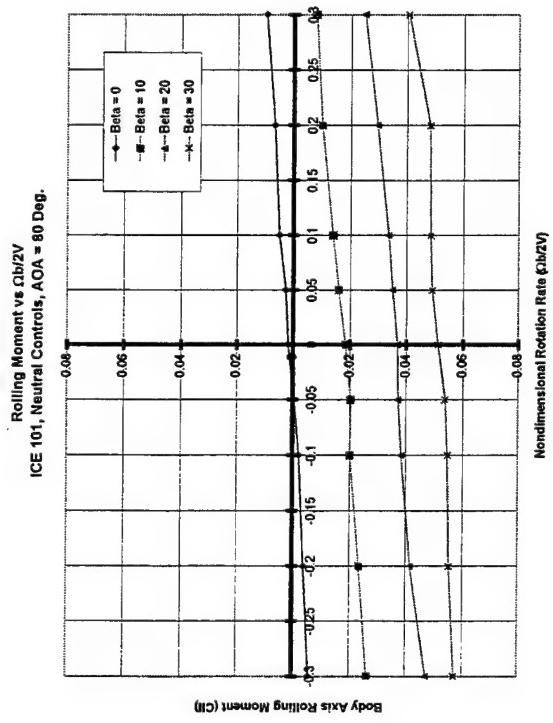
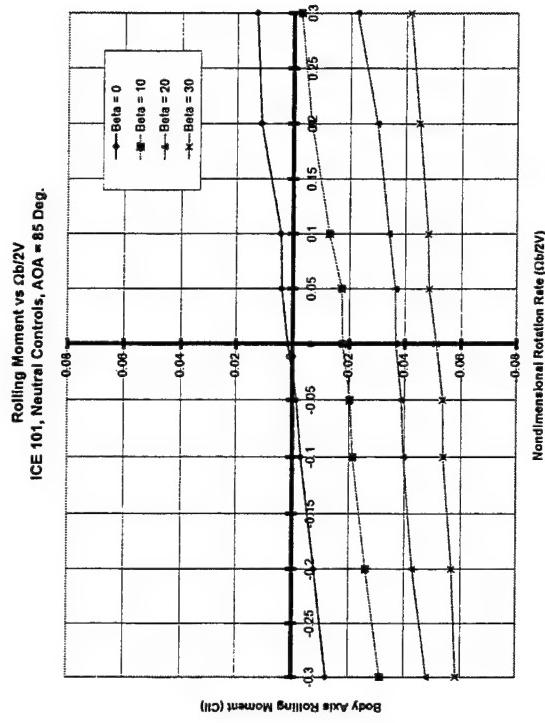


ICE 101, Neutral Controls, AOA = 30 Deg.



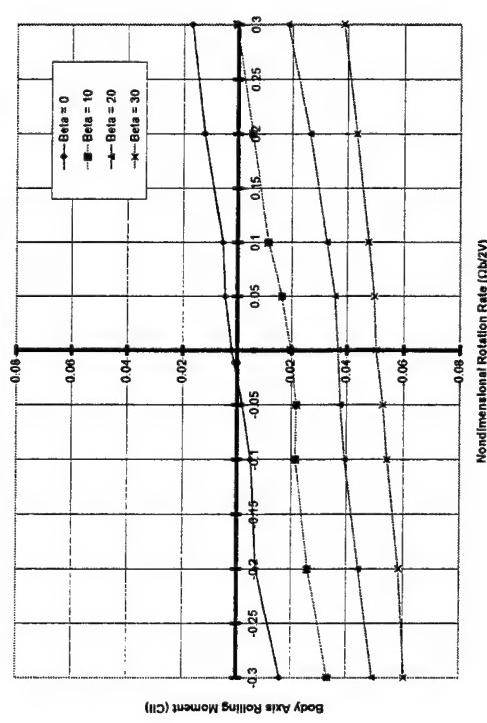






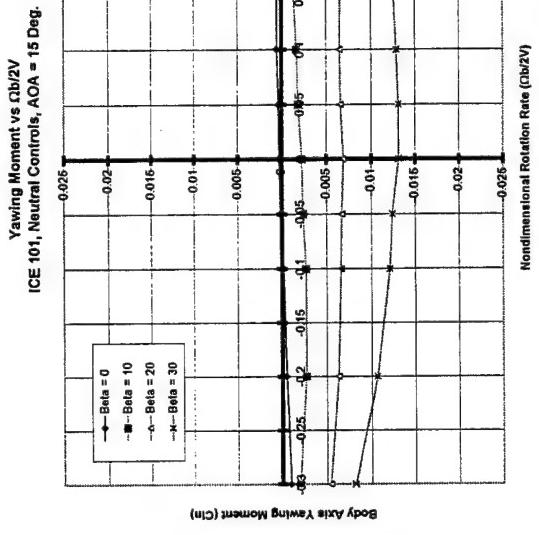
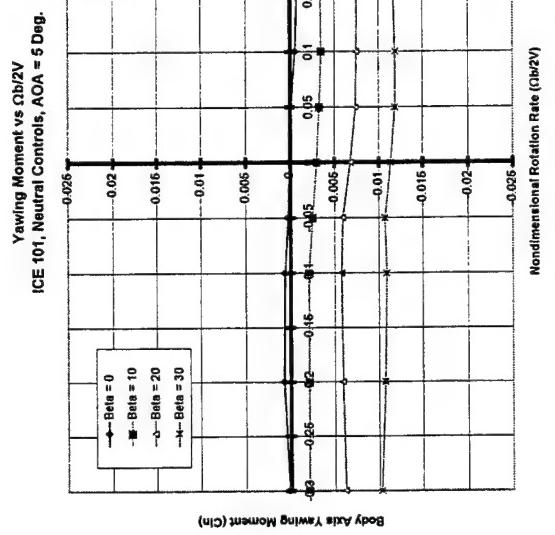
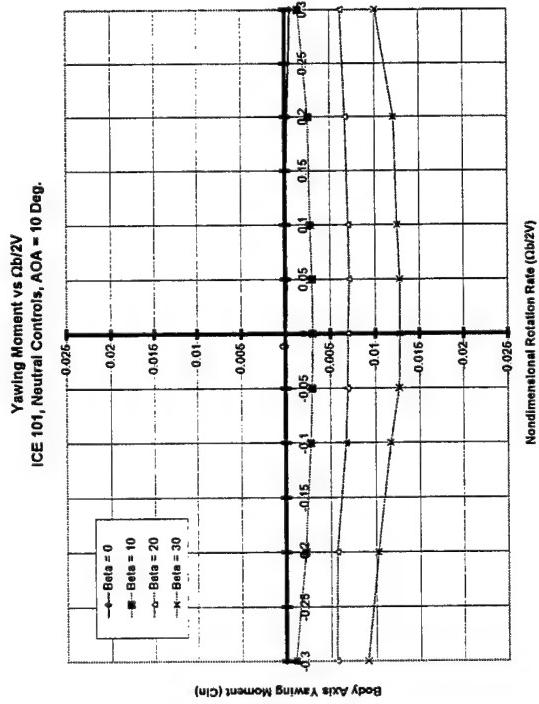
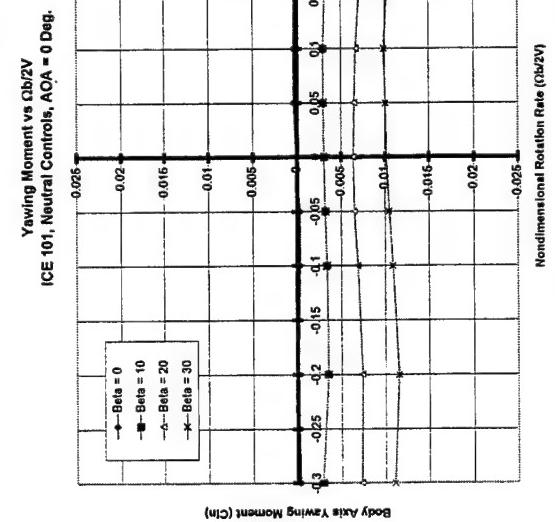
Nondimensional Rotation Rate ($\Omega b/2V$)

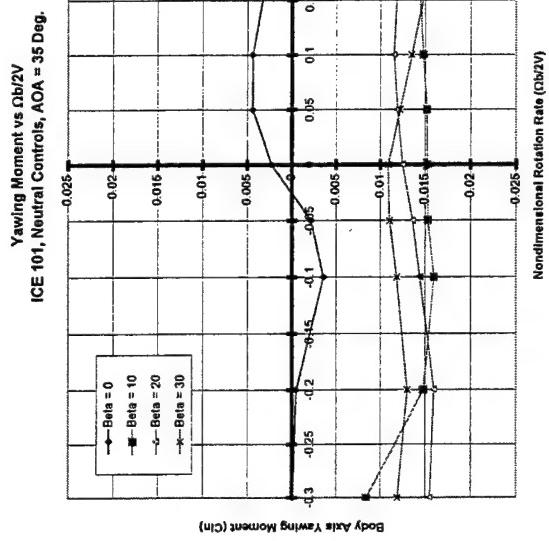
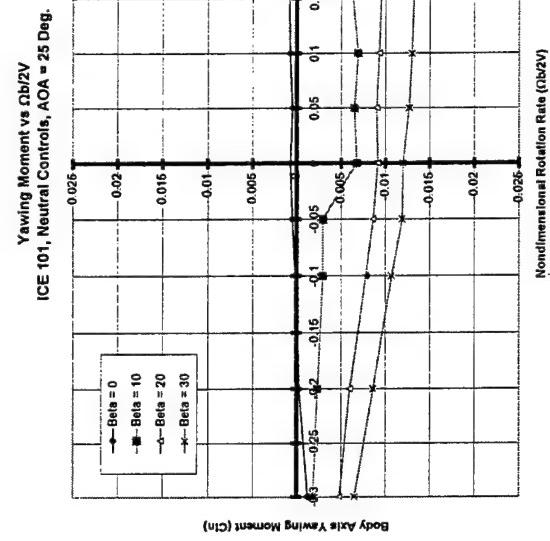
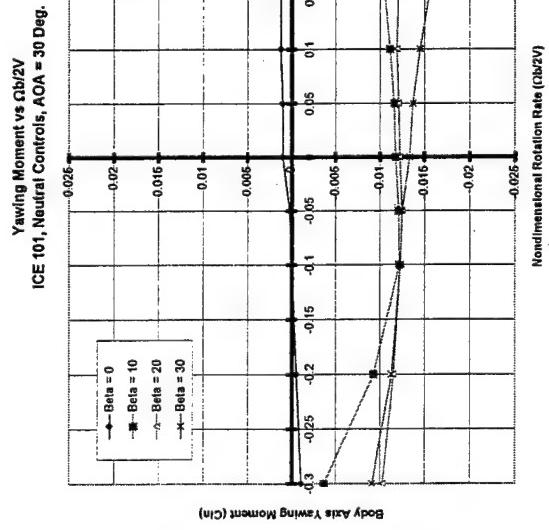
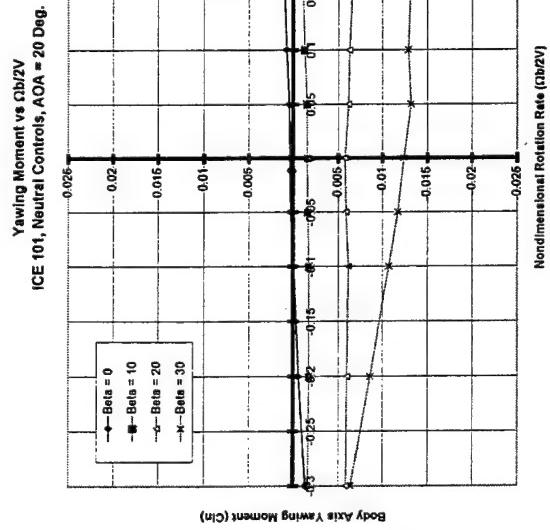
Nondimensional Rotation Rate ($\Omega b/2V$)

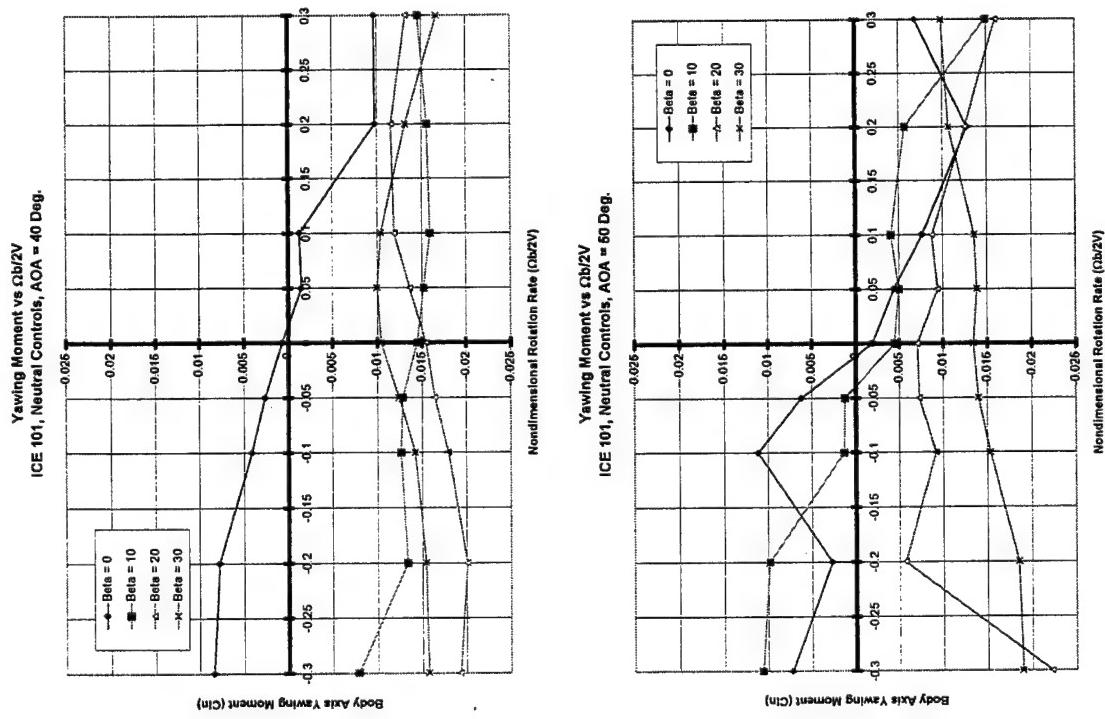
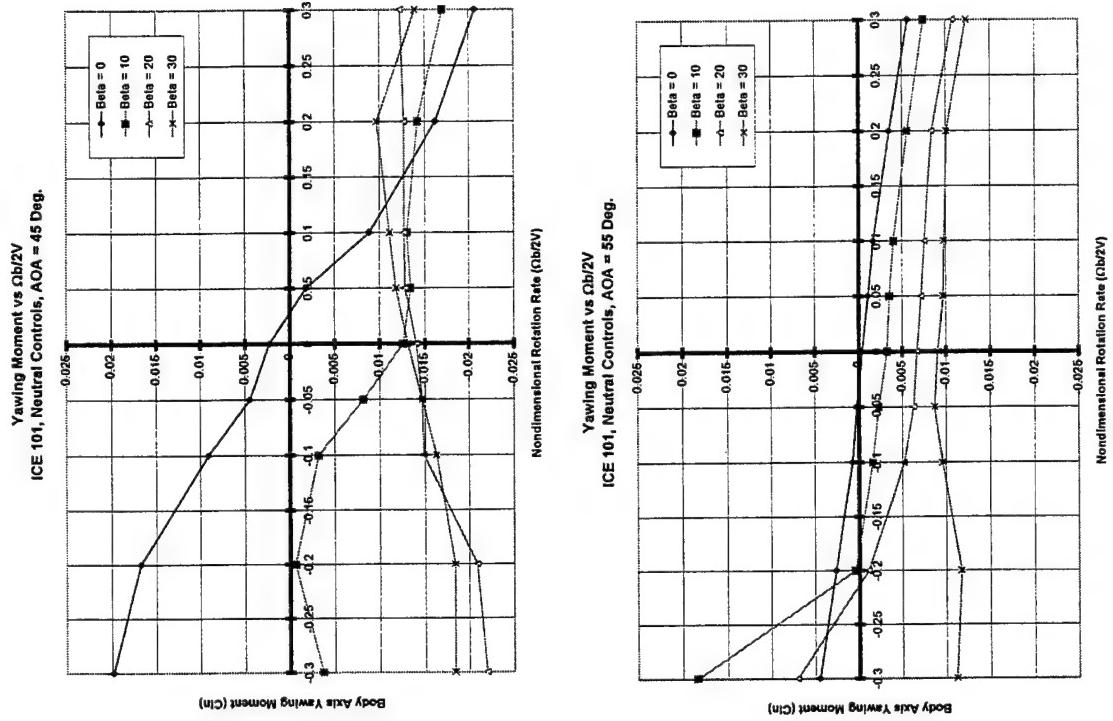


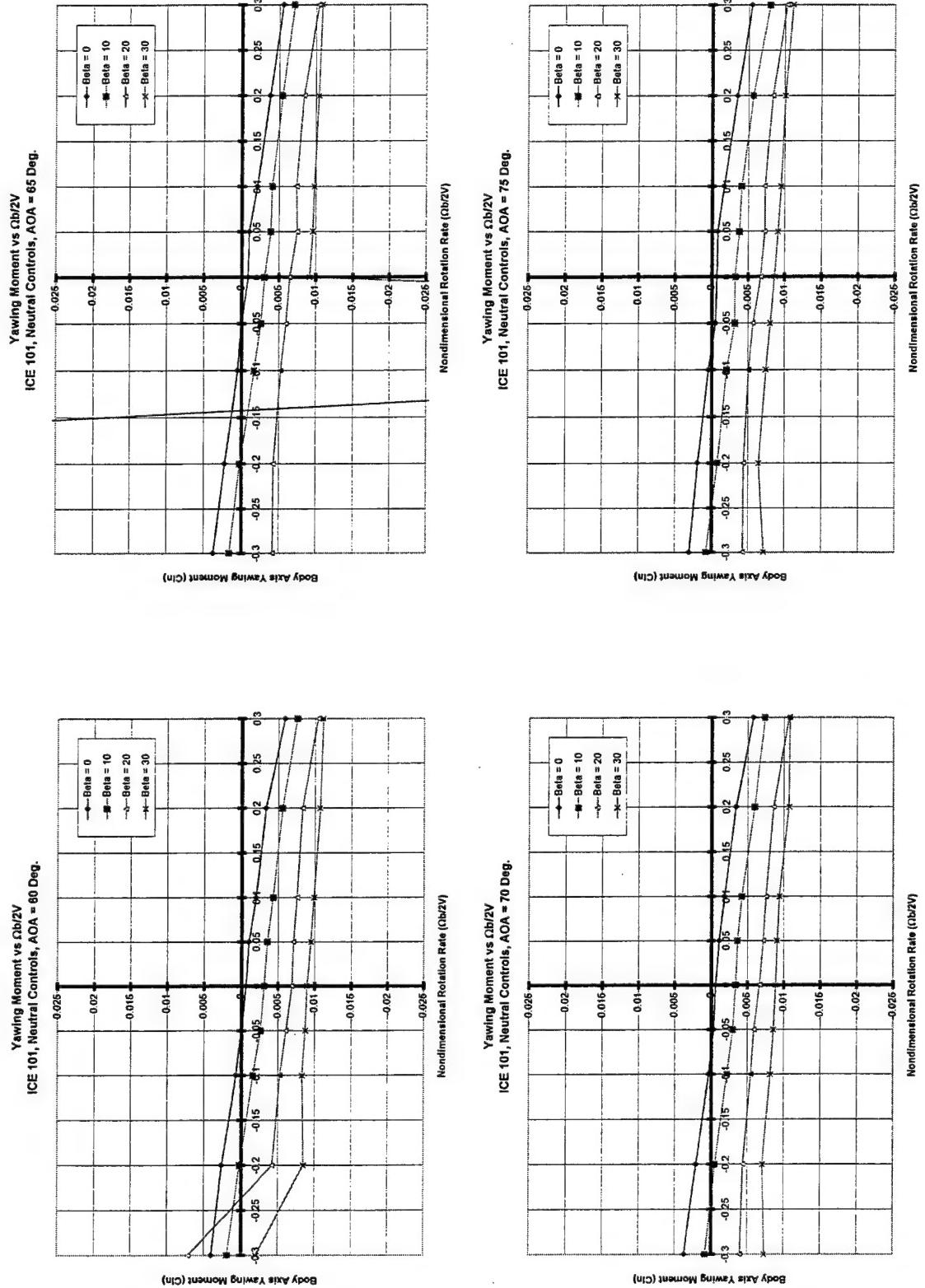
BODY AXIS ROLLING MOMENT (CL)

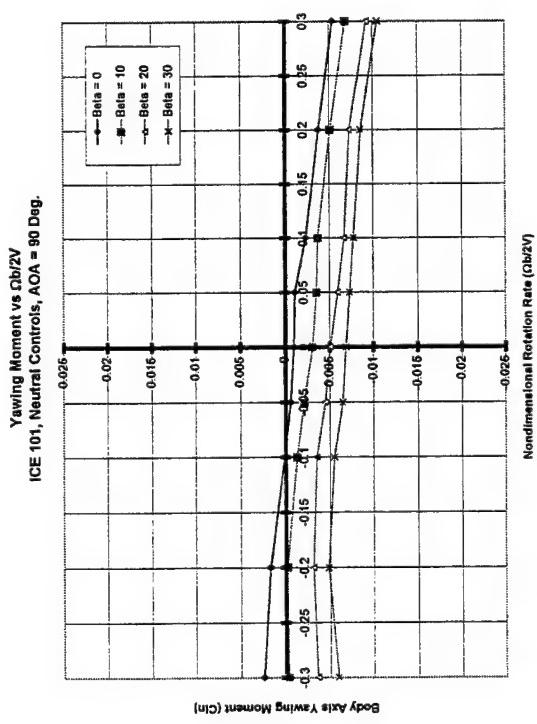
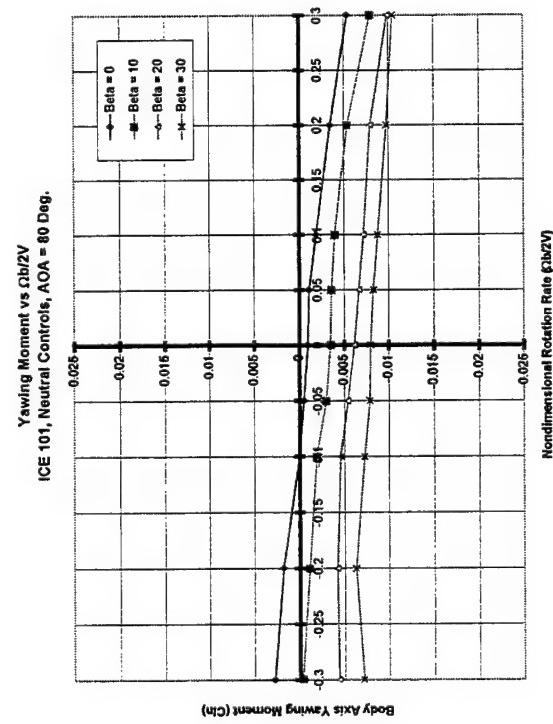
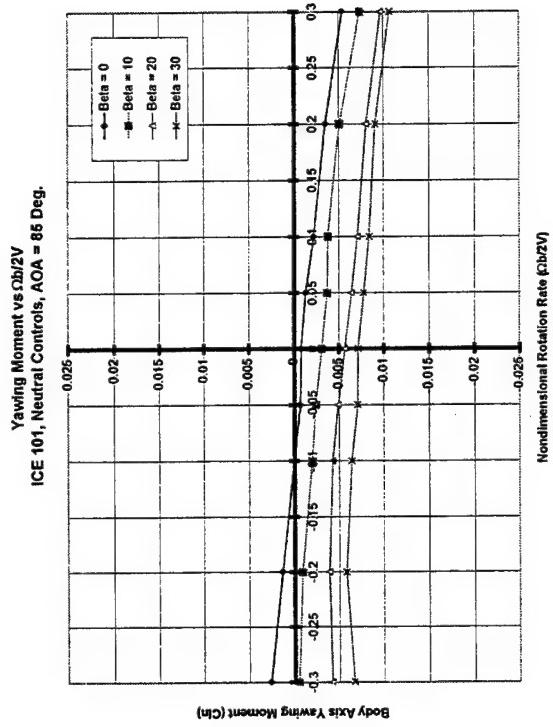
Nondimensional Rotation Rate ($\Omega b/2V$)









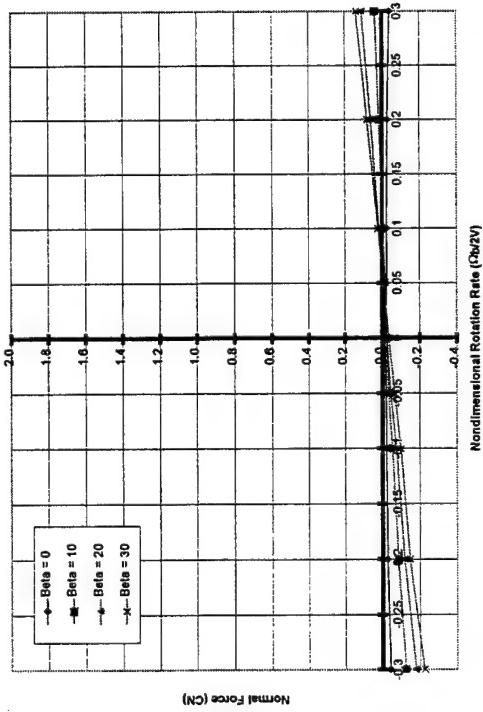


Appendix B

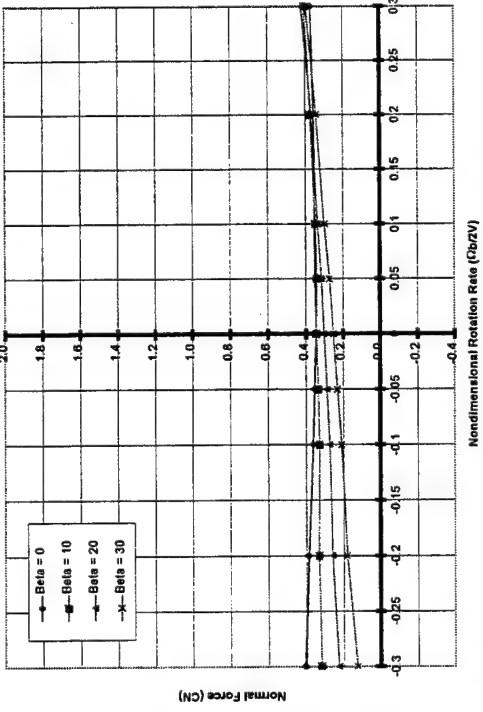
Rotary Balance Data Plots

Neutral Controls, LEF = 30/30

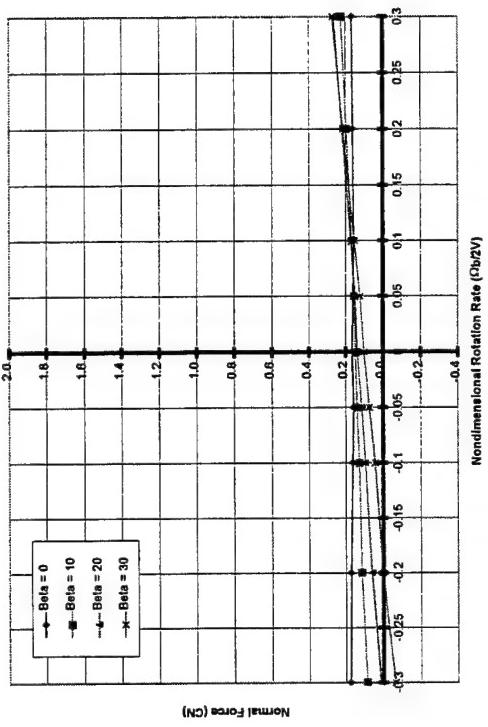
Normal Force vs $\bar{Q}_b/2V$
ICE 101, LEF = 30/30, AOA = 0 Deg.



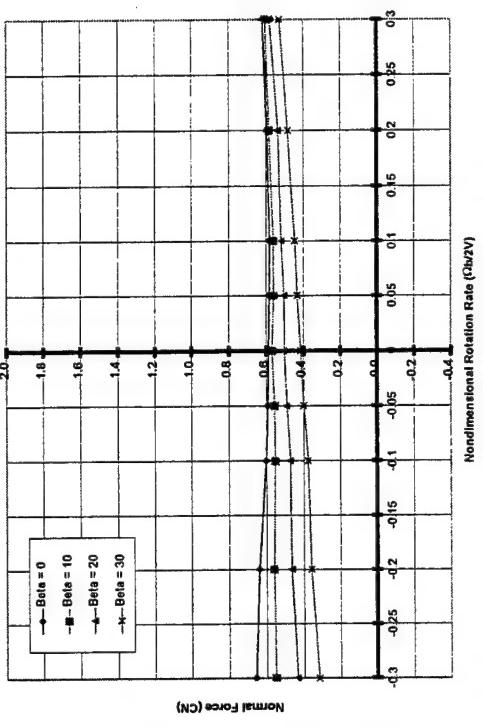
Normal Force vs $\bar{Q}_b/2V$
ICE 101, LEF = 30/30, AOA = 10 Deg.



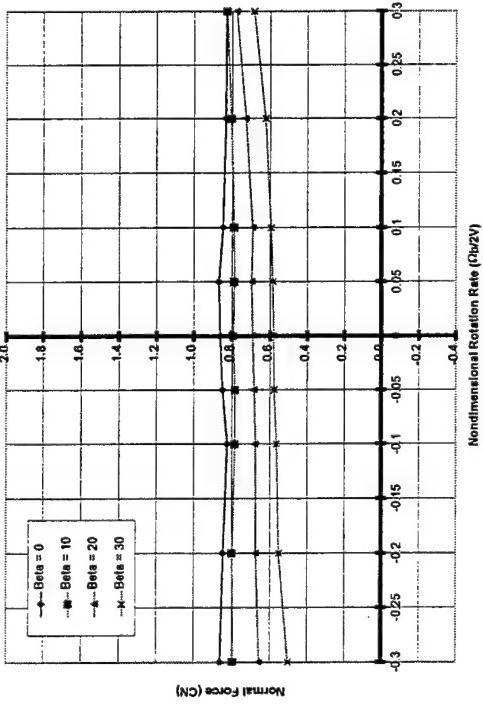
Normal Force vs $\bar{Q}_b/2V$
ICE 101, LEF = 30/30, AOA = 5 Deg.



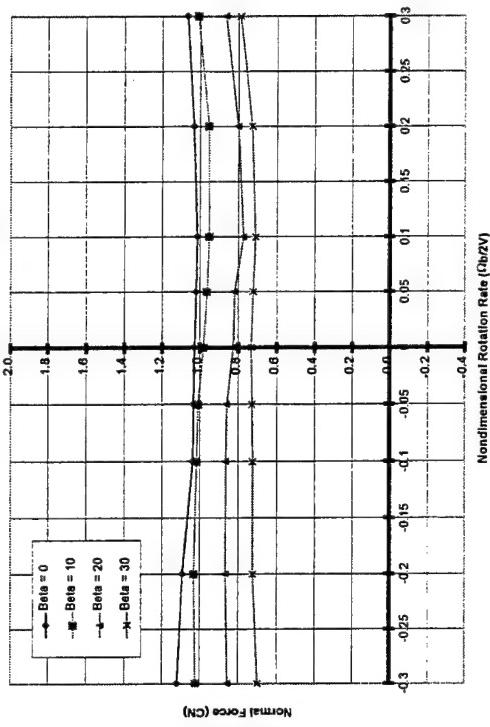
Normal Force vs $\bar{Q}_b/2V$
ICE 101, LEF = 30/30, AOA = 15 Deg.



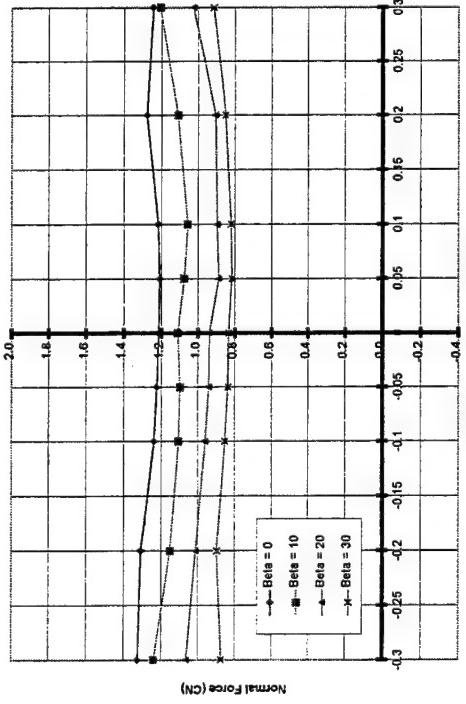
Normal Force vs $\Omega b/2V$
ICE 101, LEF = 30/30, AOA = 20 Deg.



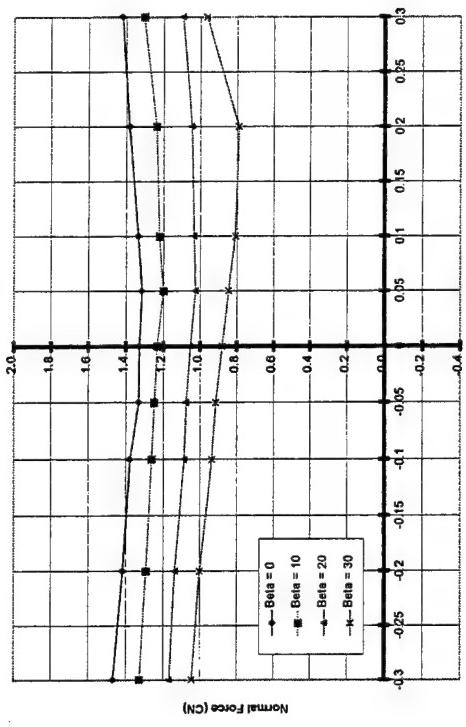
Normal Force vs $\Omega b/2V$
ICE 101, LEF = 30/30, AOA = 25 Deg.

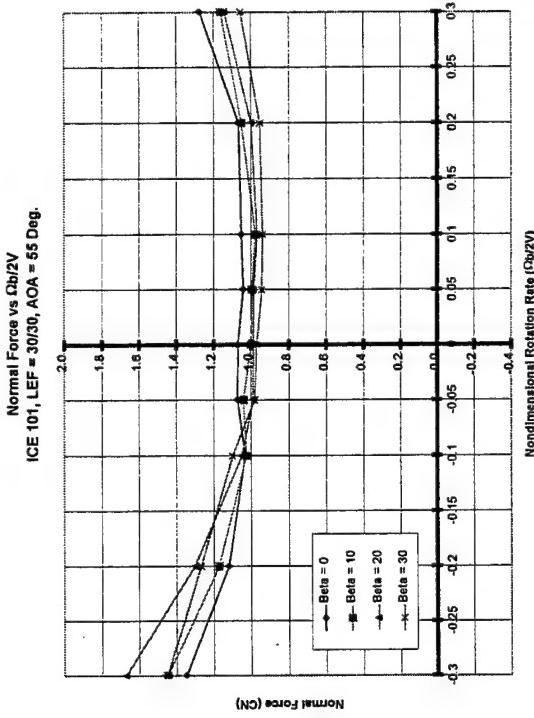
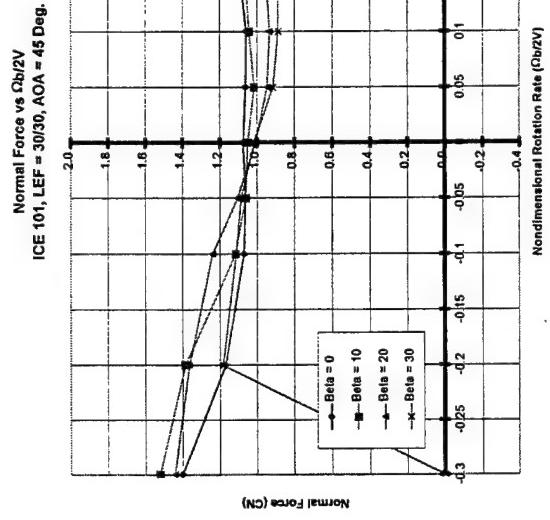
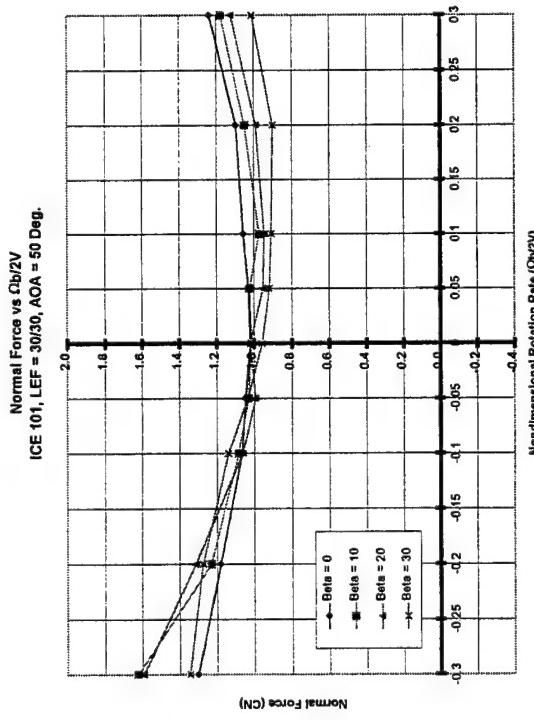
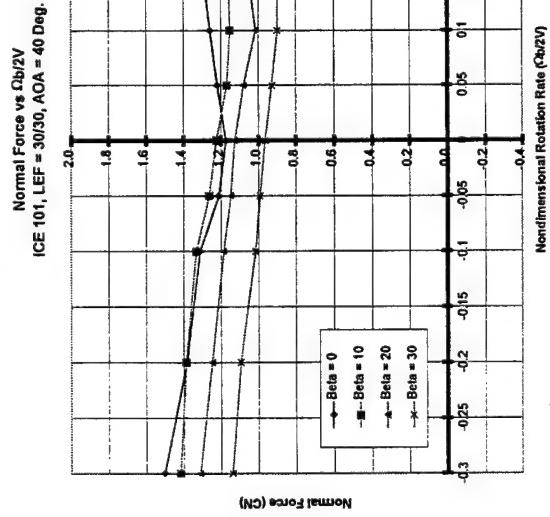


Normal Force vs $\Omega b/2V$
ICE 101, LEF = 30/30, AOA = 30 Deg.

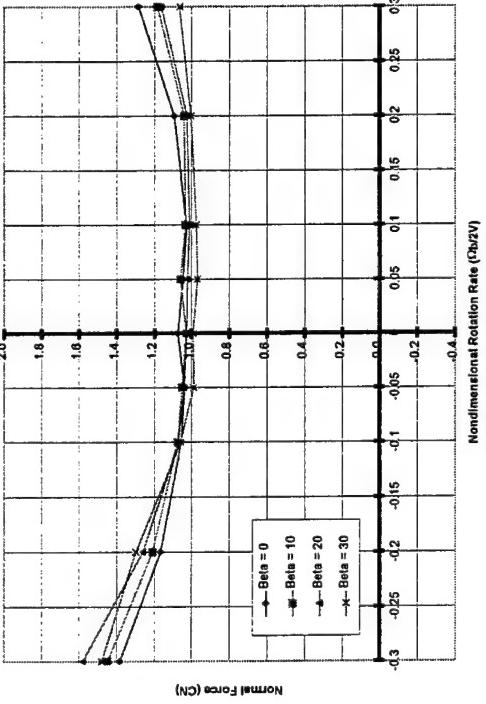


Normal Force vs $\Omega b/2V$
ICE 101, LEF = 30/30, AOA = 35 Deg.

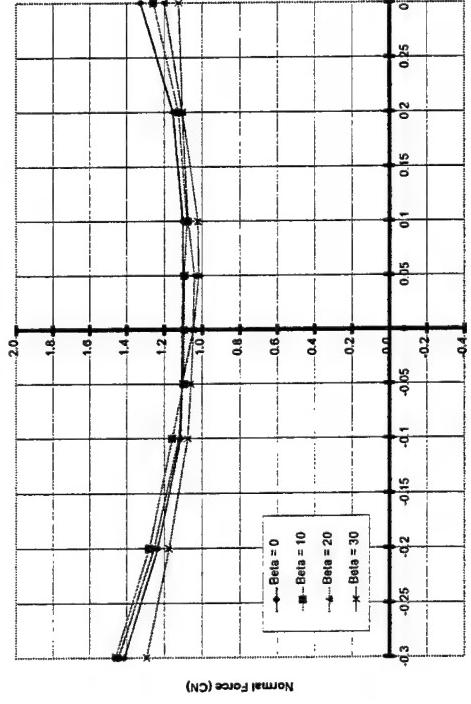




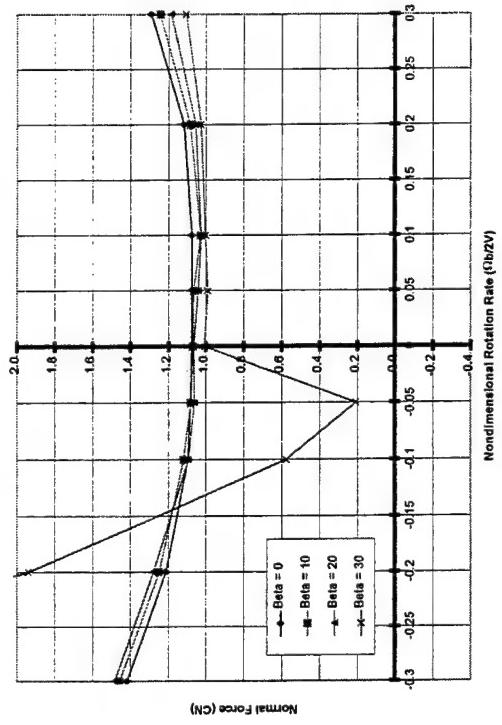
Normal Force vs $\Omega b/2V$
ICE 101, LEF = 30/30, AOA = 60 Deg.



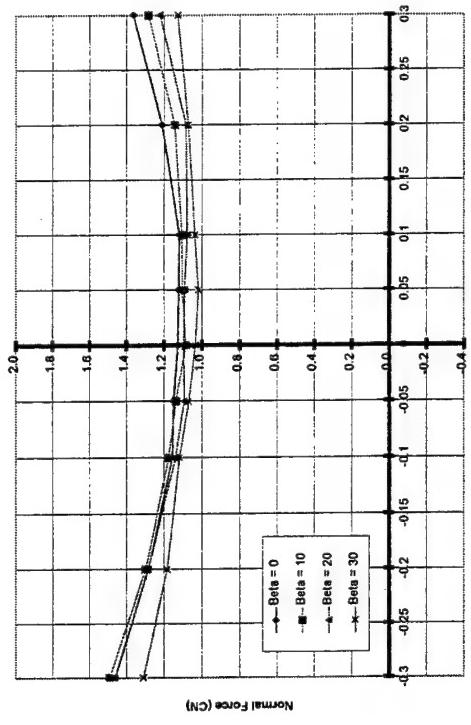
Normal Force vs $\Omega b/2V$
ICE 101, LEF = 30/30, AOA = 70 Deg.



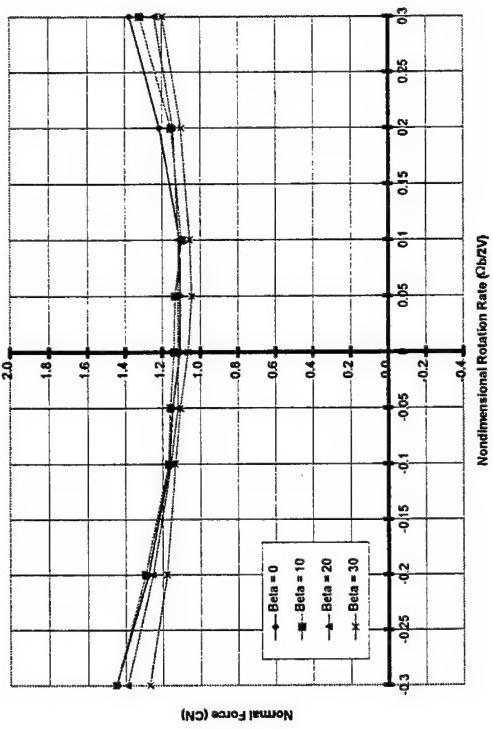
Normal Force vs $\Omega b/2V$
ICE 101, LEF = 30/30, AOA = 65 Deg.



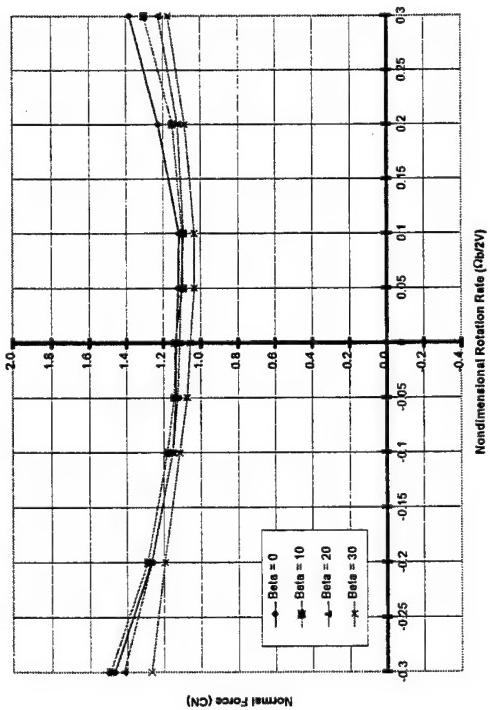
Normal Force vs $\Omega b/2V$
ICE 101, LEF = 30/30, AOA = 75 Deg.



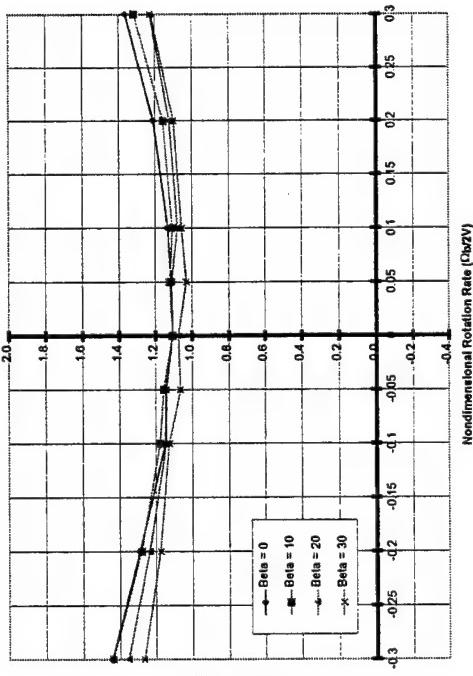
Normal Force vs $\Omega b/2V$
ICE 101, LEF = 30/30, AOA = 85 Deg.

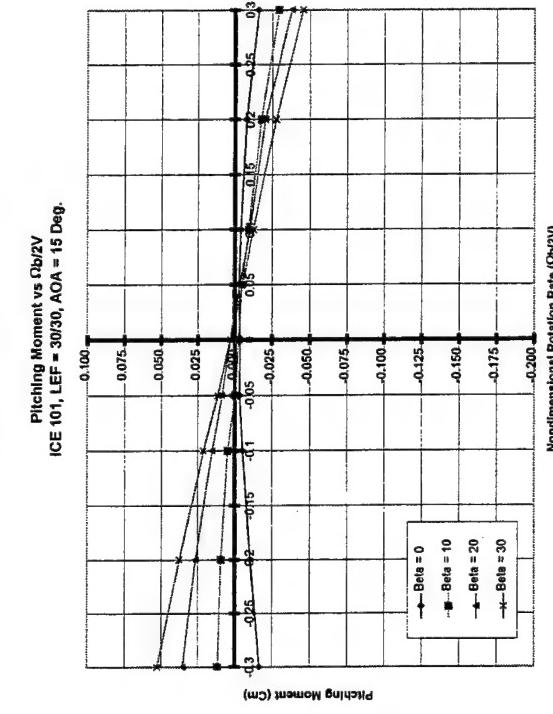
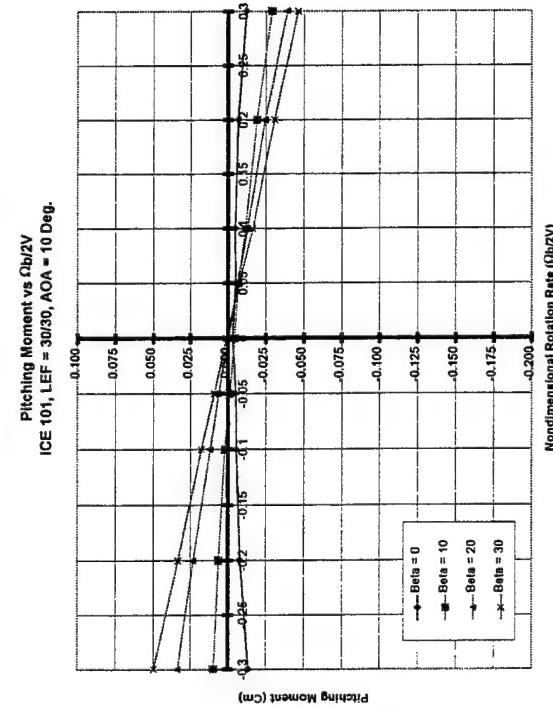
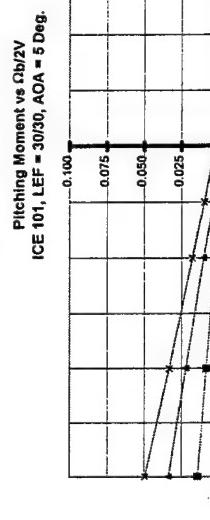
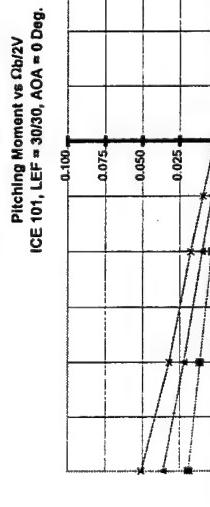


Normal Force vs $\Omega b/2V$
ICE 101, LEF = 30/30, AOA = 80 Deg.

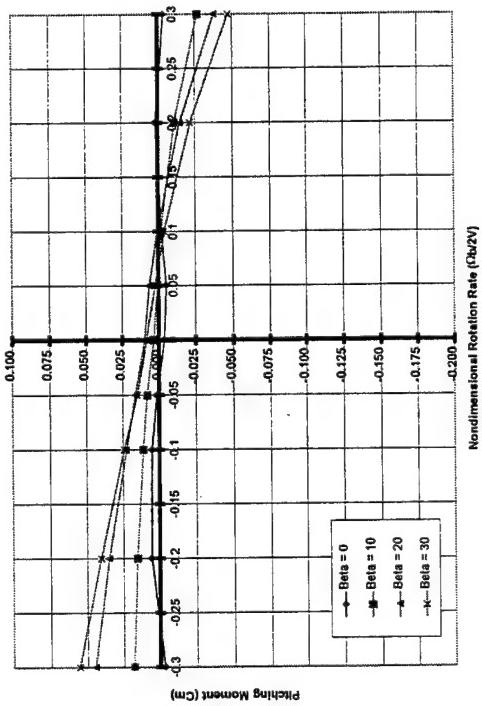


Normal Force vs $\Omega b/2V$
ICE 101, LEF = 30/30, AOA = 90 Deg.

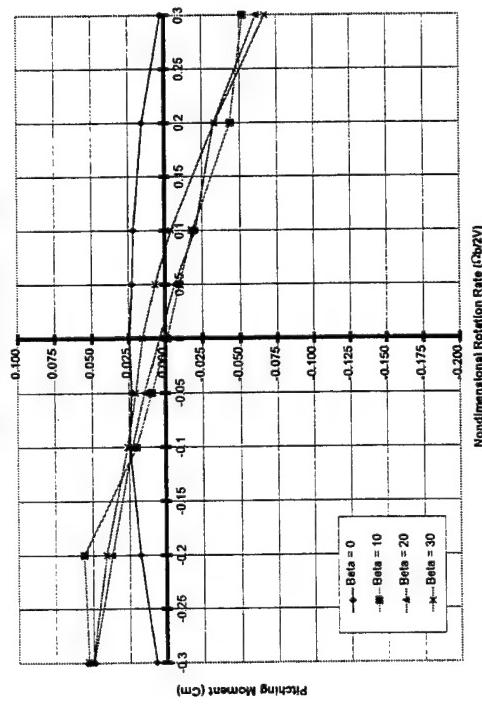




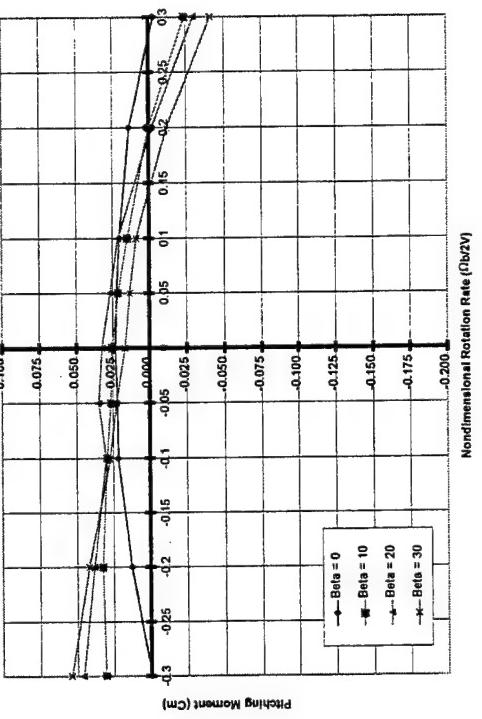
Pitching Moment vs $\Omega b/2V$
ICE 101, LEF = 30/30, AOA = 20 Deg.



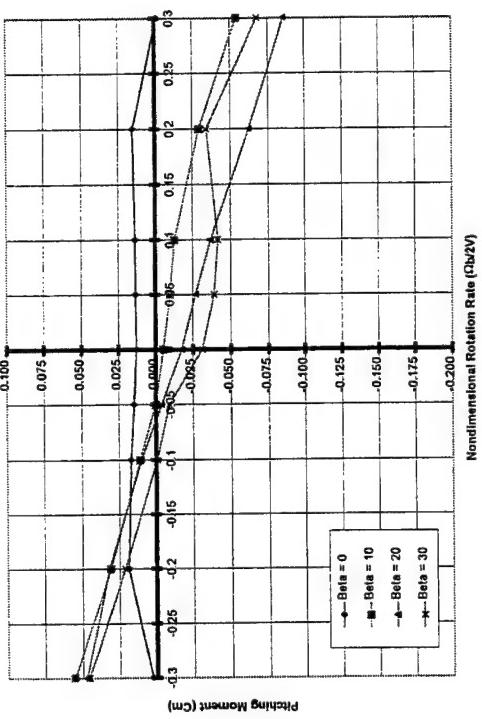
Pitching Moment vs $\Omega b/2V$
ICE 101, LEF = 30/30, AOA = 30 Deg.

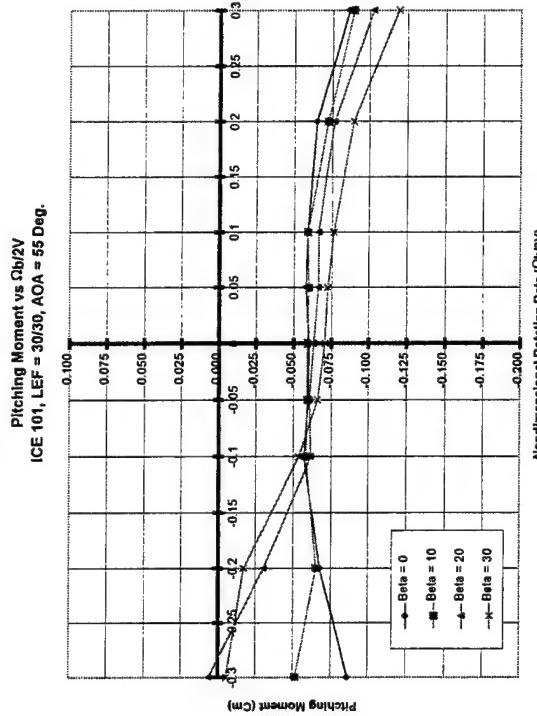
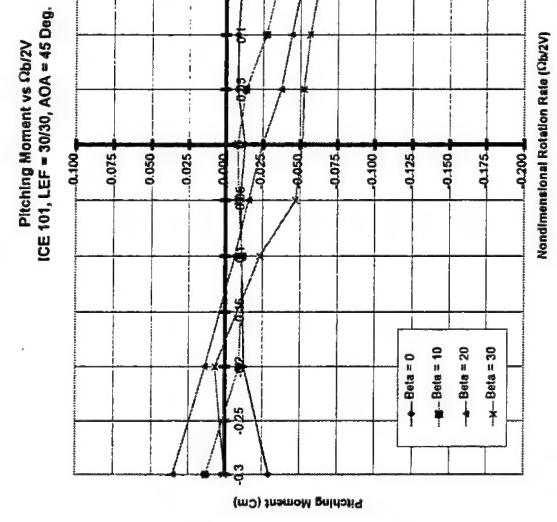
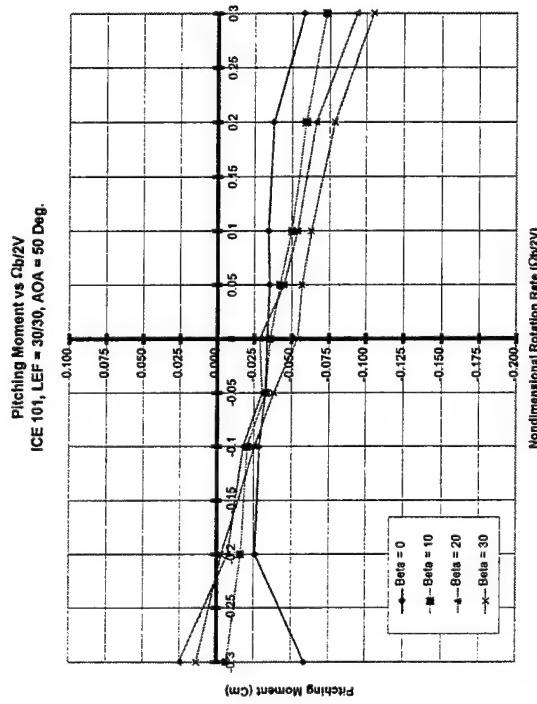
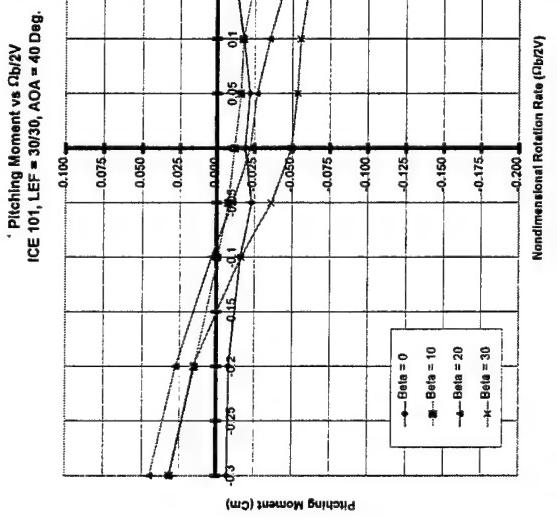


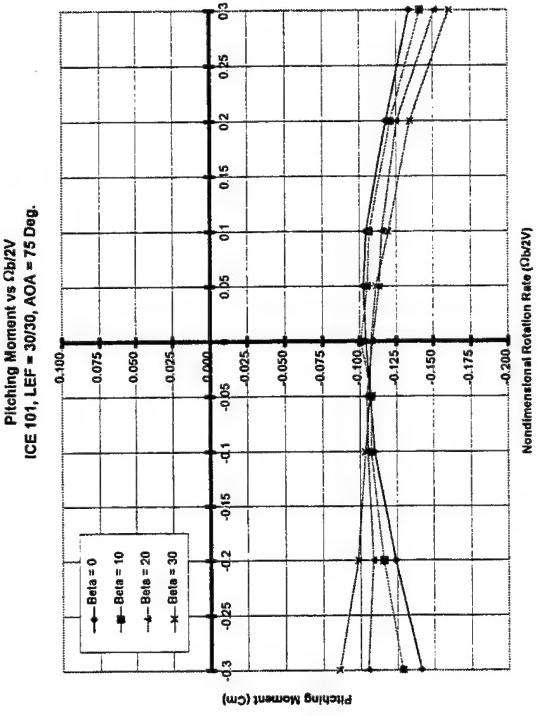
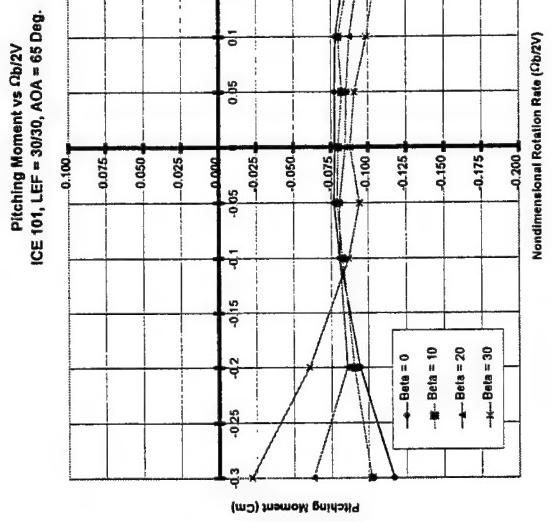
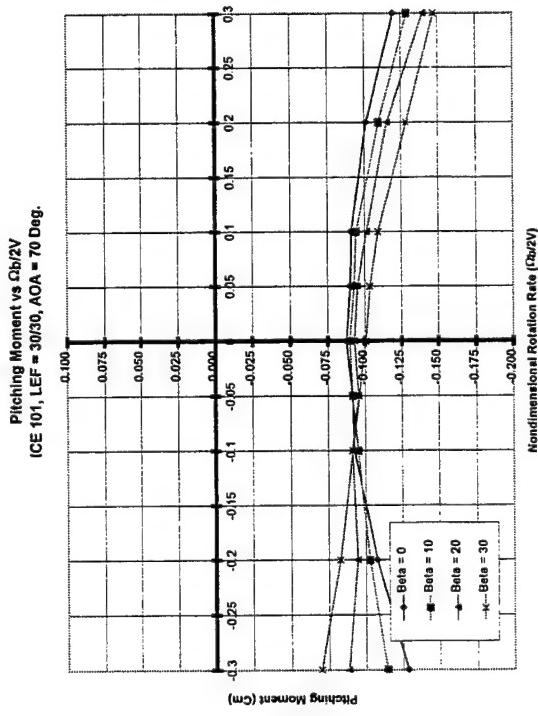
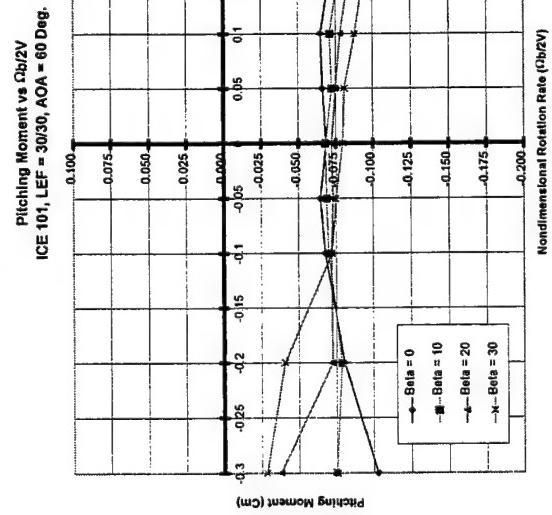
Pitching Moment vs $\Omega b/2V$
ICE 101, LEF = 30/30, AOA = 25 Deg.

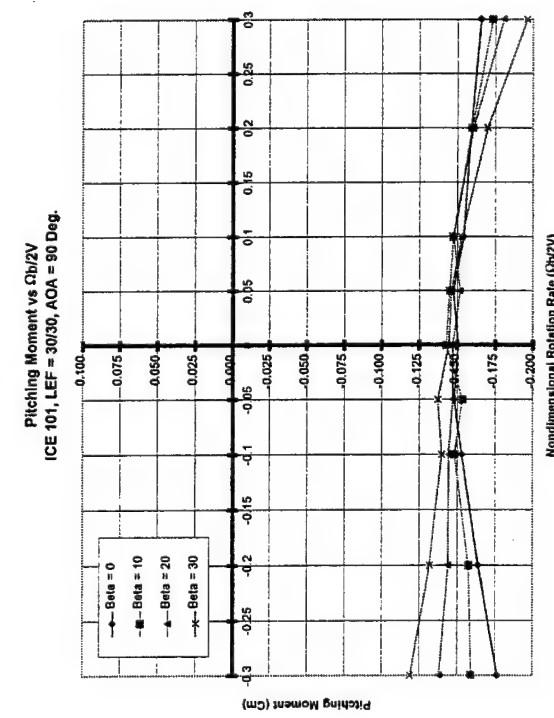
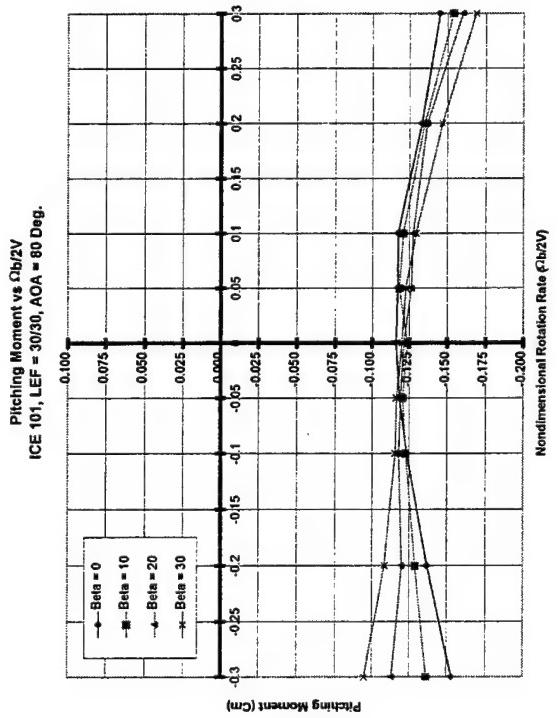
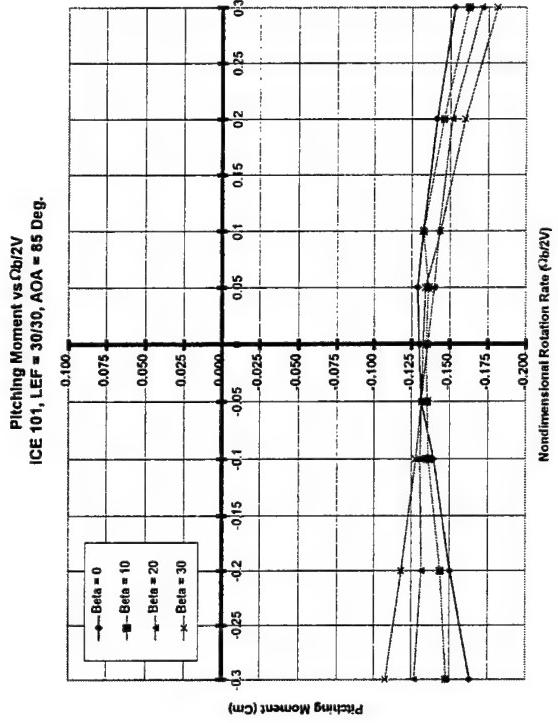


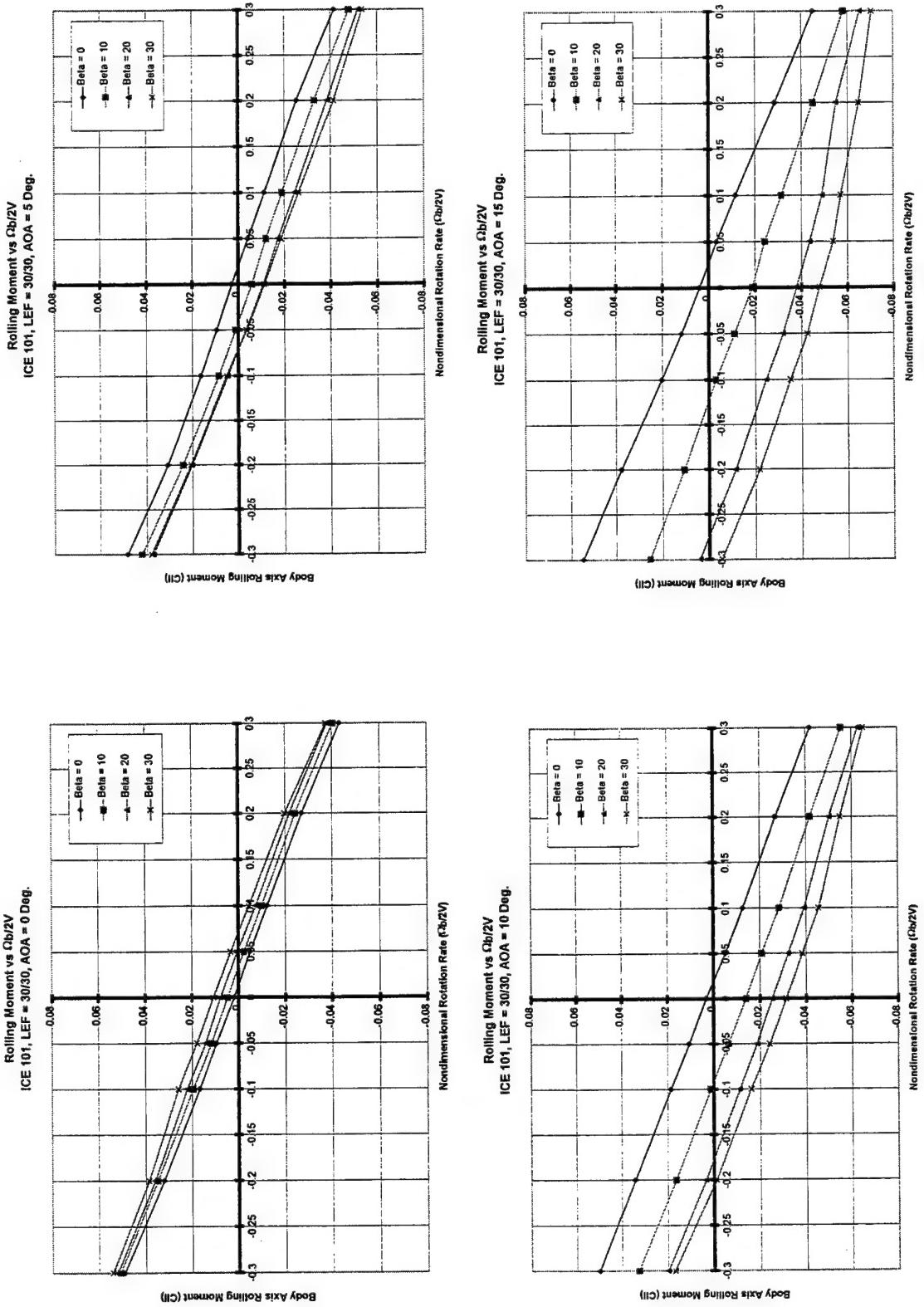
Pitching Moment vs $\Omega b/2V$
ICE 101, LEF = 30/30, AOA = 35 Deg.

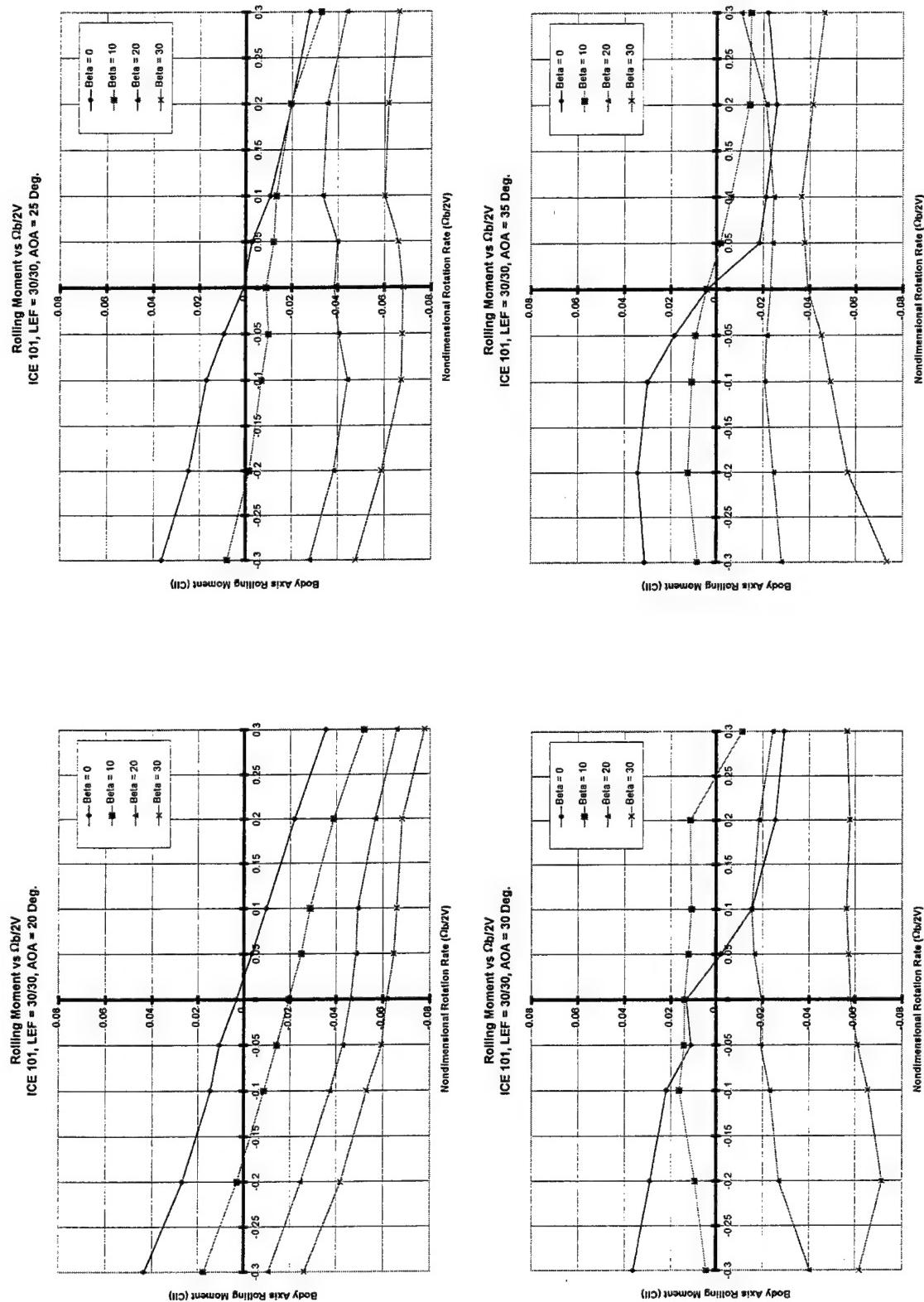


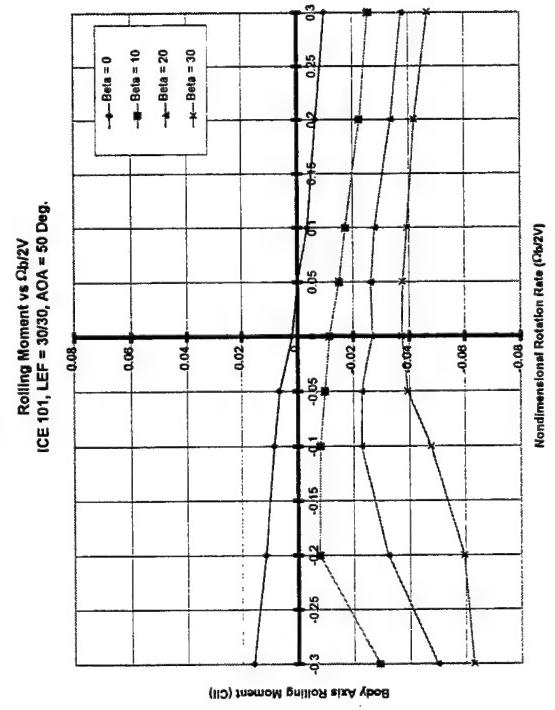
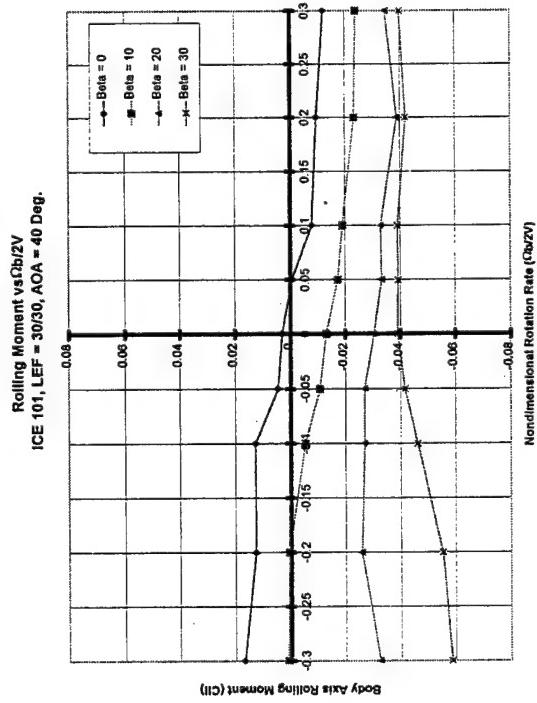
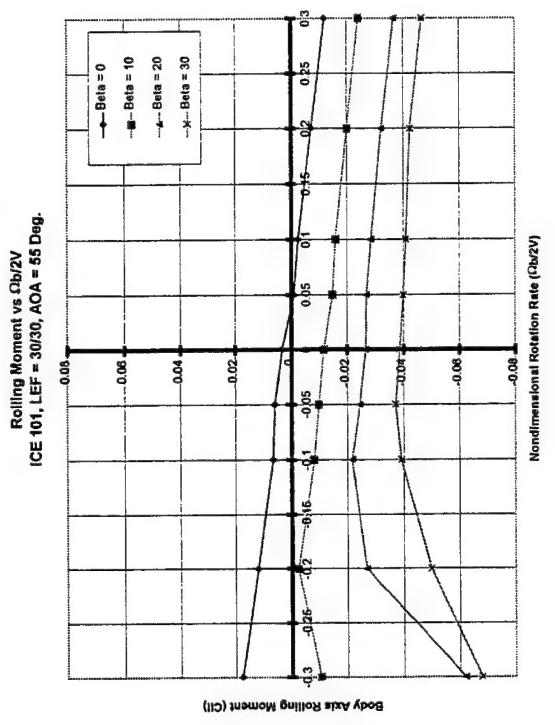
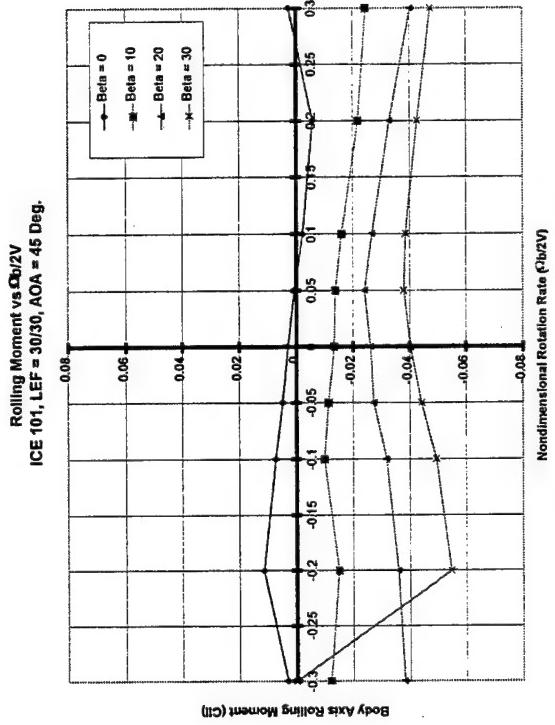




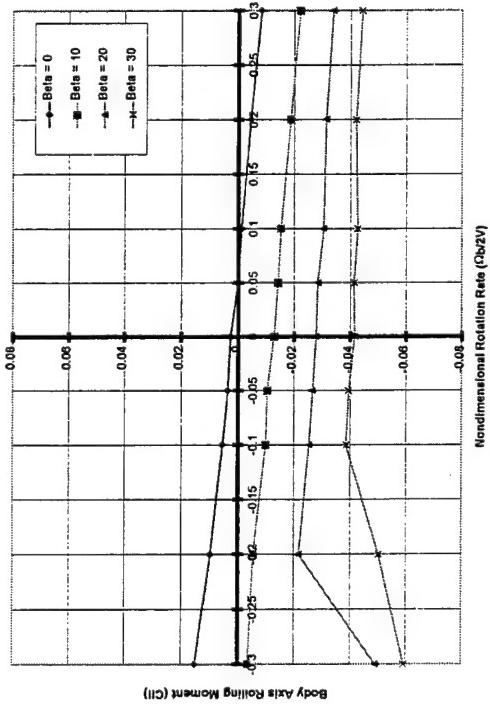




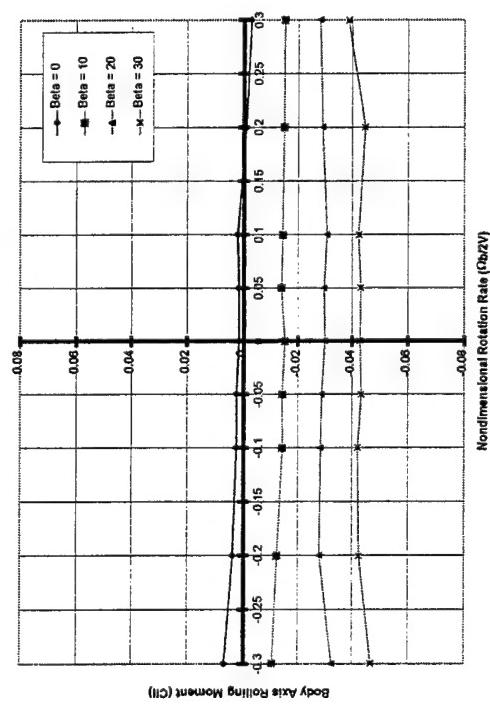




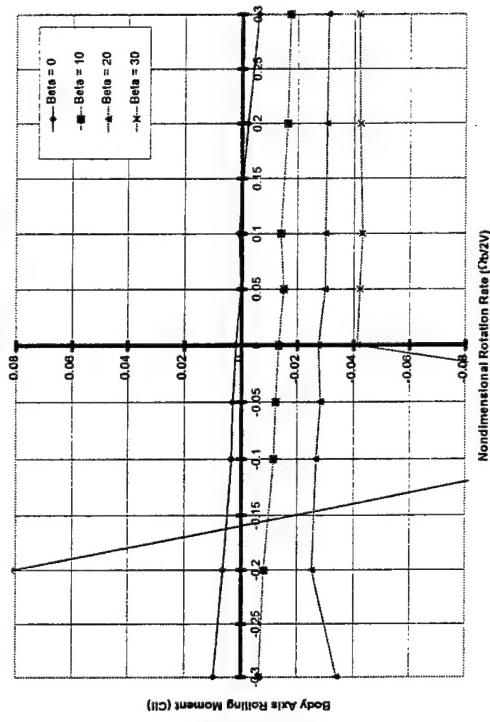
Rolling Moment vs $\Omega b/2V$
ICE 101, LEF = 30/30, AOA = 60 Deg.



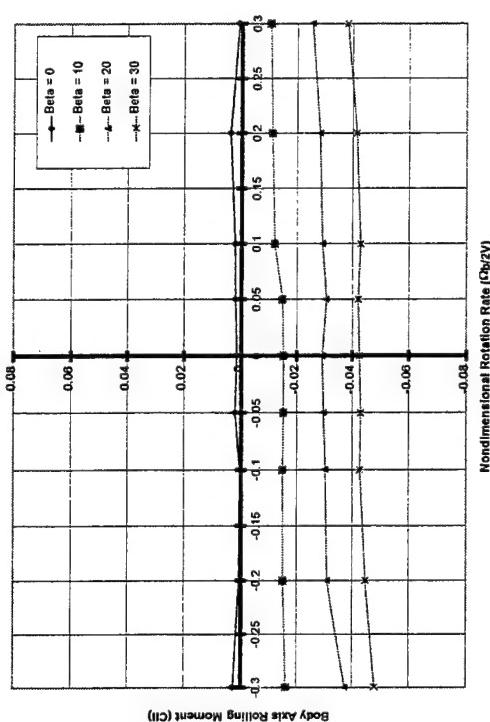
Rolling Moment vs $\Omega b/2V$
ICE 101, LEF = 30/30, AOA = 70 Deg.



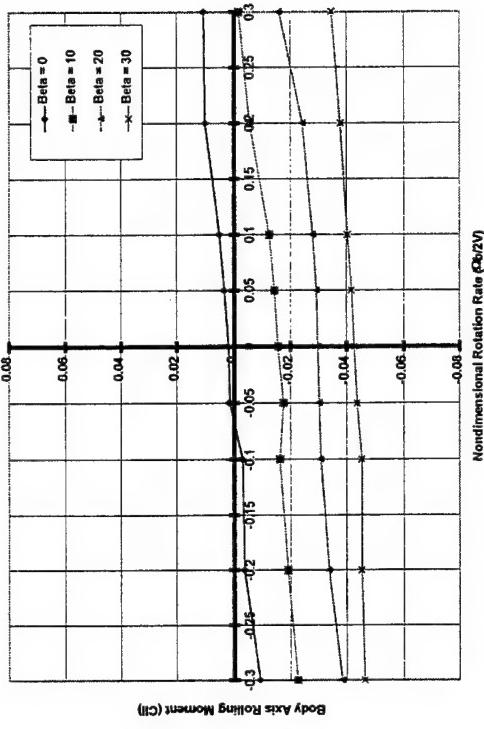
Rolling Moment vs $\Omega b/2V$
ICE 101, LEF = 30/30, AOA = 65 Deg.



Rolling Moment vs $\Omega b/2V$
ICE 101, LEF = 30/30, AOA = 75 Deg.



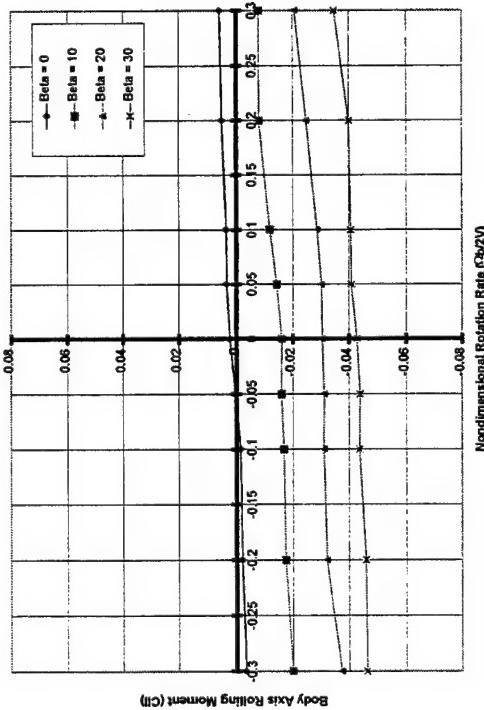
Rolling Moment vs $\Omega b/2V$
ICE 101, LEF = 30/30, AOA = 85 Deg.



Nondimensional Rotation Rate ($\Omega b/2V$)

Body Axis Rolling Moment (Cl)

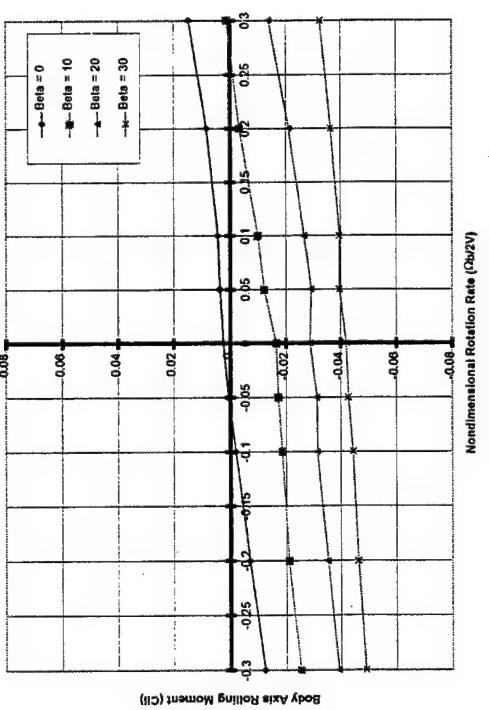
Rolling Moment vs $\Omega b/2V$
ICE 101, LEF = 30/30, AOA = 80 Deg.



Nondimensional Rotation Rate ($\Omega b/2V$)

Body Axis Rolling Moment (Cl)

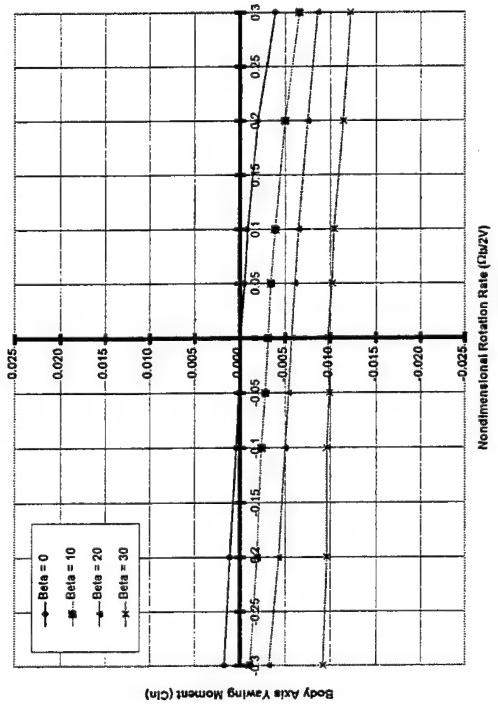
Rolling Moment vs $\Omega b/2V$
ICE 101, LEF = 30/30, AOA = 90 Deg.



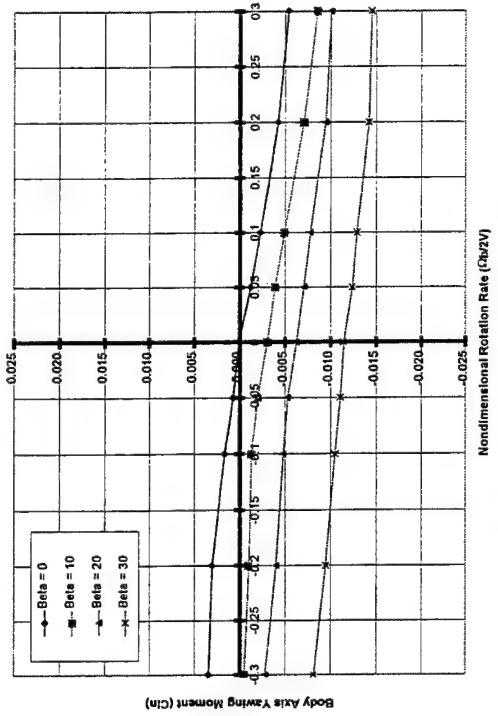
Nondimensional Rotation Rate ($\Omega b/2V$)

Body Axis Rolling Moment (Cl)

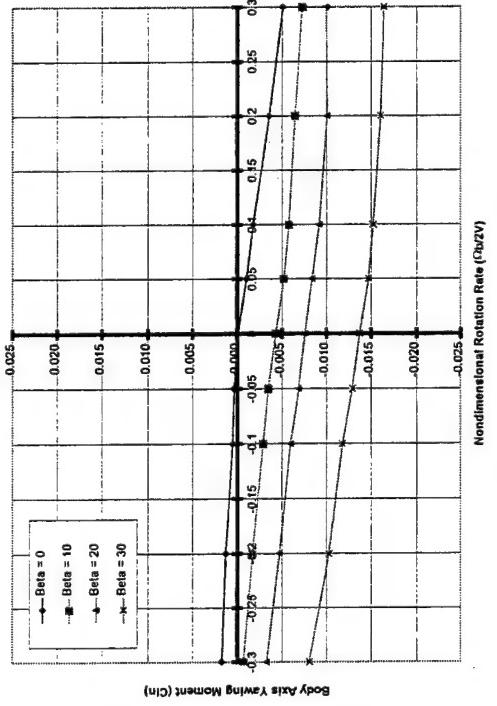
Yawing Moment vs $\Omega_b/2V$
ICE 101, LEF = 30/30, AOA = 0 Deg.



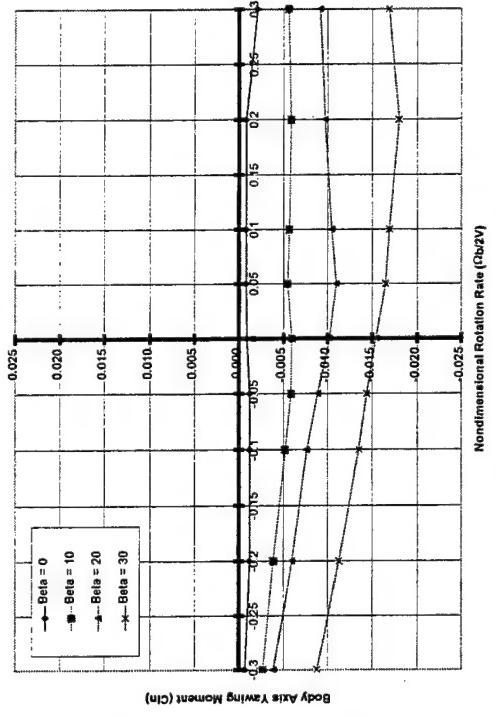
Yawing Moment vs $\Omega_b/2V$
ICE 101, LEF = 30/30, AOA = 5 Deg.

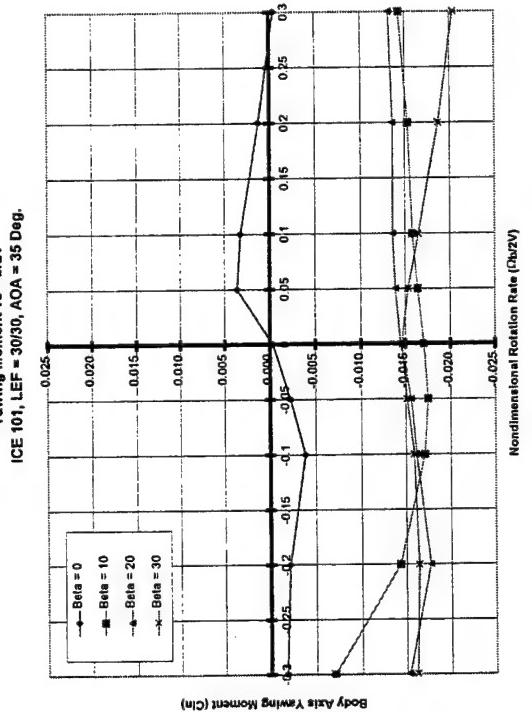
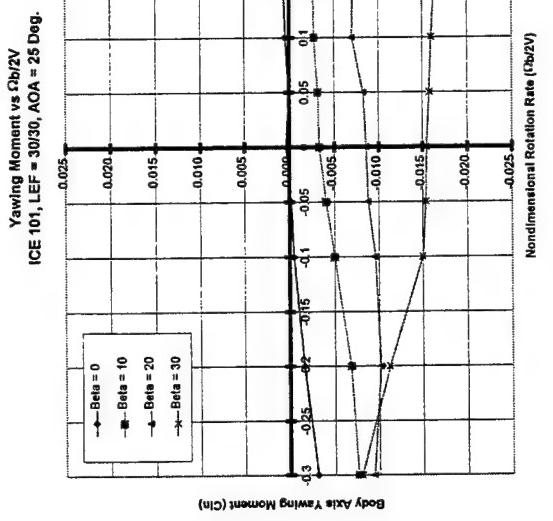
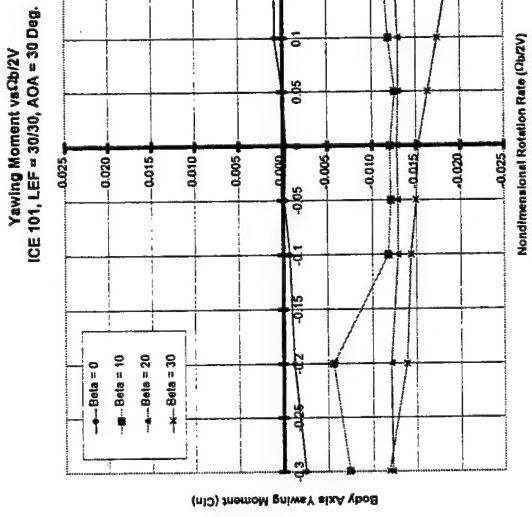
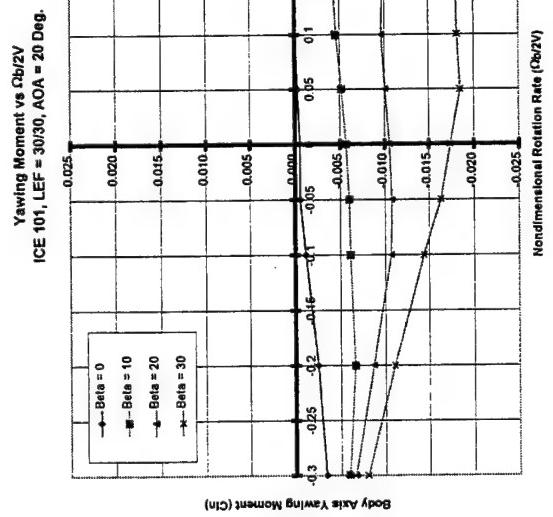


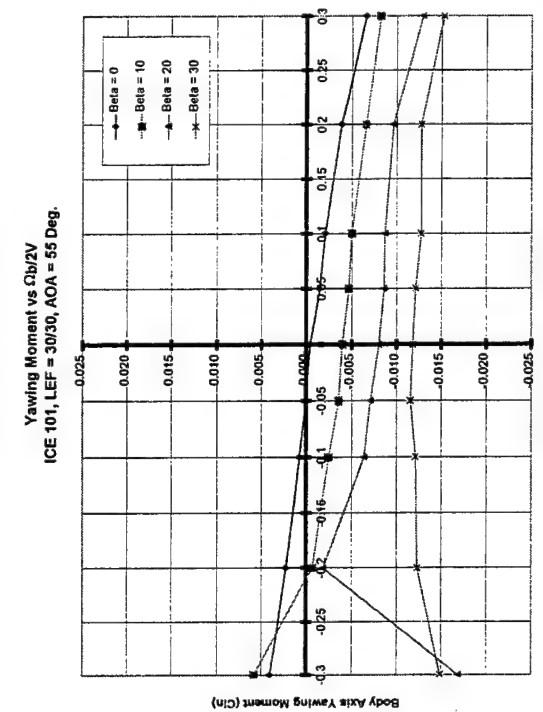
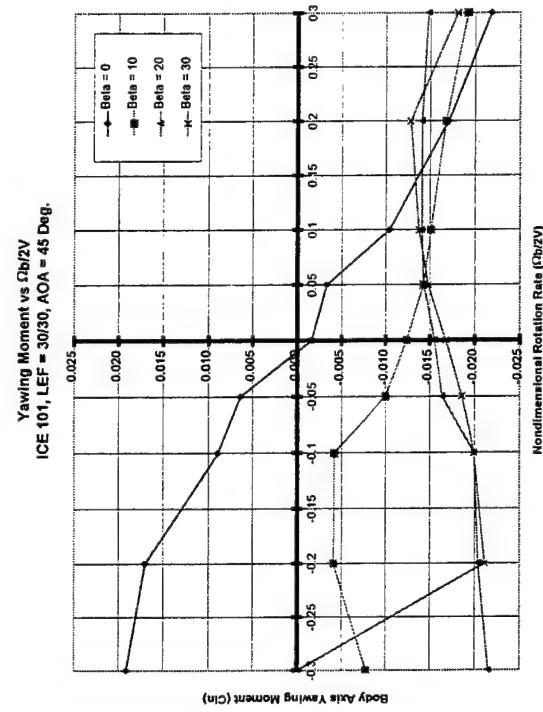
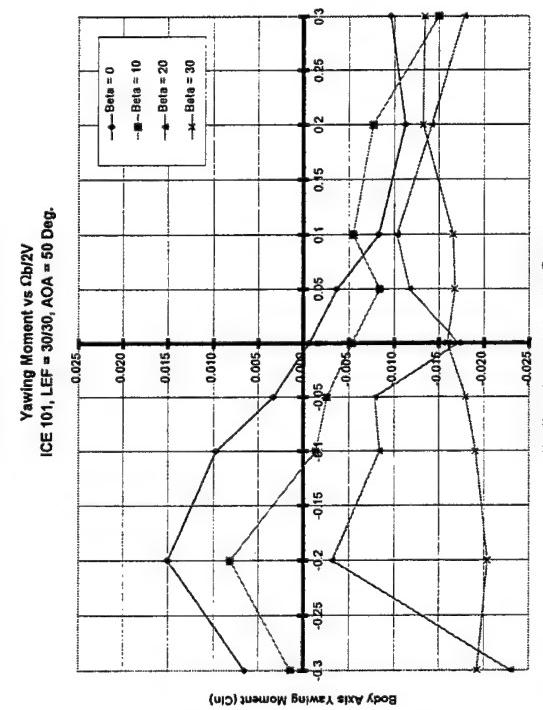
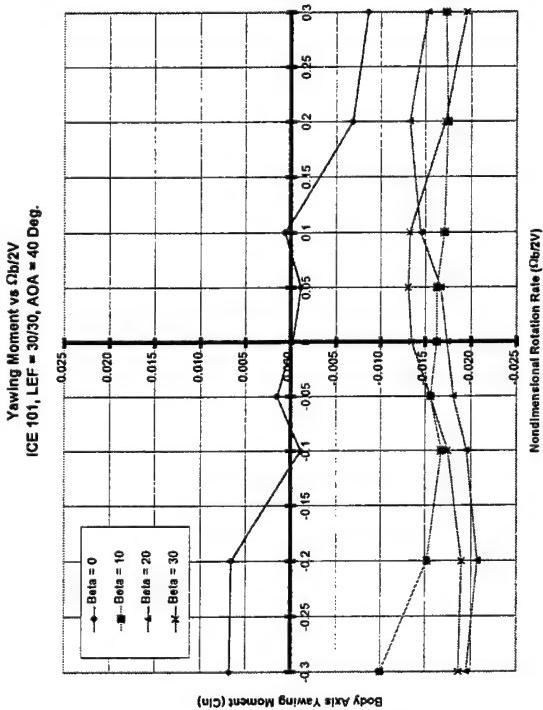
Yawing Moment vs $\Omega_b/2V$
ICE 101, LEF = 30/30, AOA = 10 Deg.

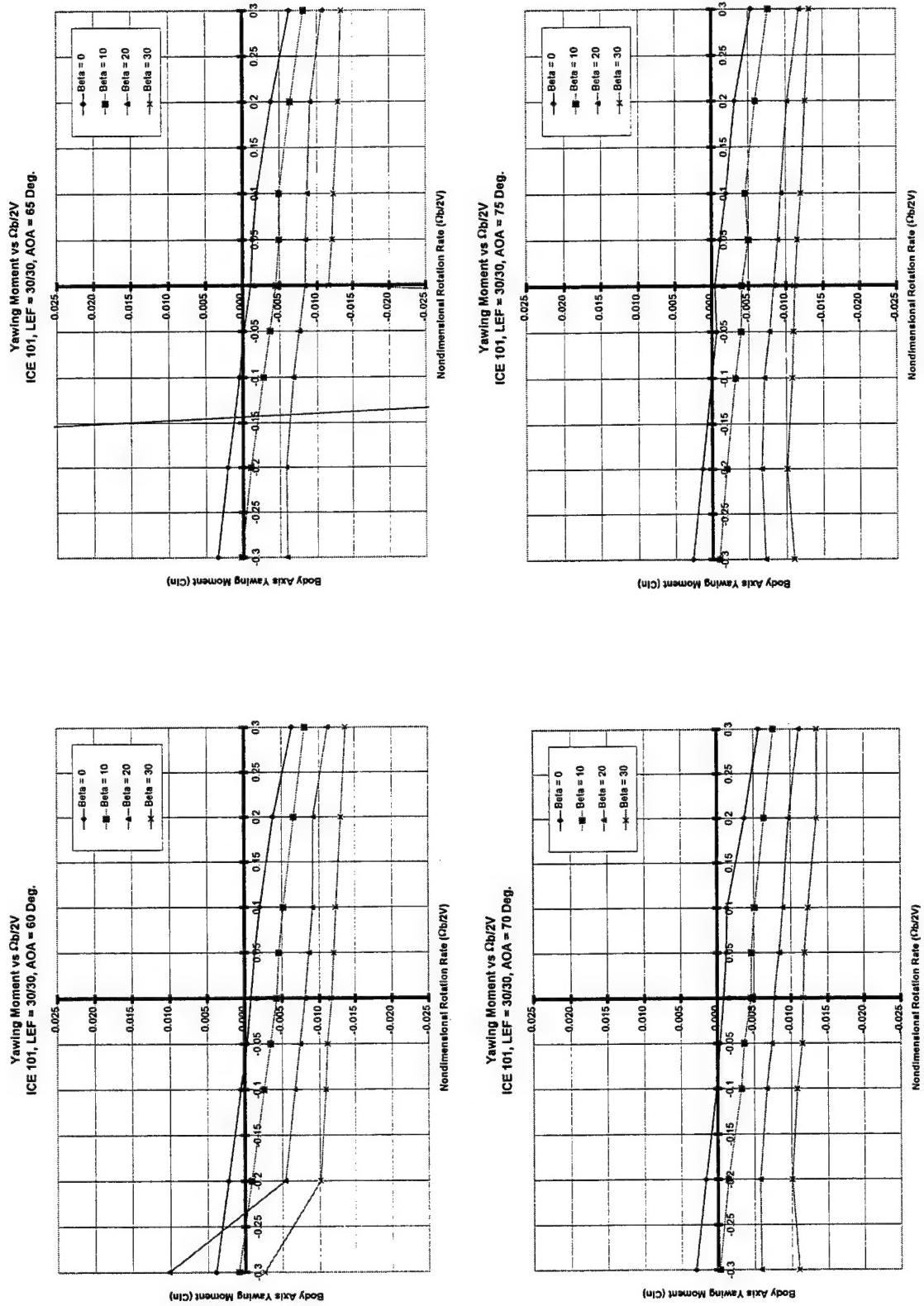


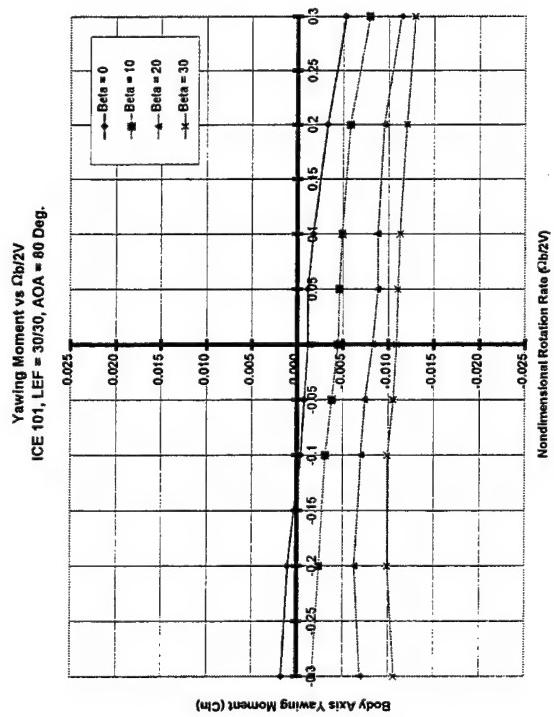
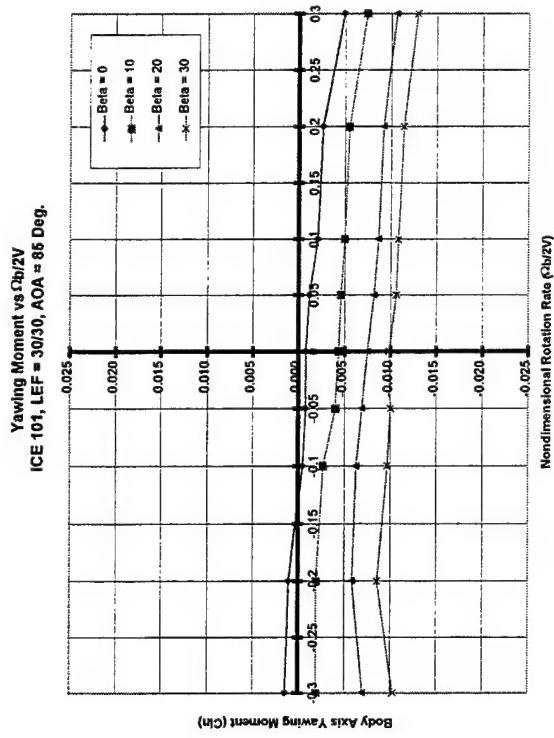
Yawing Moment vs $\Omega_b/2V$
ICE 101, LEF = 30/30, AOA = 15 Deg.



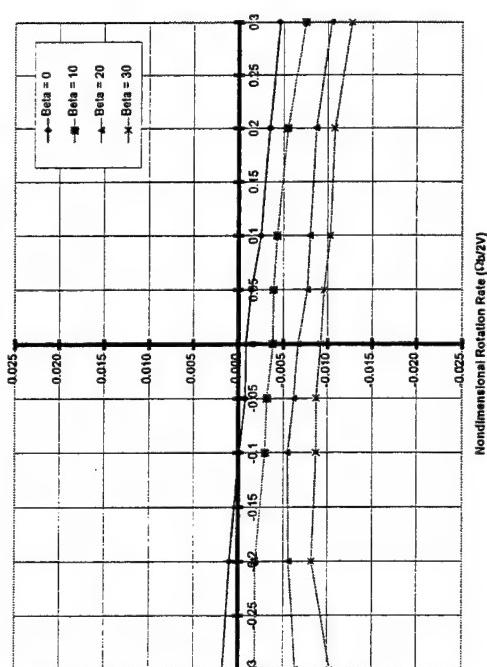








Body Axes Yawing Moment (Cin)

Non-dimensional Rotation Rate ($\Omega_b/2V$)

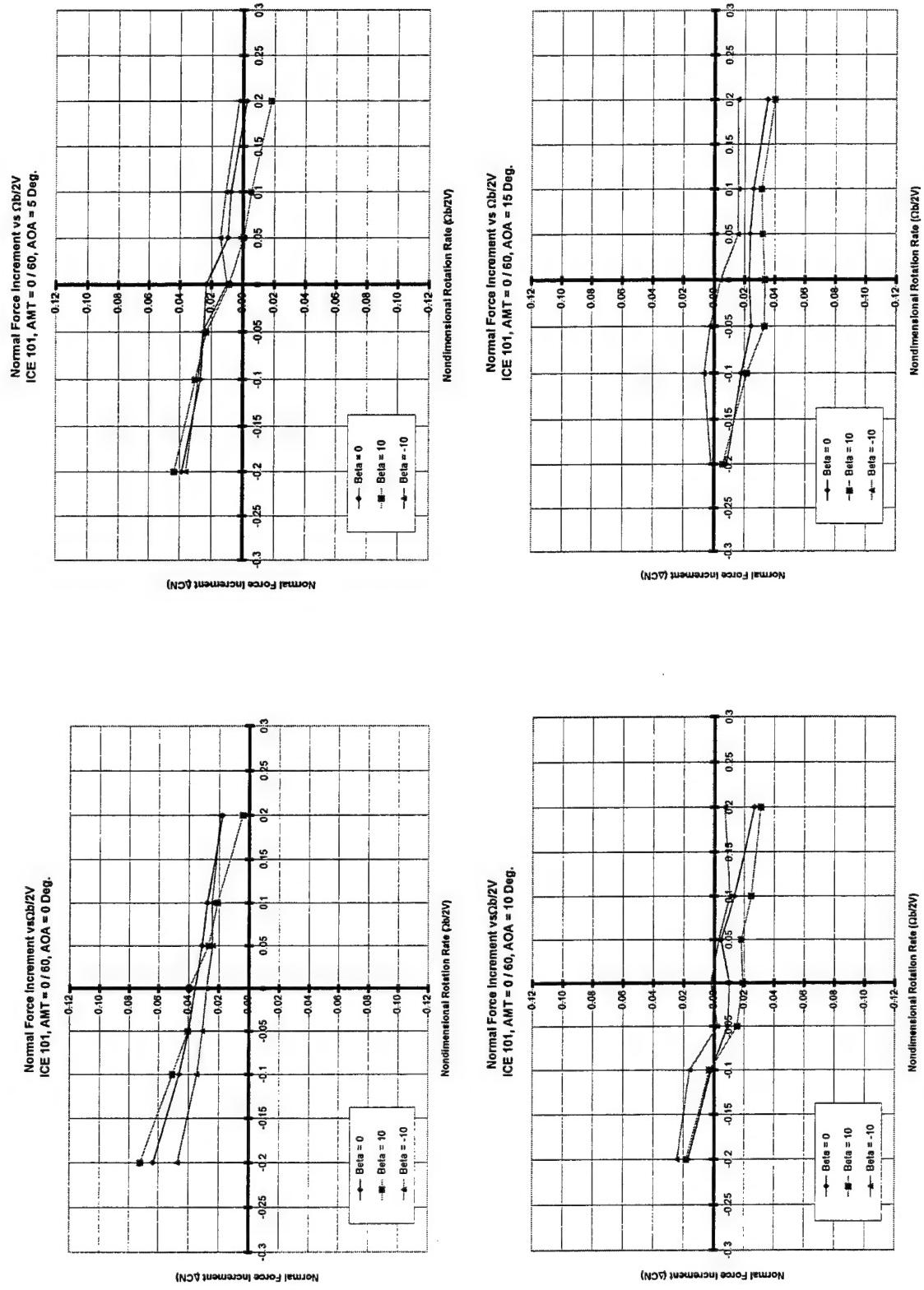
Body Axes Yawing Moment (Cin)

Non-dimensional Rotation Rate ($\Omega_b/2V$)

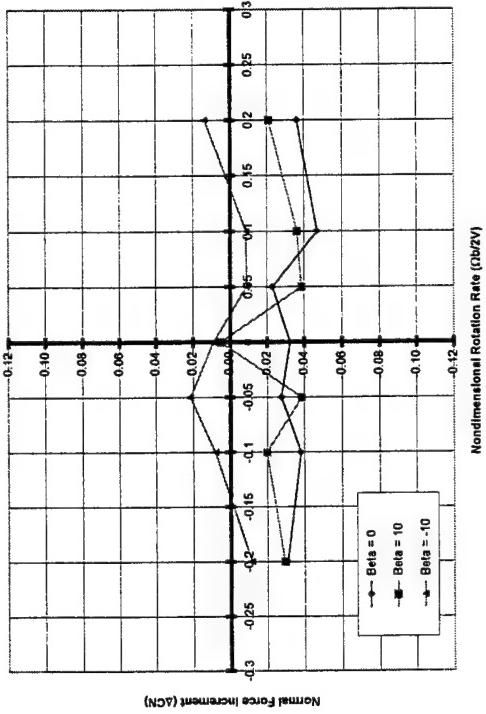
Appendix C

Rotary Balance Data Plots

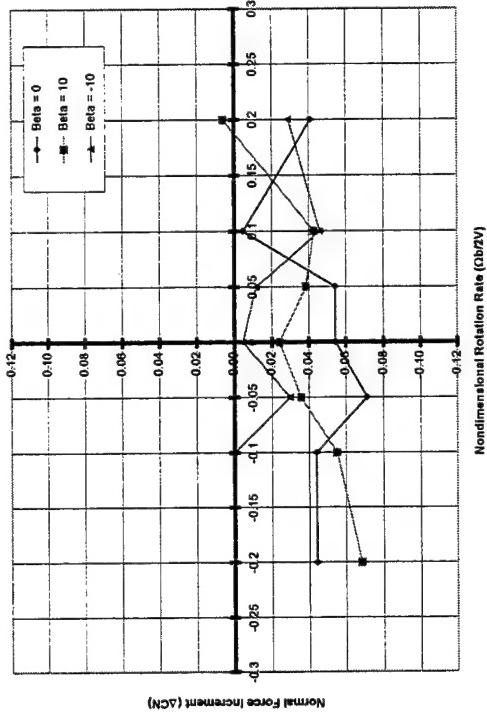
LEF = 0/0, AMT = 0/60



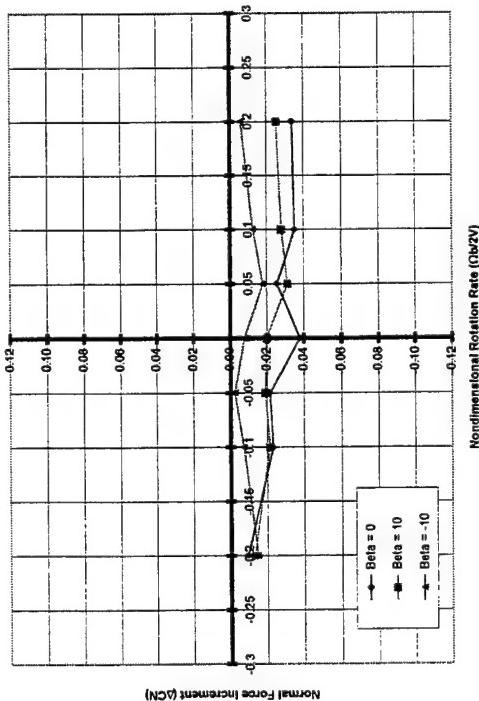
Normal Force Increment vs $\Omega b/2V$
ICE 101, AMT = 0 / 60, AOA = 25 Deg.



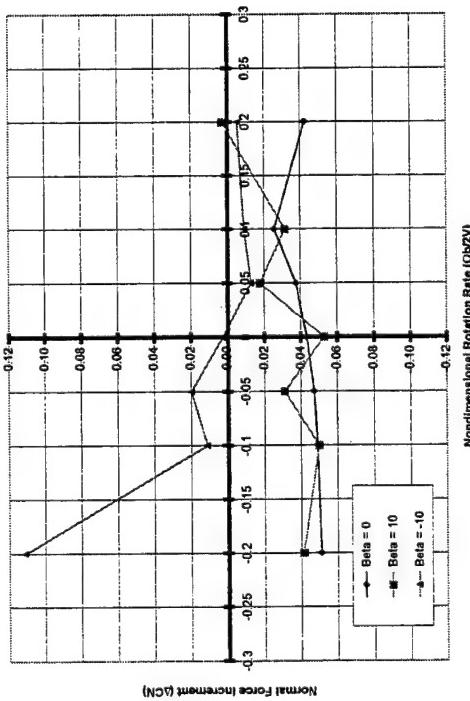
Normal Force Increment vs $\Omega b/2V$
ICE 101, AMT = 0 / 60, AOA = 35 Deg.

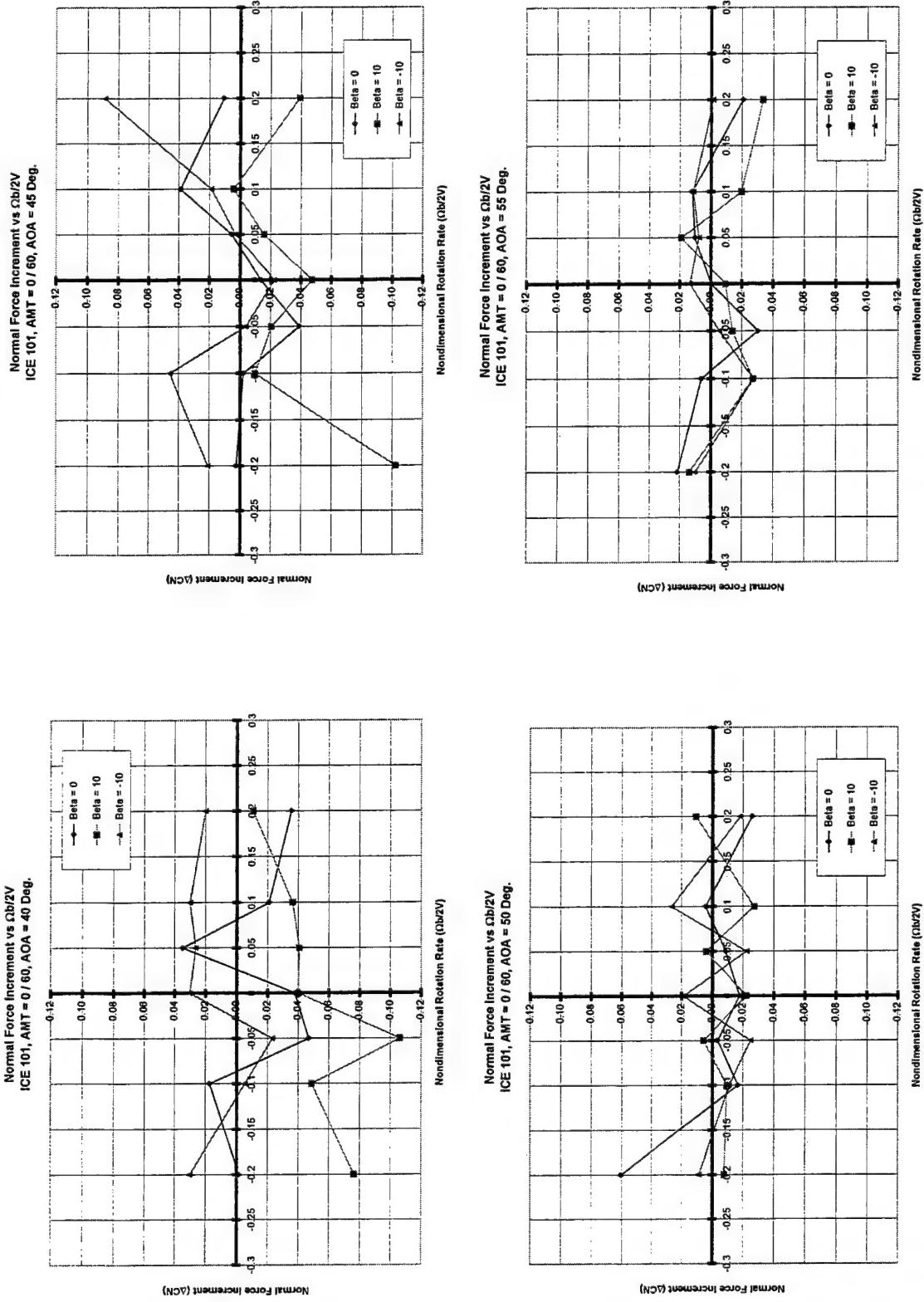


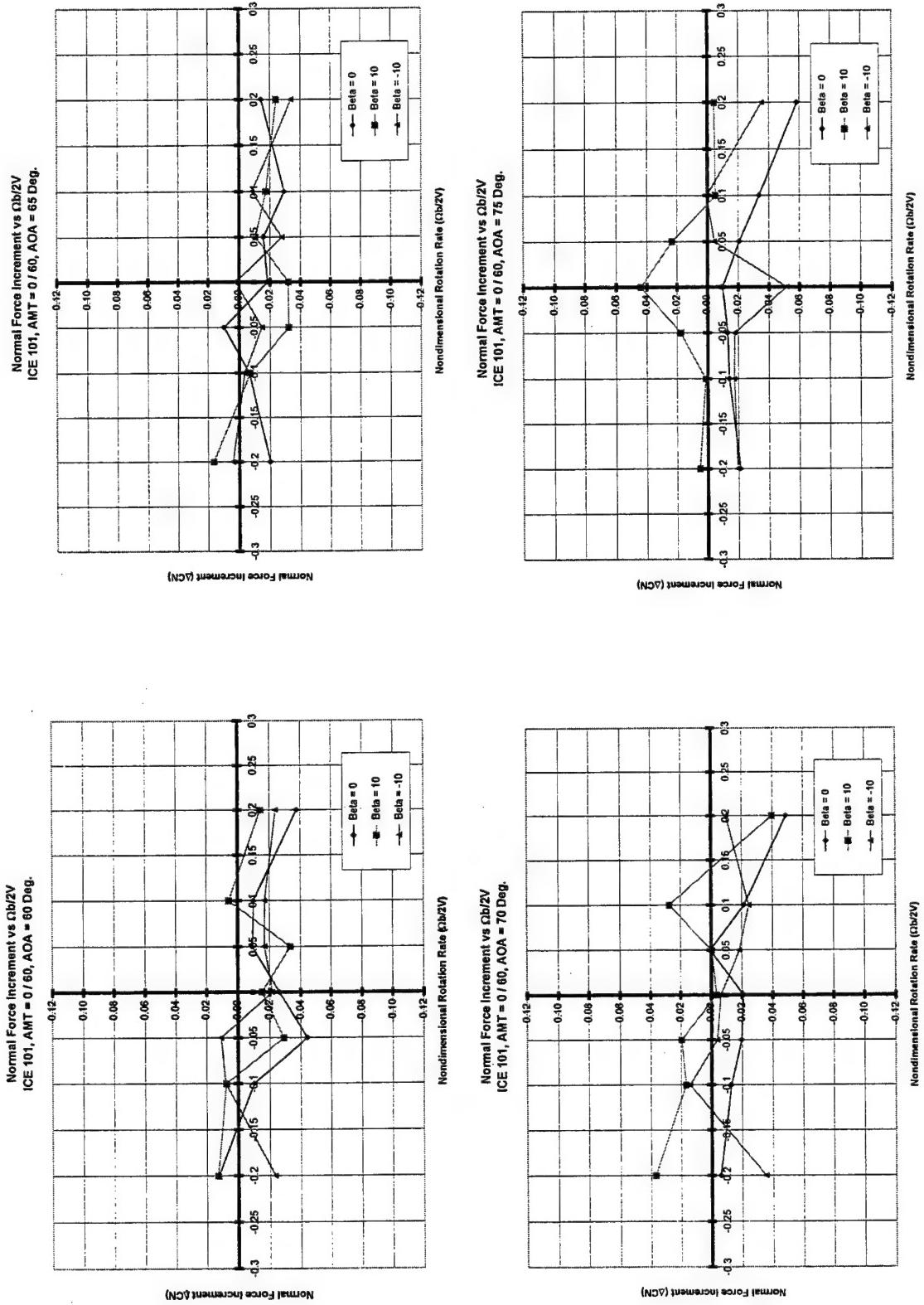
Normal Force Increment vs $\Omega b/2V$
ICE 101, AMT = 0 / 60, AOA = 20 Deg.

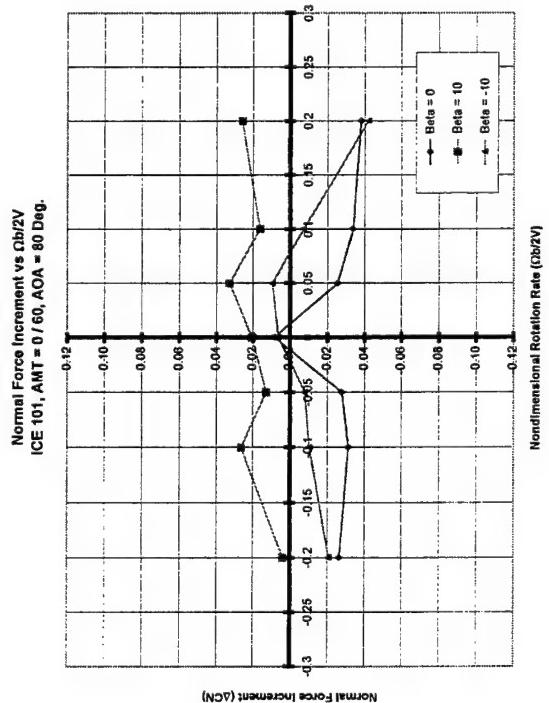
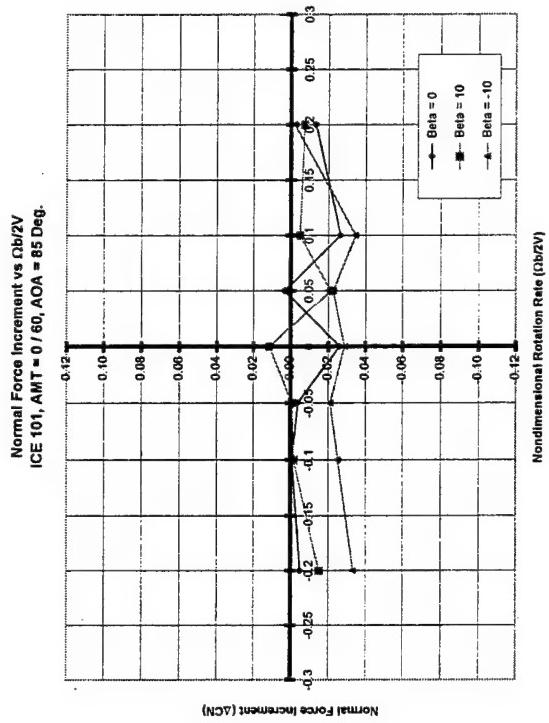


Normal Force Increment vs $\Omega b/2V$
ICE 101, AMT = 0 / 60, AOA = 30 Deg.

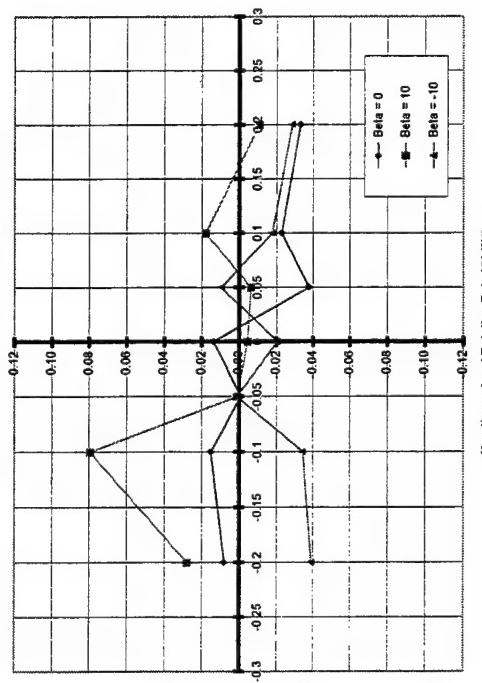






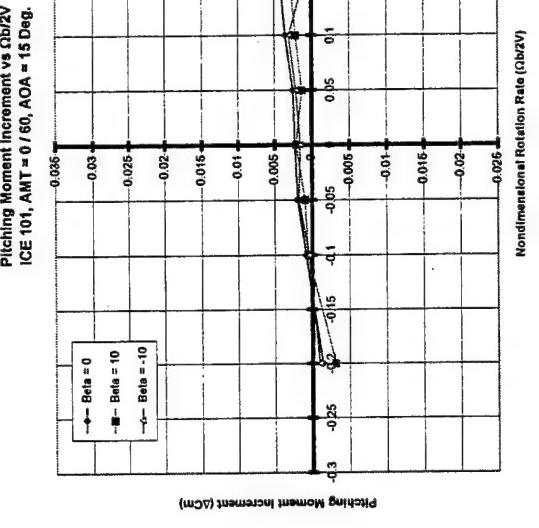
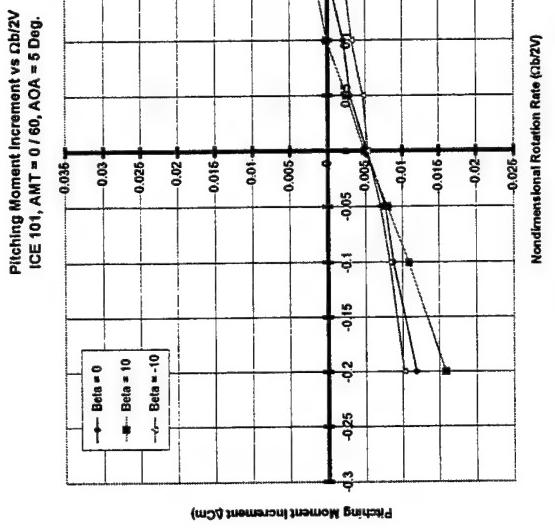
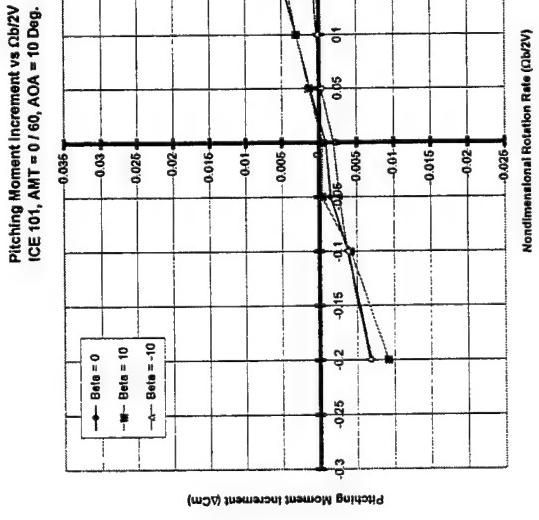
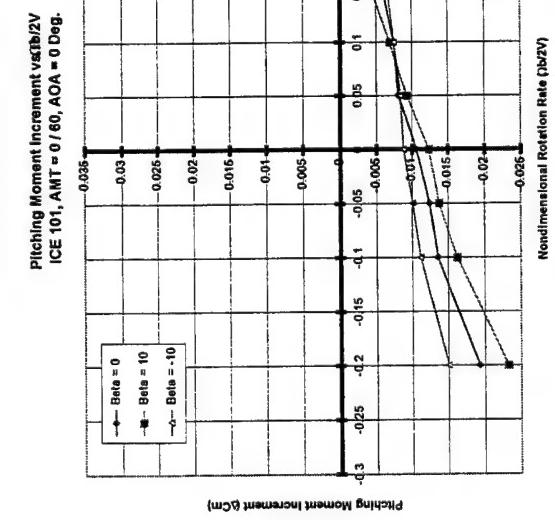


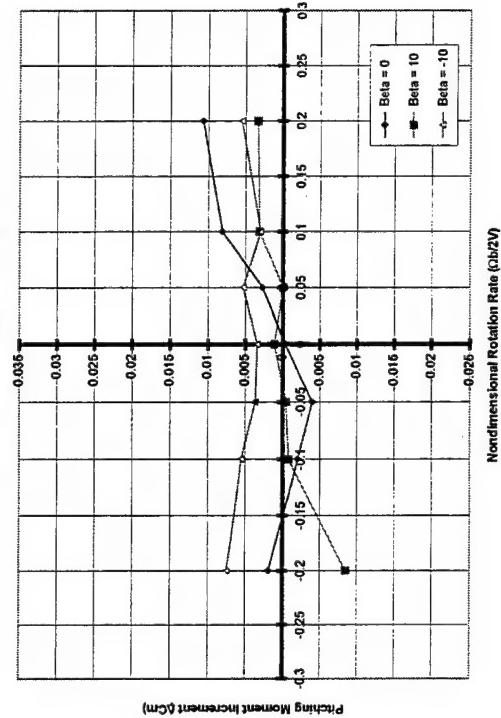
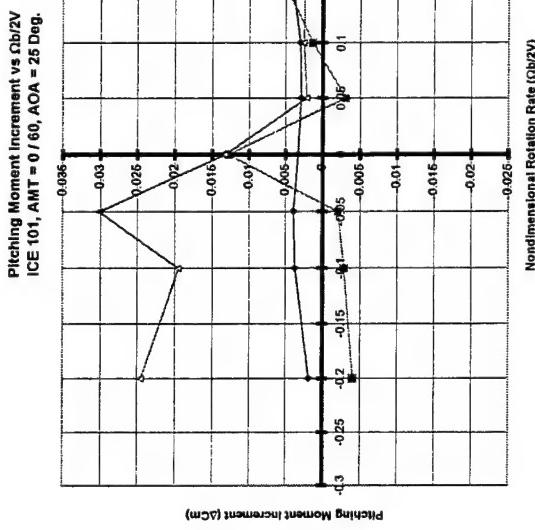
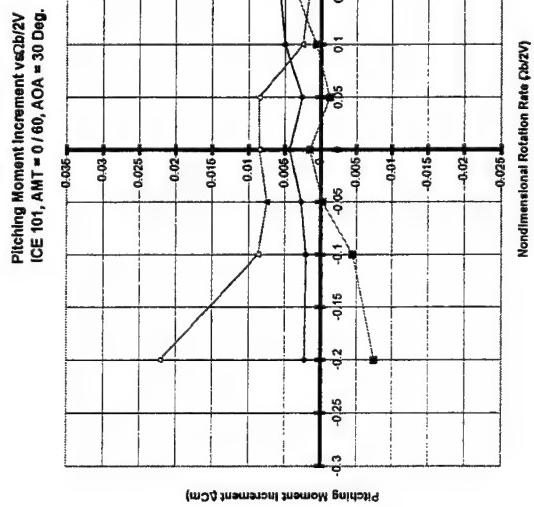
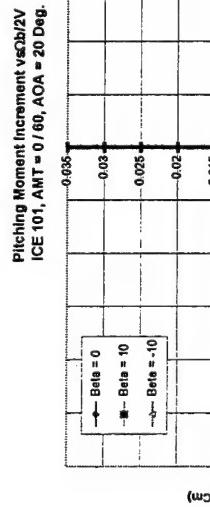
Normal Force Increment (ACN)

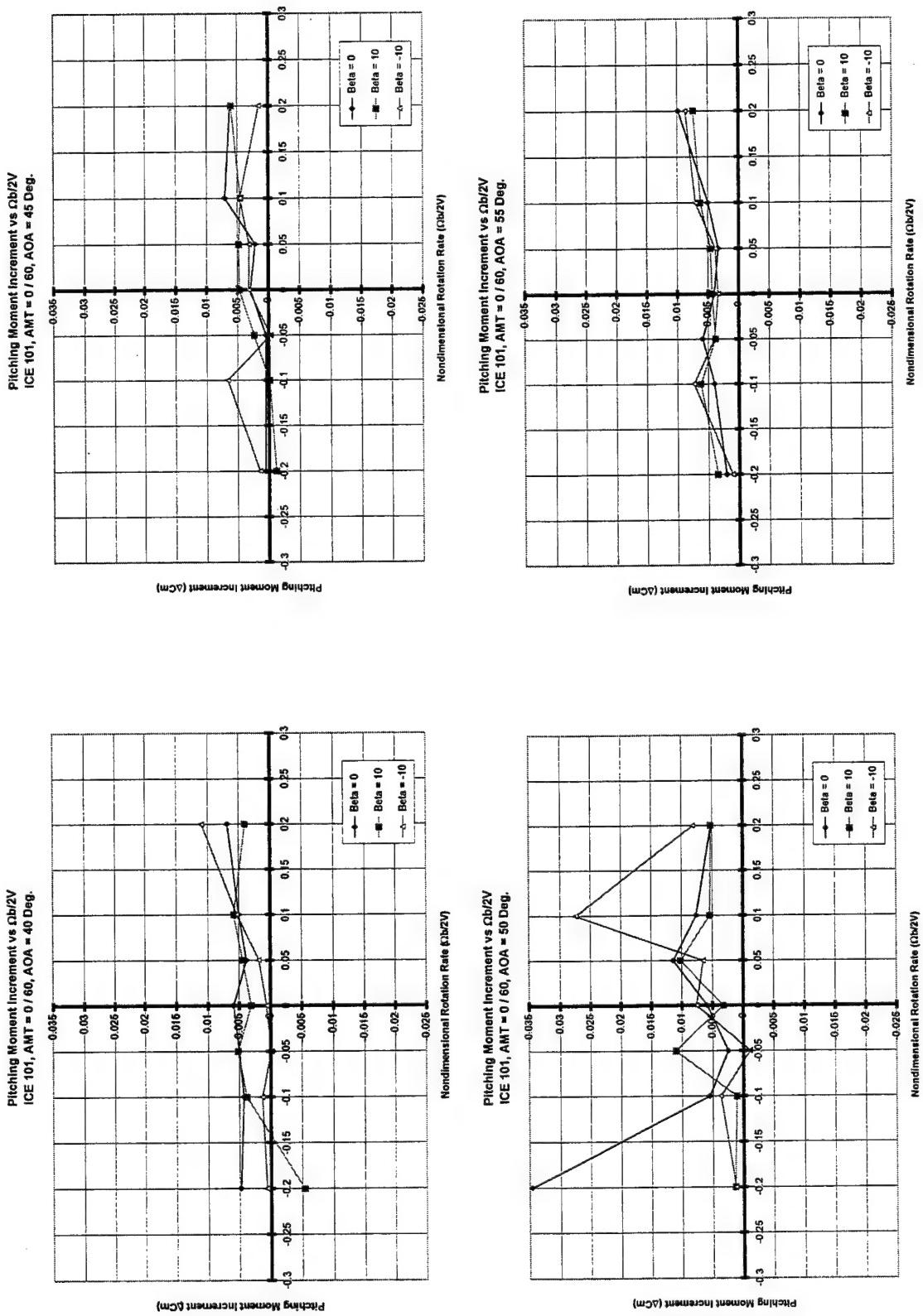
Nondimensional Rotation Rate ($\Omega b/2V$)

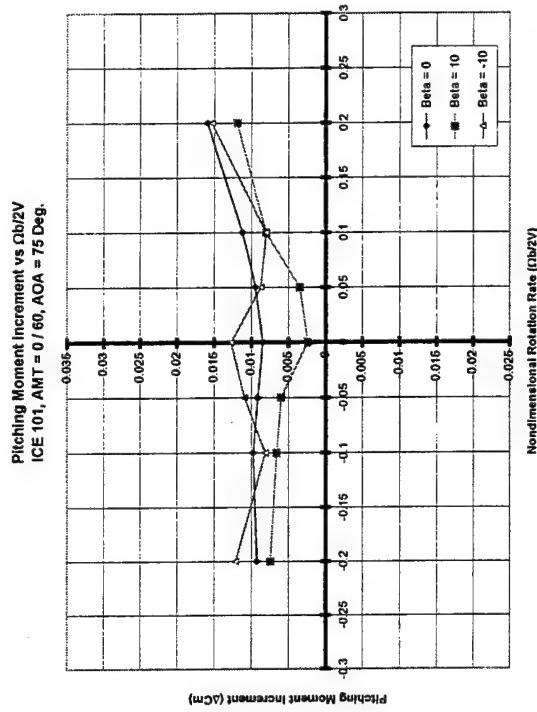
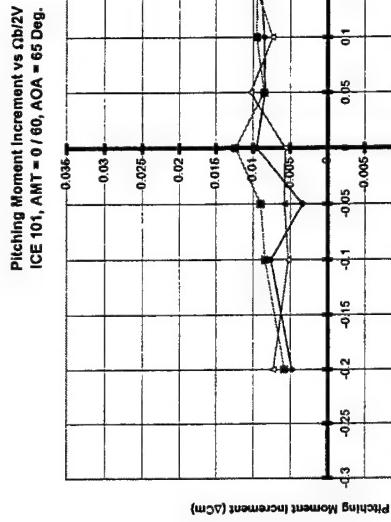
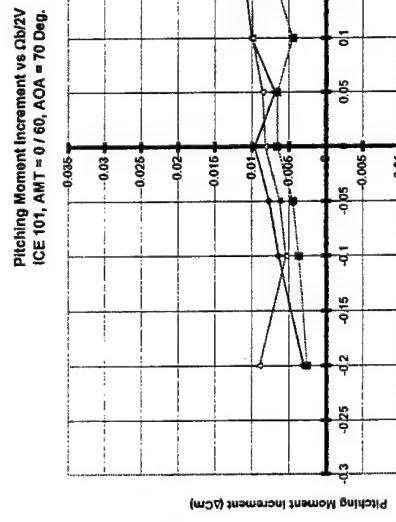
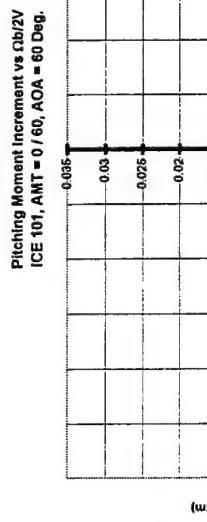
Normal Force Increment (ACN)

Nondimensional Rotation Rate ($\Omega b/2V$)

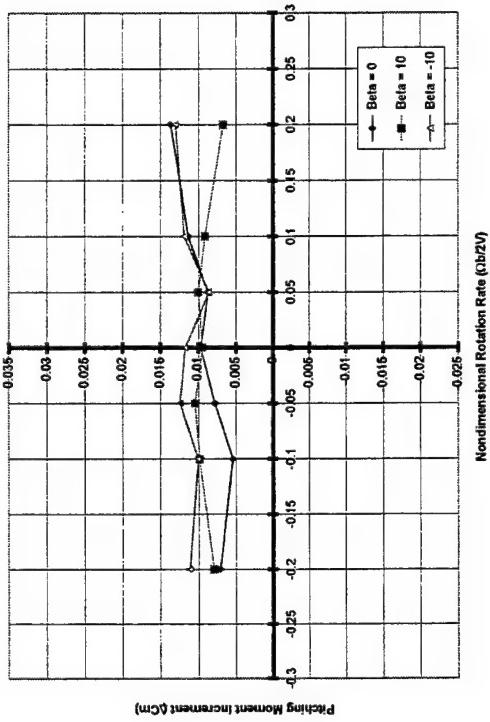




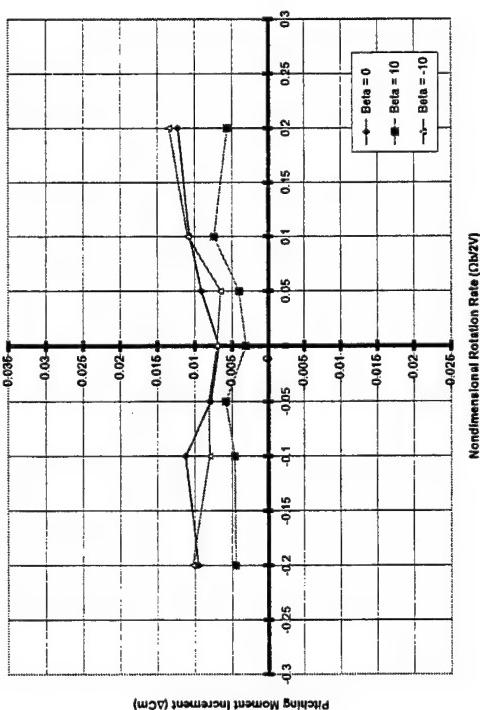




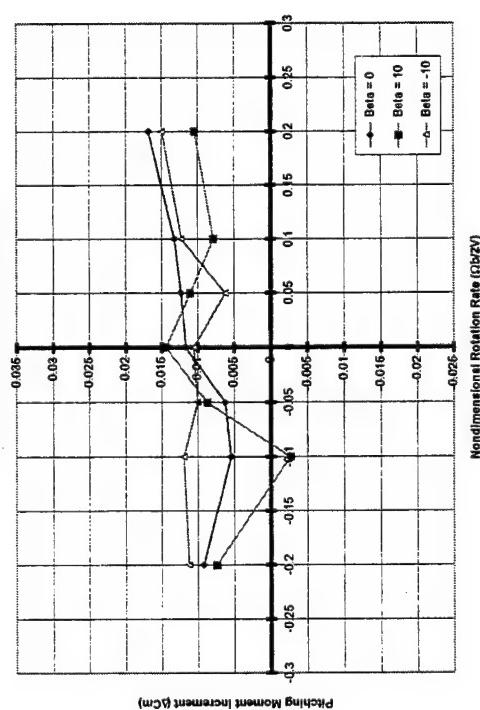
Pitching Moment Increment vs $\Omega b/2V$
ICE 101, AMT = 0 / 60, AOA = 85 Deg.



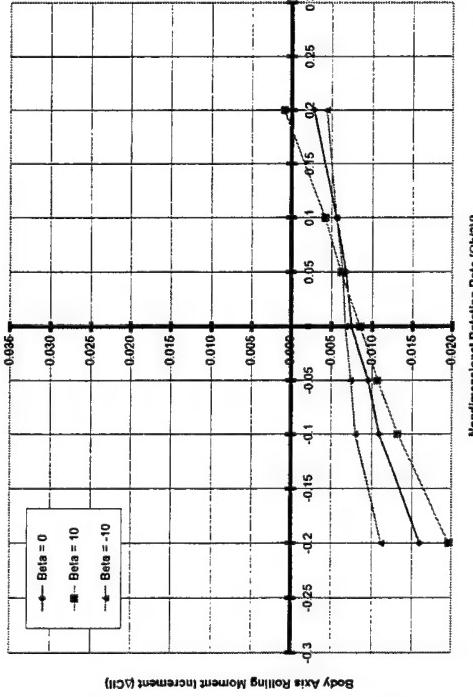
Pitching Moment Increment vs $\Omega b/2V$
ICE 101, AMT = 0 / 60, AOA = 80 Deg.



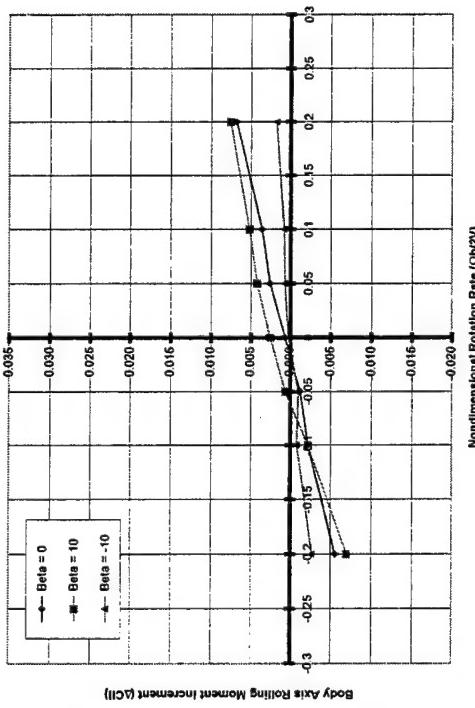
Pitching Moment Increment vs $\Omega b/2V$
ICE 101, AMT = 0 / 60, AOA = 90 Deg.



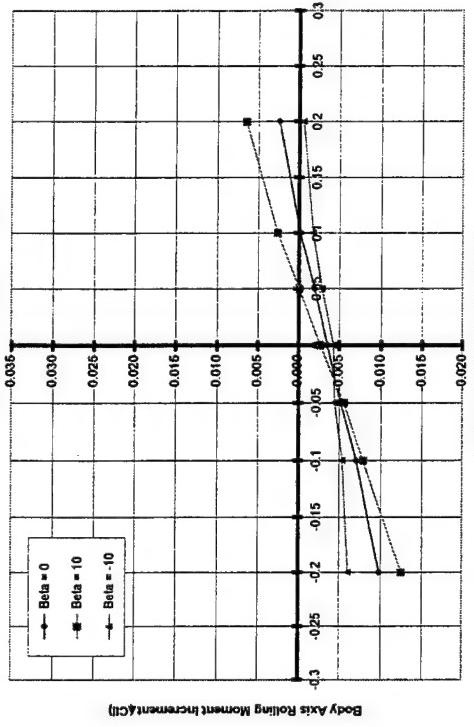
Rolling Moment Increment vs $\Omega b/2V$
ICE 101, AMT = 0 / 60, AOA = 0 Deg.



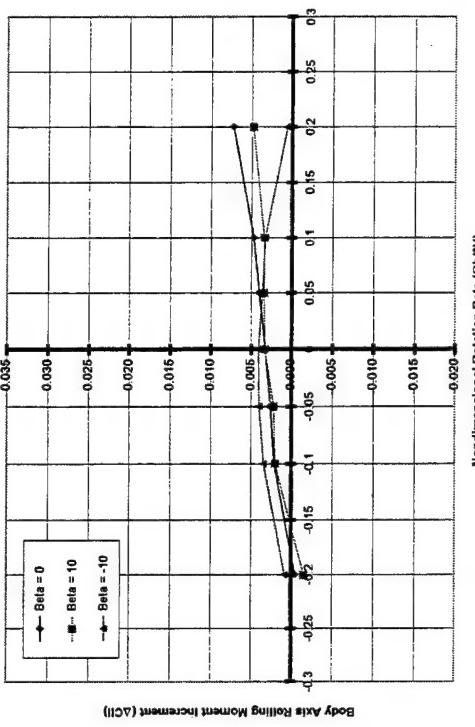
Rolling Moment Increment vs $\Omega b/2V$
ICE 101, AMT = 0 / 60, AOA = 10 Deg.



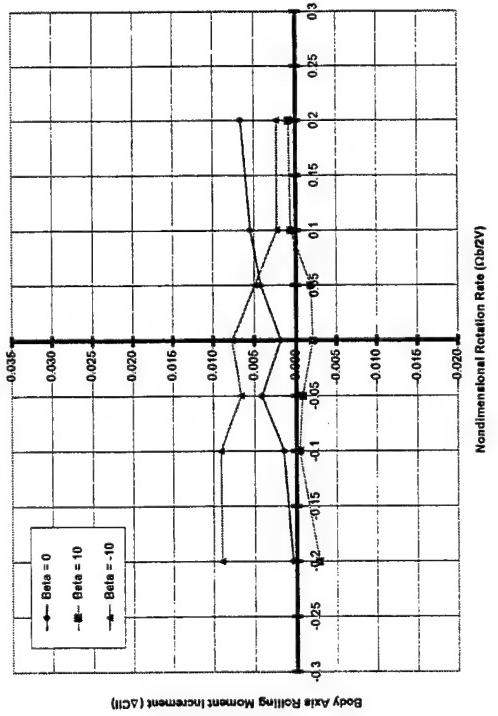
Rolling Moment Increment vs $\Omega b/2V$
ICE 101, AMT = 0 / 60, AOA = 5 Deg.



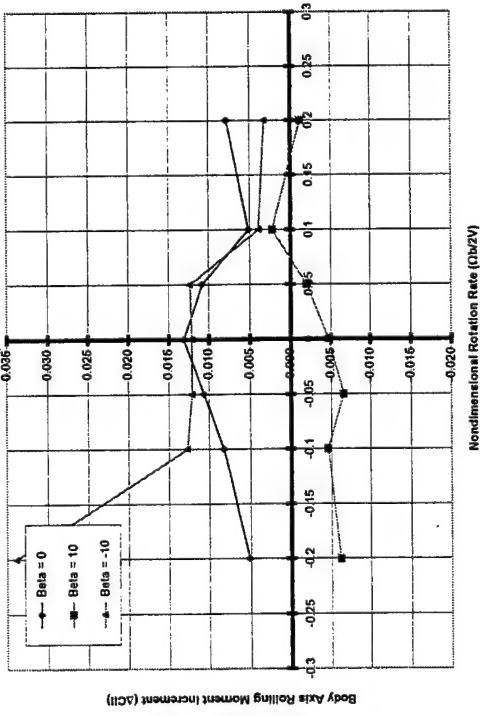
Rolling Moment Increment vs $\Omega b/2V$
ICE 101, AMT = 0 / 60, AOA = 15 Deg.



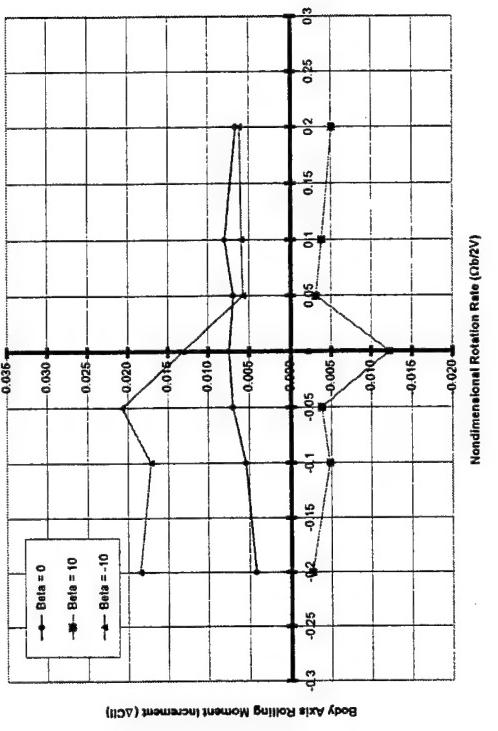
Rolling Moment Increment vs $\Omega b/2V$
ICE 101, AMT = 0 / 60, AOA = 20 Deg.



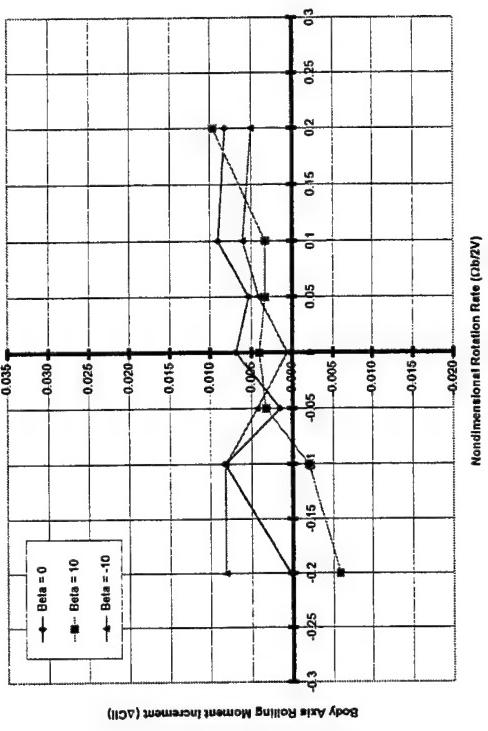
Rolling Moment Increment vs $\Omega b/2V$
ICE 101, AMT = 0 / 60, AOA = 30 Deg.



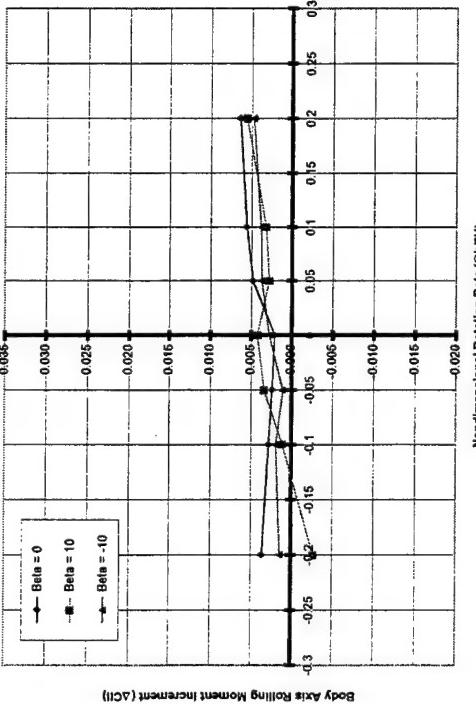
Rolling Moment Increment vs $\Omega b/2V$
ICE 101, AMT = 0 / 60, AOA = 25 Deg.



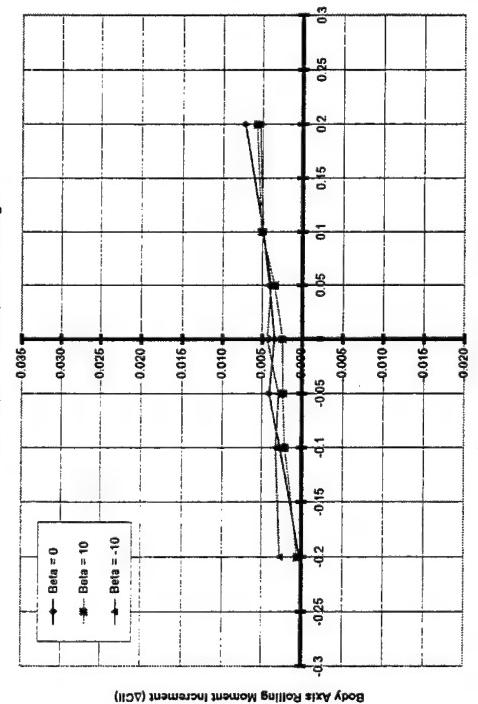
Rolling Moment Increment vs $\Omega b/2V$
ICE 101, AMT = 0 / 60, AOA = 35 Deg.



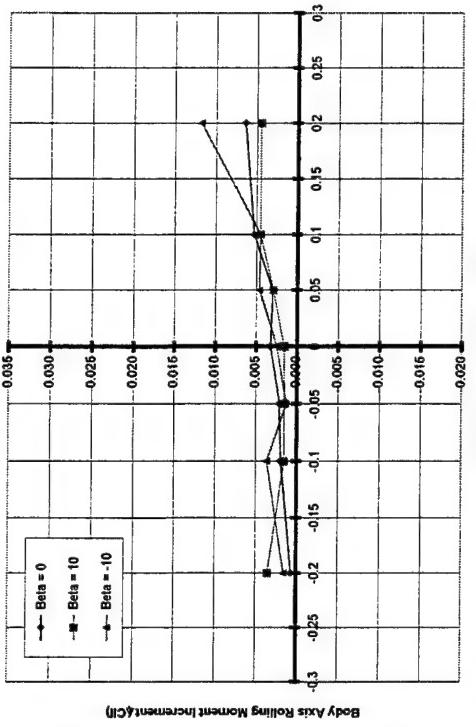
Rolling Moment Increment vs $\Omega b/2V$
ICE 101, AMT = 0 / 60, AOA = 40 Deg.



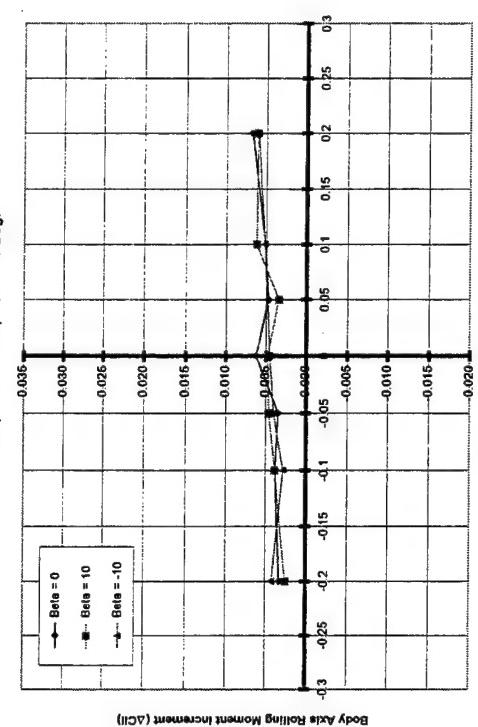
Rolling Moment Increment vs $\Omega b/2V$
ICE 101, AMT = 0 / 60, AOA = 50 Deg.

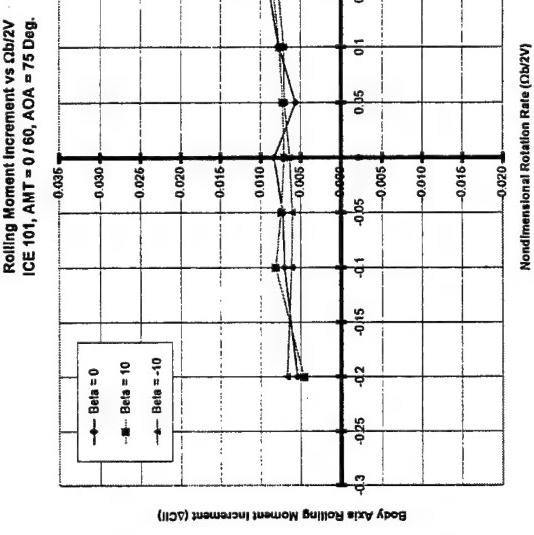
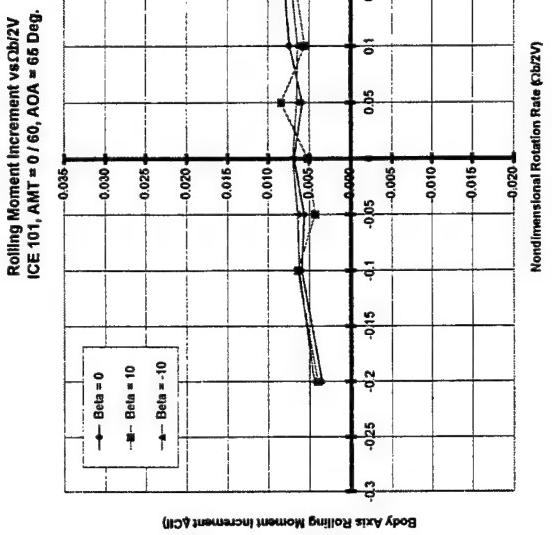
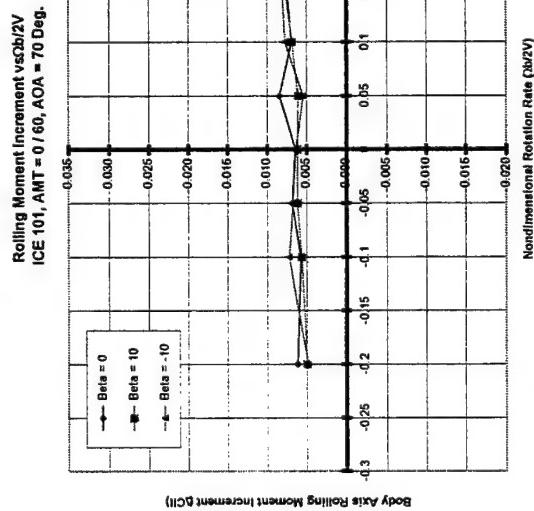
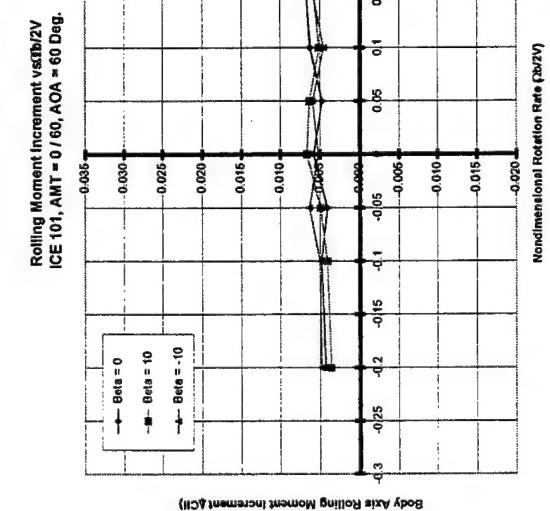


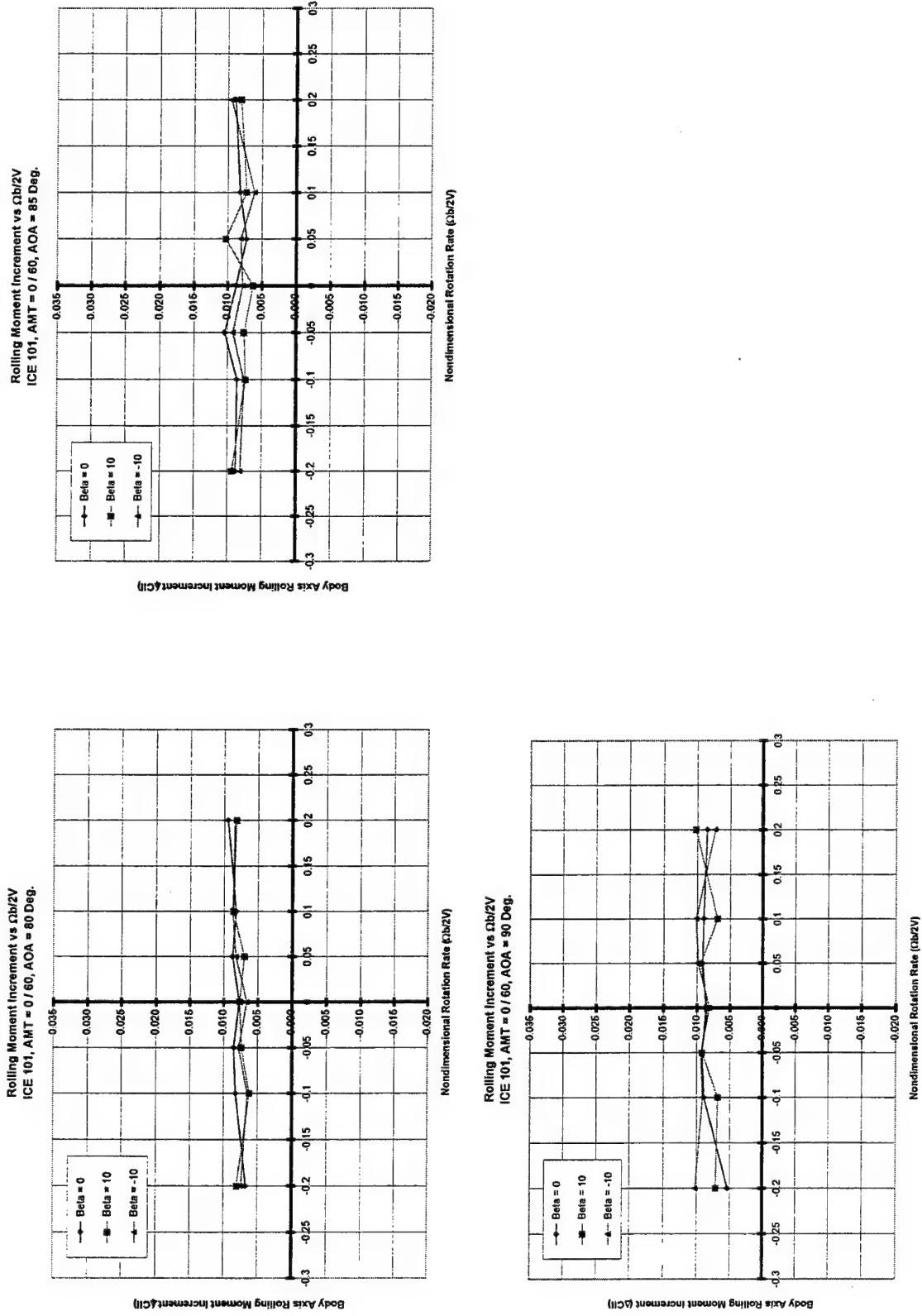
Rolling Moment Increment vs $\Omega b/2V$
ICE 101, AMT = 0 / 60, AOA = 45 Deg.

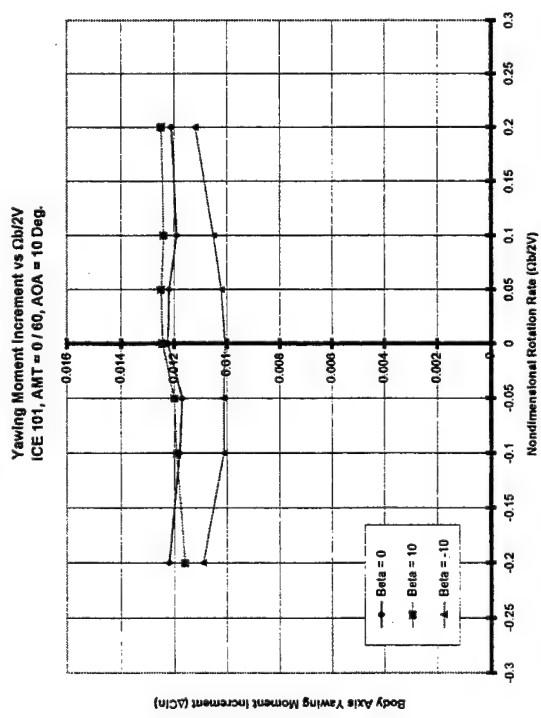
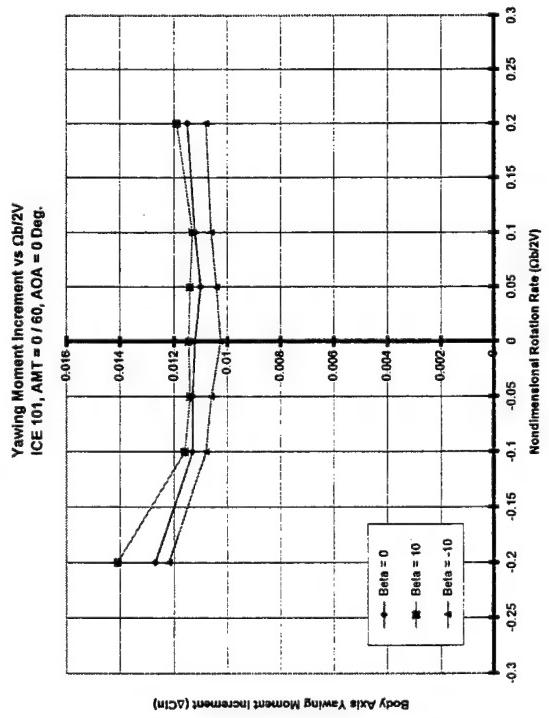
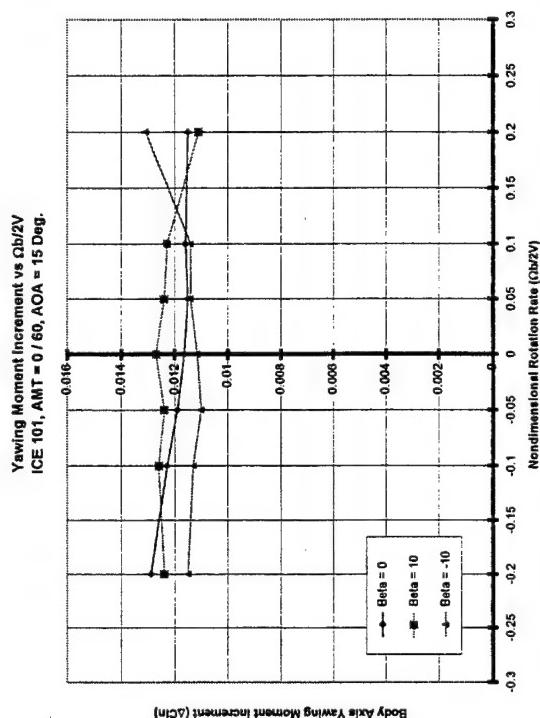
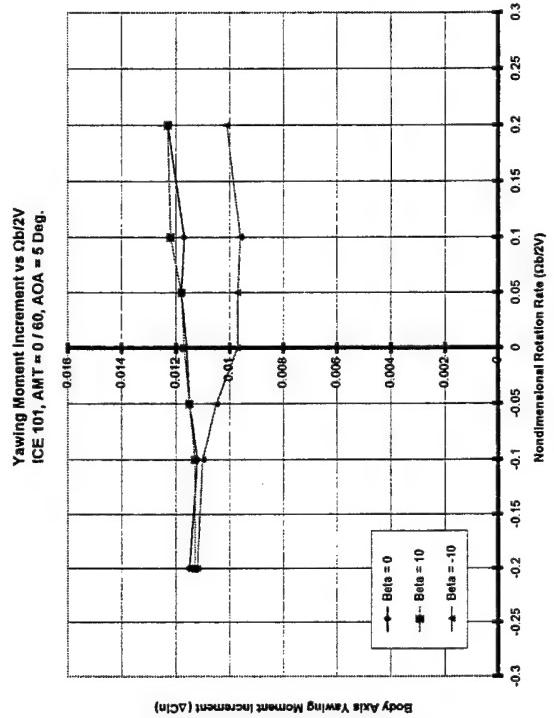


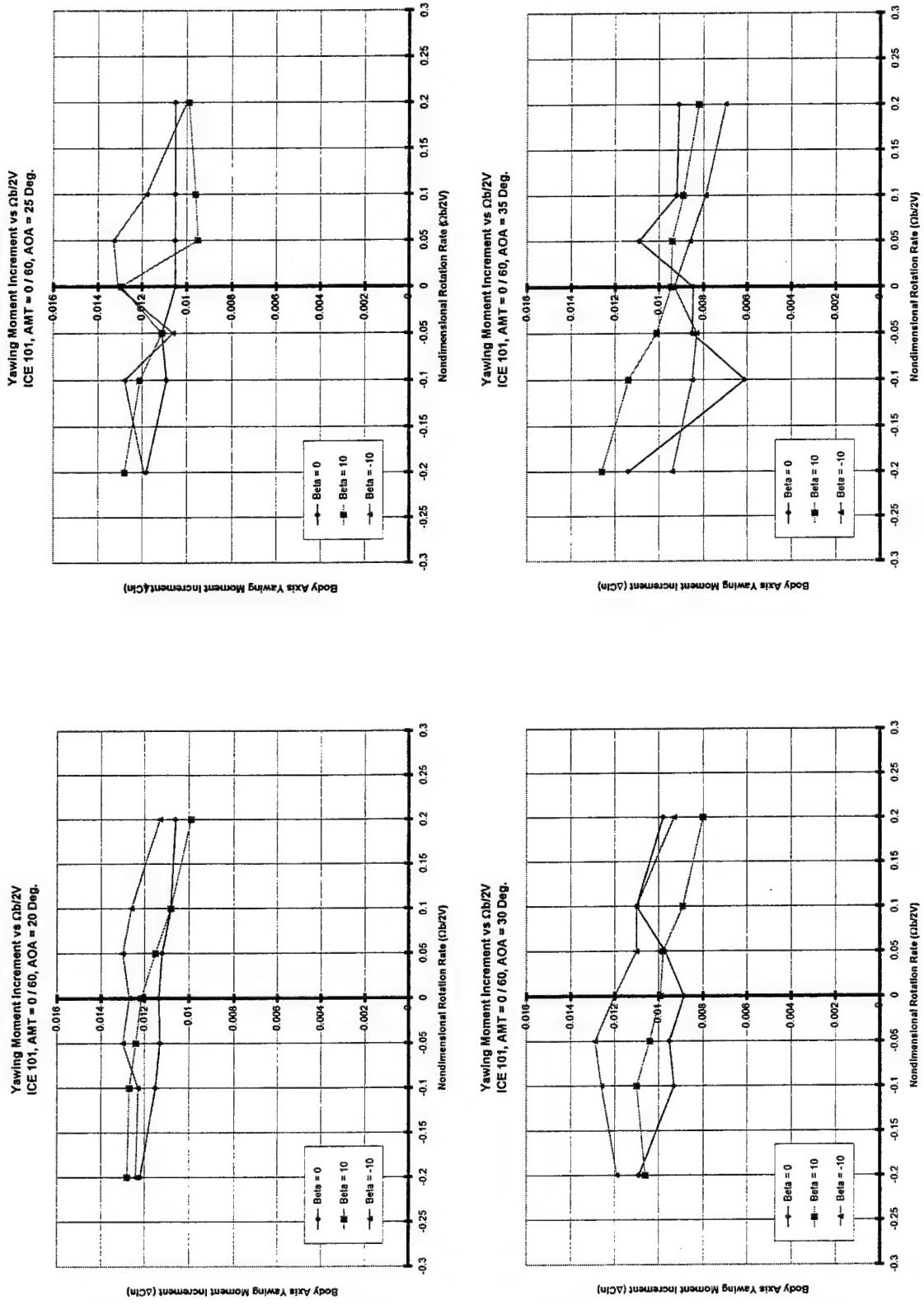
Rolling Moment Increment vs $\Omega b/2V$
ICE 101, AMT = 0 / 60, AOA = 55 Deg.

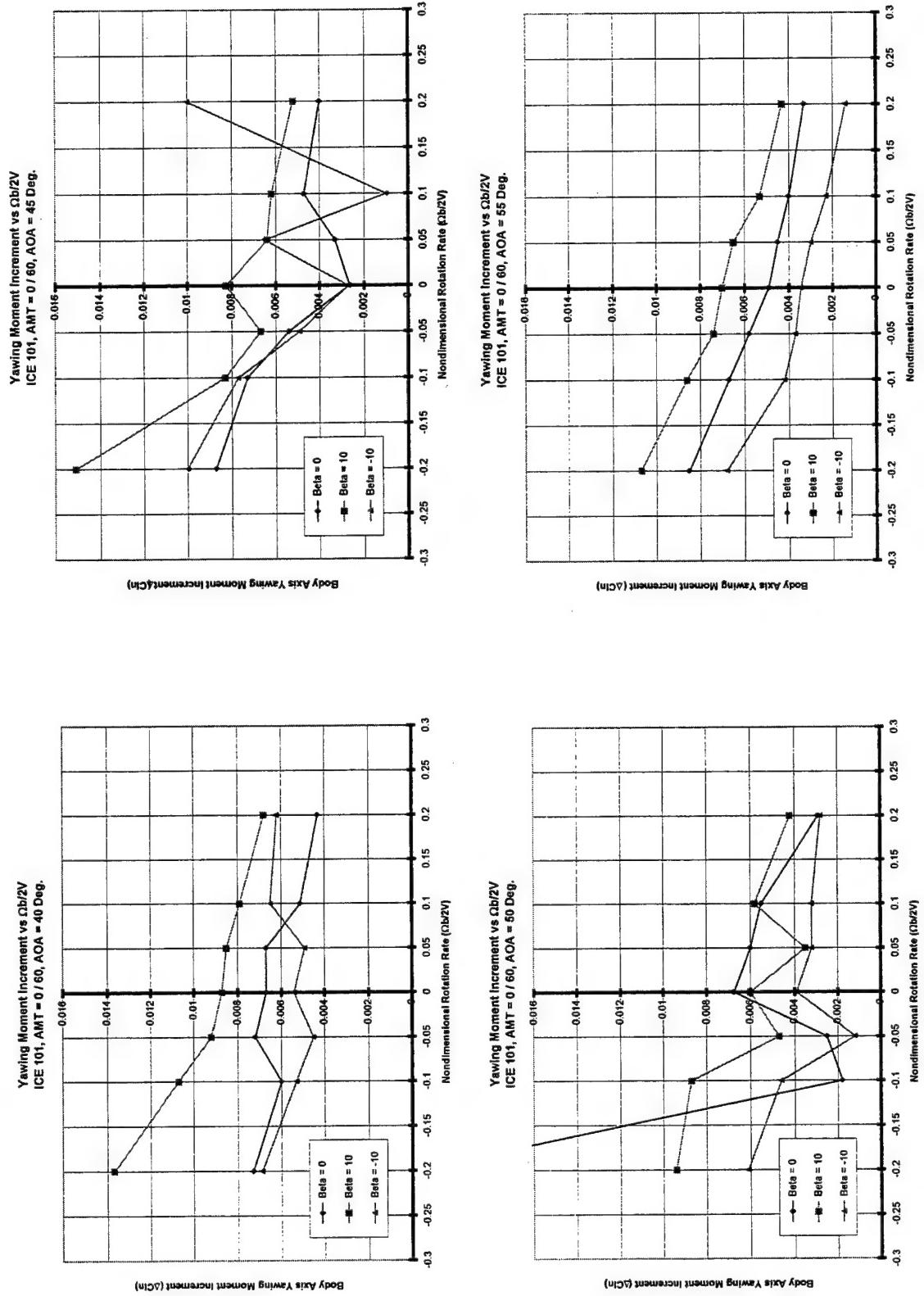




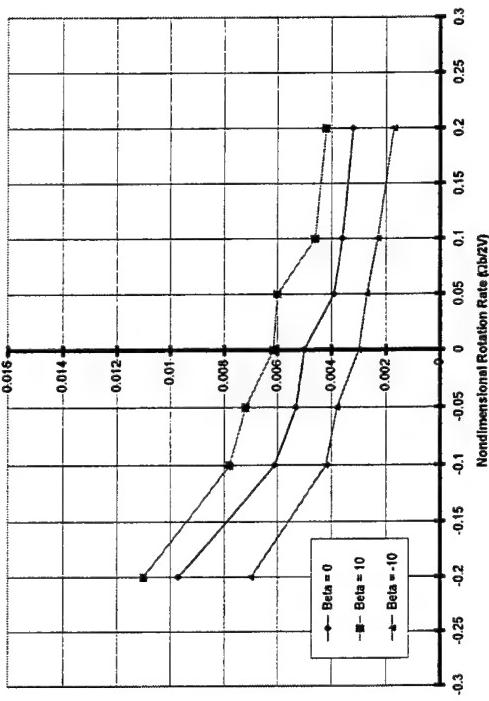




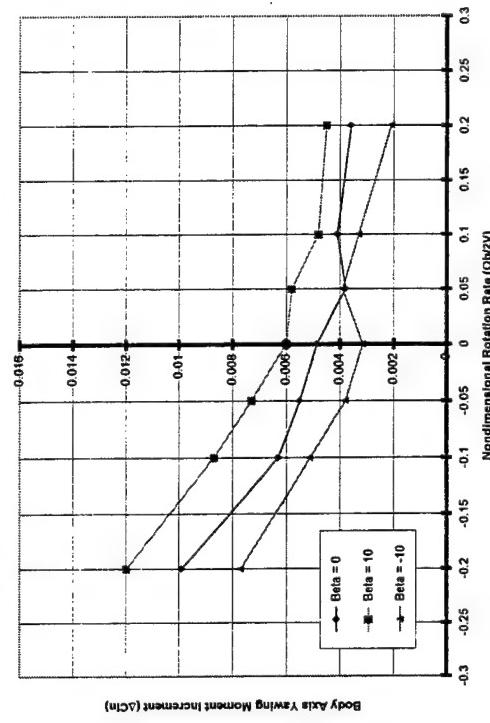




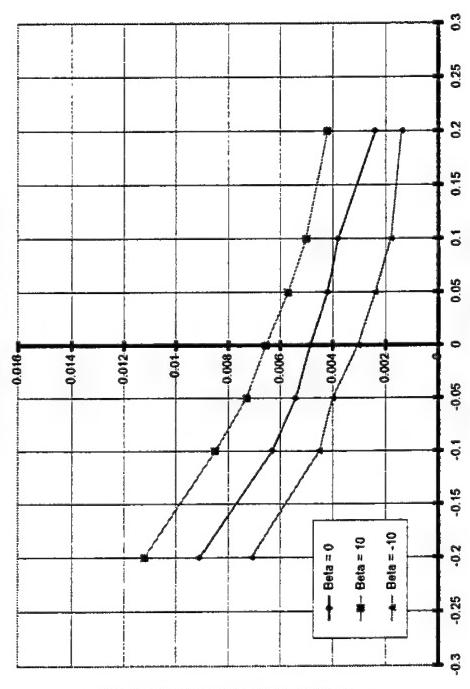
Yawing Moment Increment vs $\Omega b/2V$
ICE 101, AMT = 0 / 60, AOA = 65 Deg.



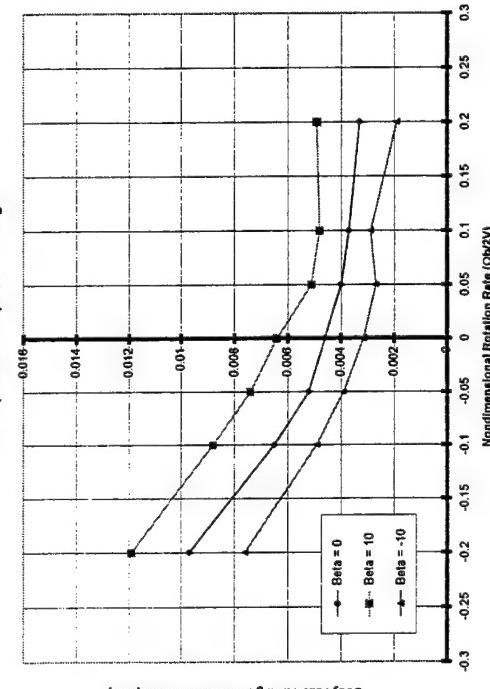
Yawing Moment Increment vs $\Omega b/2V$
ICE 101, AMT = 0 / 60, AOA = 75 Deg.



Yawing Moment Increment vs $\Omega b/2V$
ICE 101, AMT = 0 / 60, AOA = 80 Deg.

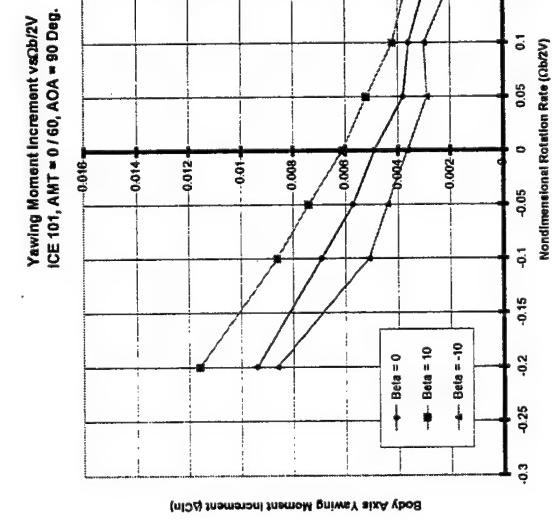
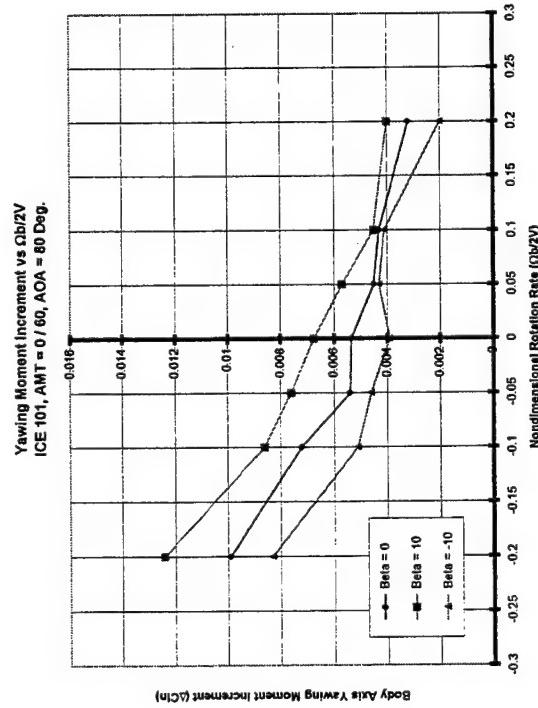
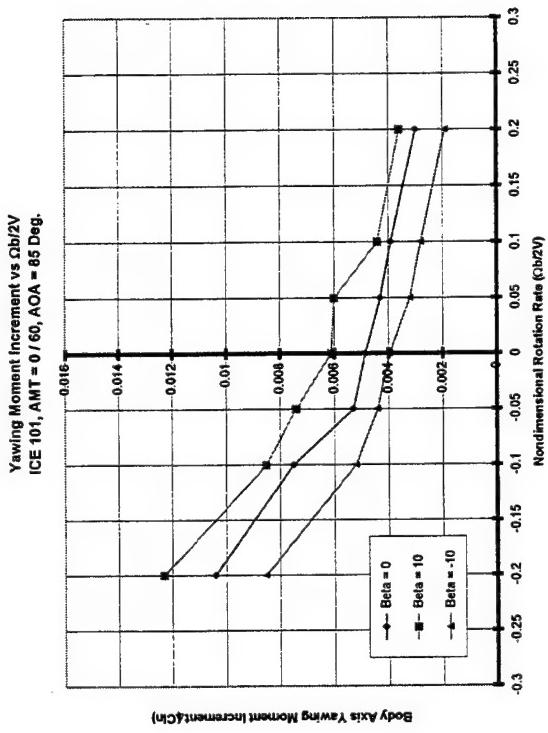


Yawing Moment Increment vs $\Omega b/2V$
ICE 101, AMT = 0 / 60, AOA = 70 Deg.



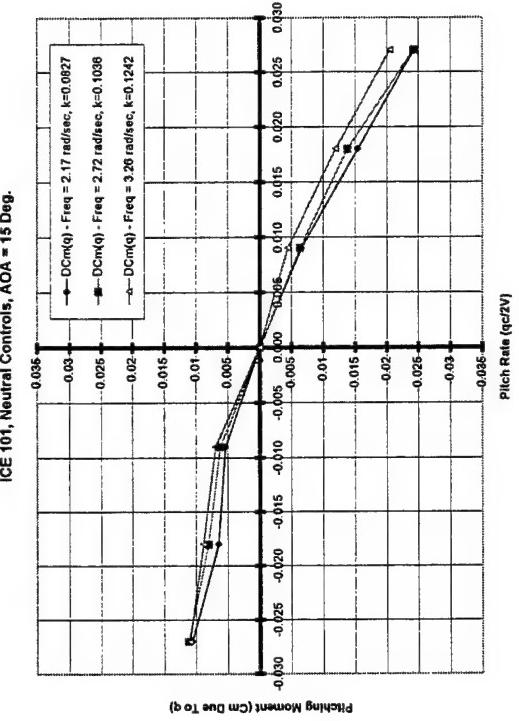
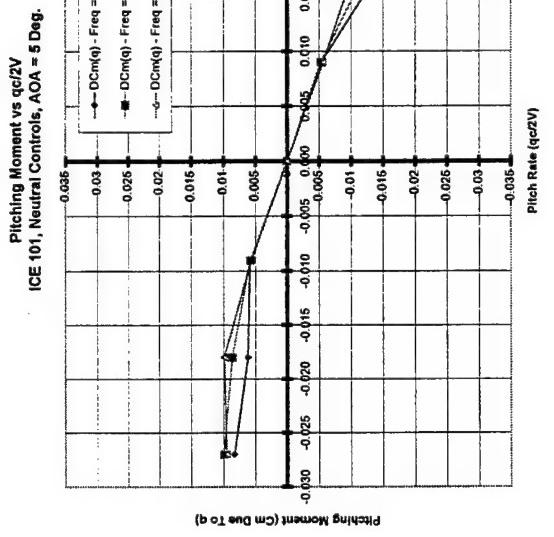
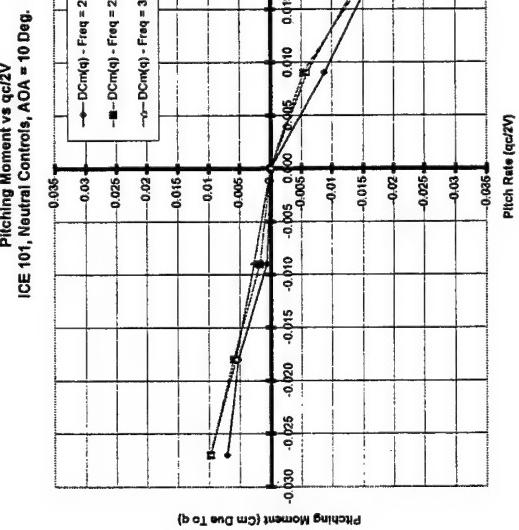
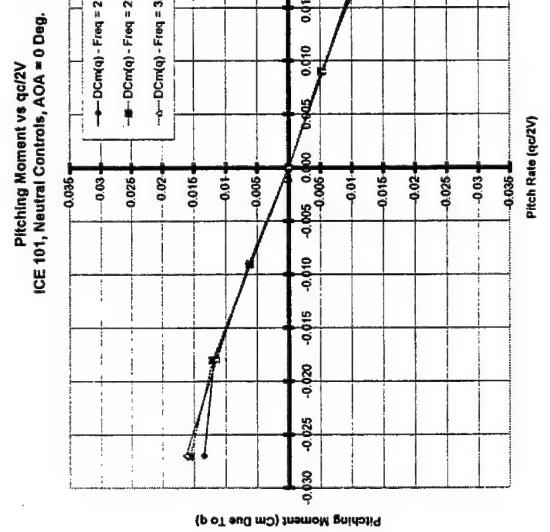
Body Axis Yawing Moment Increment (lb/in)

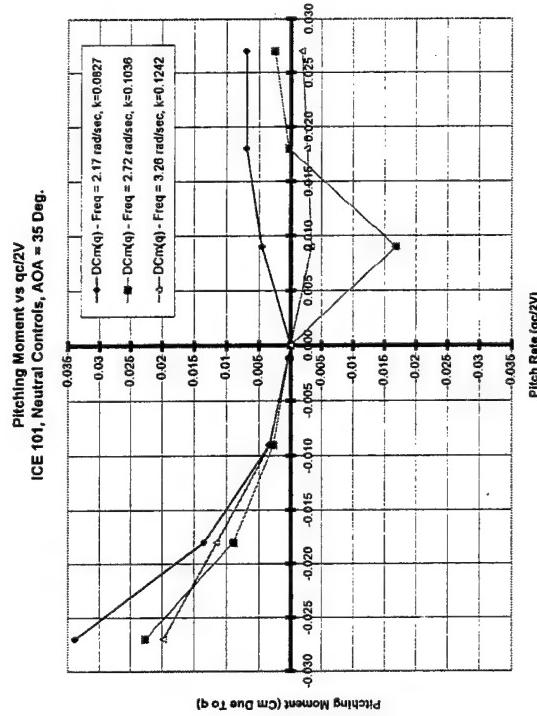
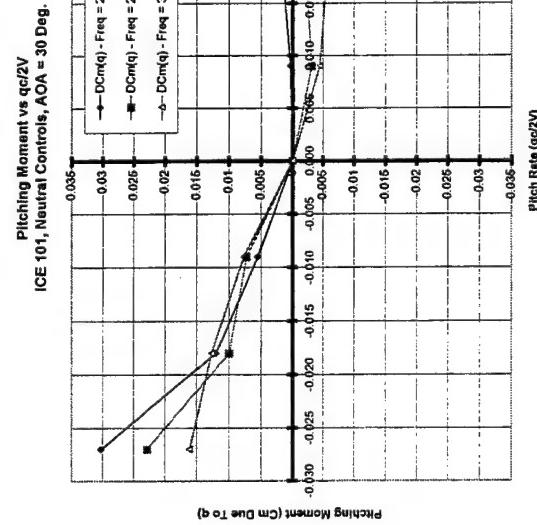
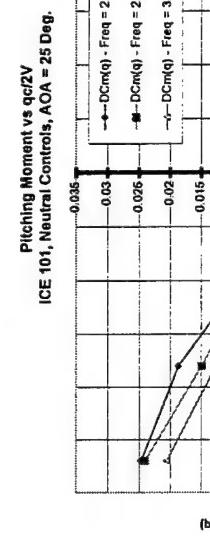
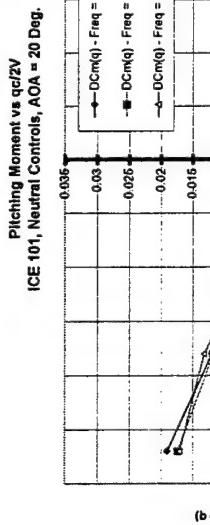
Body Axis Yawing Moment Increment (lb/in)



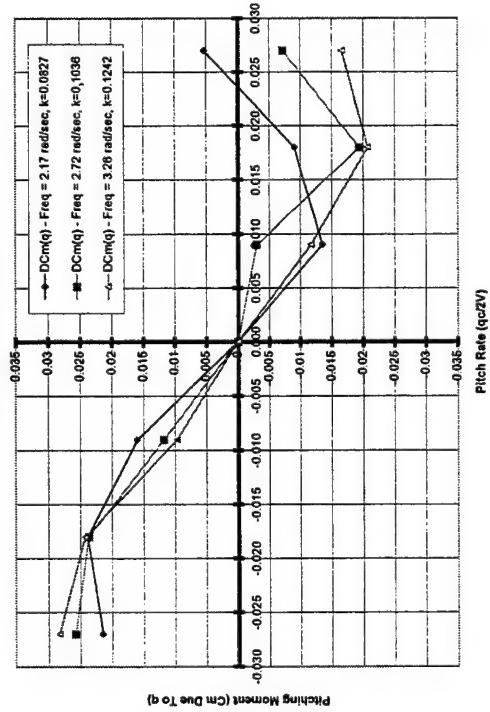
Appendix D

Pitch Forced Oscillation Data Plots

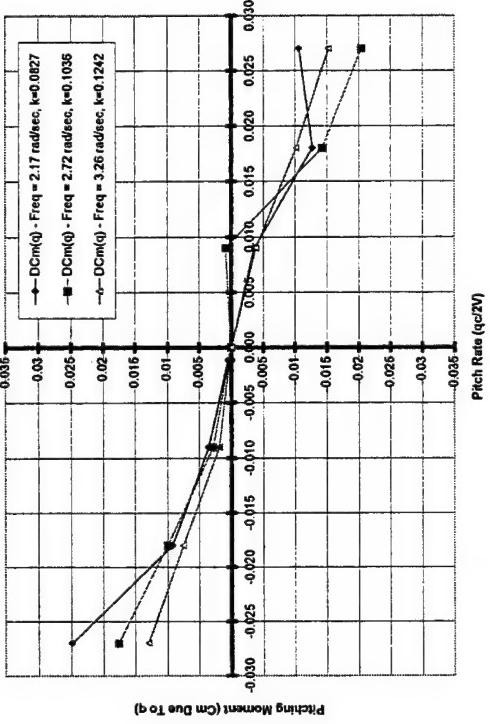




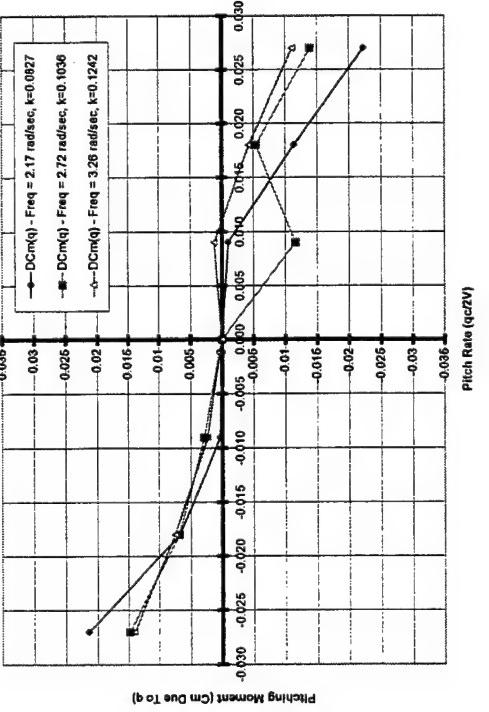
Pitching Moment vs $q/c/2V$
ICE 101, Neutral Controls, AOA = 40 Deg.



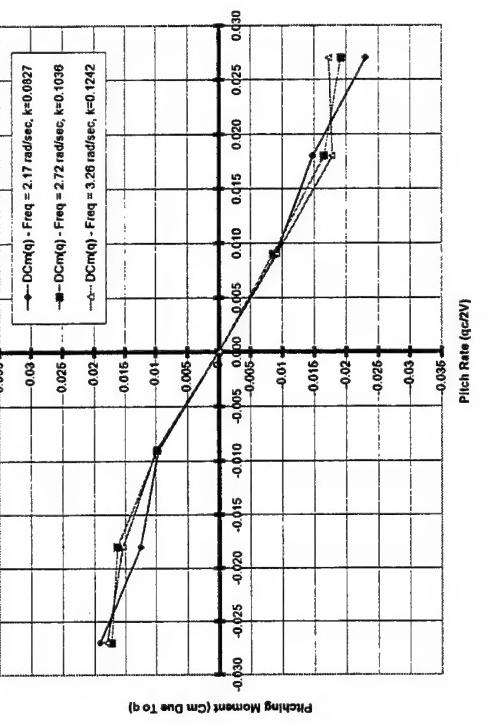
Pitching Moment vs $q/c/2V$
ICE 101, Neutral Controls, AOA = 45 Deg.



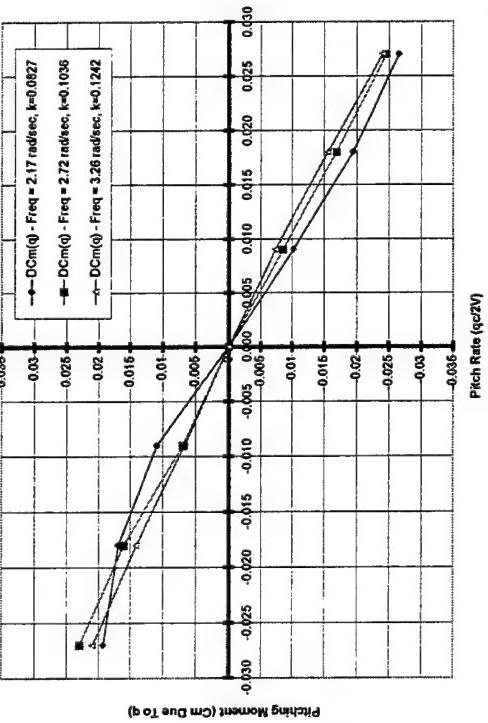
Pitching Moment vs $q/c/2V$
ICE 101, Neutral Controls, AOA = 50 Deg.



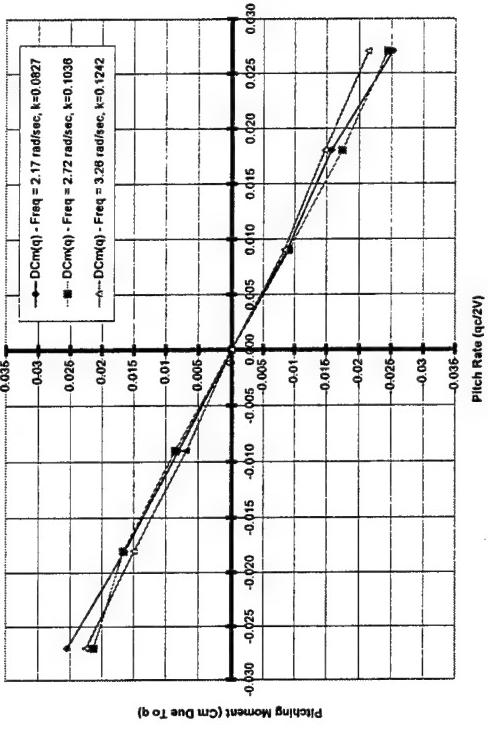
Pitching Moment vs $q/c/2V$
ICE 101, Neutral Controls, AOA = 55 Deg.



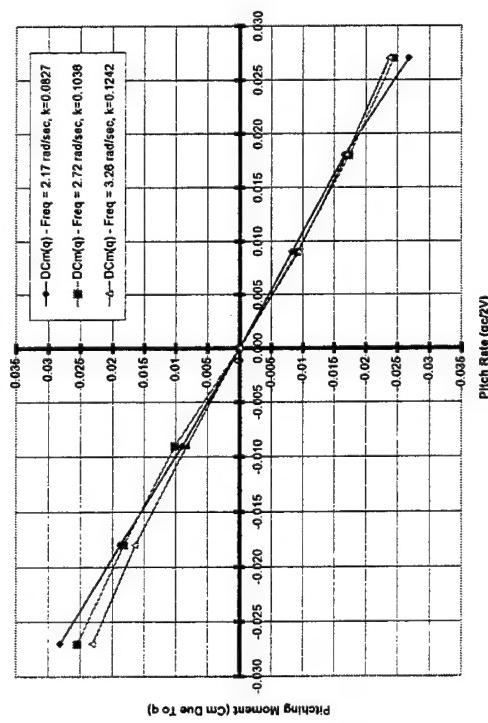
Pitching Moment vs $qc/2V$
ICE 101, Neutral Controls, AOA = 60 Deg.



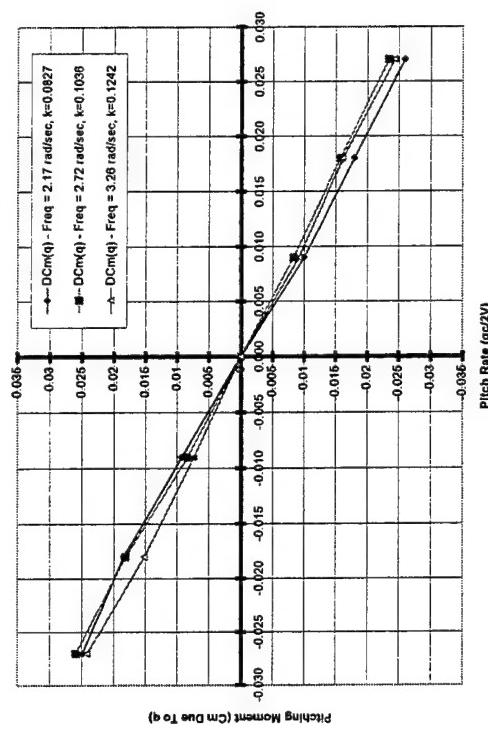
Pitching Moment vs $qc/2V$
ICE 101, Neutral Controls, AOA = 65 Deg.



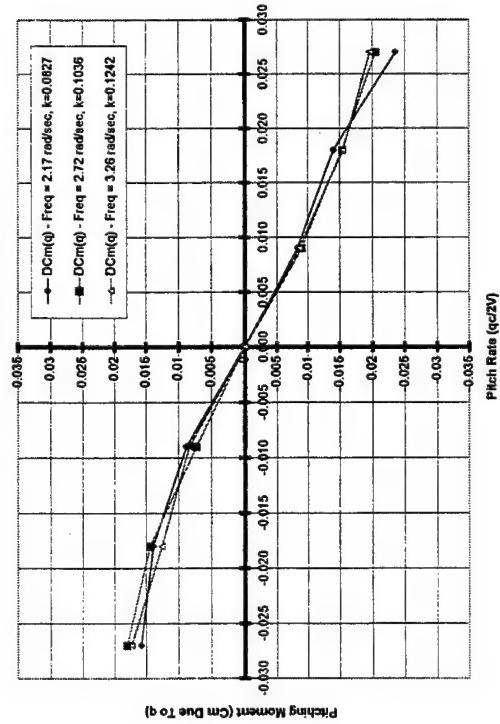
Pitching Moment vs $qc/2V$
ICE 101, Neutral Controls, AOA = 70 Deg.



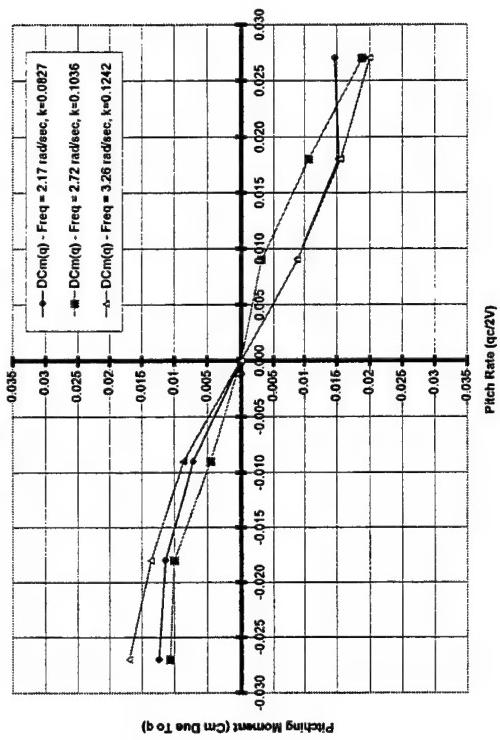
Pitching Moment vs $qc/2V$
ICE 101, Neutral Controls, AOA = 75 Deg.



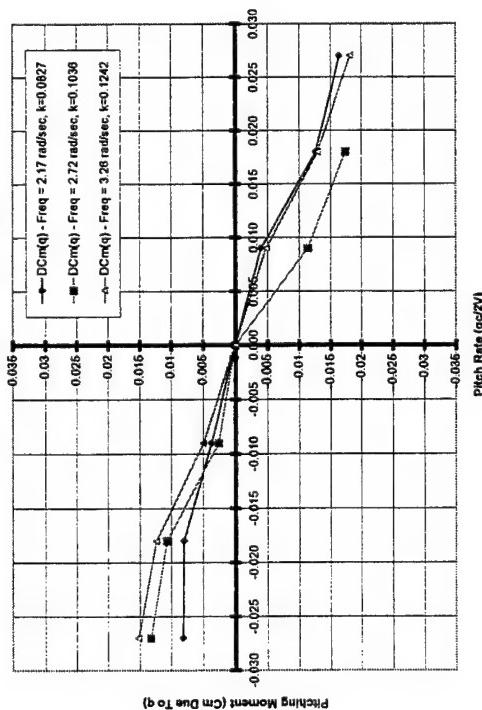
Pitching Moment vs $q/c/2V$
ICE 101, Neutral Controls, AOA = 80 Deg.

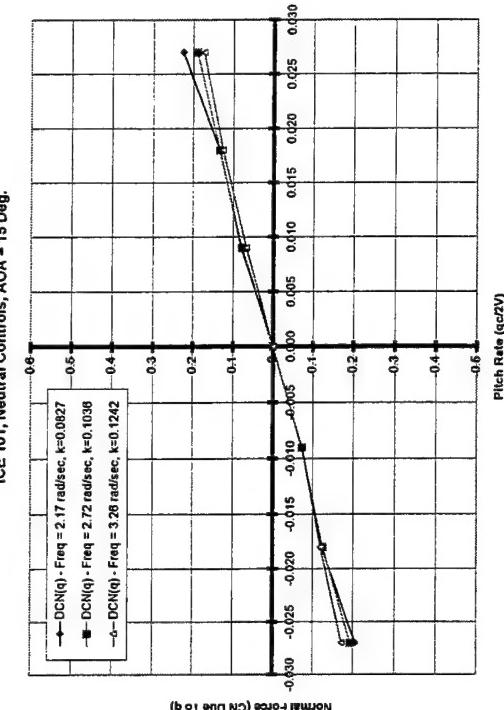
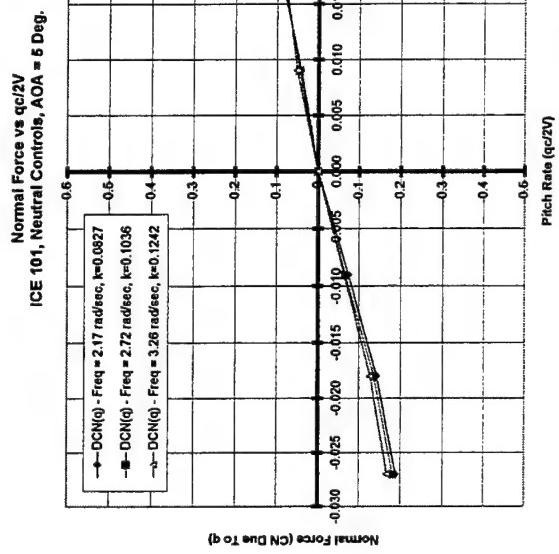
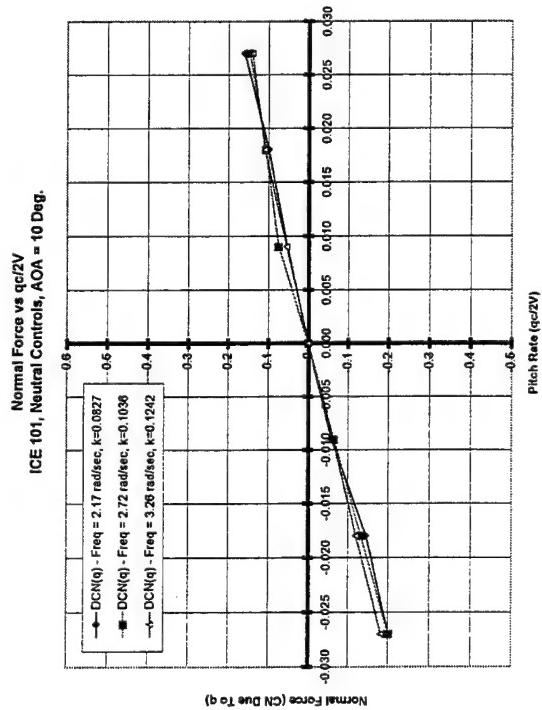
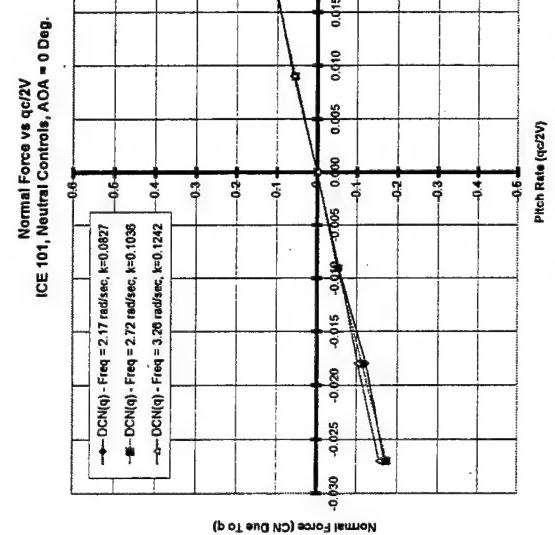


Pitching Moment vs $qc/2V$
ICE 101, Neutral Controls, AOA = 85 Deg.

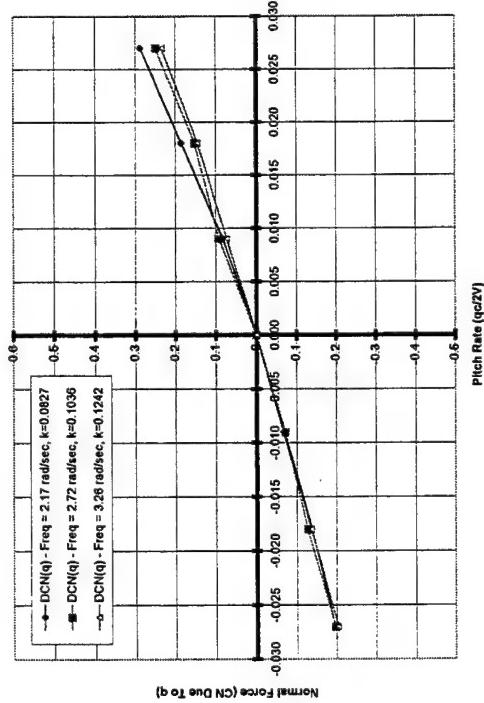


Pitching Moment vs $qc/2V$
ICE 101, Neutral Controls, AOA = 90 Deg.

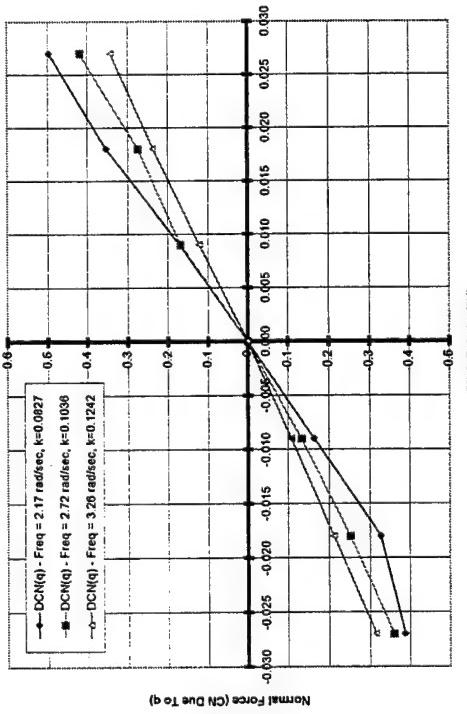




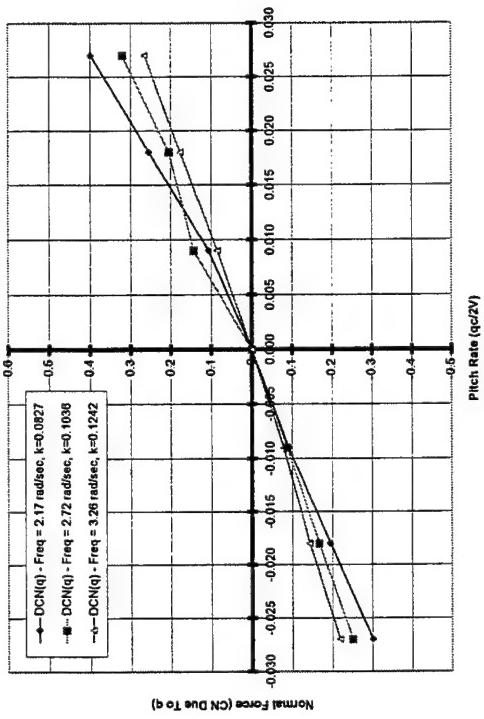
ICE 101, Neutral Controls, AOA = 20 Deg.



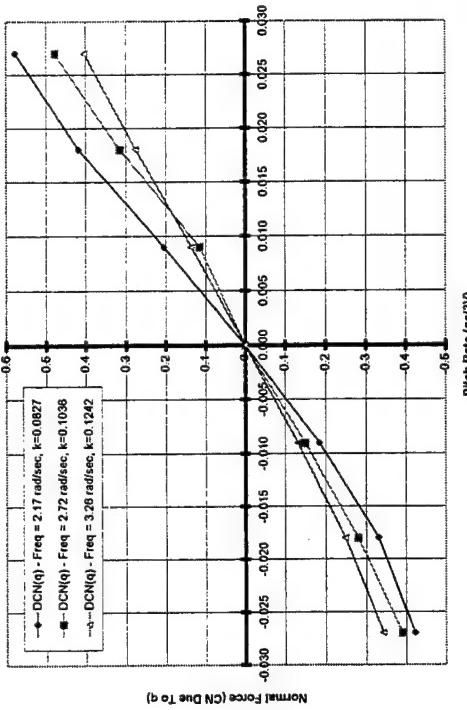
ICE 101, Neutral Controls, AOA = 30 Deg.

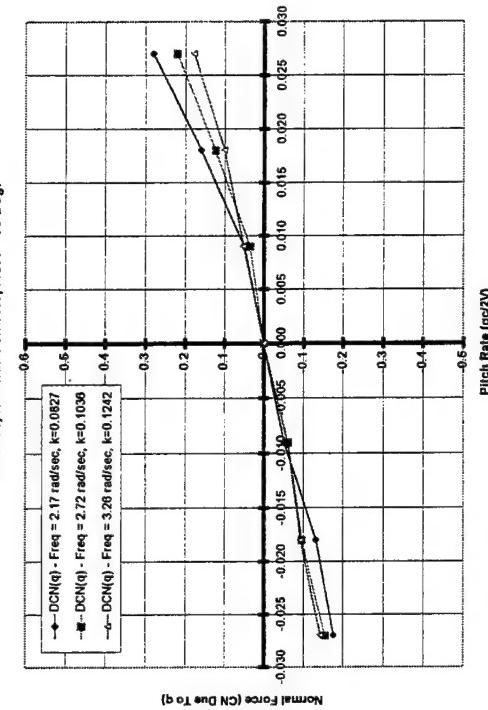
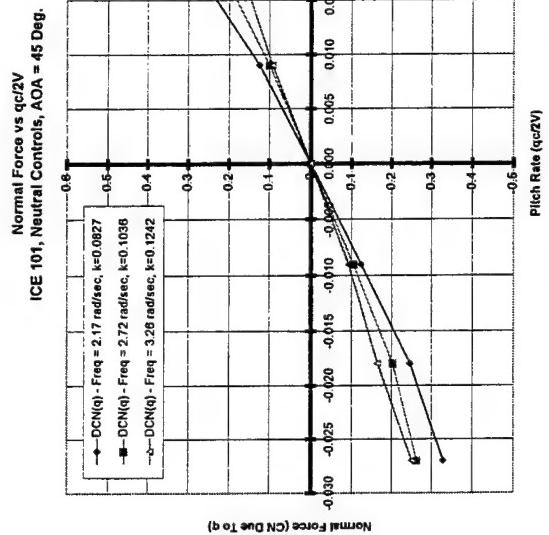
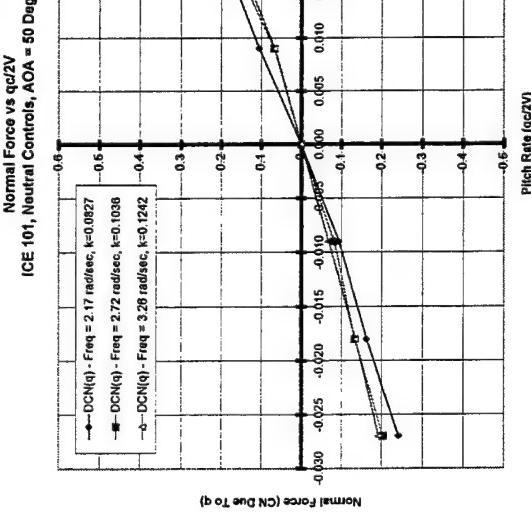
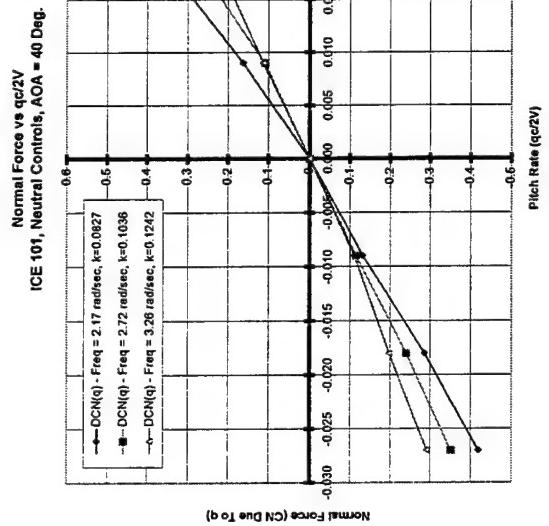


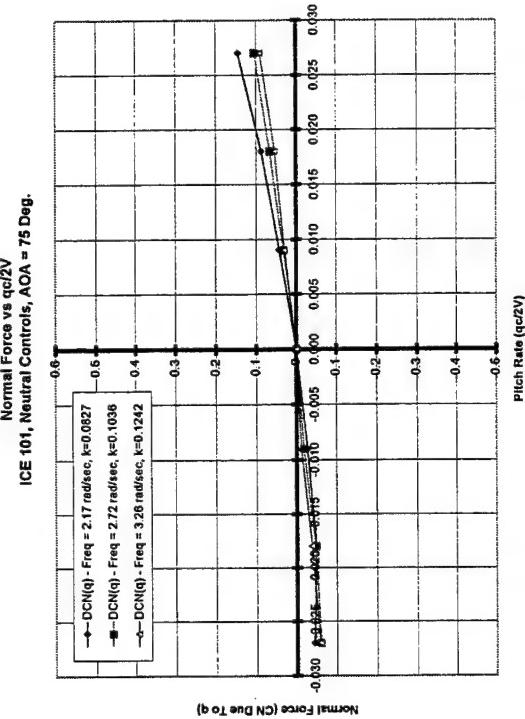
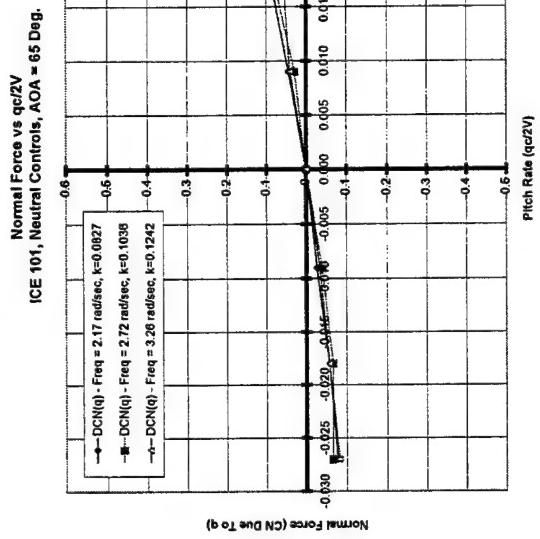
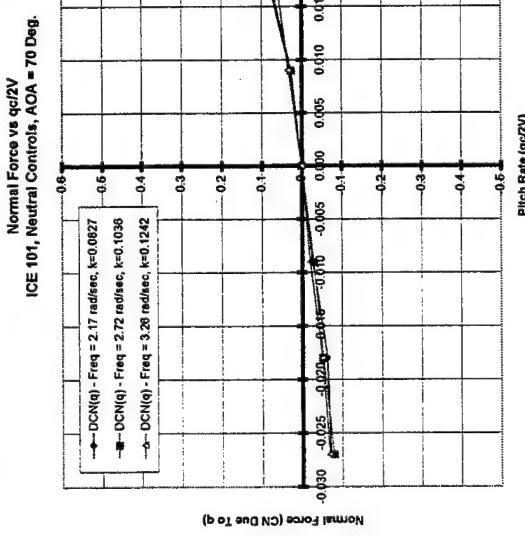
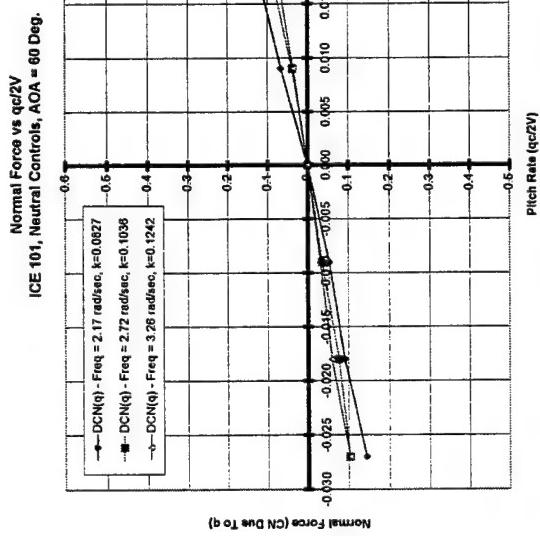
ICE 101, Neutral Controls, AOA = 25 Deg.



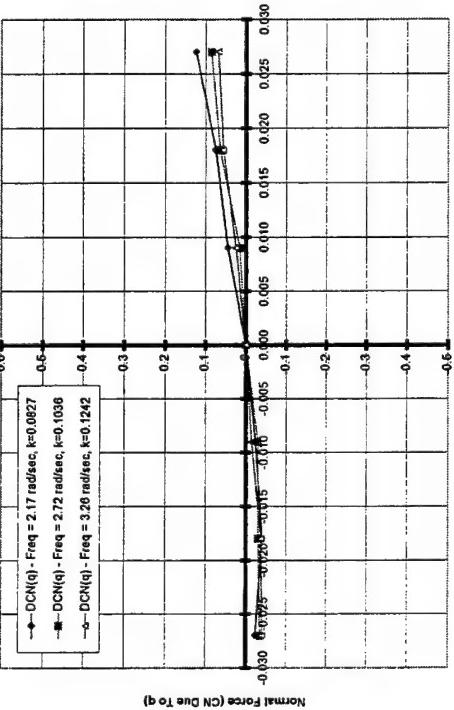
ICE 101, Neutral Controls, AOA = 35 Deg.



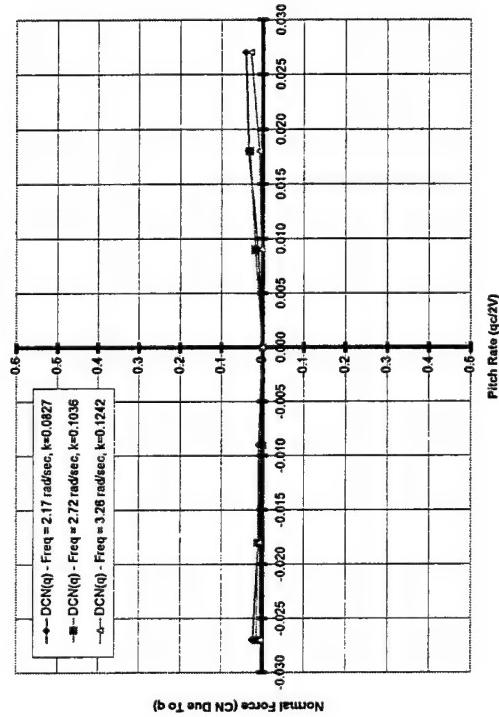




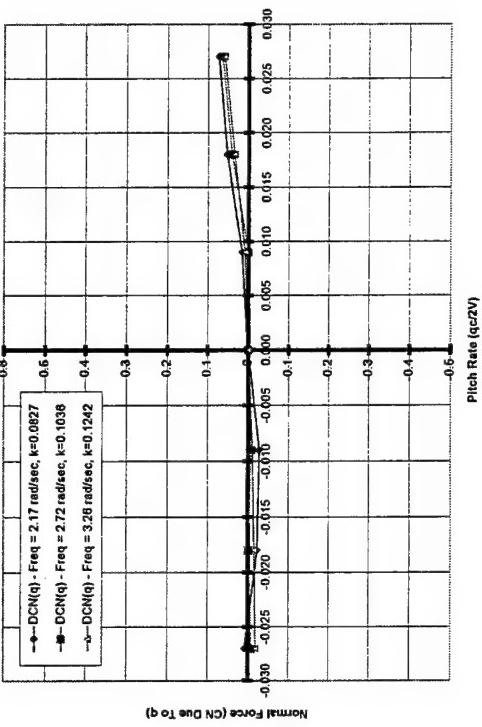
Normal Force vs $qc/2V$
ICE 101, Neutral Controls, AOA = 80 Deg.

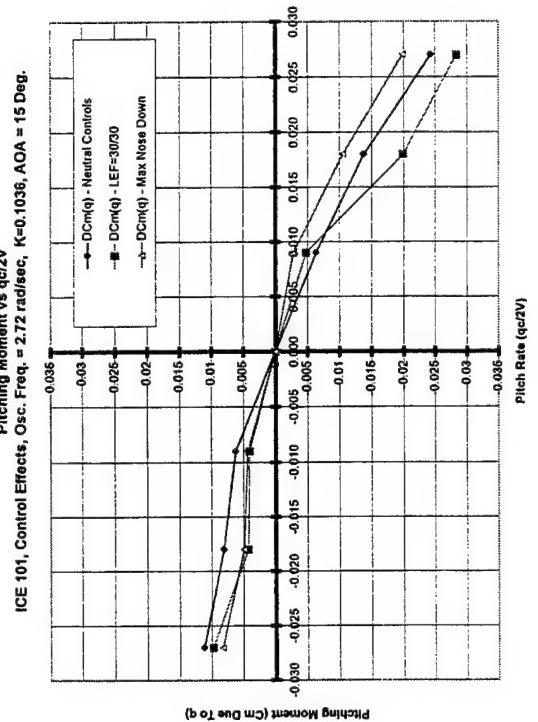
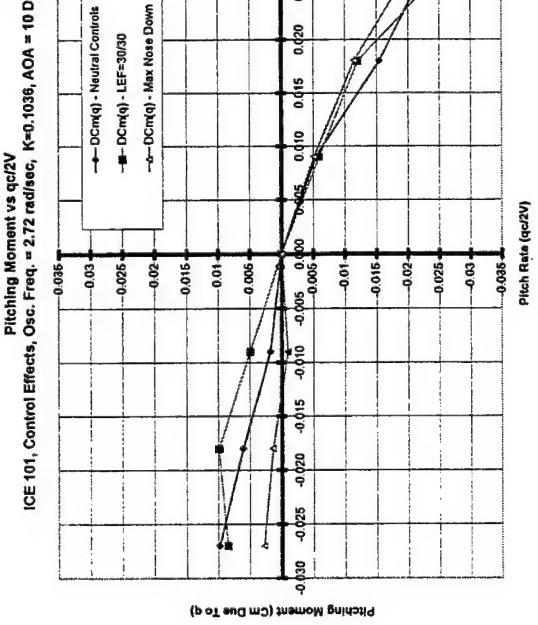
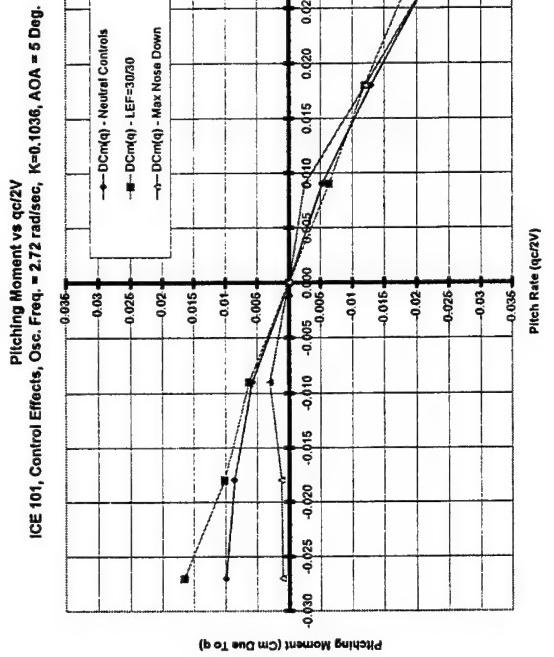
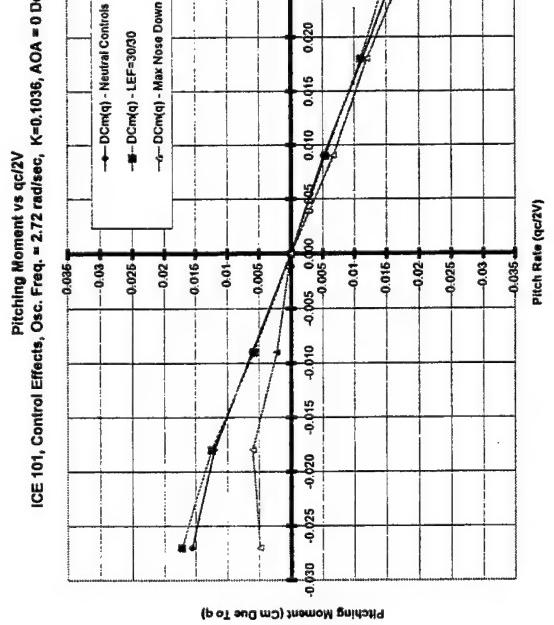


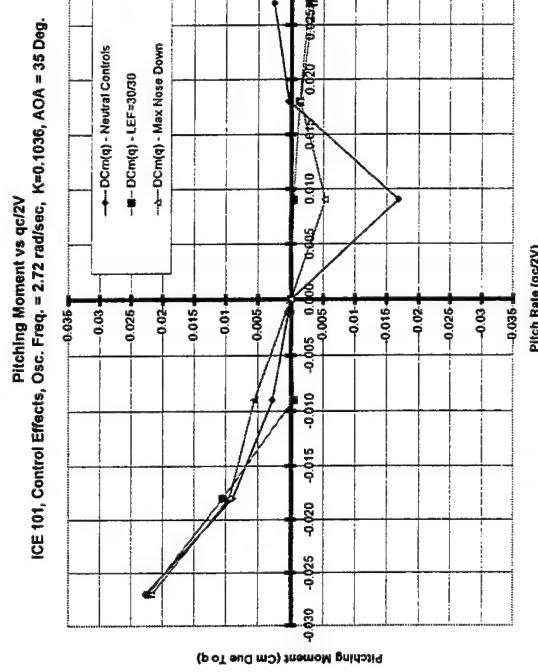
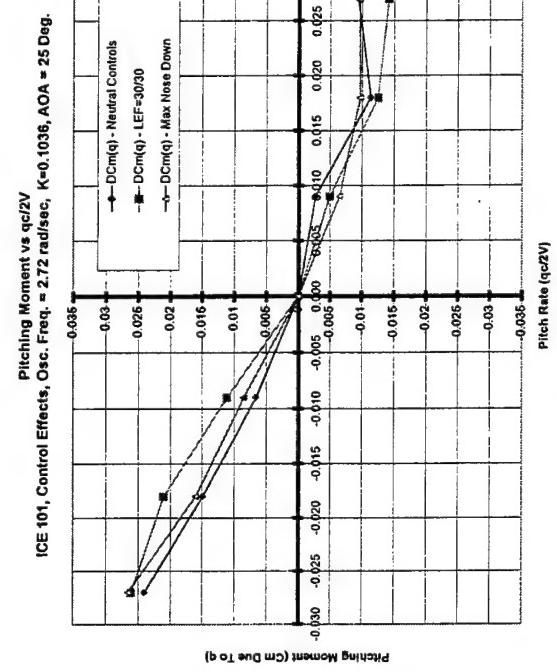
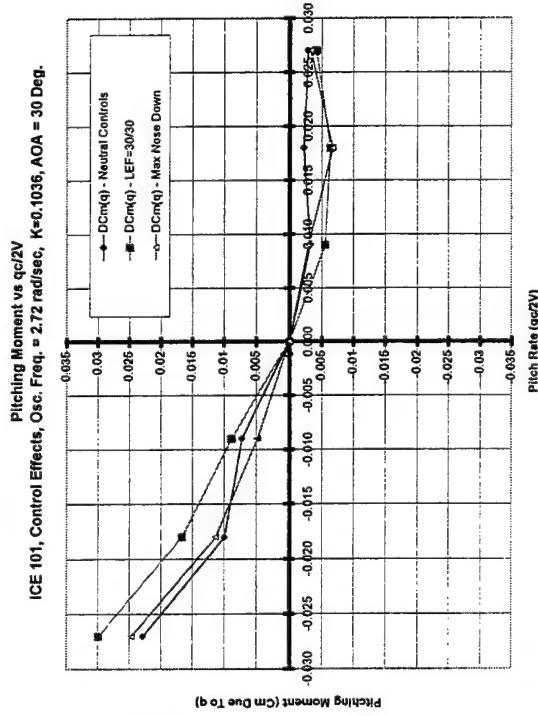
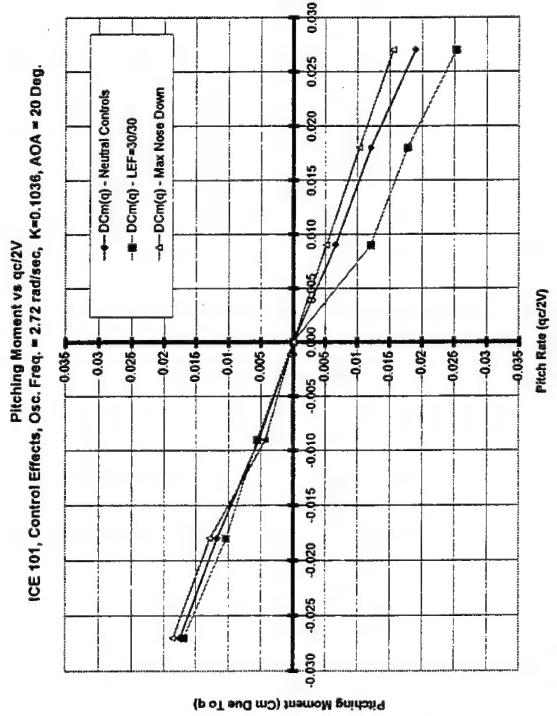
Normal Force vs $qc/2V$
ICE 101, Neutral Controls, AOA = 90 Deg.



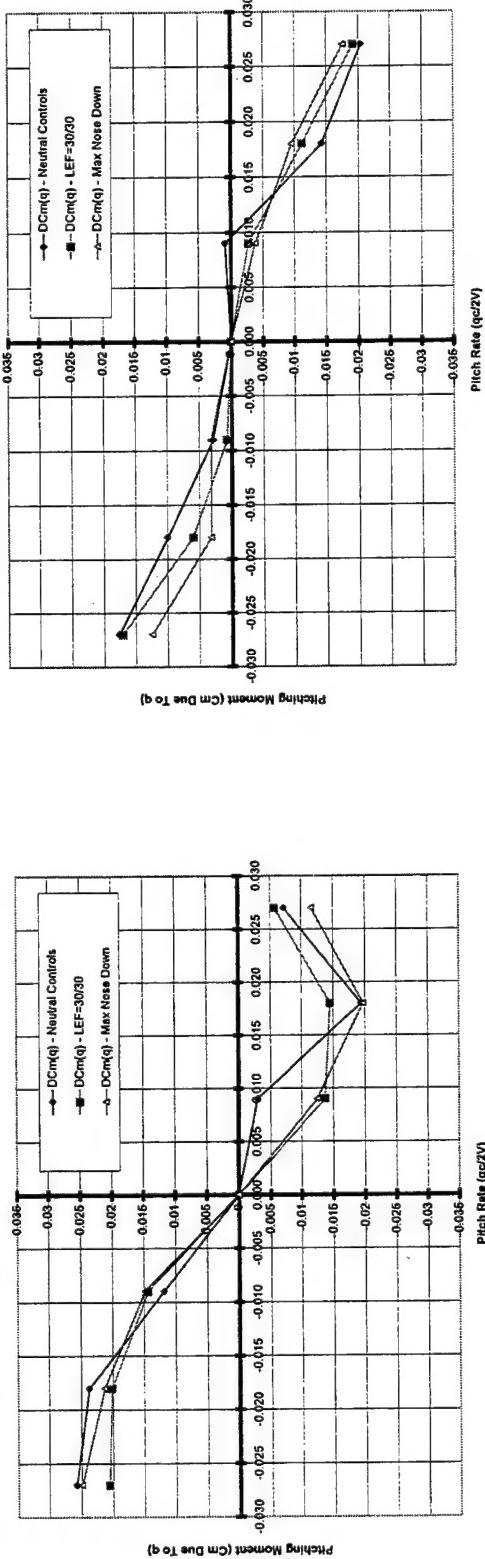
Normal Force vs $qc/2V$
ICE 101, Neutral Controls, AOA = 85 Deg.



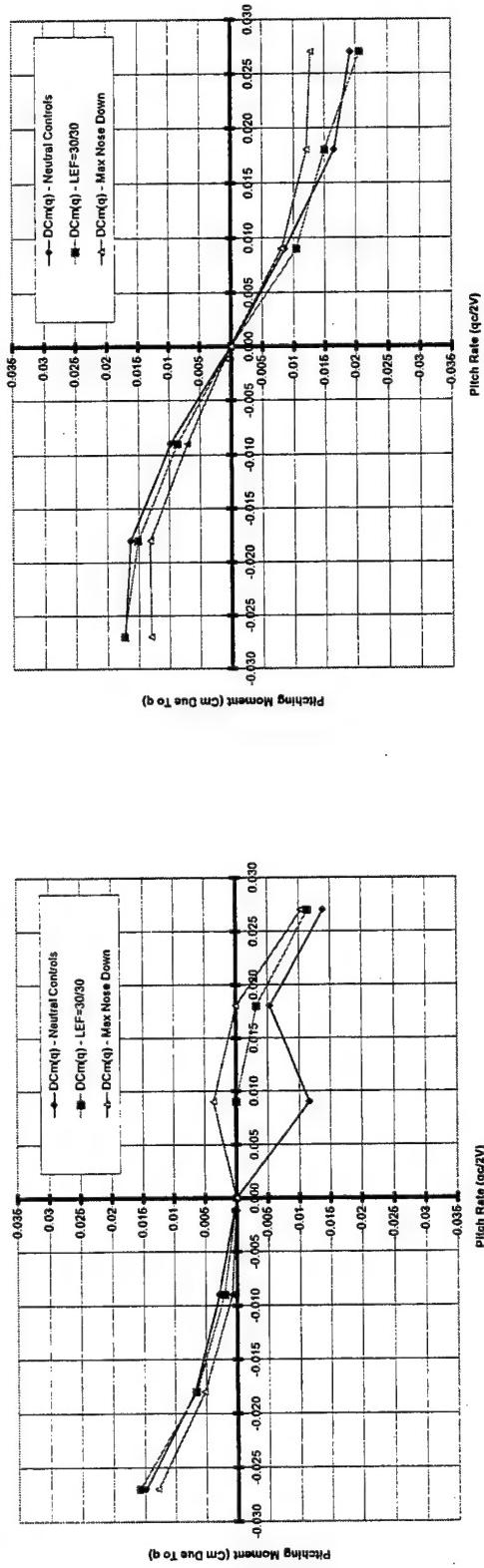


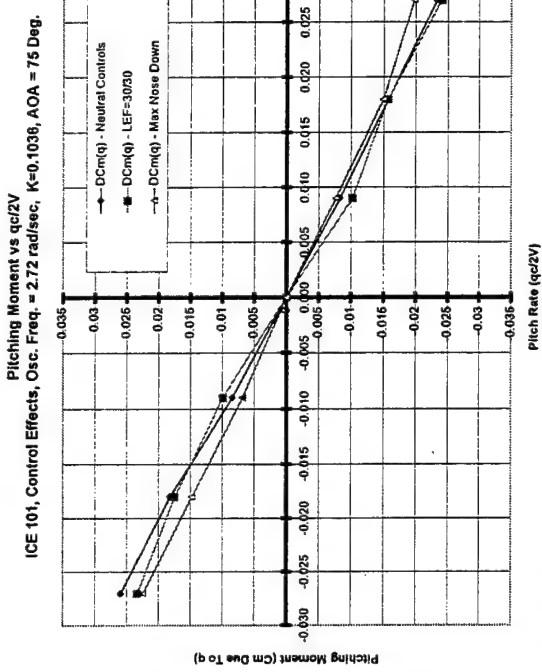
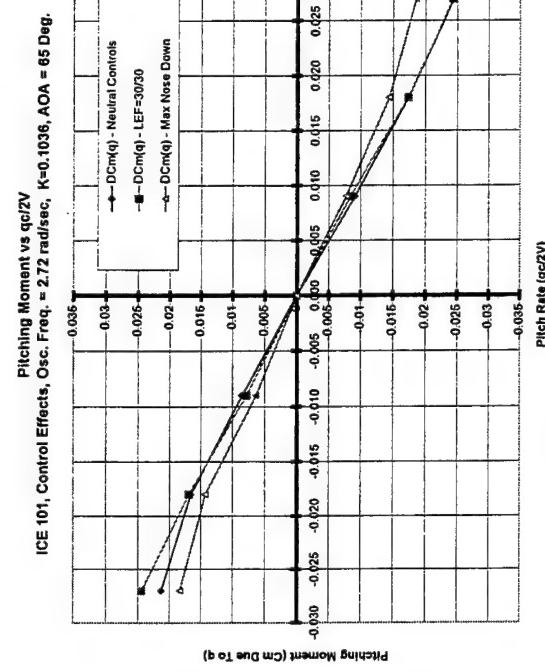
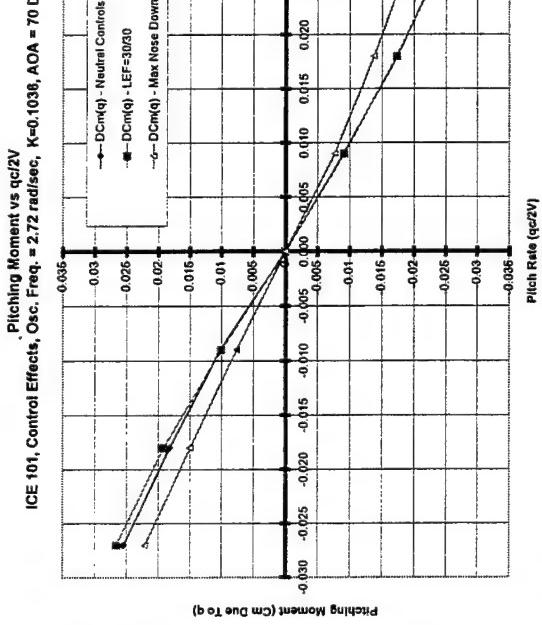
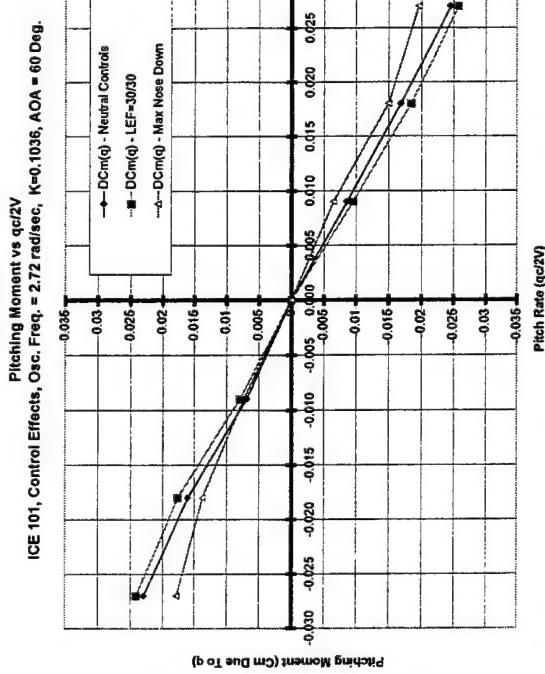


ICE 101, Control Effects, Osc. Freq. = 2.72 rad/sec, K=0.1036, AOA = 45 Deg.

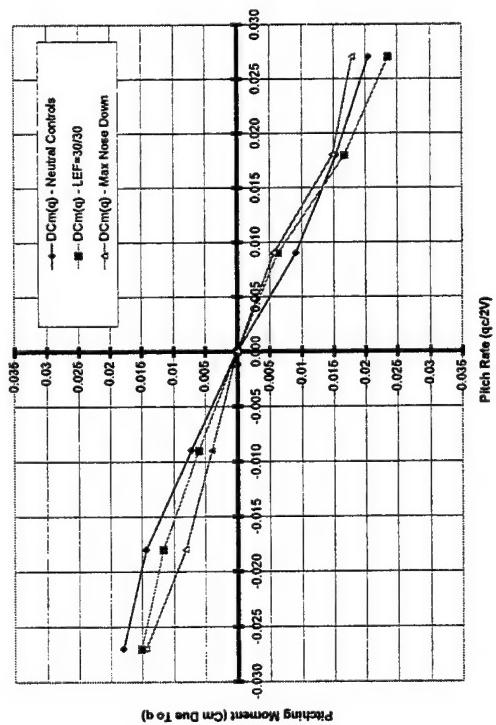


ICE 101, Control Effects, Osc. Freq. = 2.72 rad/sec, K=0.1036, AOA = 55 Deg.

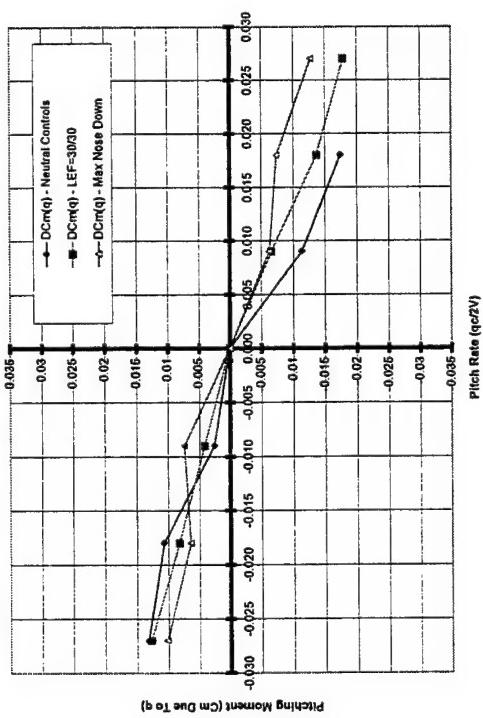




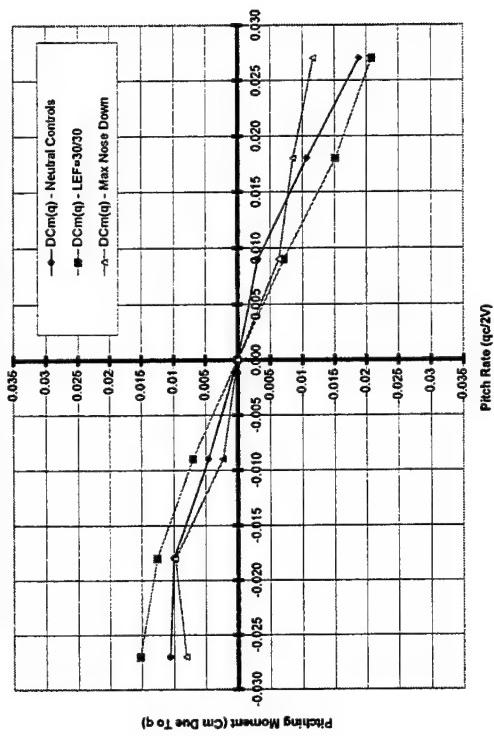
ICE 101, Control Effects, Osc. Freq. = 2.72 rad/sec, K=0.1036, AOA = 80 Deg.

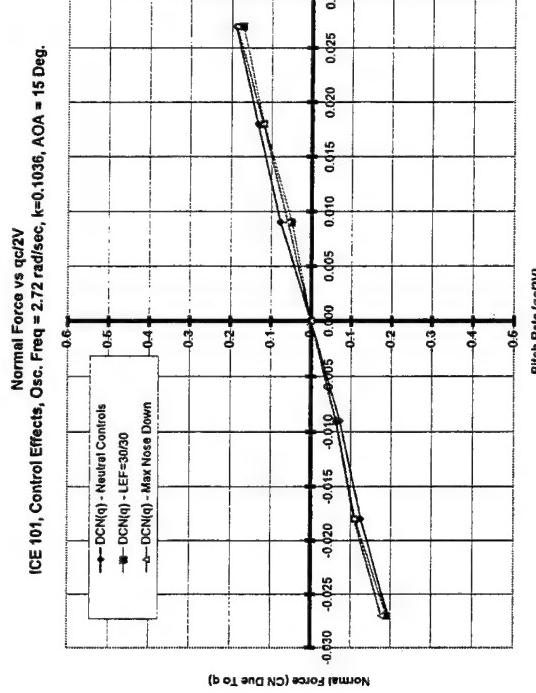
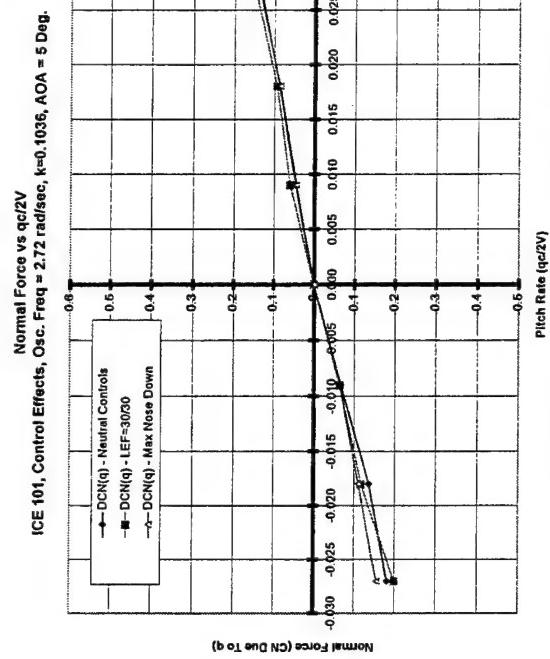
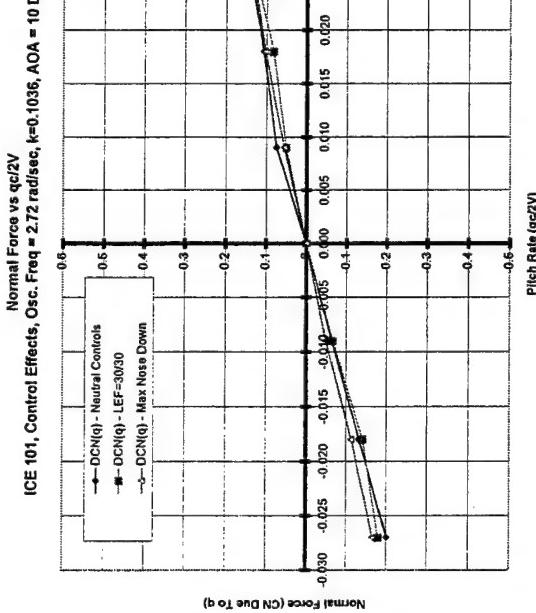
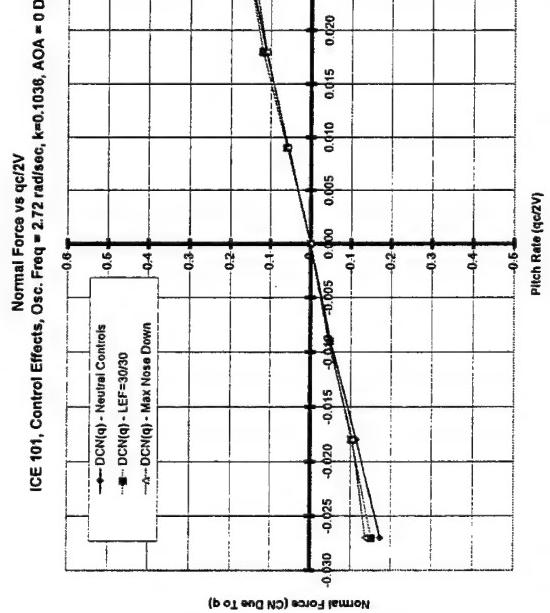


ICE 101, Control Effects, Osc. Freq. = 2.72 rad/sec, K=0.1036, AOA = 80 Deg.

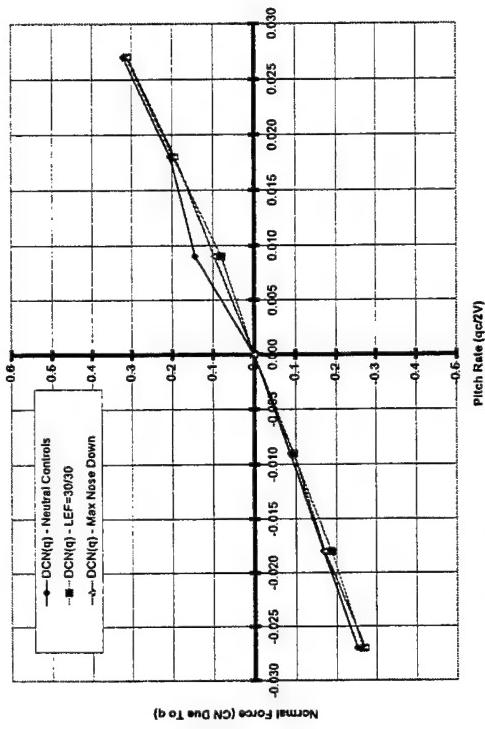


ICE 101, Control Effects, Osc. Freq. = 2.72 rad/sec, K=0.1036, AOA = 85 Deg.

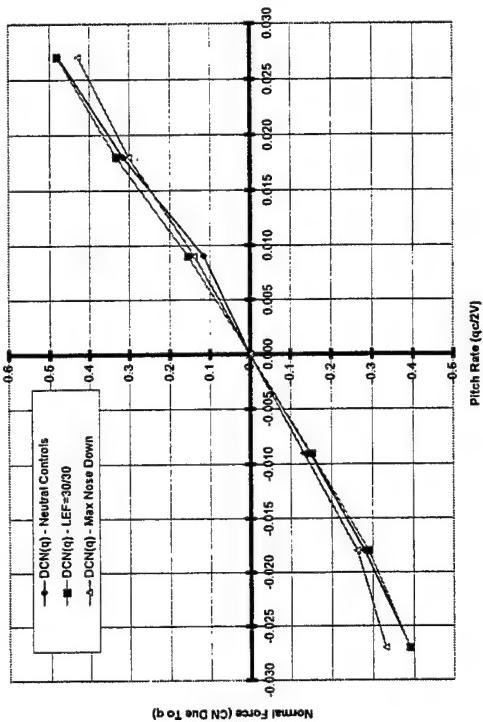




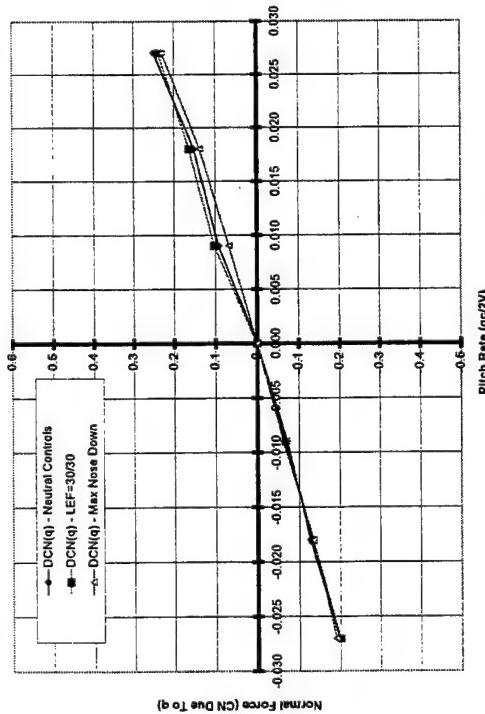
ICE 101, Control Effects, Osc. Freq = 2.72 rad/sec, k=0.1036, AOA = 25 Deg.



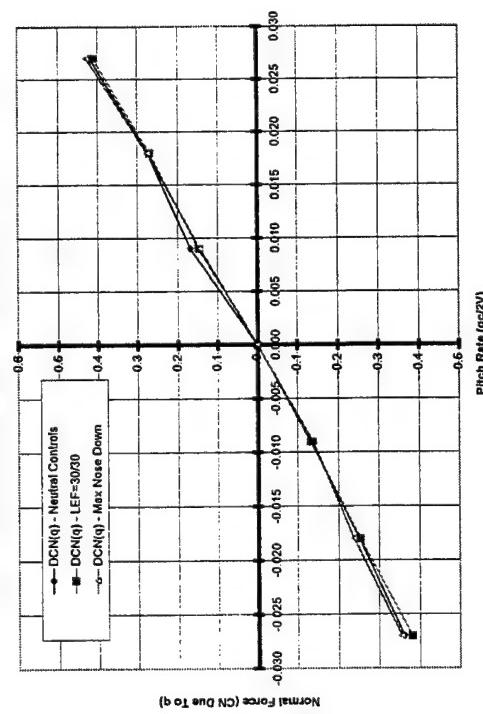
ICE 101, Control Effects, Osc. Freq = 2.72 rad/sec, k=0.1036, AOA = 35 Deg.

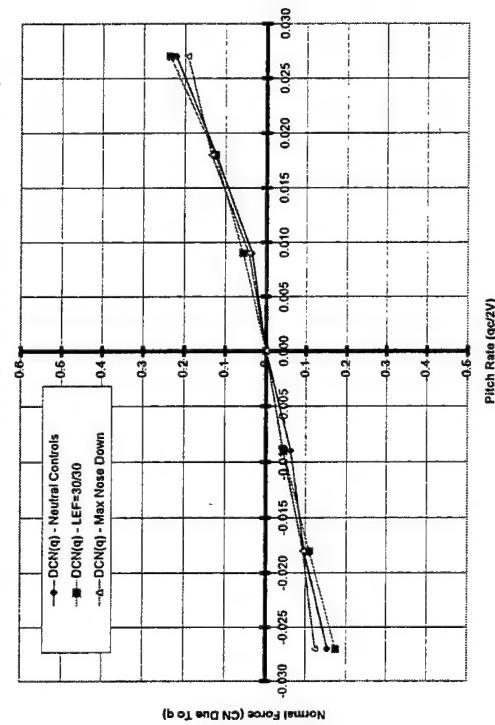
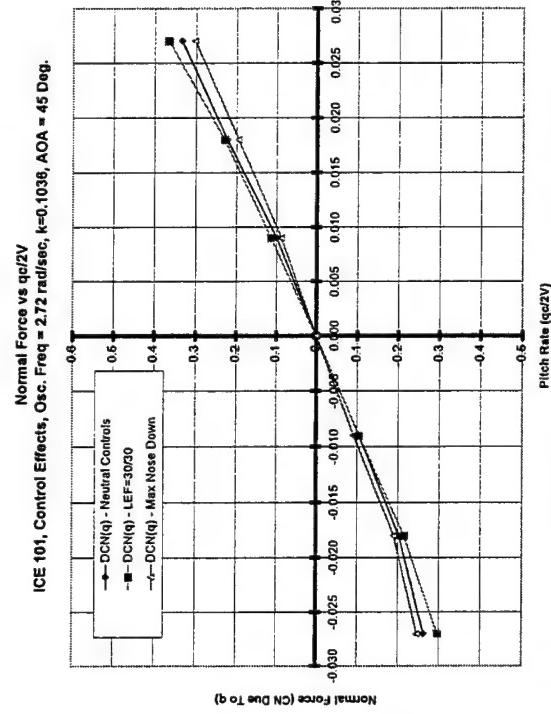
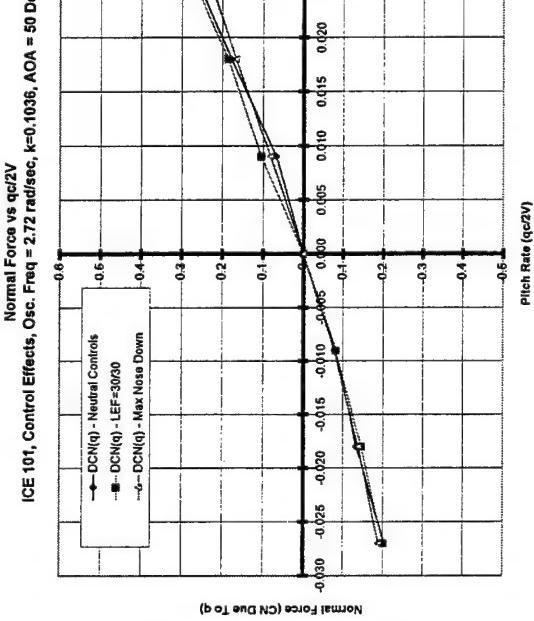
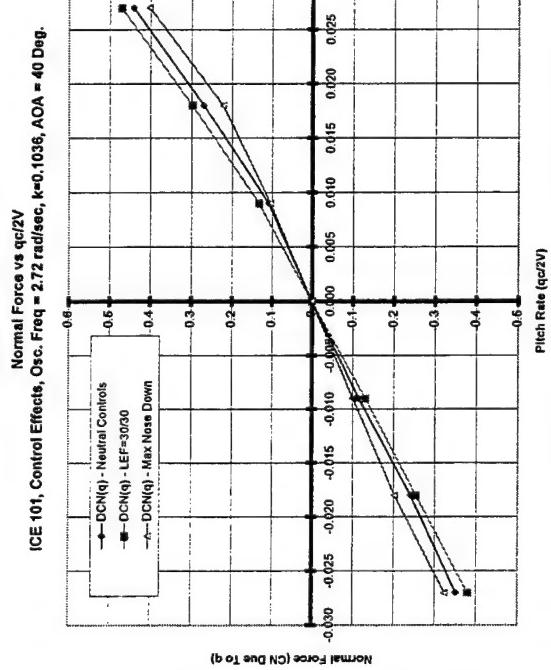


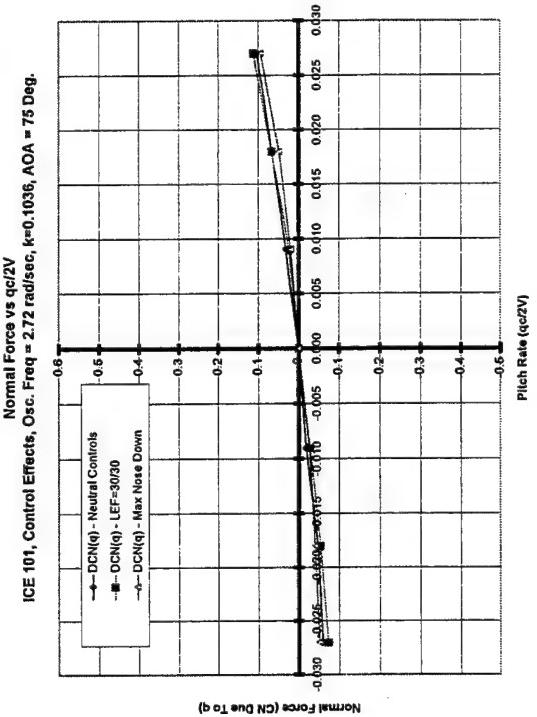
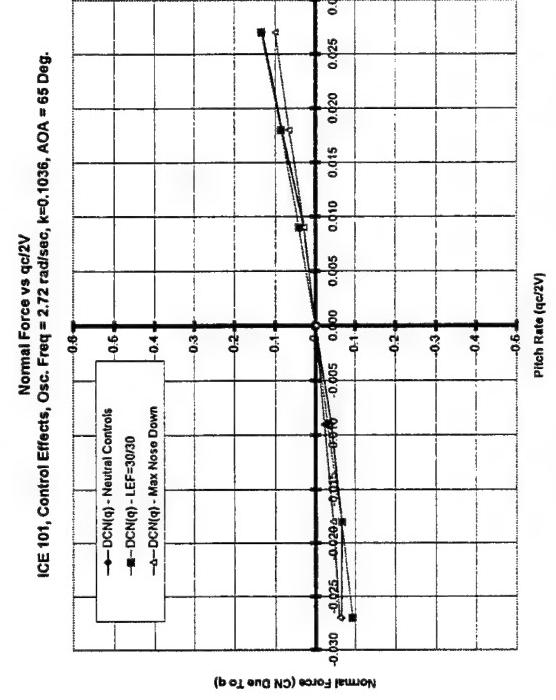
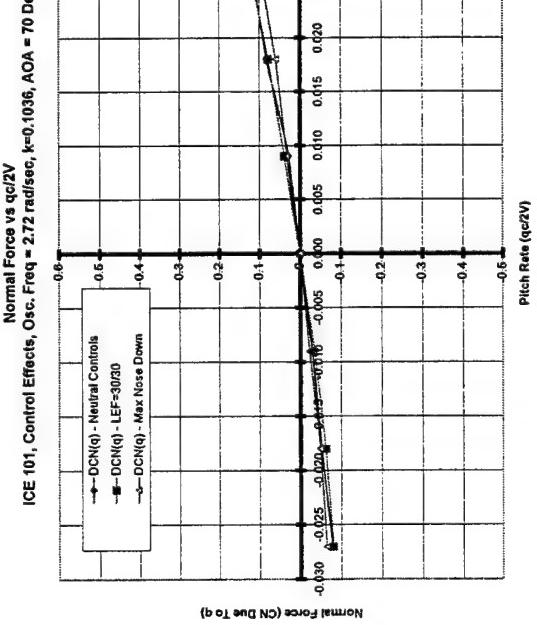
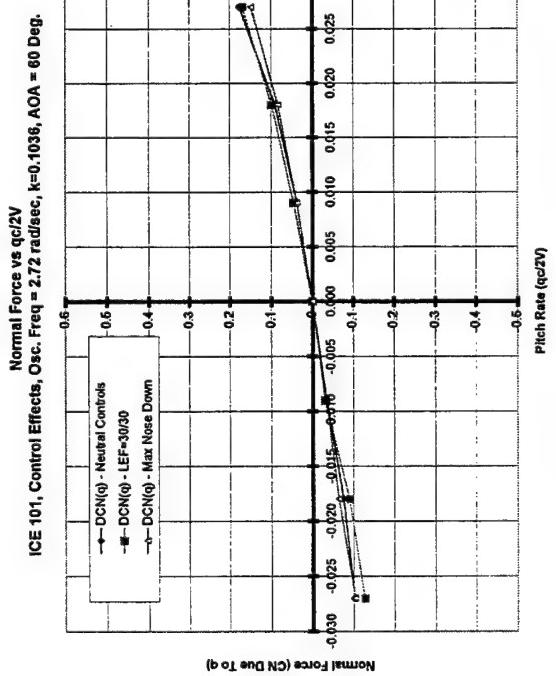
ICE 101, Control Effects, Osc. Freq = 2.72 rad/sec, k=0.1036, AOA = 20 Deg.

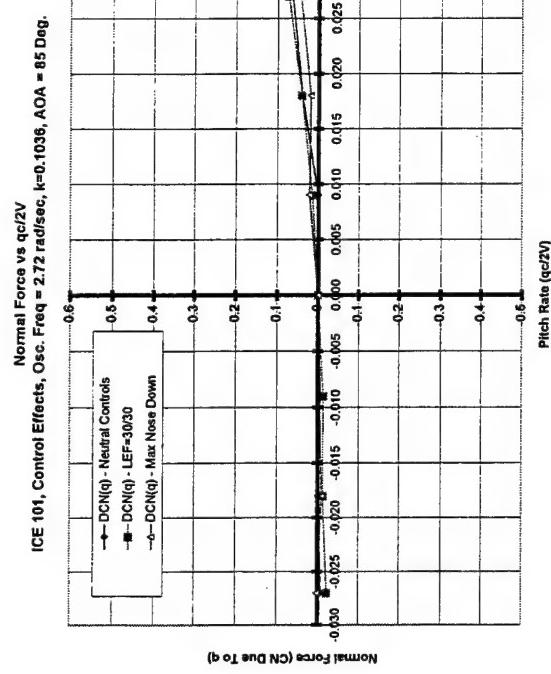
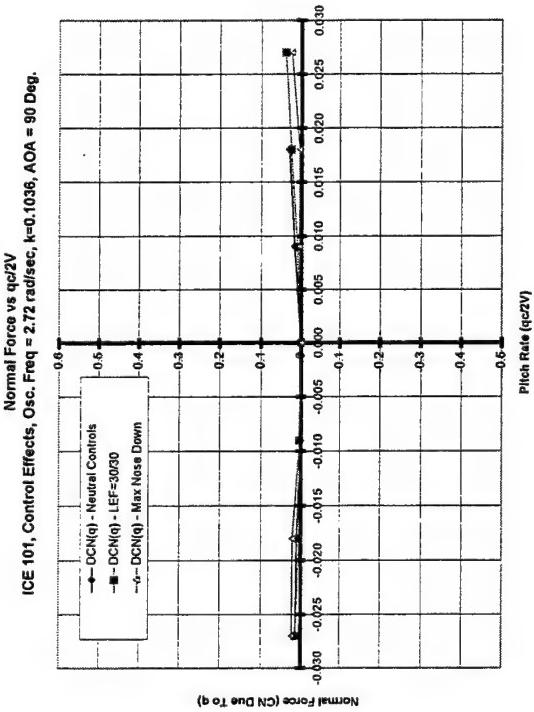
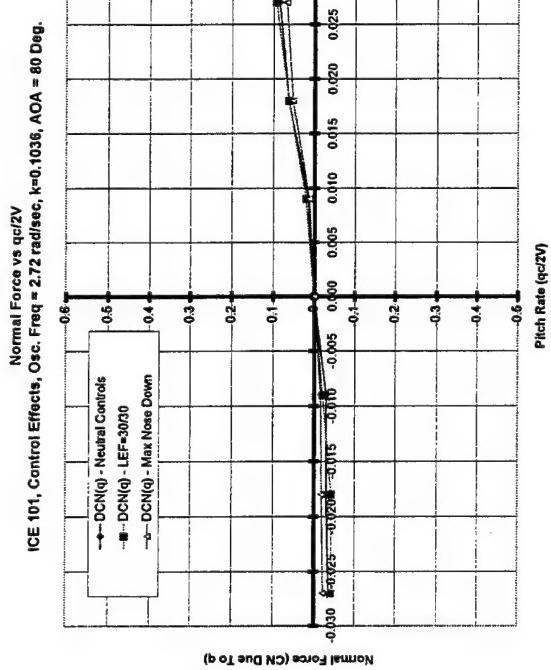


ICE 101, Control Effects, Osc. Freq = 2.72 rad/sec, k=0.1036, AOA = 30 Deg.



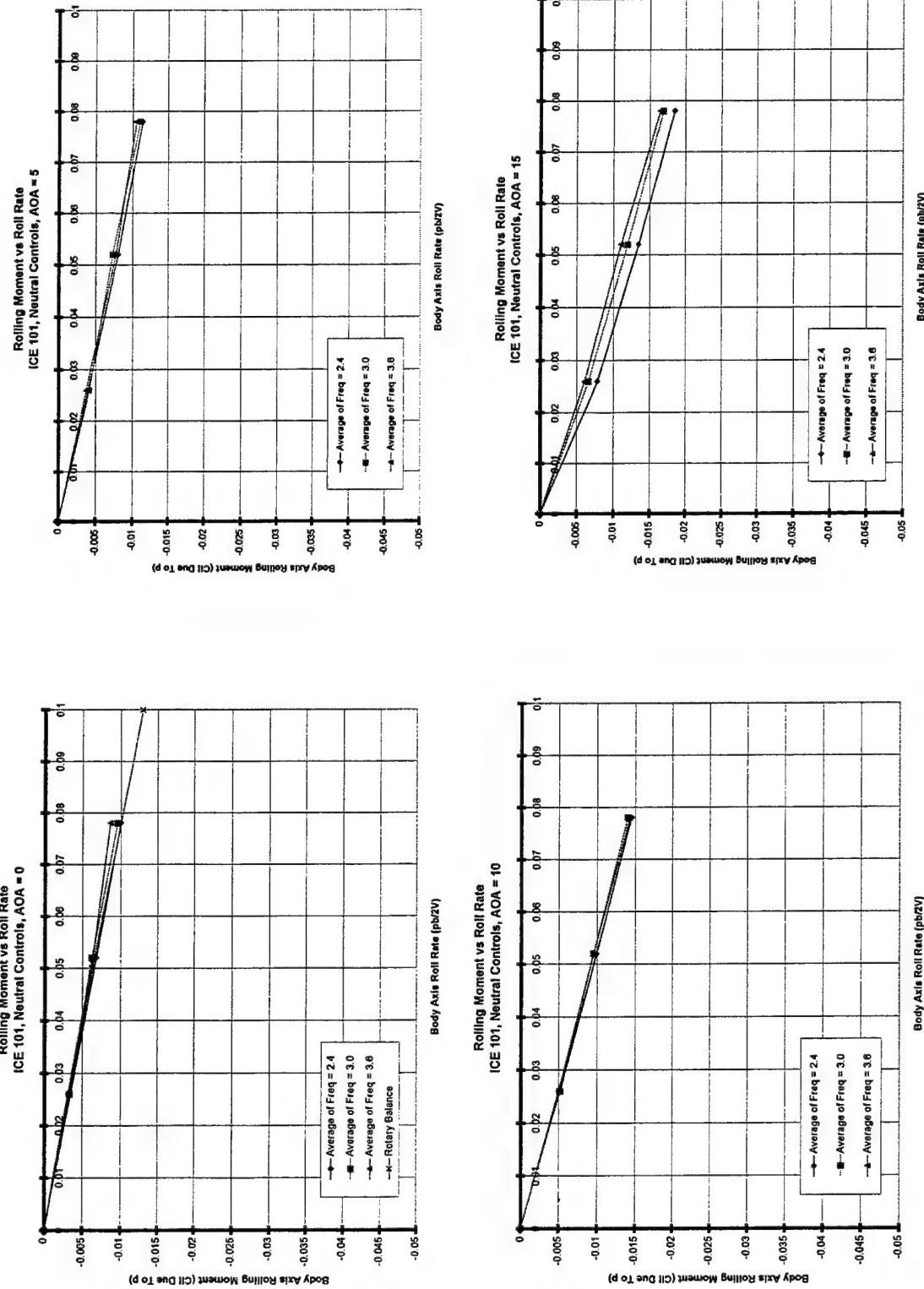


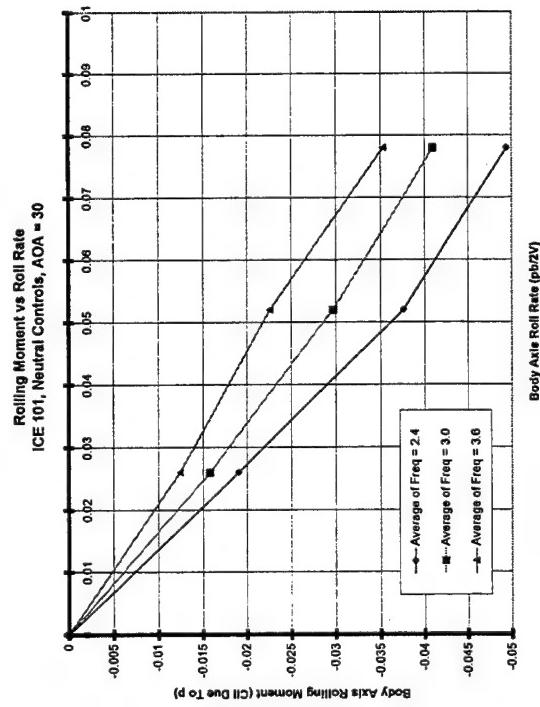
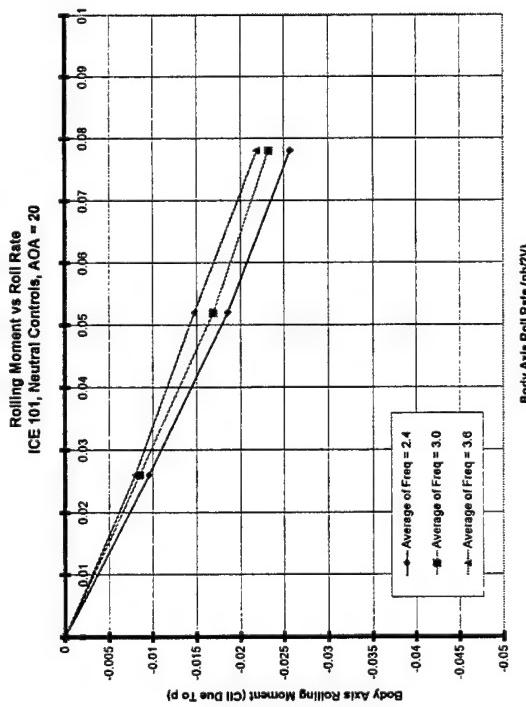
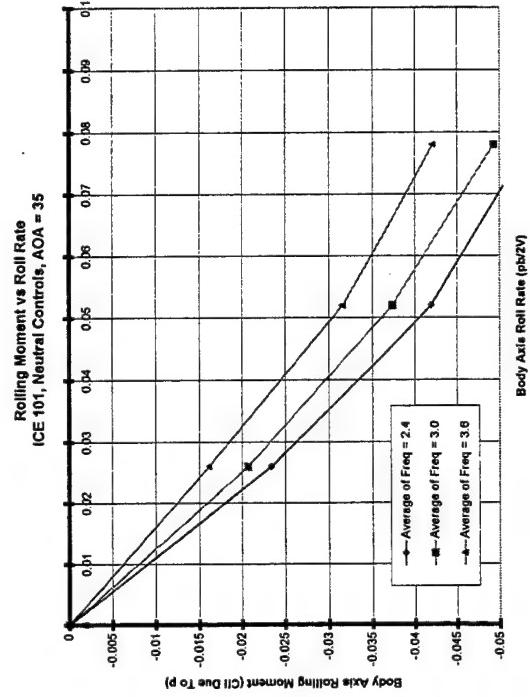
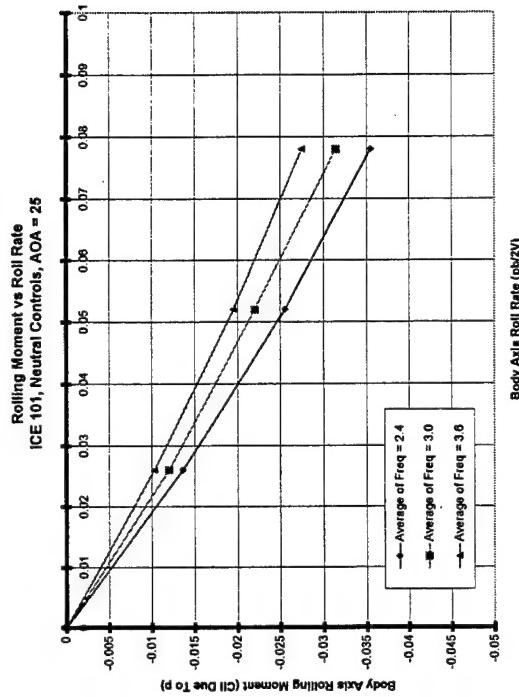


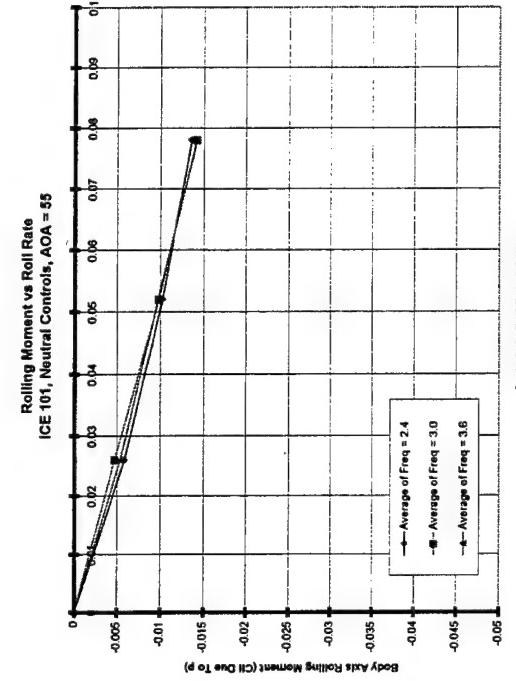
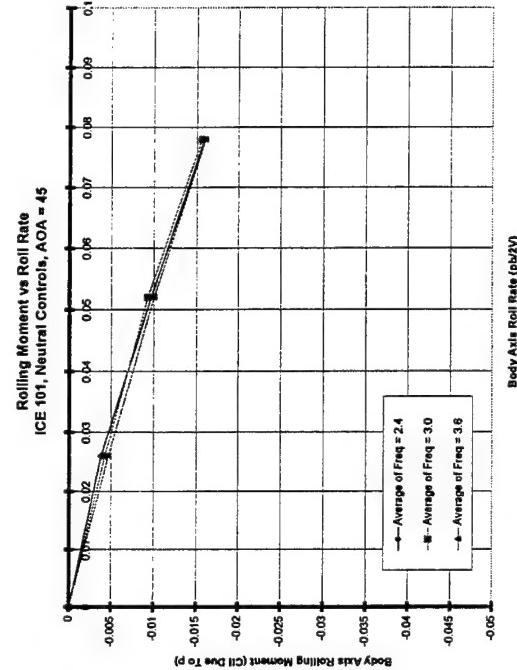
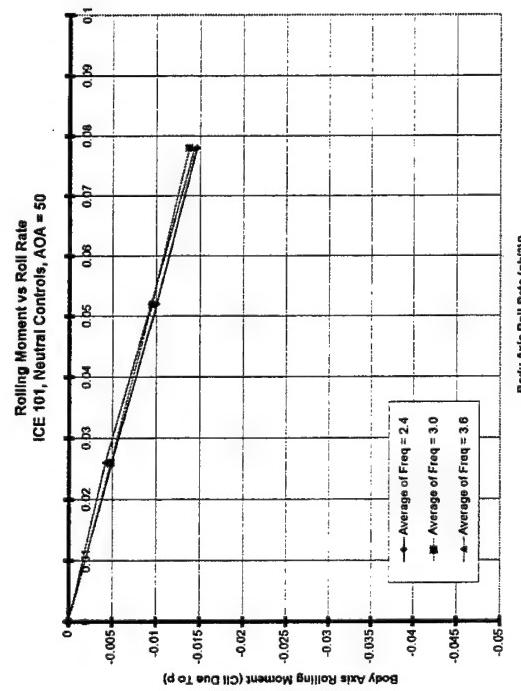
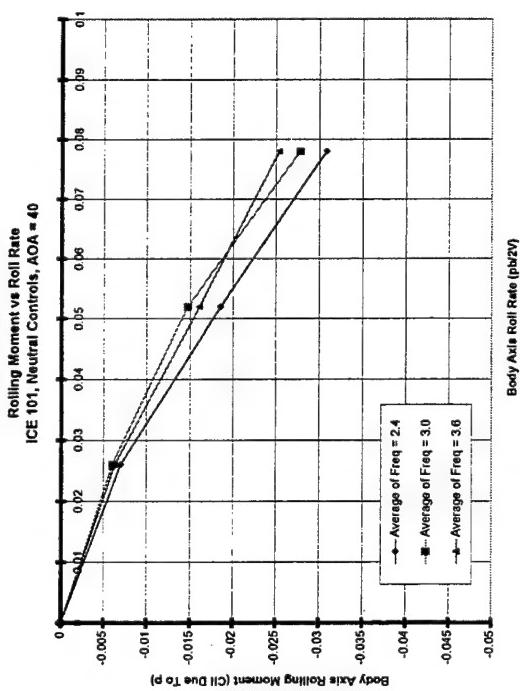


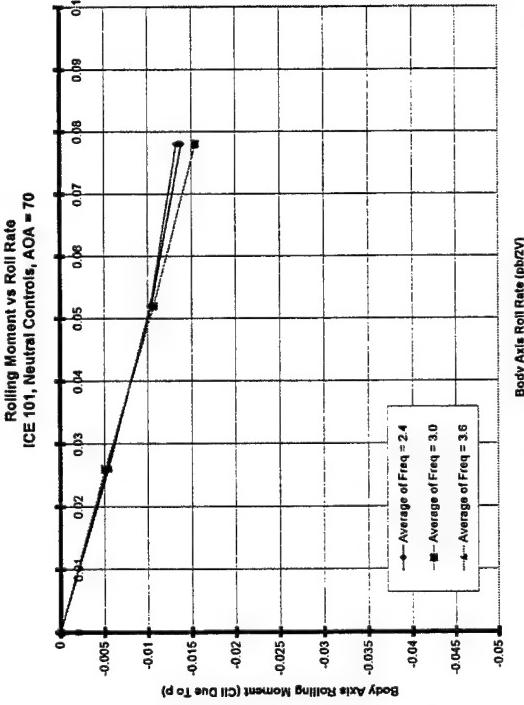
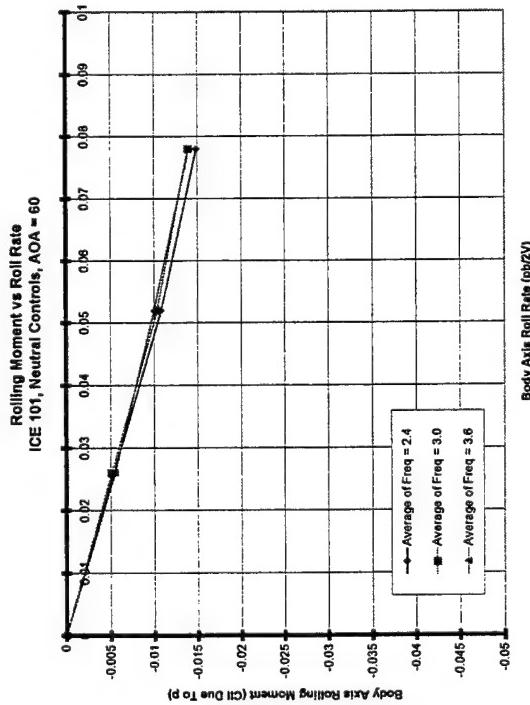
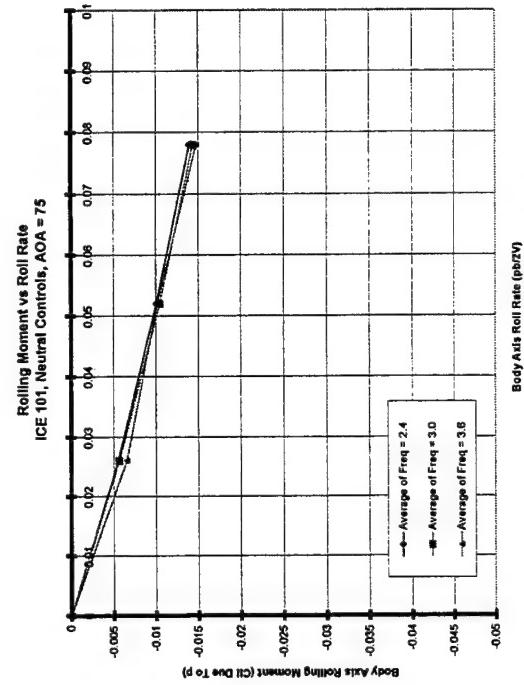
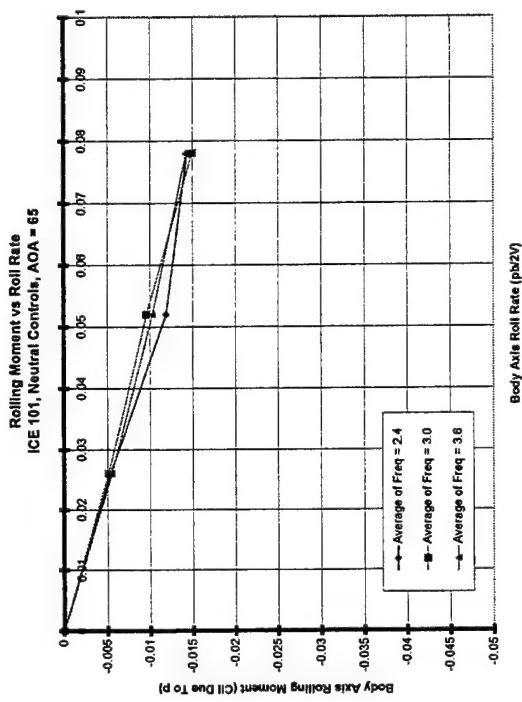
Appendix E

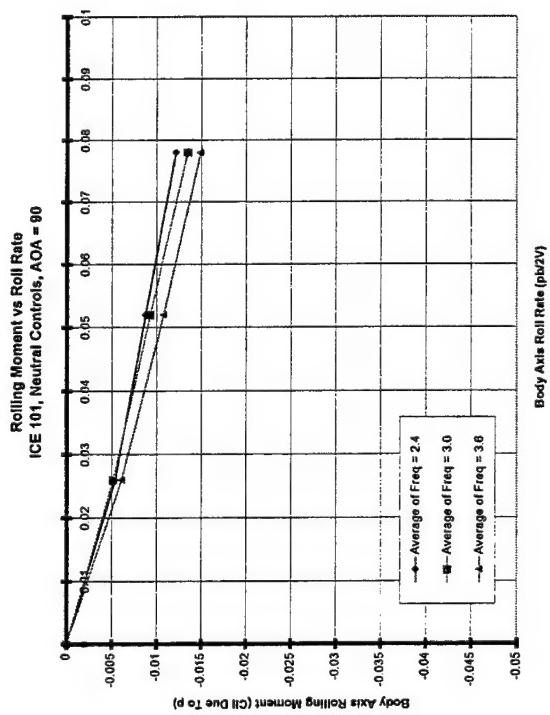
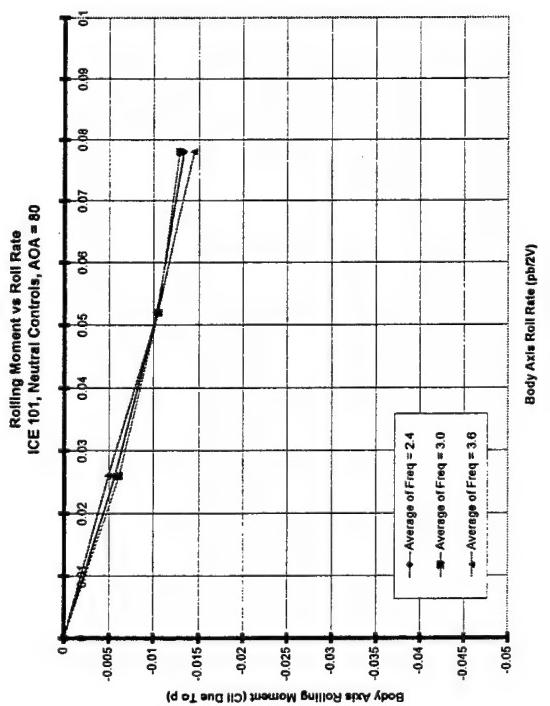
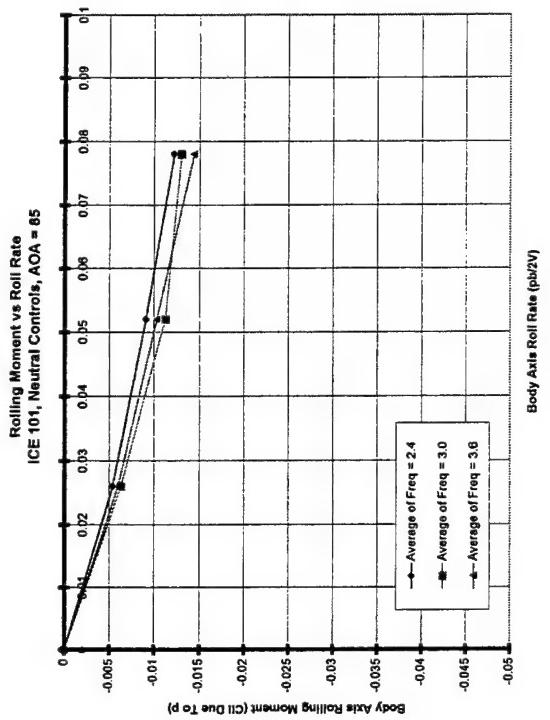
Roll Forced Oscillation Data Plots

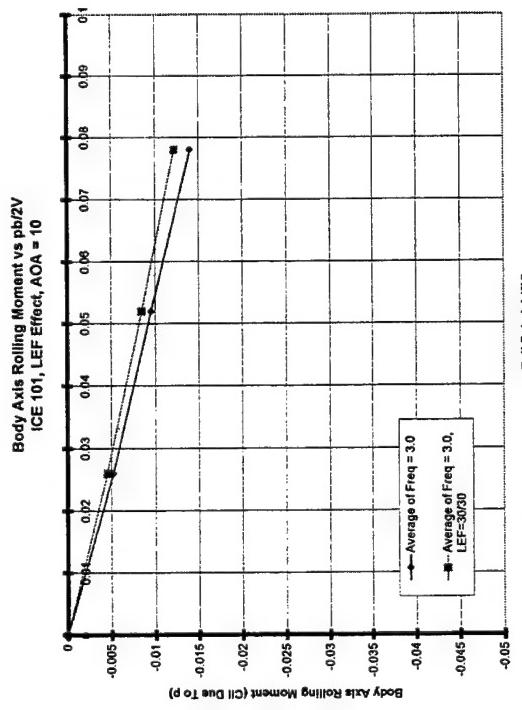
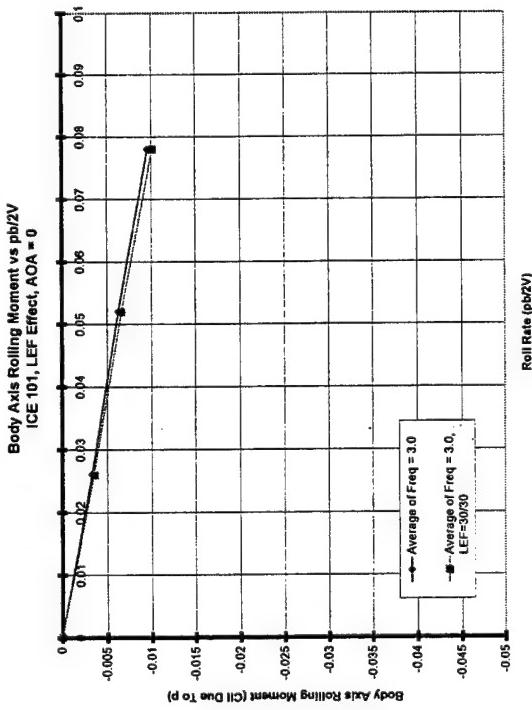
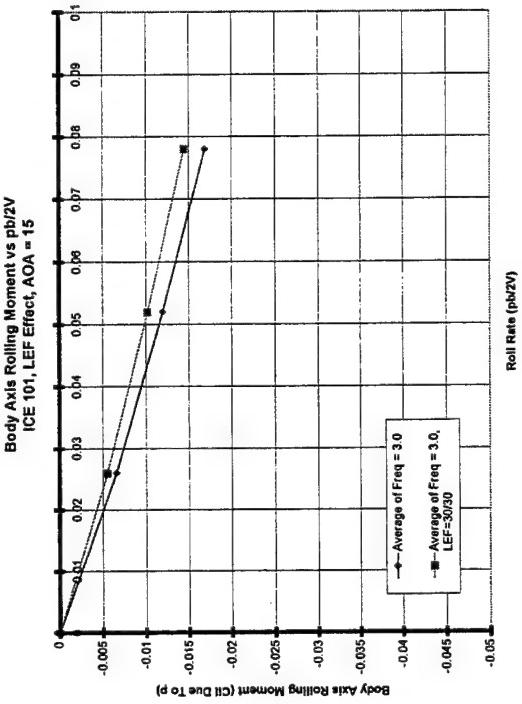
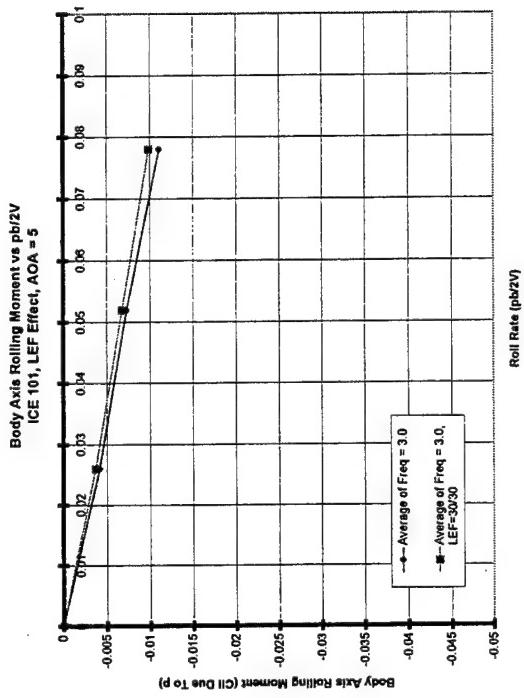


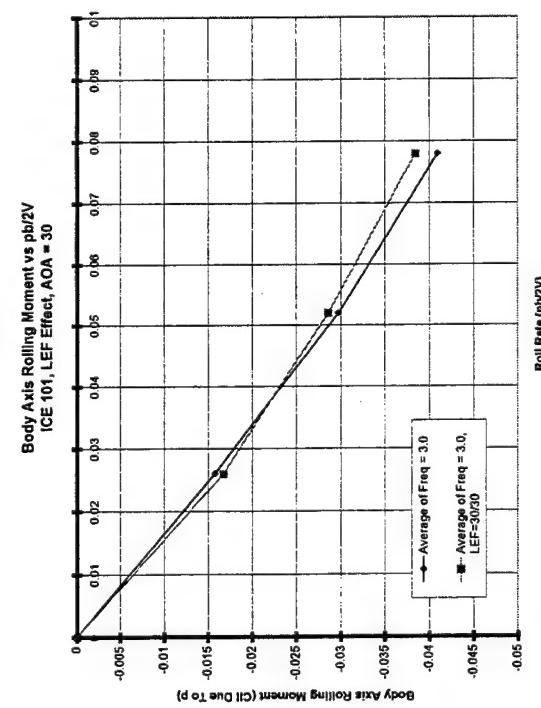
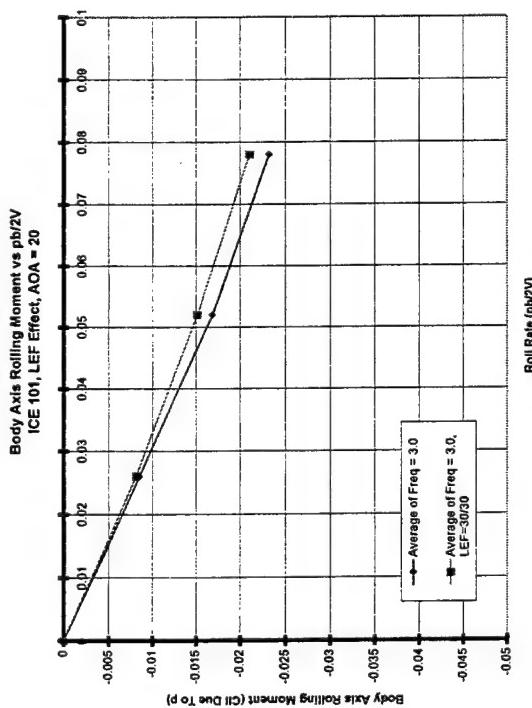
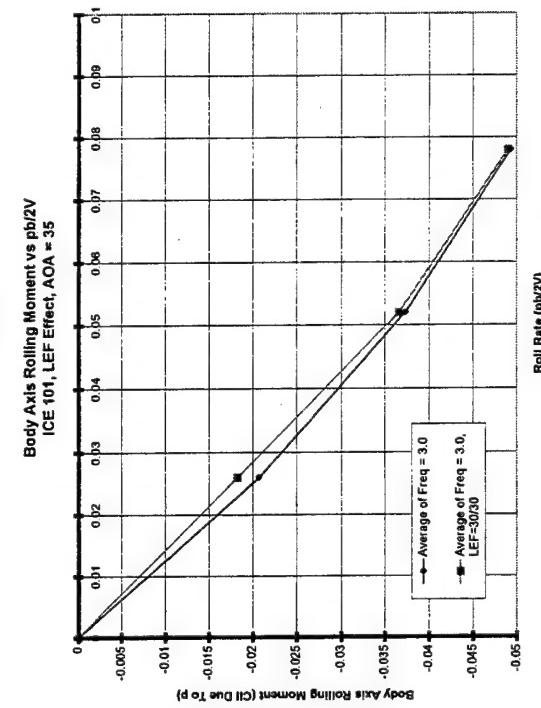
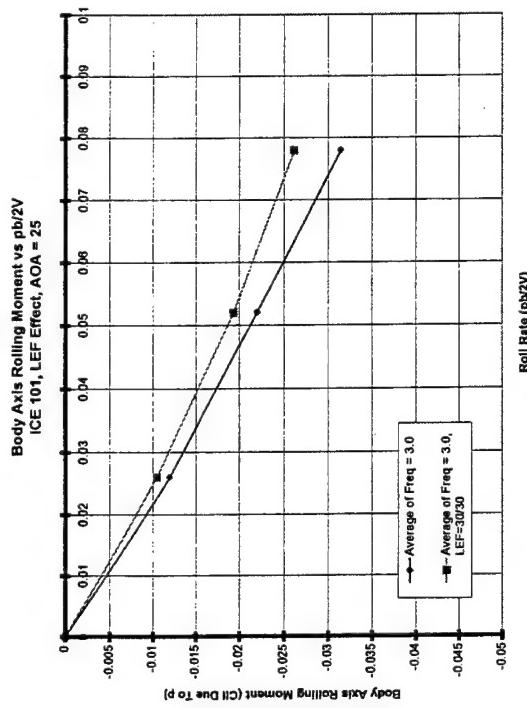


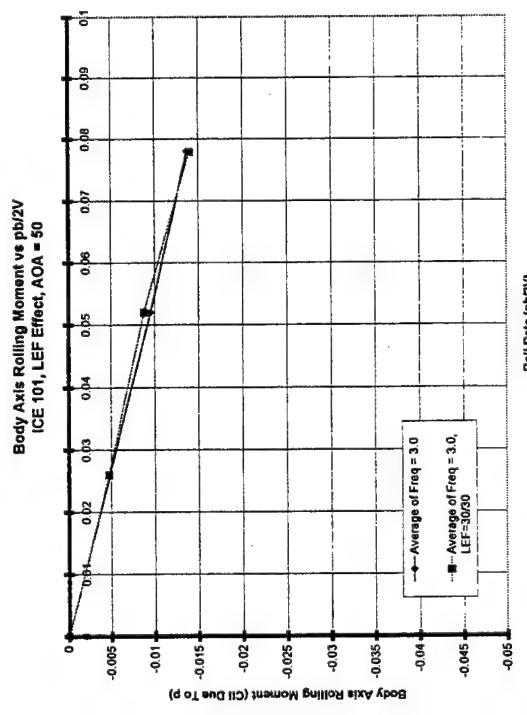
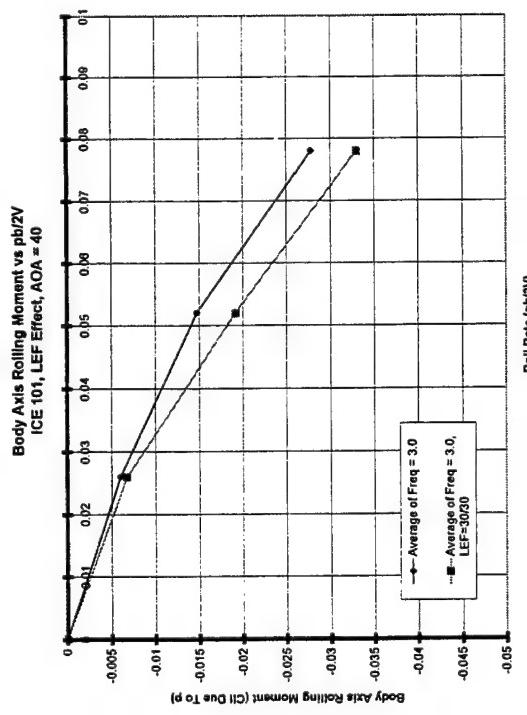
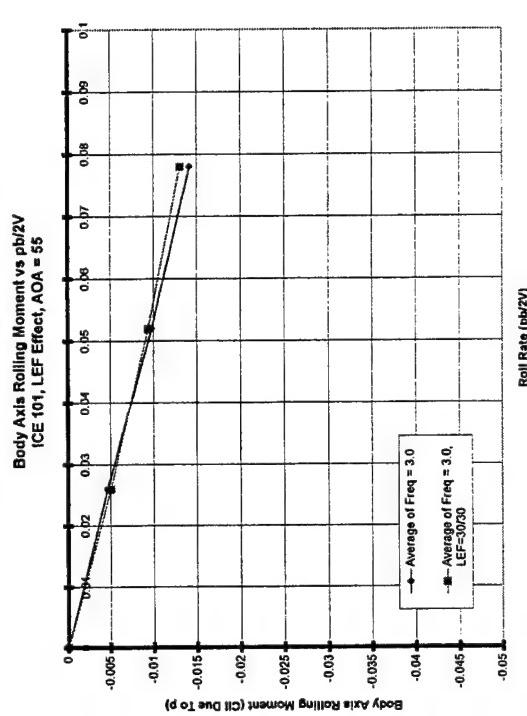
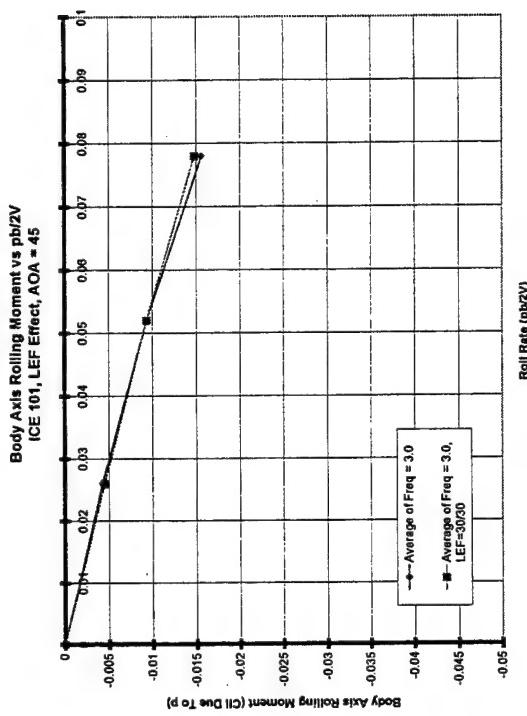


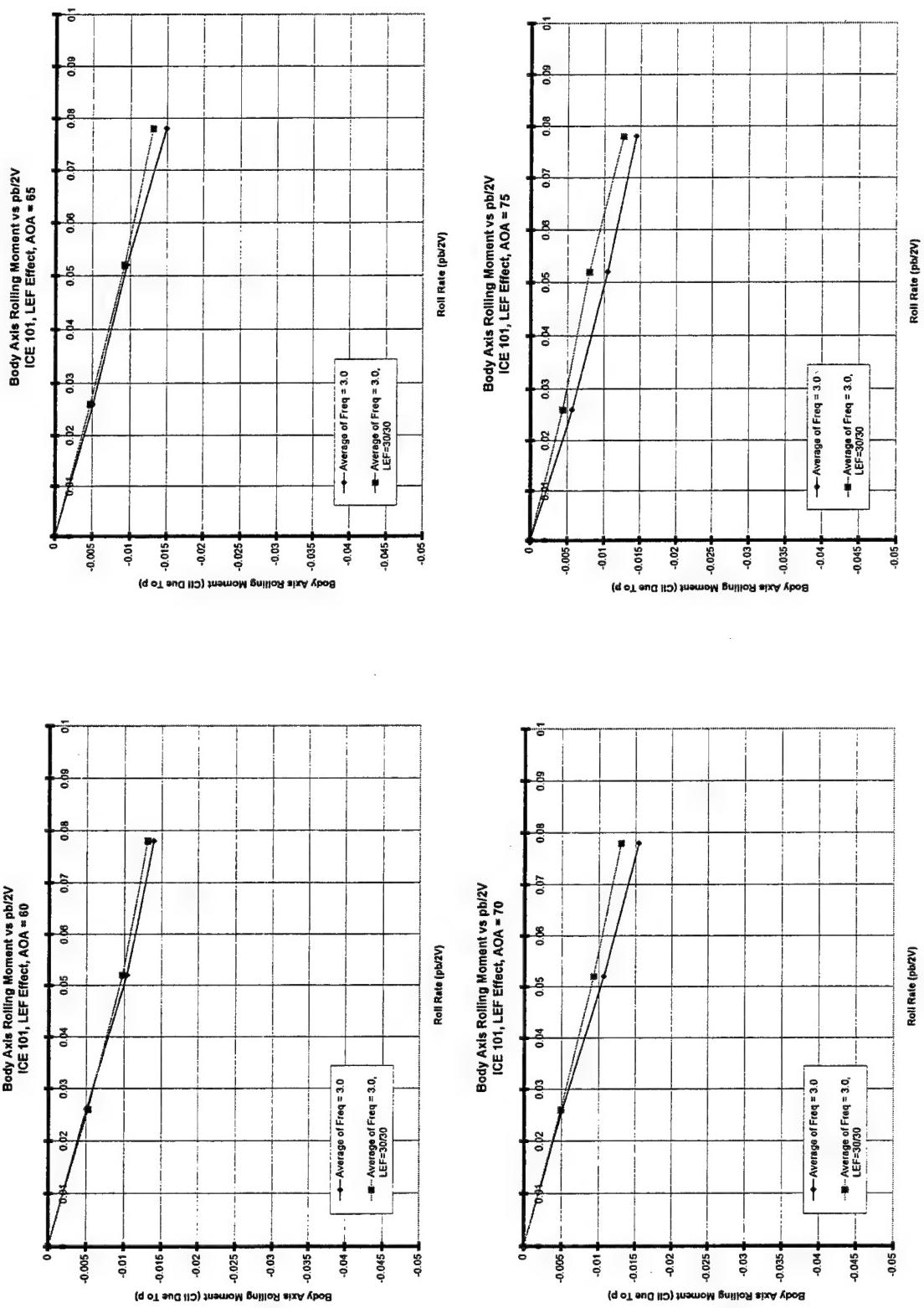


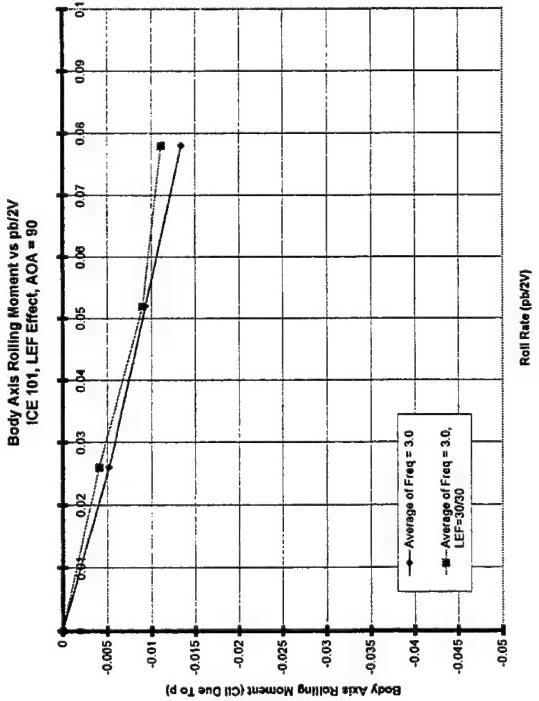
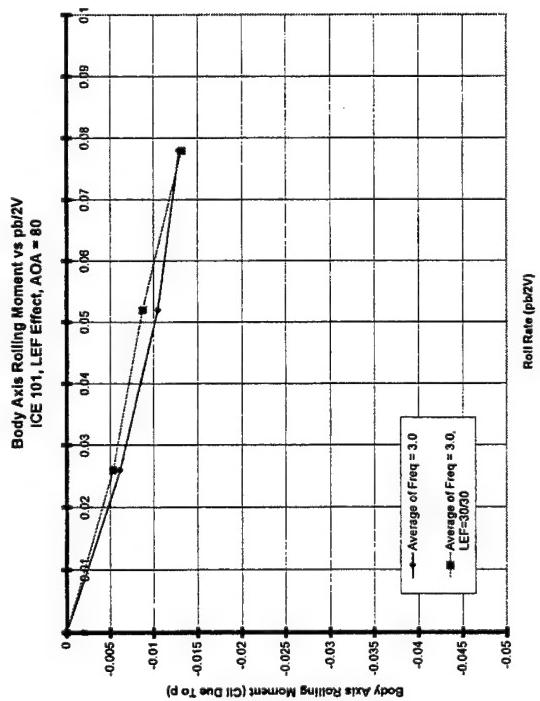
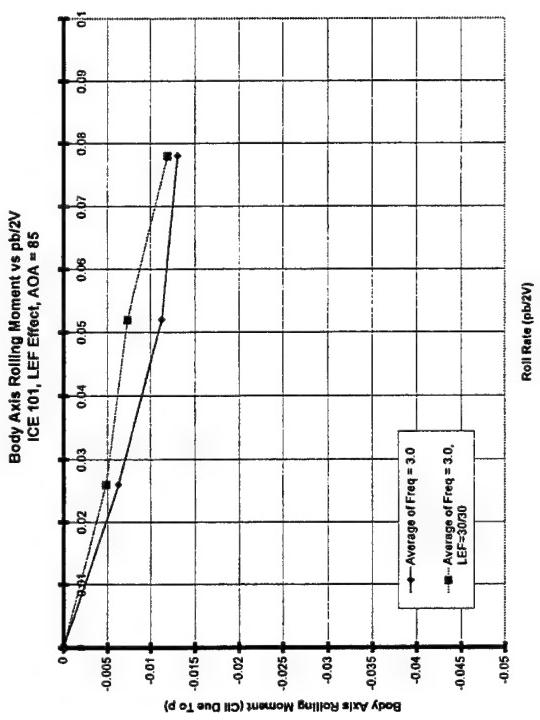


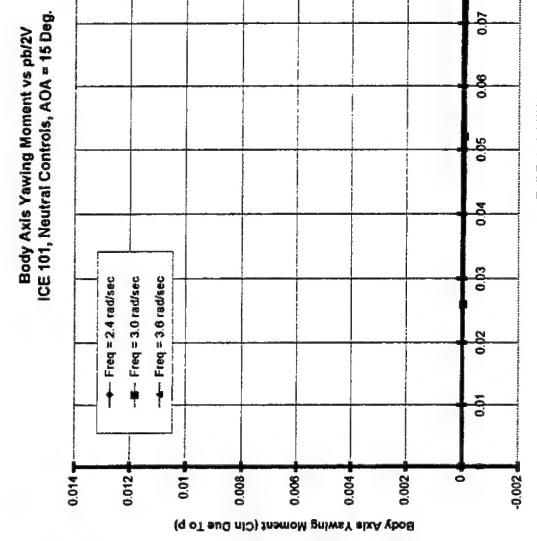
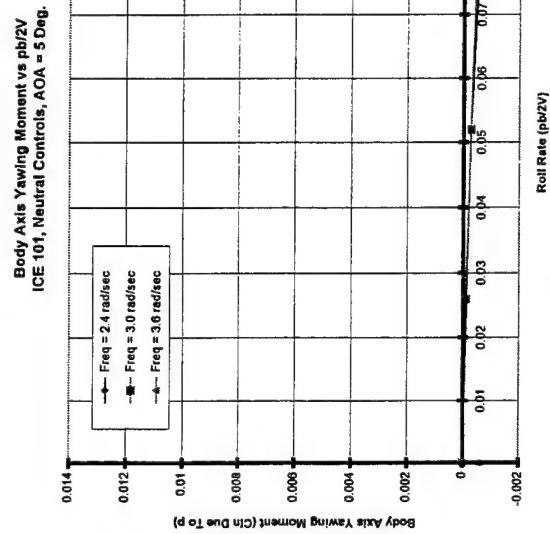
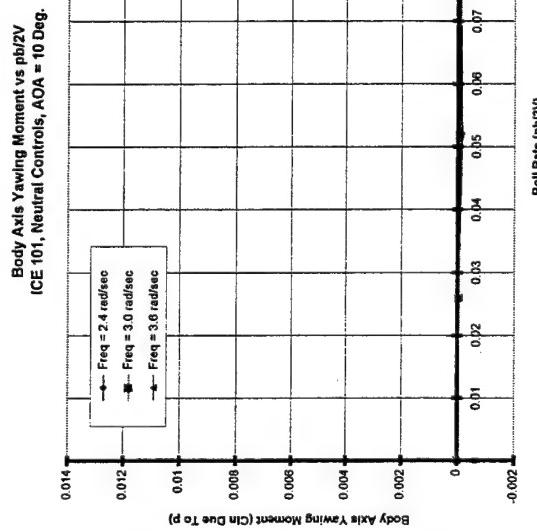
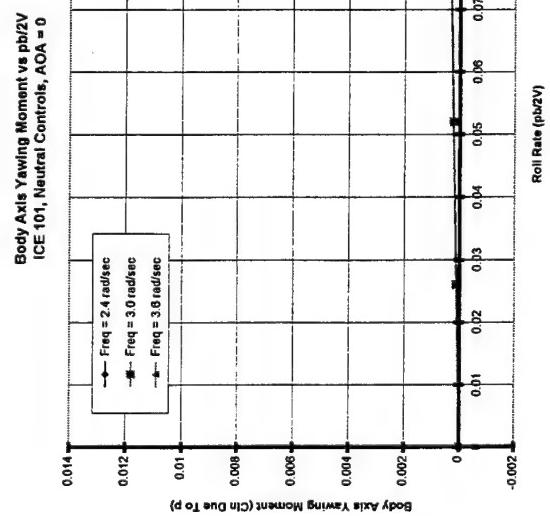


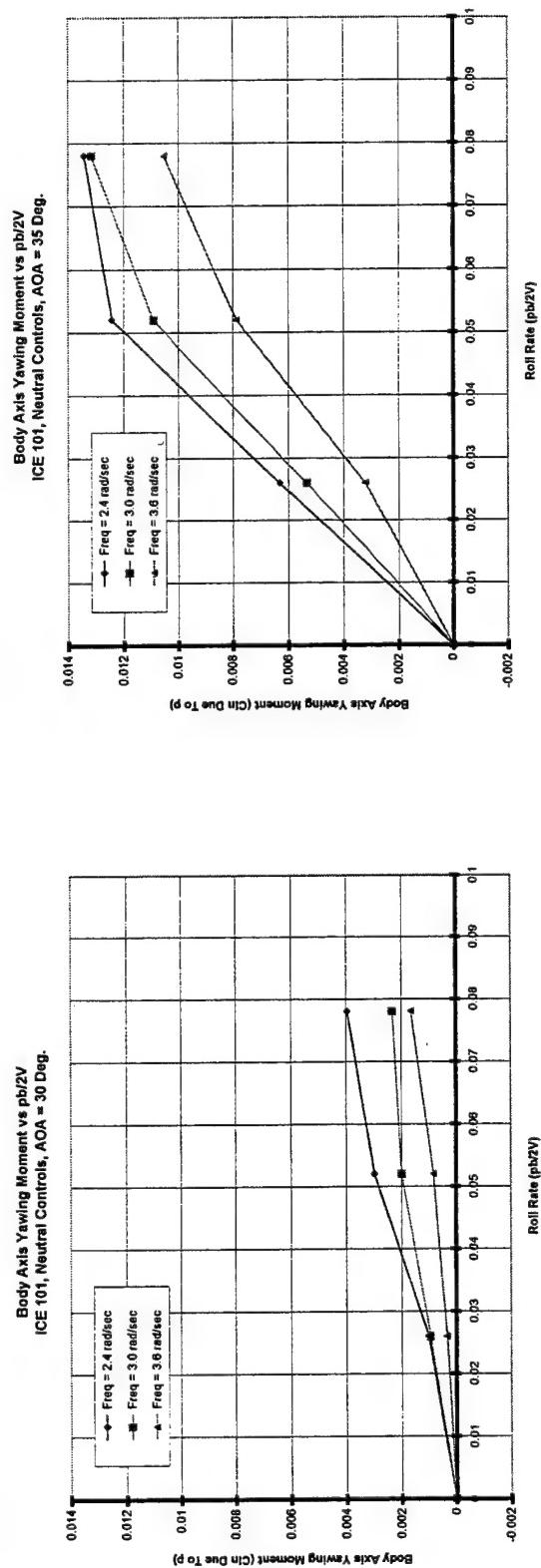
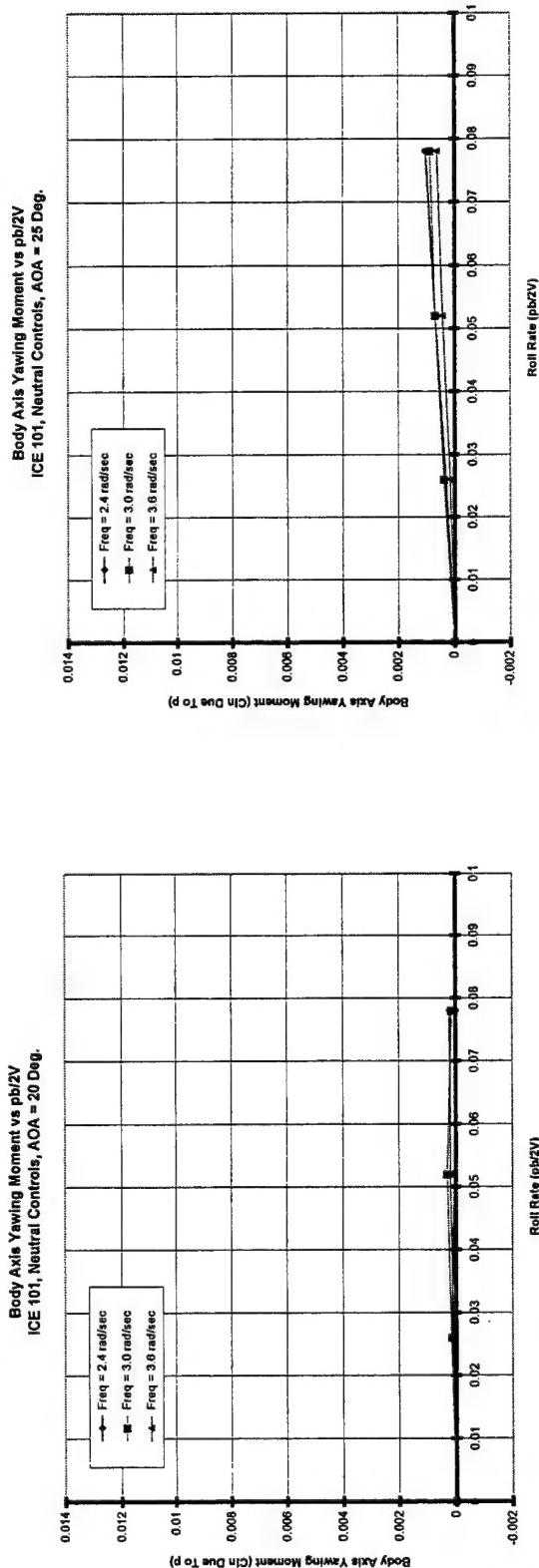




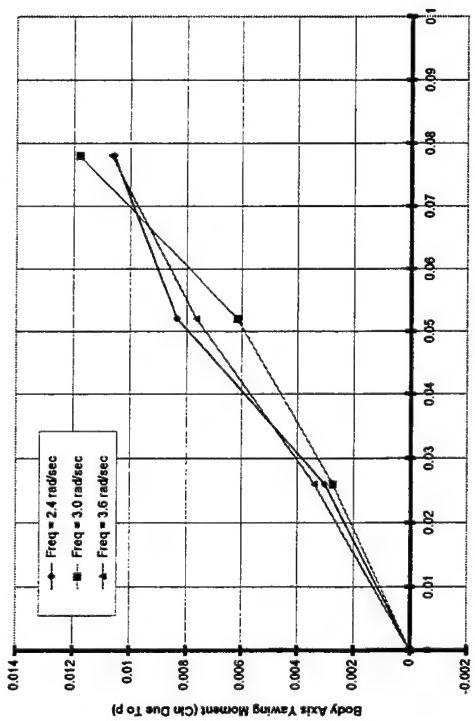




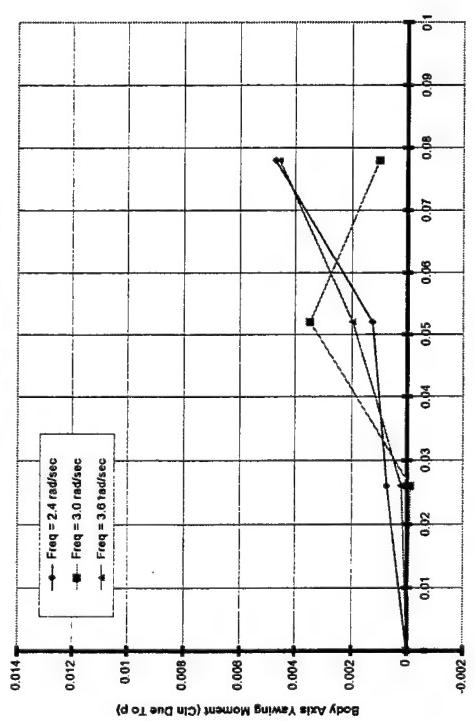




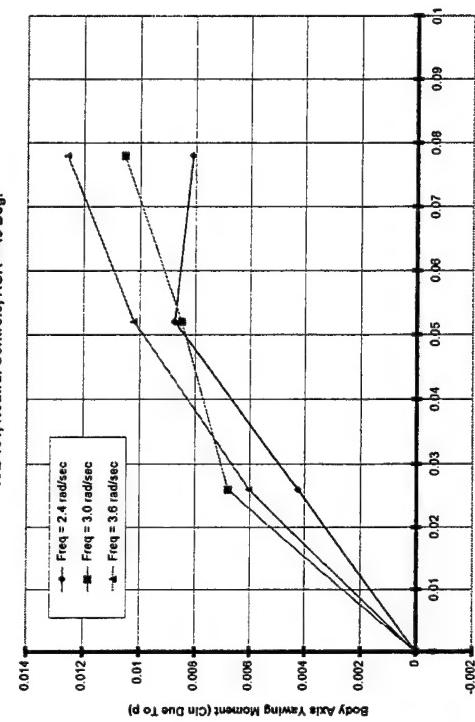
Body Axis Yawing Moment vs pb/2V
ICE 101, Neutral Controls, AOA = 40 Deg.



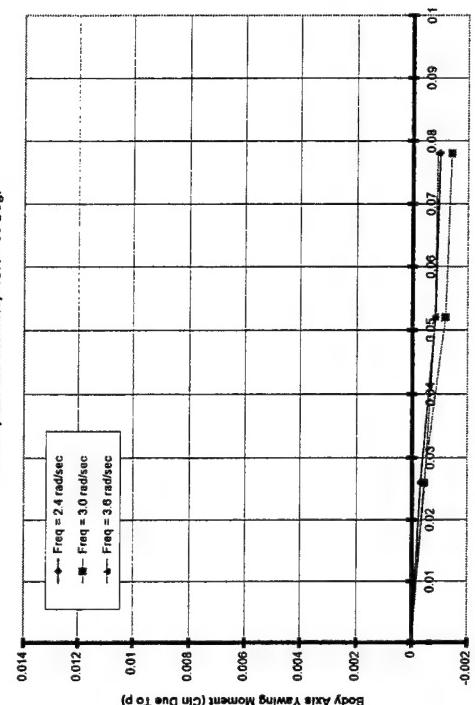
Body Axis Yawing Moment vs pb/2V
ICE 101, Neutral Controls, AOA = 50 Deg.



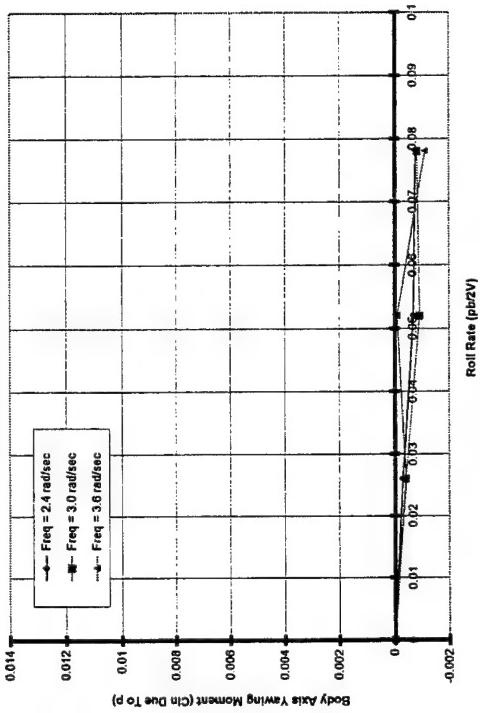
Body Axis Yawing Moment vs pb/2V
ICE 101, Neutral Controls, AOA = 45 Deg.



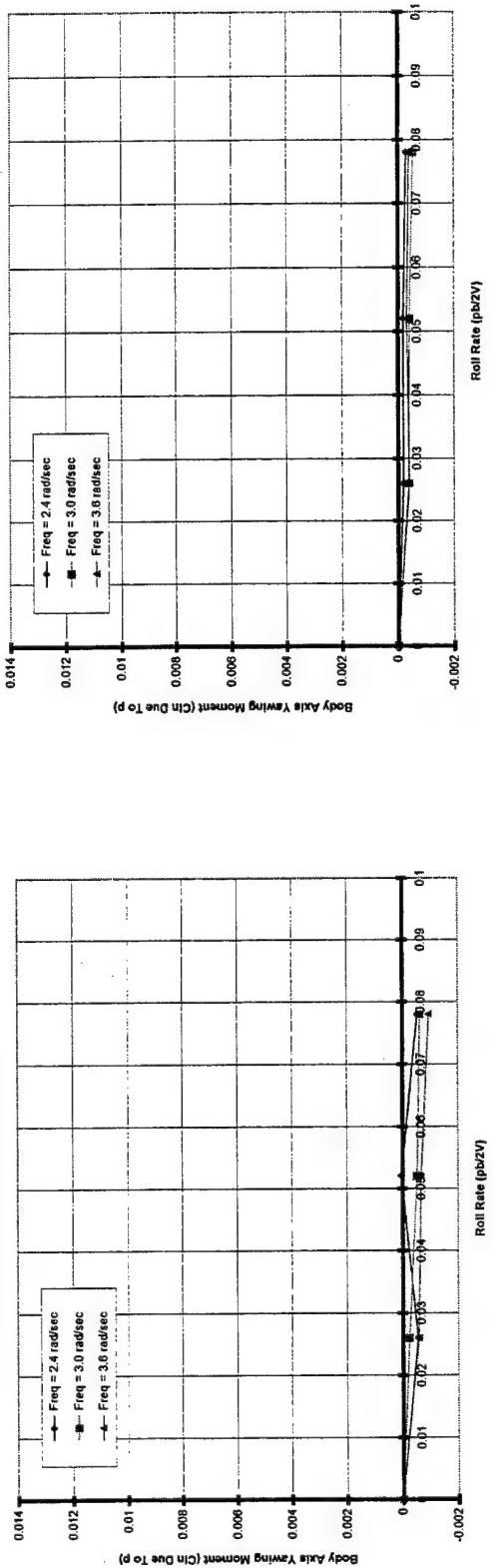
Body Axis Yawing Moment vs pb/2V
ICE 101, Neutral Controls, AOA = 55 Deg.

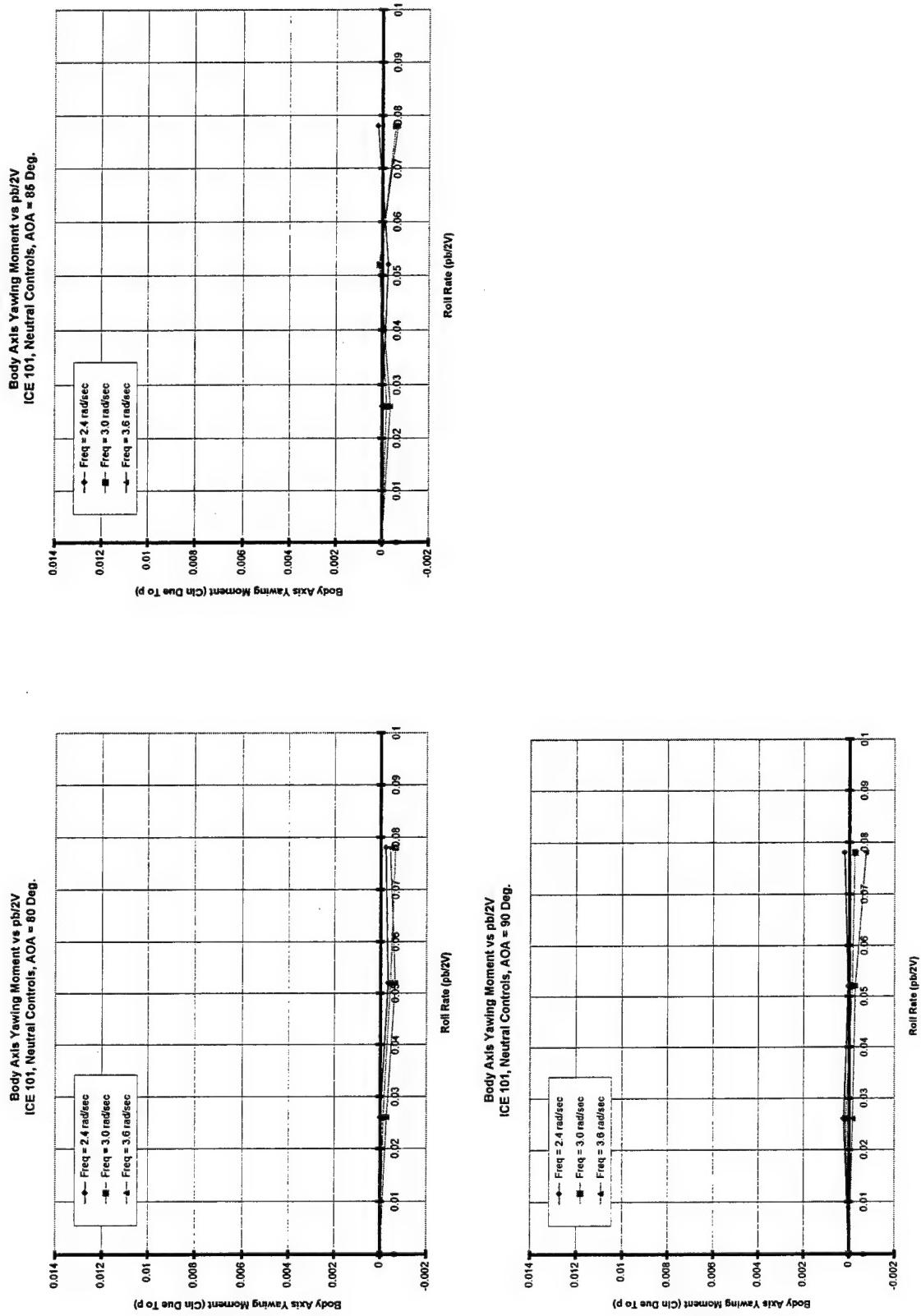


Body Axis Yawing Moment vs pb/2V
ICE 101, Neutral Controls, AOA = 65 Deg.



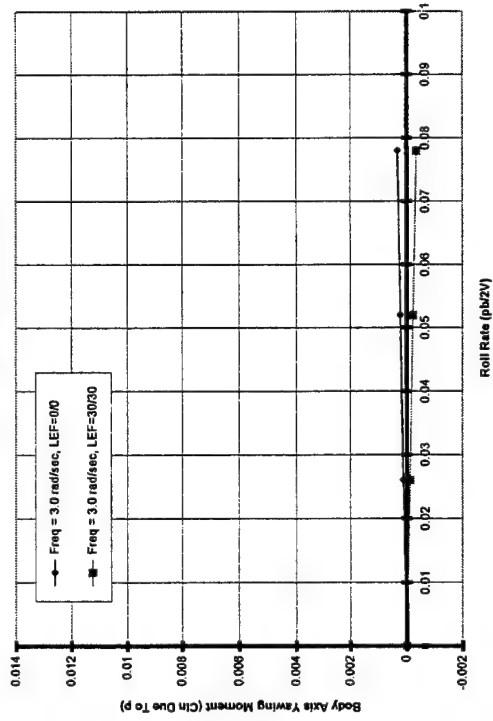
Body Axis Yawing Moment vs pb/2V
ICE 101, Neutral Controls, AOA = 75 Deg.





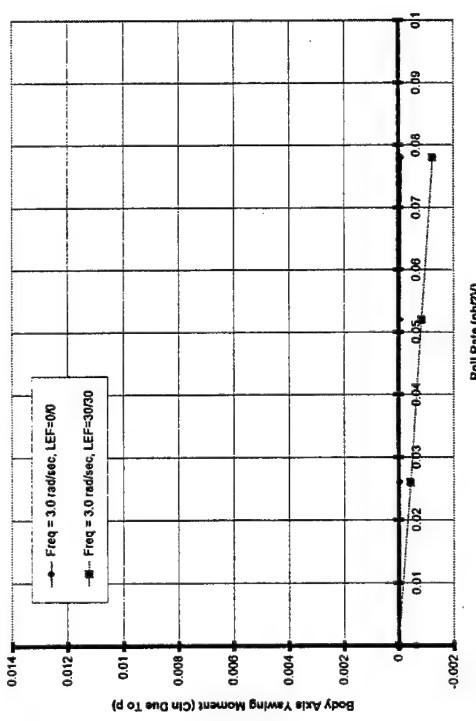
Body Axis Yawing Moment vs phi/2V

ICE 101, LEF Effects, AOA = 0 Deg.



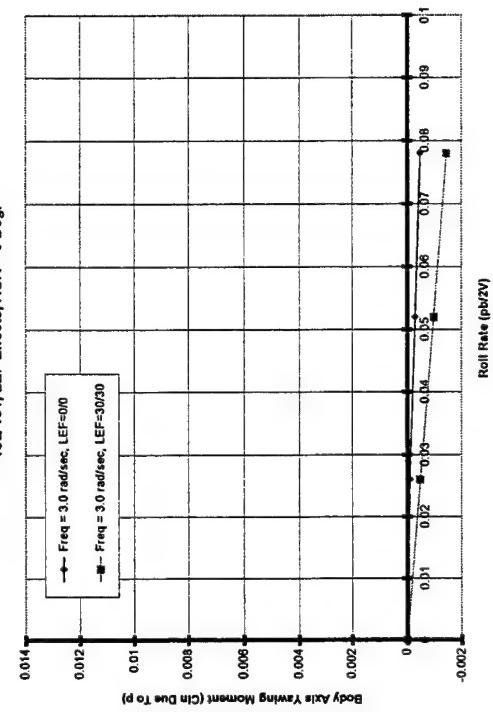
Body Axis Yawing Moment vs phi/2V

ICE 101, LEF Effects, AOA = 5 Deg.



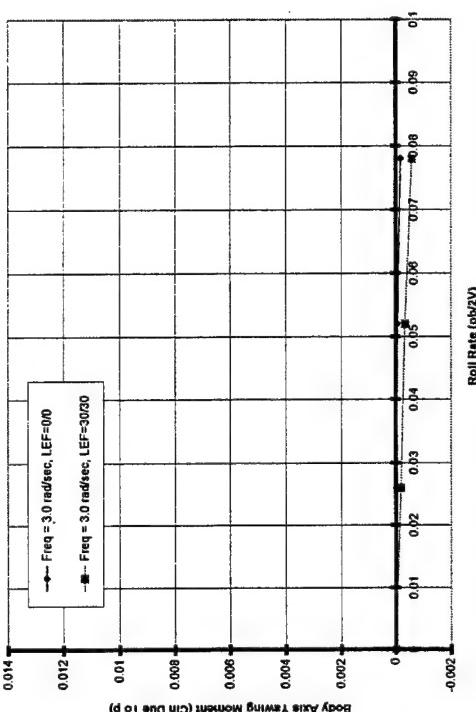
Body Axis Yawing Moment vs phi/2V

ICE 101, LEF Effects, AOA = 15 Deg.



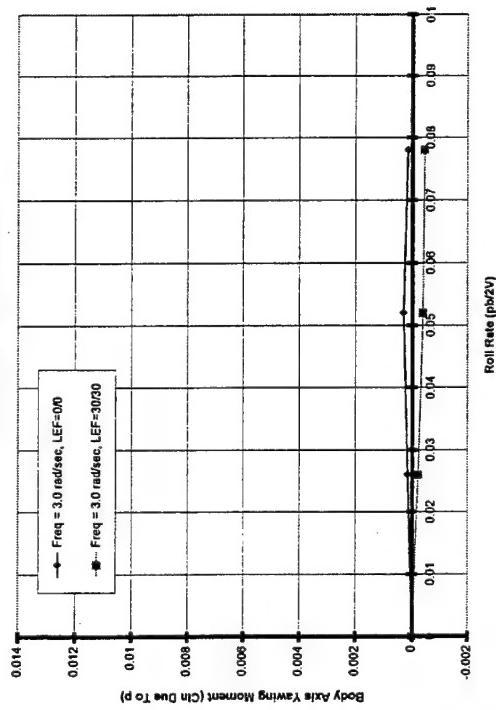
Body Axis Yawing Moment vs phi/2V

ICE 101, LEF Effects, AOA = 15 Deg.



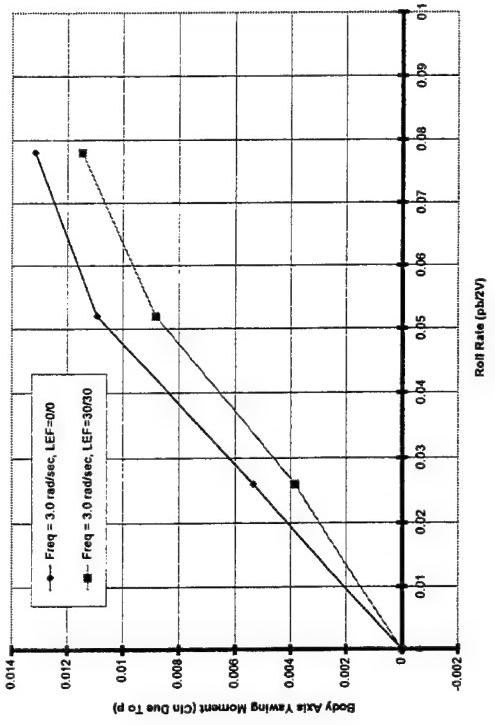
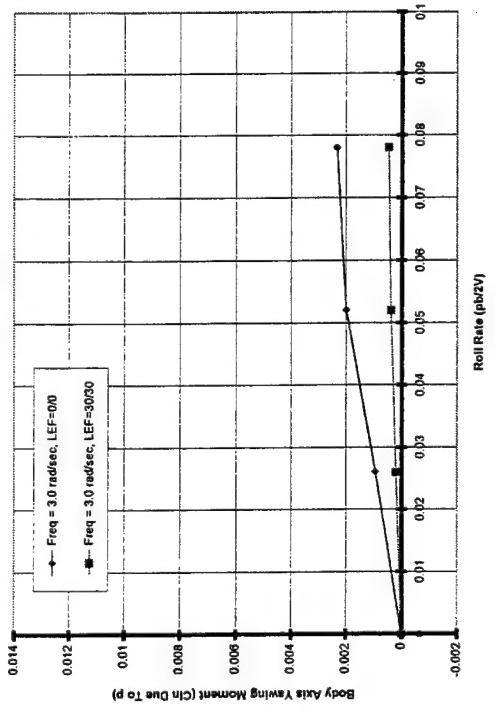
Body Axis Yawing Moment vs pbj2V
ICE 101, LEF Effects, AOA = 20 Deg.

Body Axis Yawing Moment vs pbj2V
ICE 101, LEF Effects, AOA = 25 Deg.

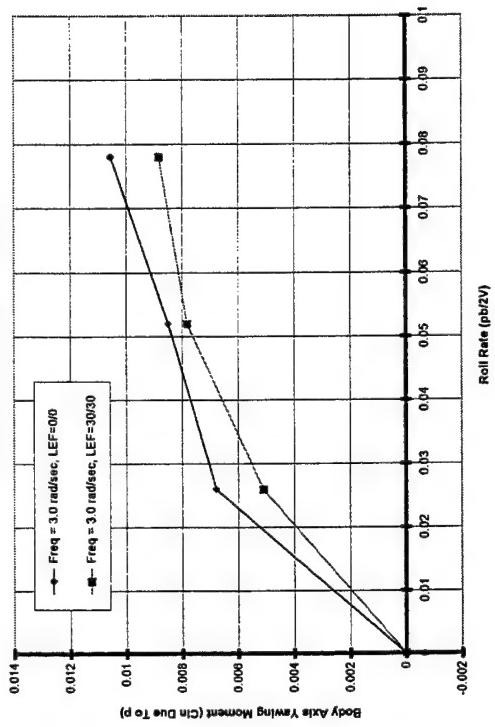


Body Axis Yawing Moment vs pbj2V
ICE 101, LEF Effects, AOA = 30 Deg.

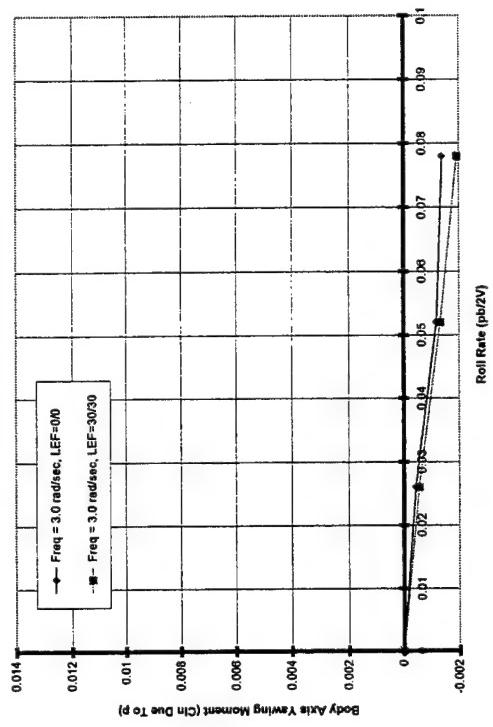
Body Axis Yawing Moment vs pbj2V
ICE 101, LEF Effects, AOA = 35 Deg.



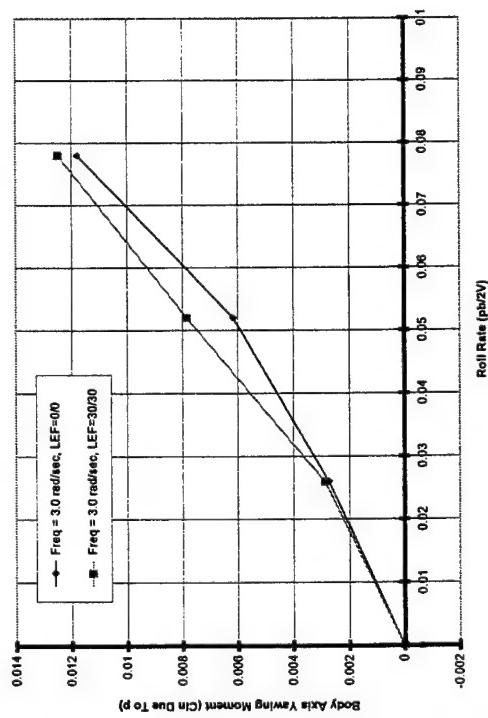
Body Axis Yawing Moment vs pb/2V
ICE 101, LEF Effects, AOA = 45 Deg.



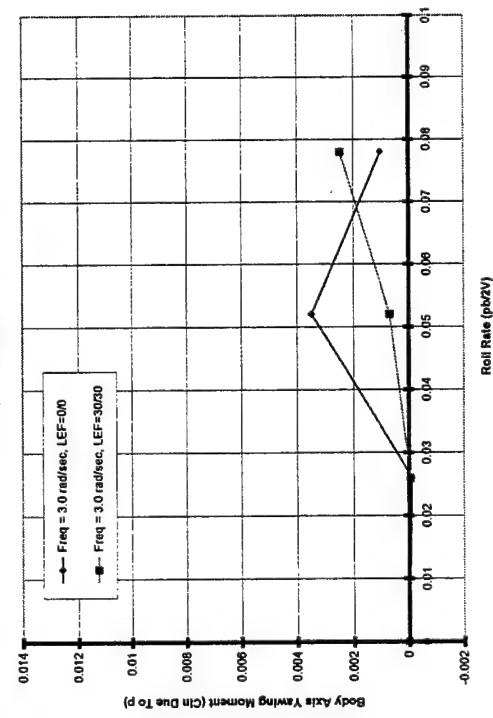
Body Axis Yawing Moment vs pb/2V
ICE 101, LEF Effects, AOA = 55 Deg.



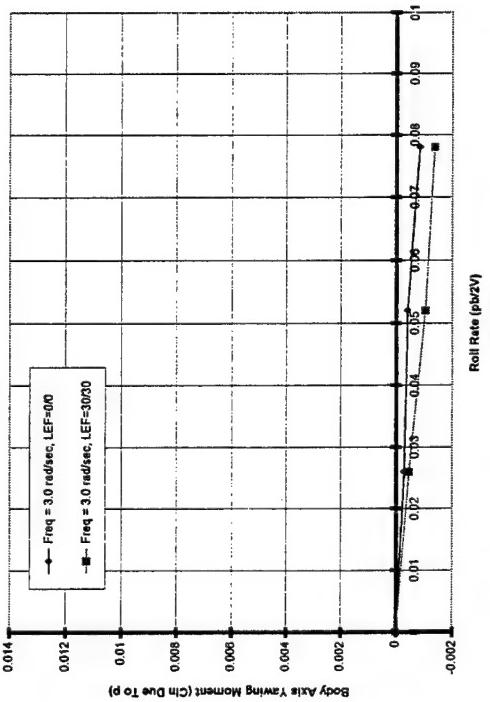
Body Axis Yawing Moment vs pb/2V
ICE 101, LEF Effects, AOA = 40 Deg.



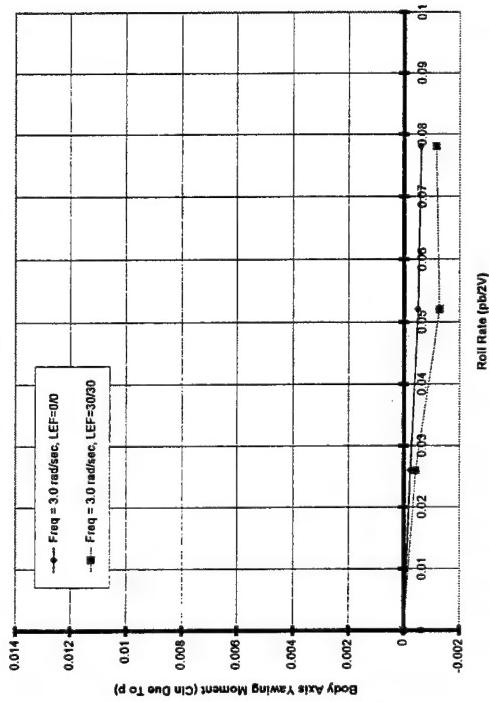
Body Axis Yawing Moment vs pb/2V
ICE 101, LEF Effects, AOA = 50 Deg.



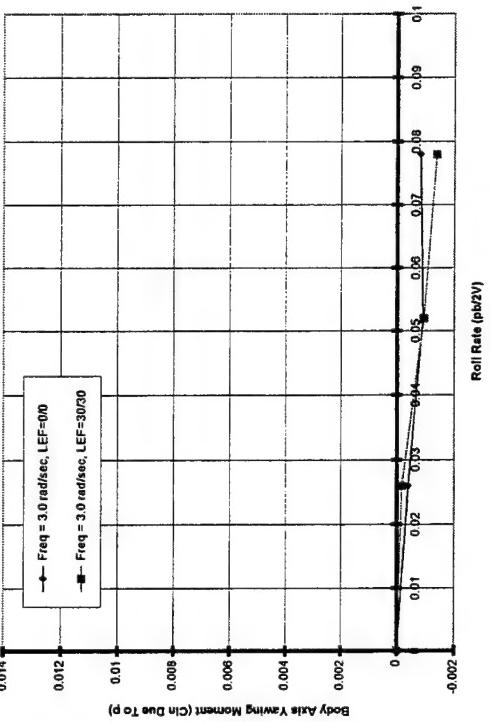
Body Axis Yawing Moment vs pb/2V
ICE 101, LEF Effects, AOA = 60 Deg.



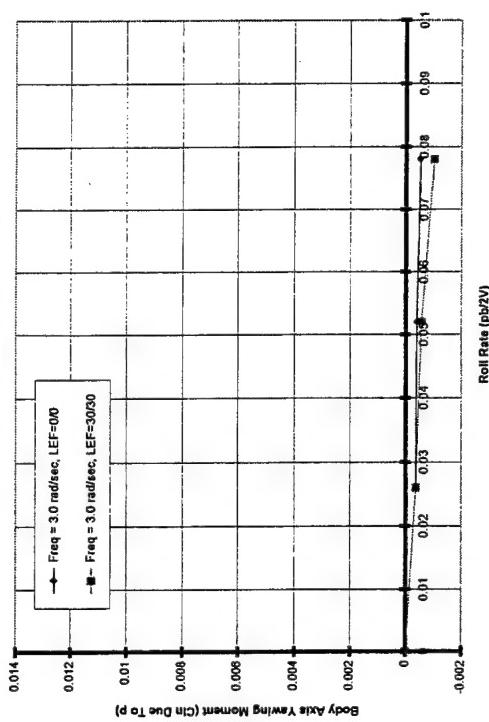
Body Axis Yawing Moment vs pb/2V
ICE 101, LEF Effects, AOA = 70 Deg.



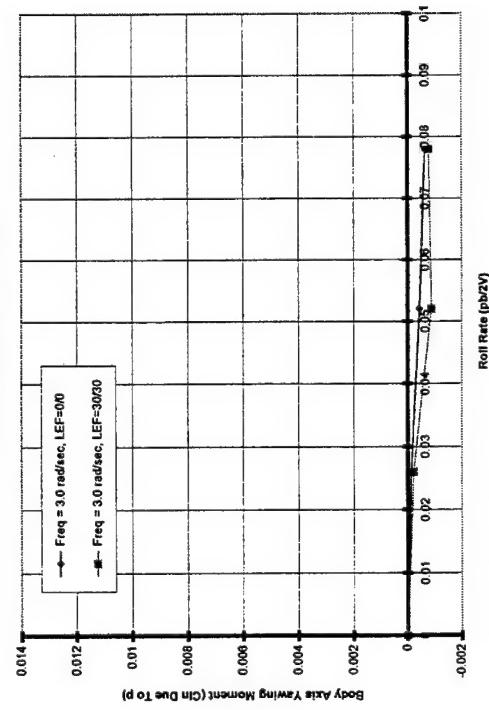
Body Axis Yawing Moment vs pb/2V
ICE 101, LEF Effects, AOA = 65 Deg.



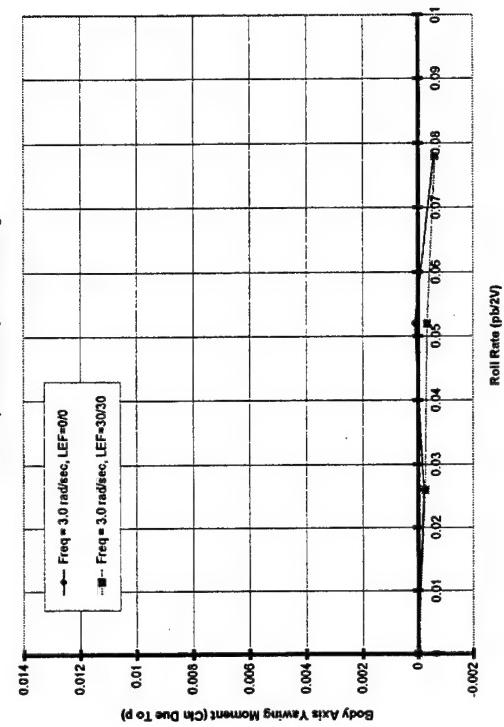
Body Axis Yawing Moment vs pb/2V
ICE 101, LEF Effects, AOA = 75 Deg.



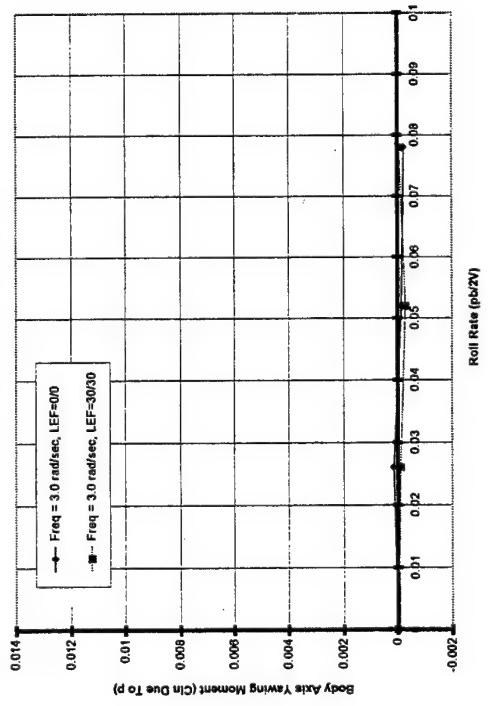
Body Axis Yawing Moment vs $\dot{\phi}/2V$
ICE 101, LEF Effects, AOA = 80 Deg.



Body Axis Yawing Moment vs $\dot{\phi}/2V$
ICE 101, LEF Effects, AOA = 85 Deg.



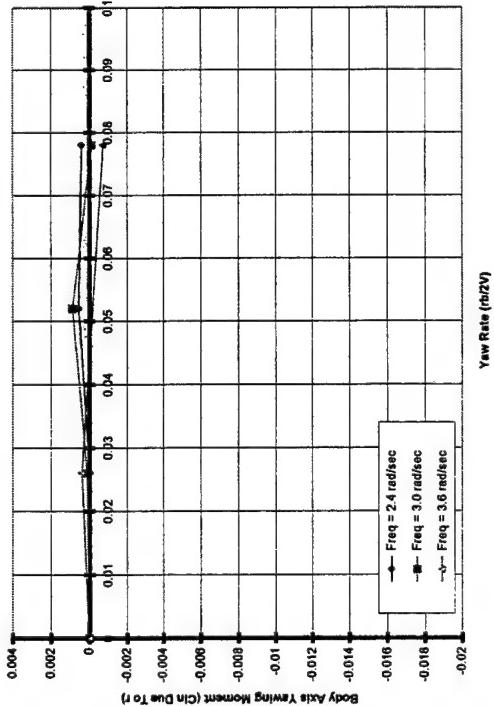
Body Axis Yawing Moment vs $\dot{\phi}/2V$
ICE 101, LEF Effects, AOA = 90 Deg.



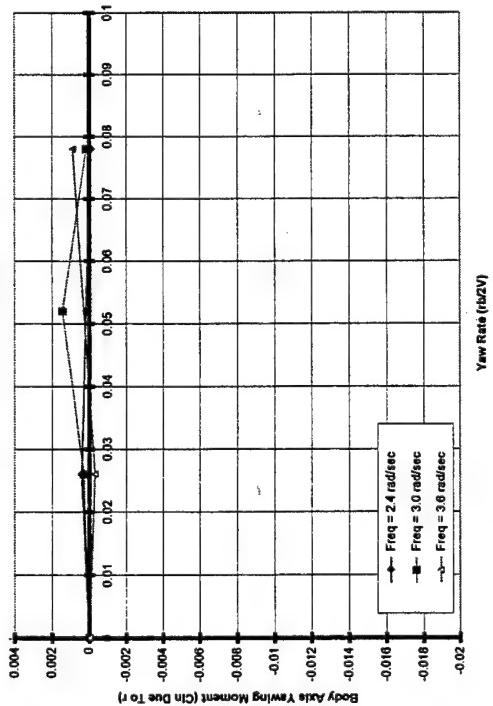
Appendix F

Yaw Forced Oscillation Data Plots

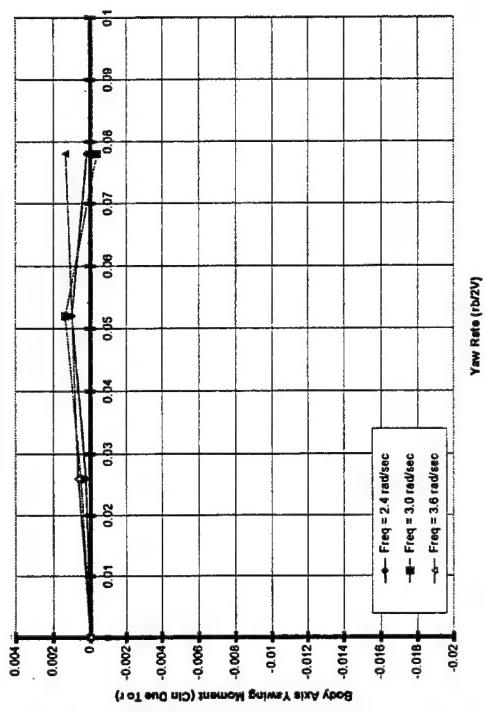
Body Axis Yawing Moment vs $\dot{\theta}/2V$
ICE 101, Neutral Controls, AOA = 0 Deg.



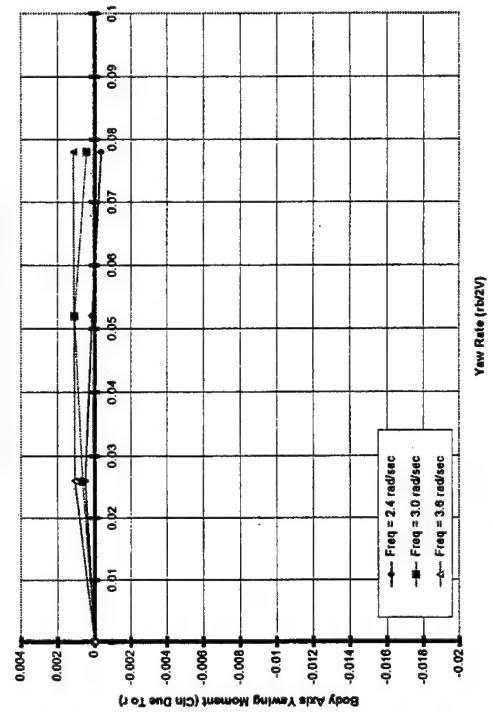
Body Axis Yawing Moment vs $\dot{\theta}/2V$
ICE 101, Neutral Controls, AOA = 10 Deg.

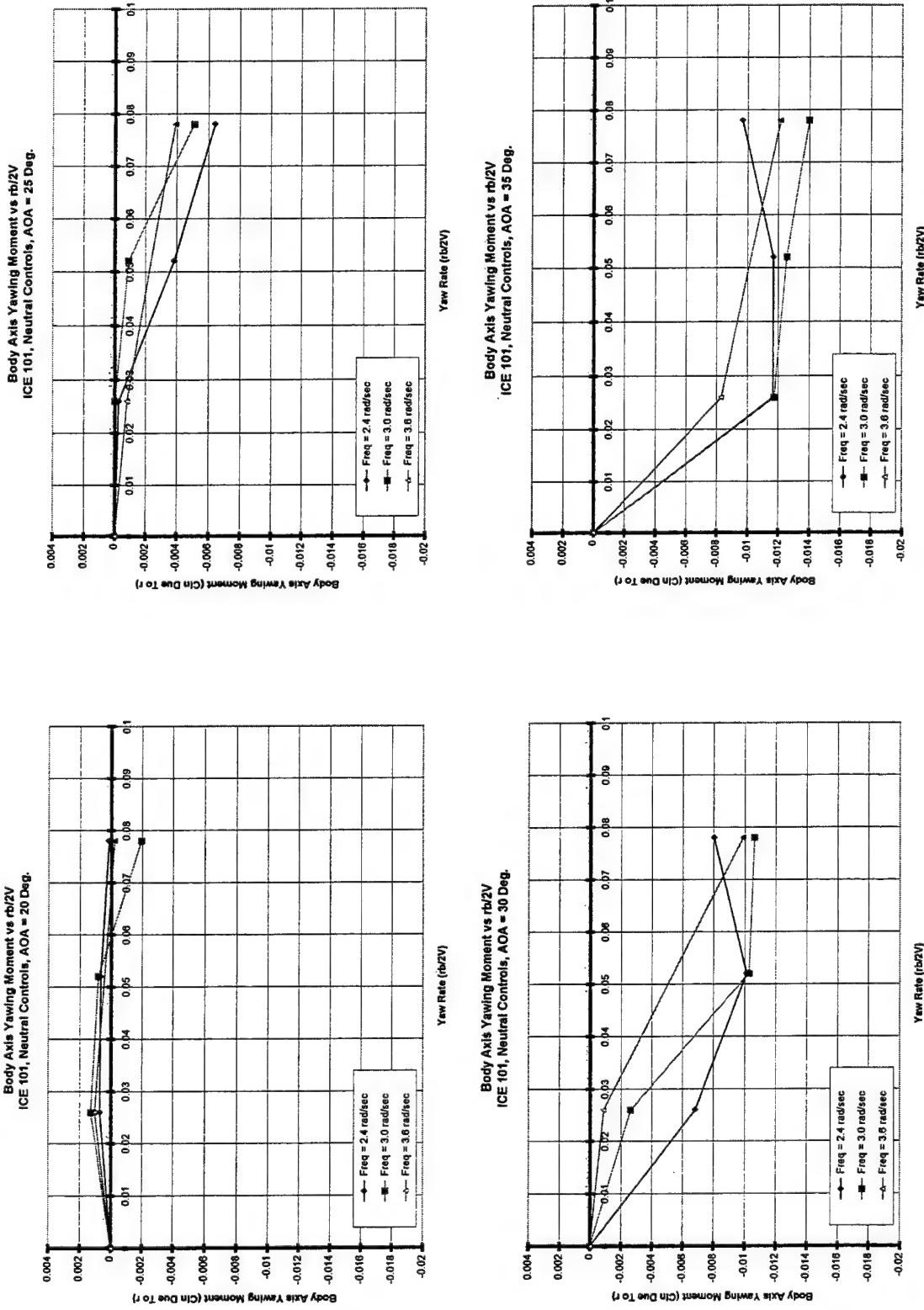


Body Axis Yawing Moment vs $\dot{\theta}/2V$
ICE 101, Neutral Controls, AOA = 5 Deg.

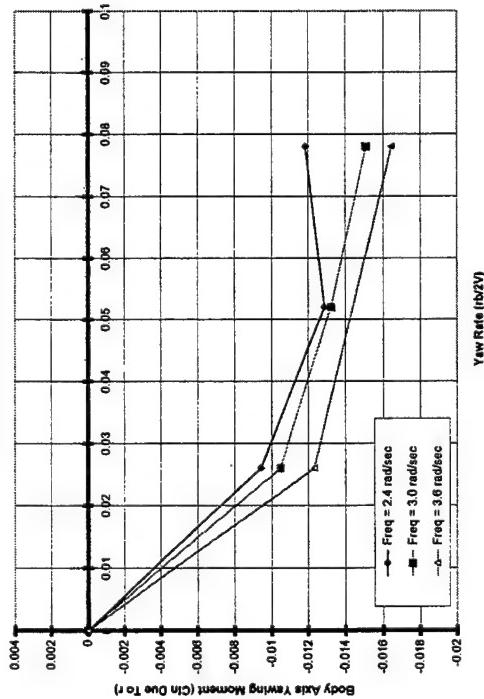


Body Axis Yawing Moment vs $\dot{\theta}/2V$
ICE 101, Neutral Controls, AOA = 15 Deg.

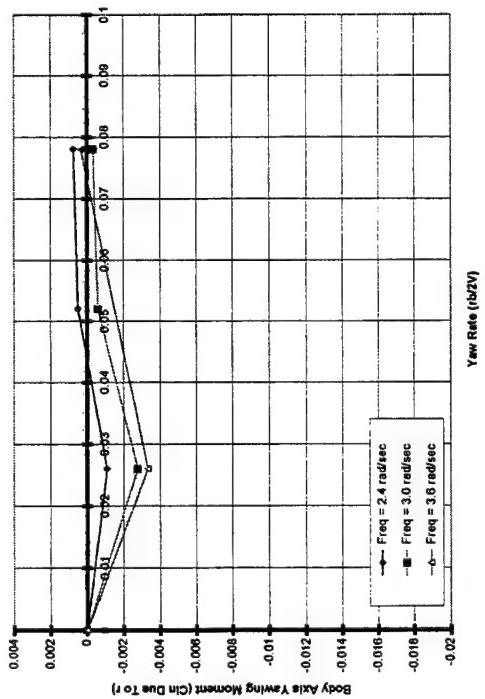




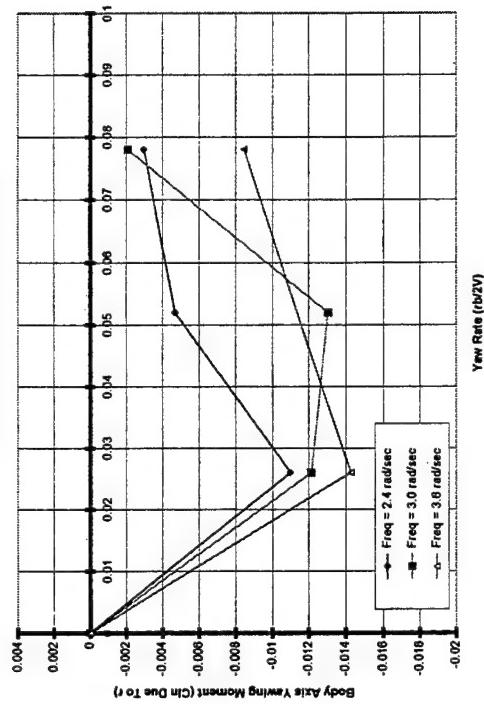
Body Axis Yawing Moment vs $\dot{\theta}/2V$
ICE 101, Neutral Controls, AOA = 40 Deg.



Body Axis Yawing Moment vs $\dot{\theta}/2V$
ICE 101, Neutral Controls, AOA = 50 Deg.



Body Axis Yawing Moment vs $\dot{\theta}/2V$
ICE 101, Neutral Controls, AOA = 45 Deg.

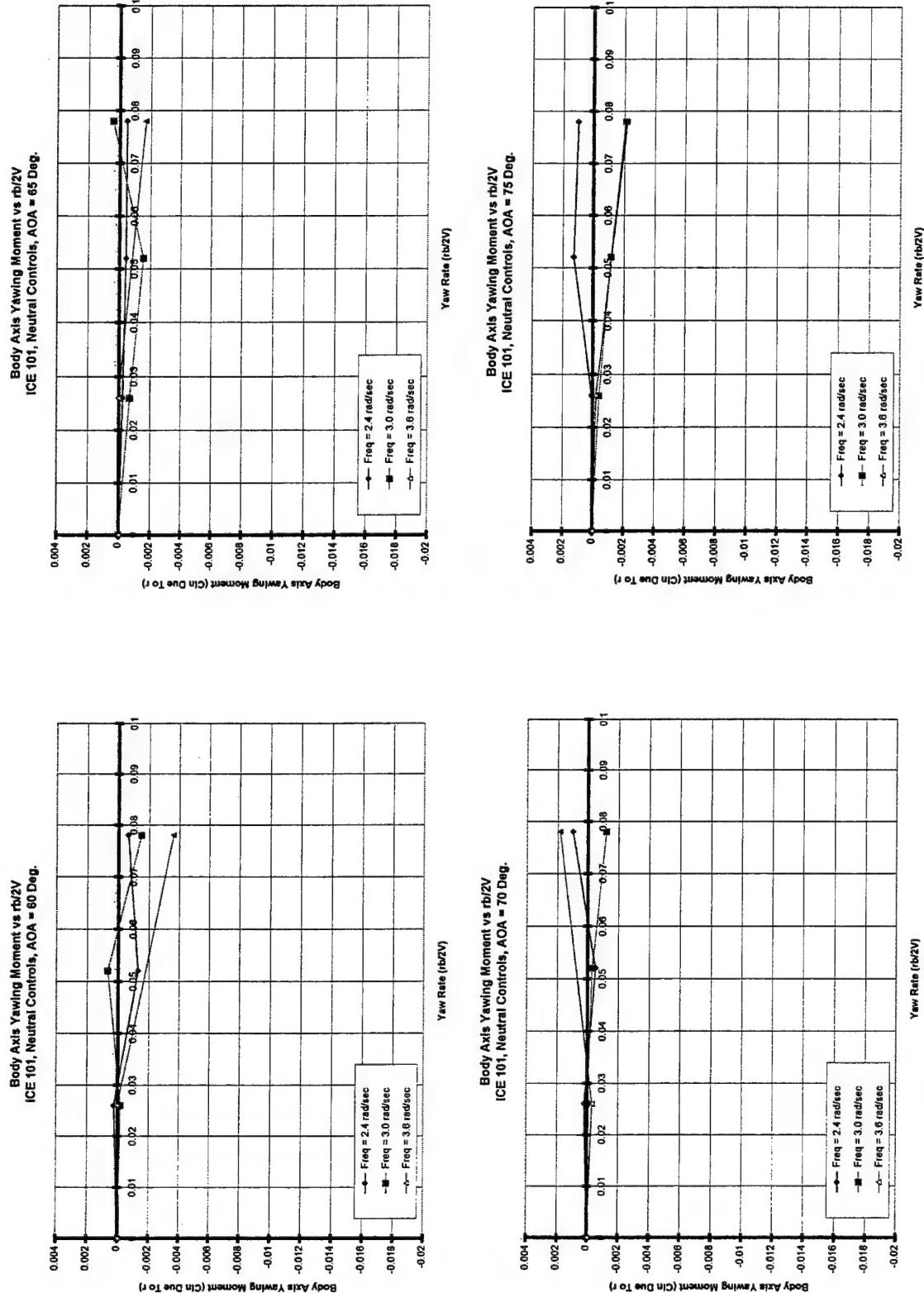


Body Axis Yawing Moment vs $\dot{\theta}/2V$

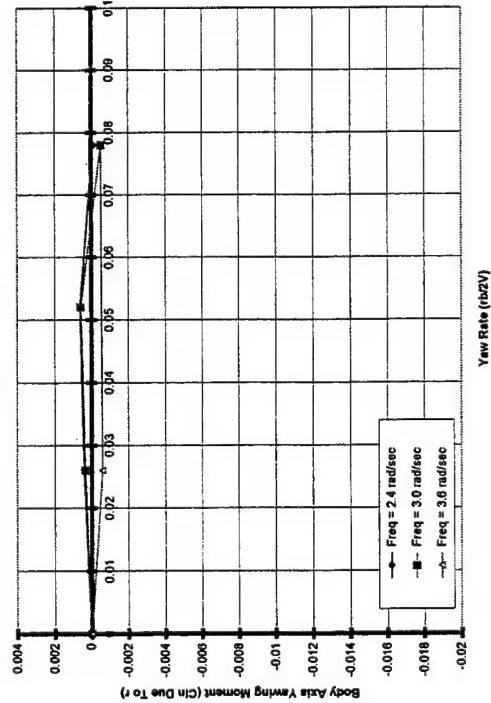
Yaw Rate ($\dot{\theta}/2V$)

Body Axis Yawing Moment vs $\dot{\theta}/2V$

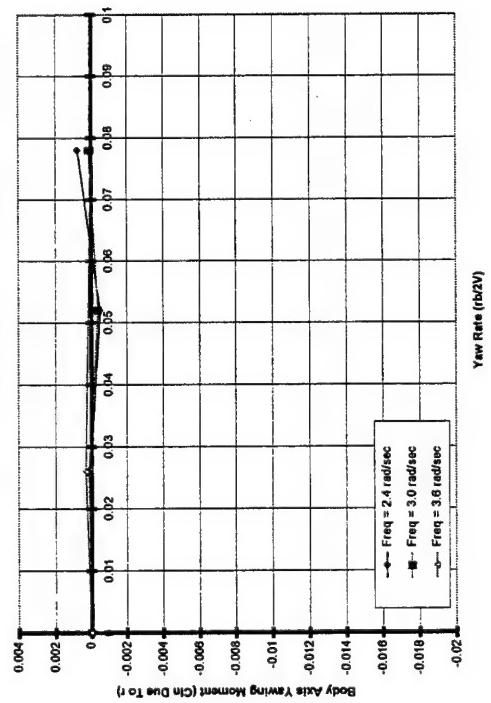
Yaw Rate ($\dot{\theta}/2V$)



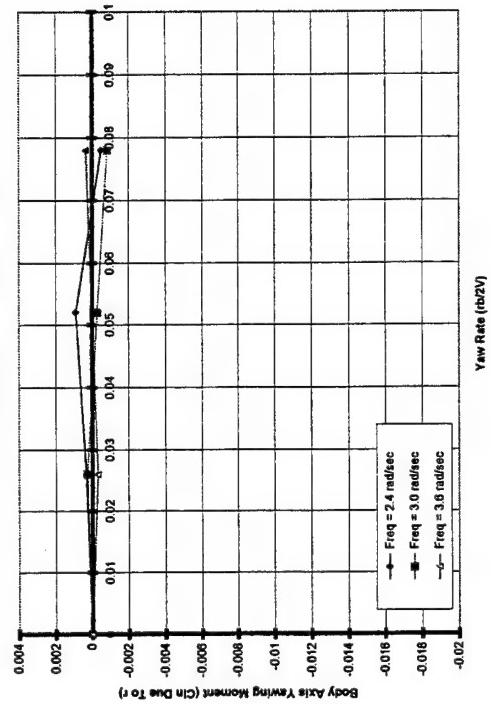
Body Axis Yawing Moment vs $rbi/2V$
ICE 101, Neutral Controls, AOA = 80 Deg.



Body Axis Yawing Moment vs $rbi/2V$
ICE 101, Neutral Controls, AOA = 85 Deg.

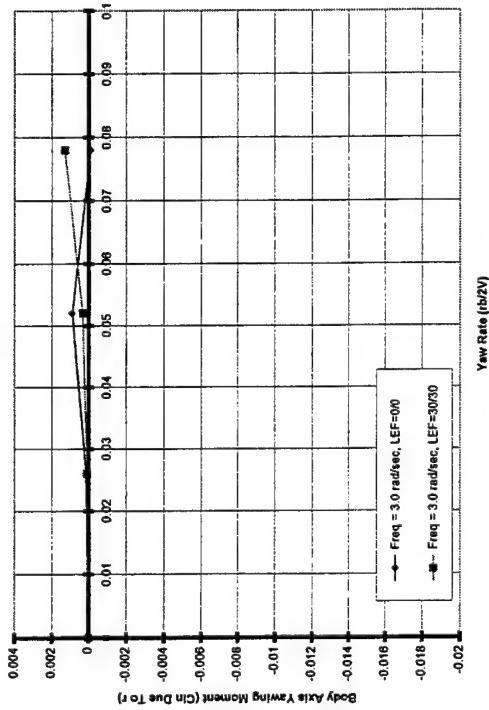


Body Axis Yawing Moment vs $rbi/2V$
ICE 101, Neutral Controls, AOA = 85 Deg.



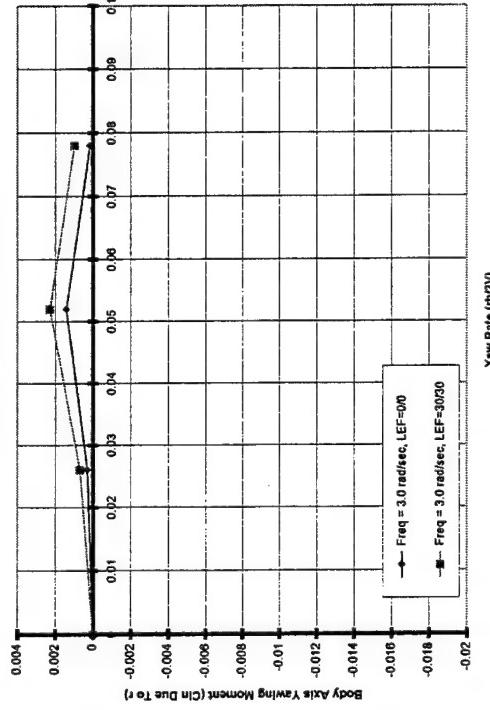
Body Axis Yawing Moment vs $\dot{\theta}/2V$
ICE 101, LEF Effects, AOA = 0 Deg.

Body Axis Yawing Moment vs $\dot{\theta}/2V$
ICE 101, LEF Effects, AOA = 5 Deg.

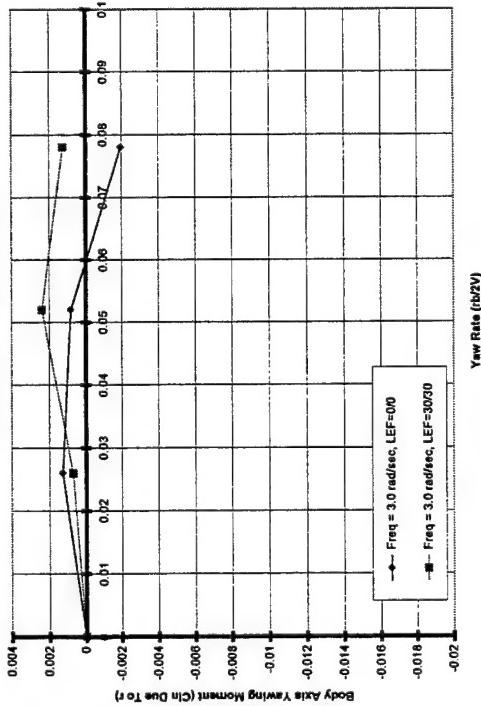


Body Axis Yawing Moment vs $\dot{\theta}/2V$
ICE 101, LEF Effects, AOA = 10 Deg.

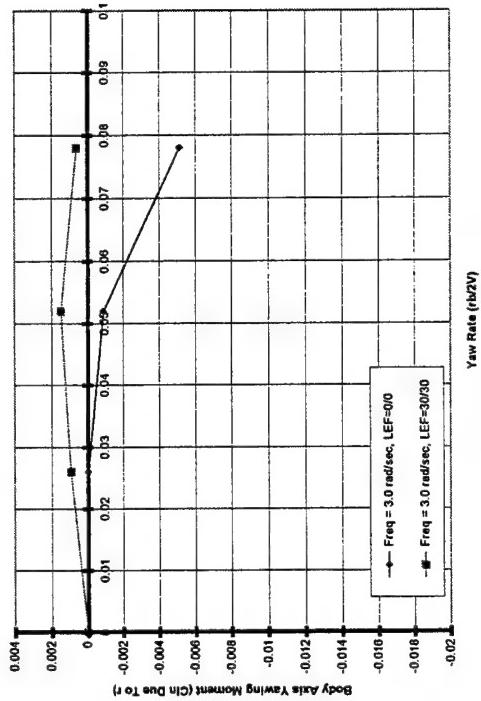
Body Axis Yawing Moment vs $\dot{\theta}/2V$
ICE 101, LEF Effects, AOA = 15 Deg.



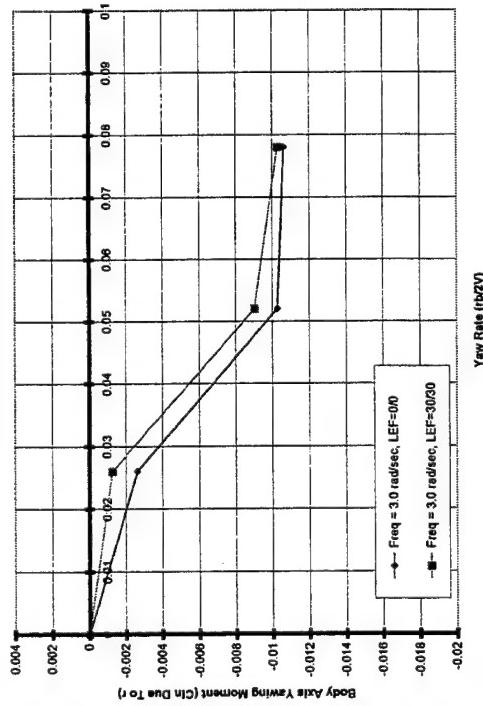
Body Axis Yawing Moment vs $r\dot{b}/2V$
ICE 101, LEF Effects, AOA = 20 Deg.

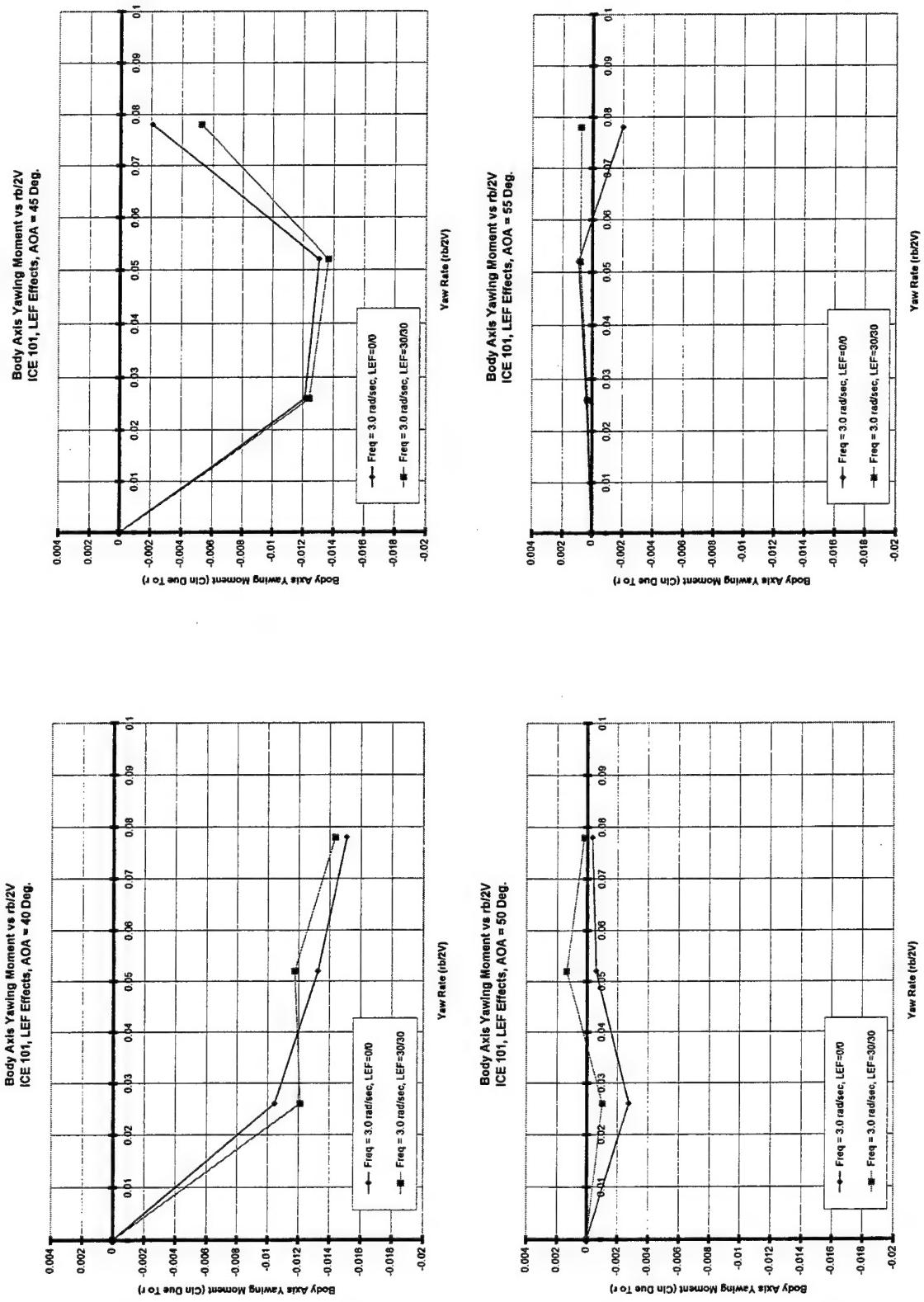


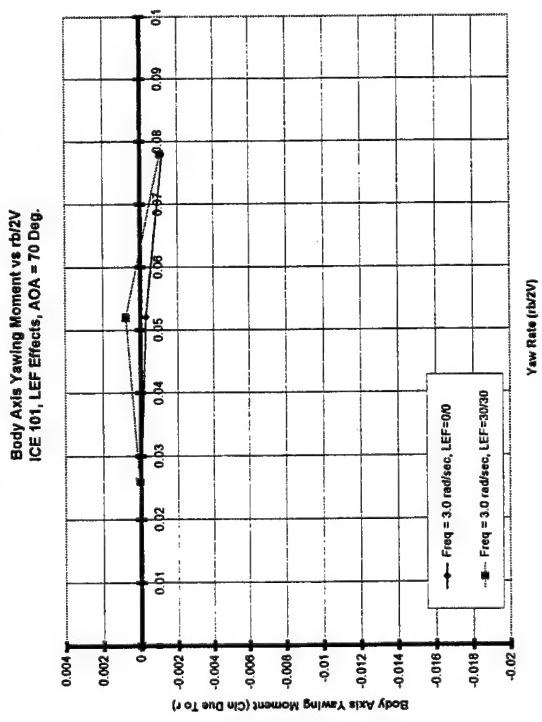
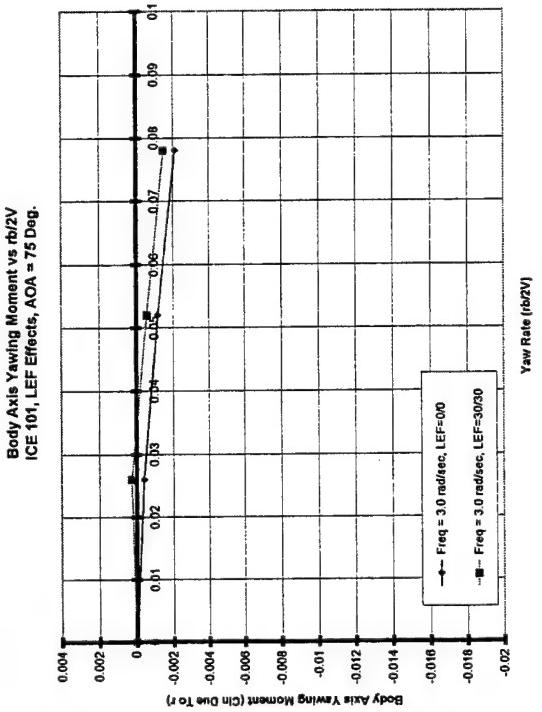
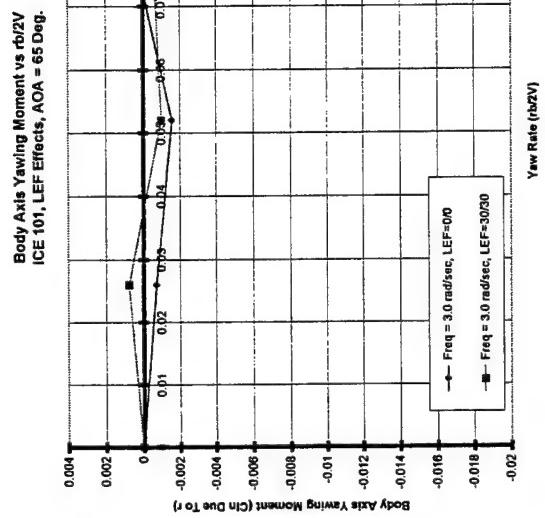
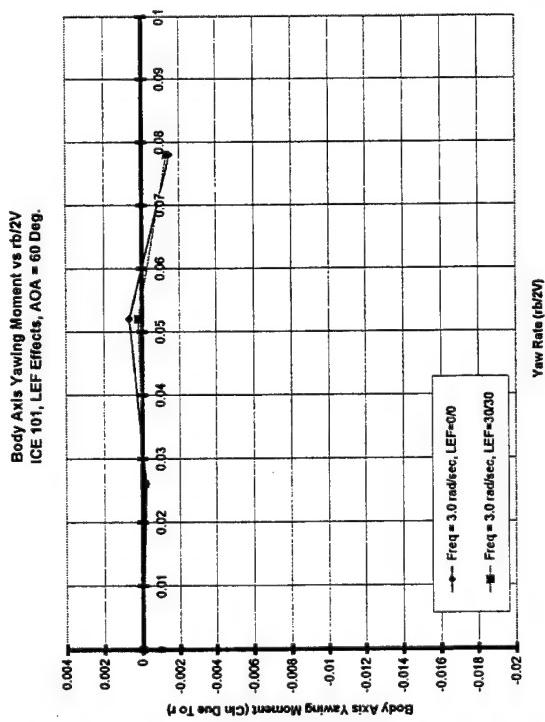
Body Axis Yawing Moment vs $r\dot{b}/2V$
ICE 101, LEF Effects, AOA = 25 Deg.

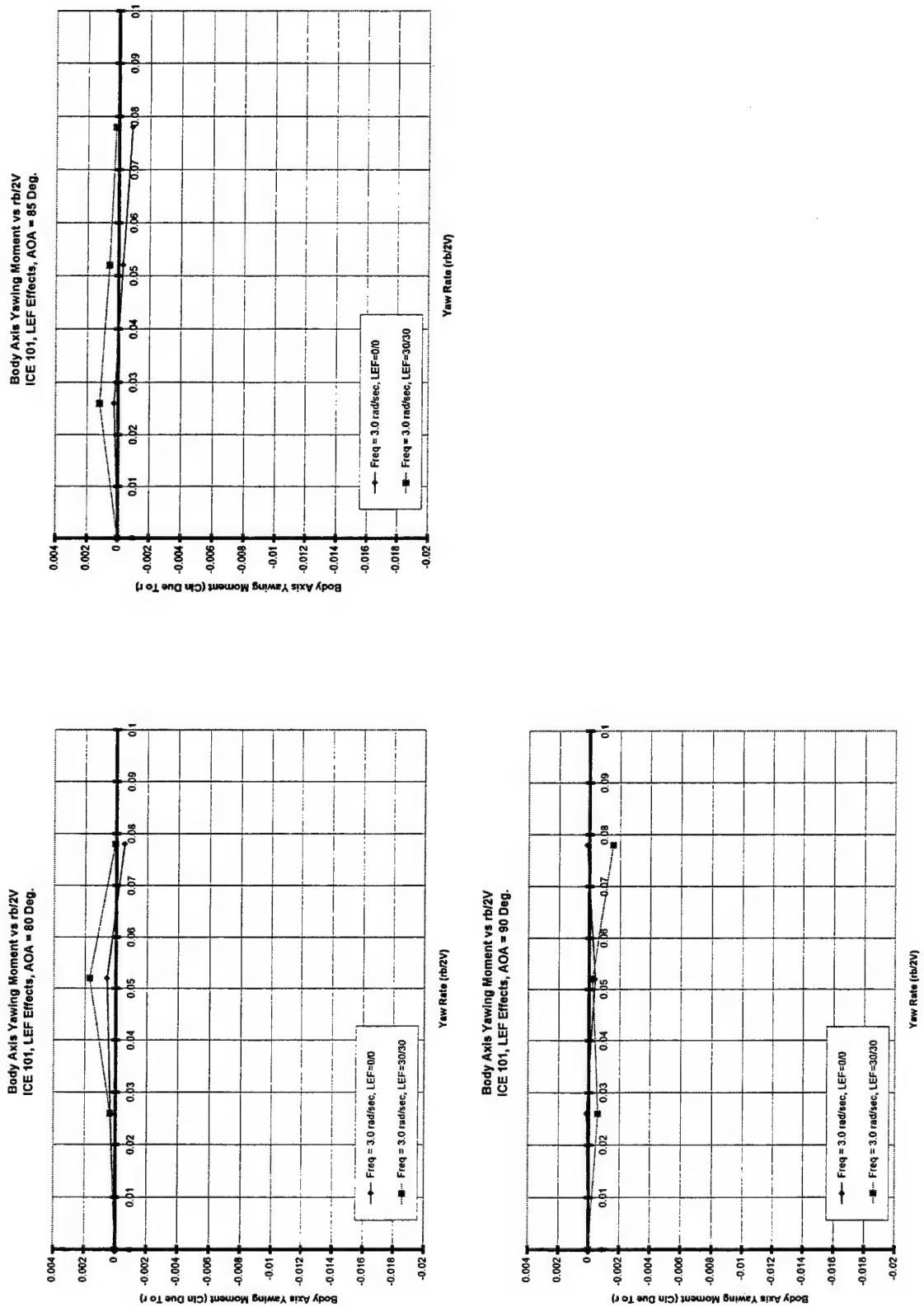


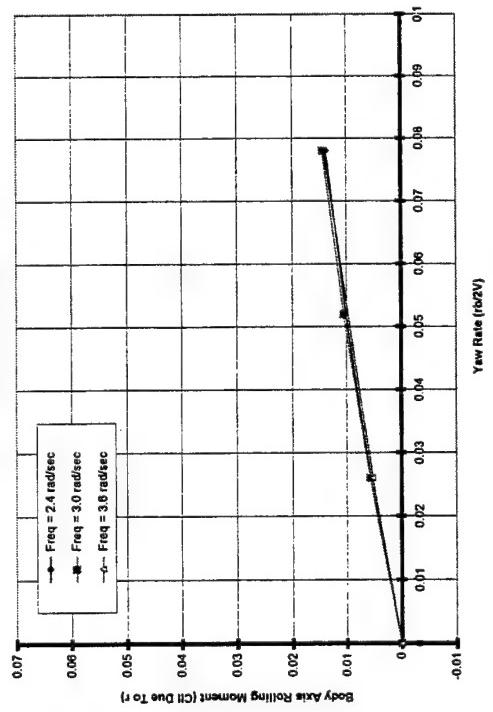
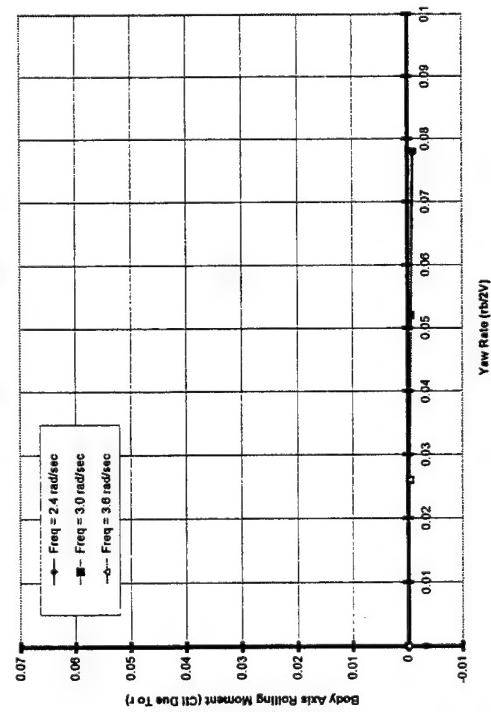
Body Axis Yawing Moment vs $r\dot{b}/2V$
ICE 101, LEF Effects, AOA = 30 Deg.

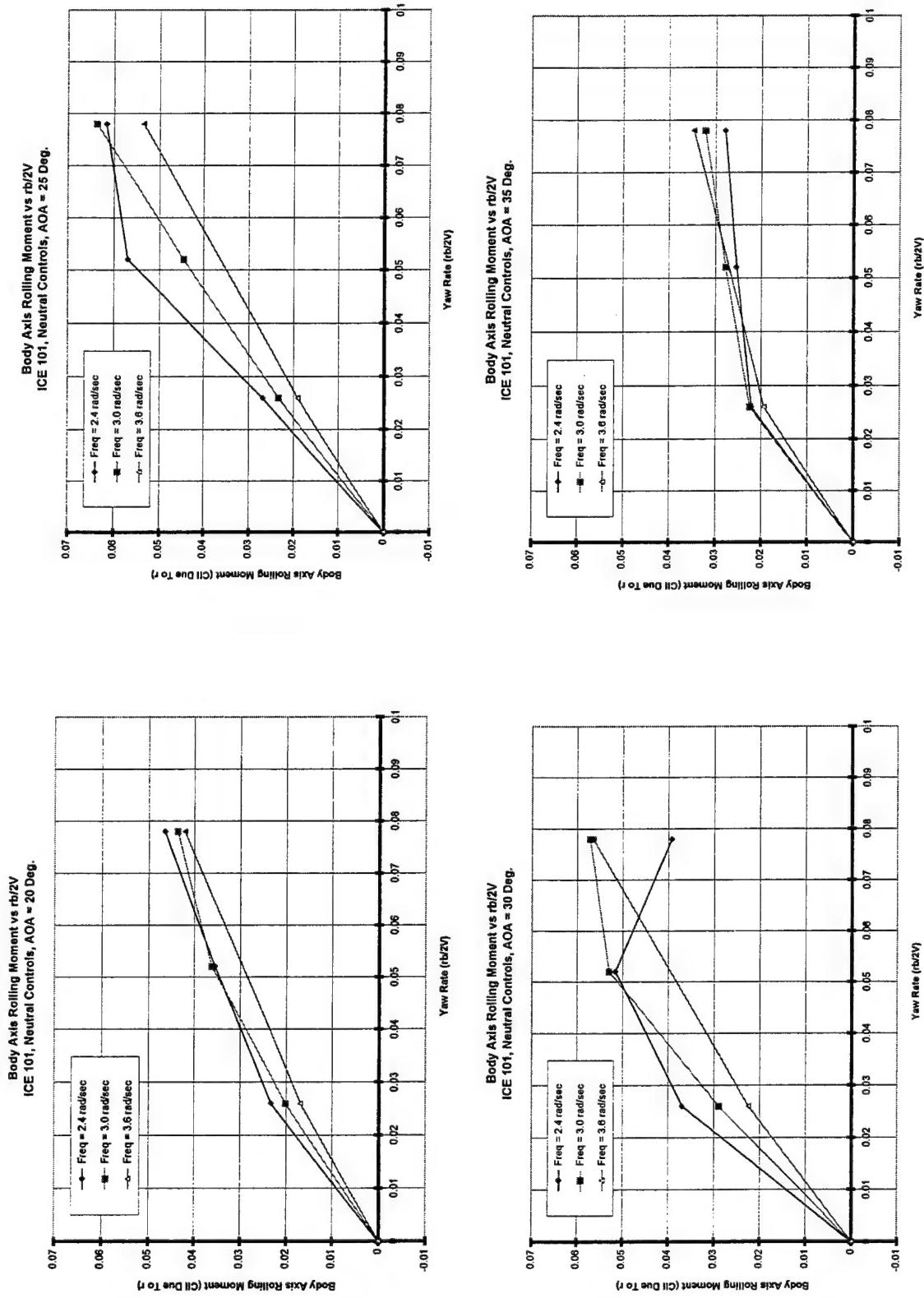


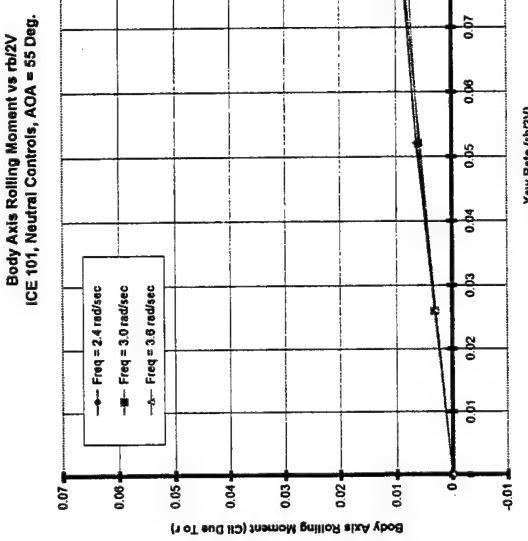
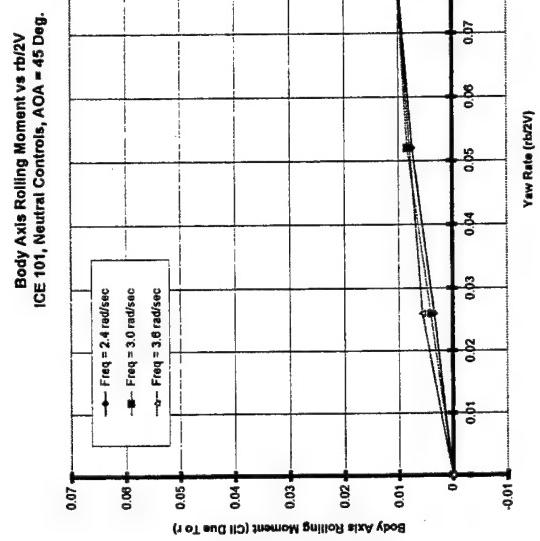
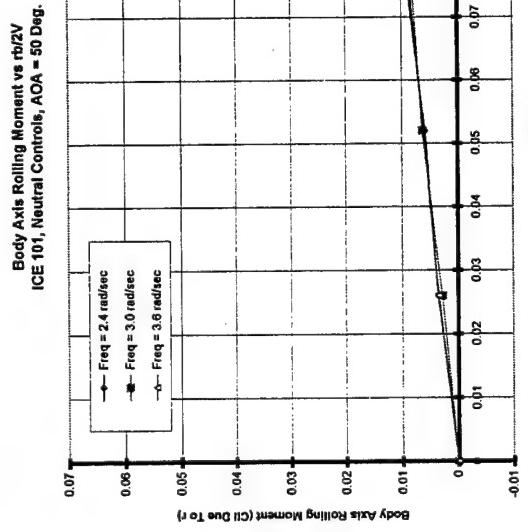
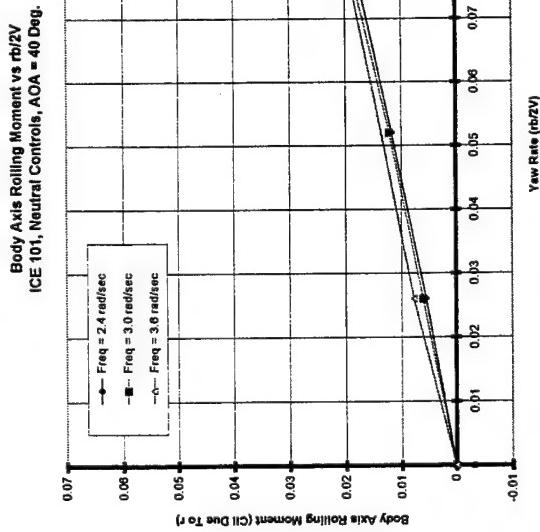




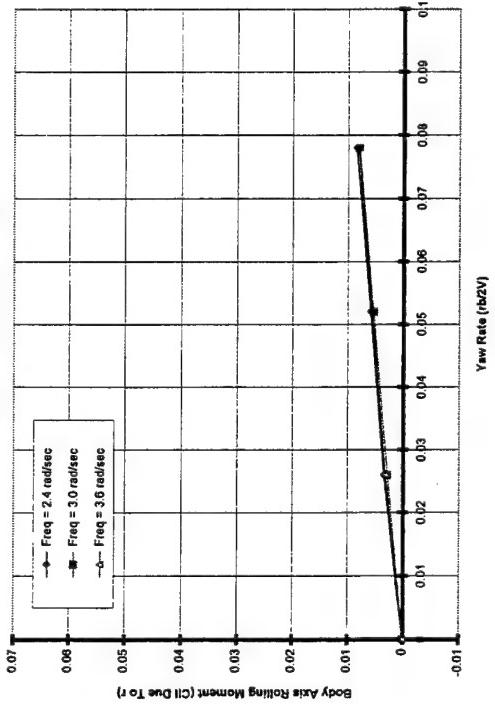




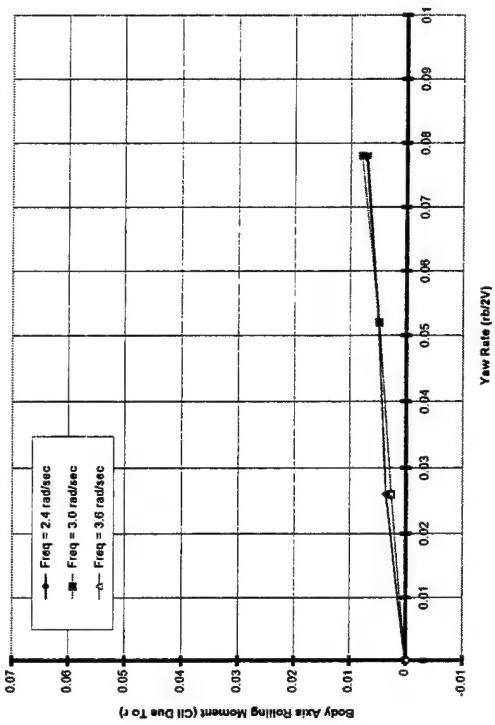




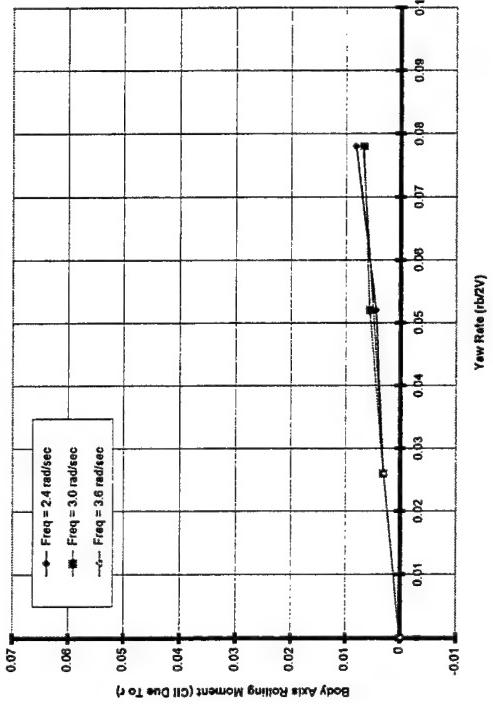
Body Axis Rolling Moment vs $r b/2V$
ICE 101, Neutral Controls, AOA = 60 Deg.



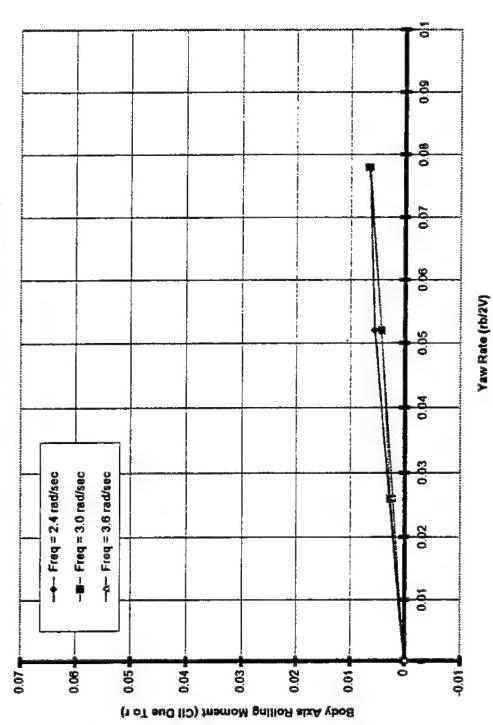
Body Axis Rolling Moment vs $r b/2V$
ICE 101, Neutral Controls, AOA = 65 Deg.



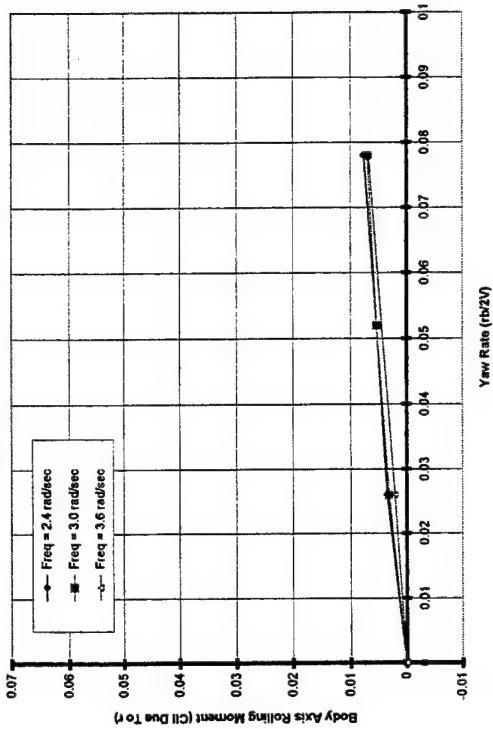
Body Axis Rolling Moment vs $r b/2V$
ICE 101, Neutral Controls, AOA = 70 Deg.



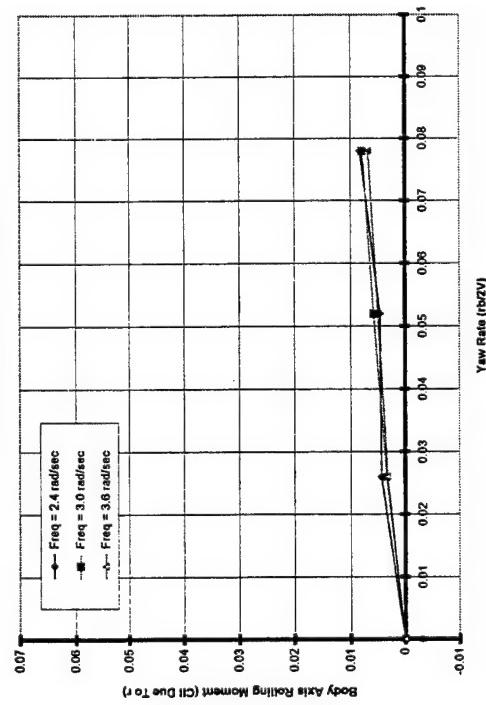
Body Axis Rolling Moment vs $r b/2V$
ICE 101, Neutral Controls, AOA = 75 Deg.



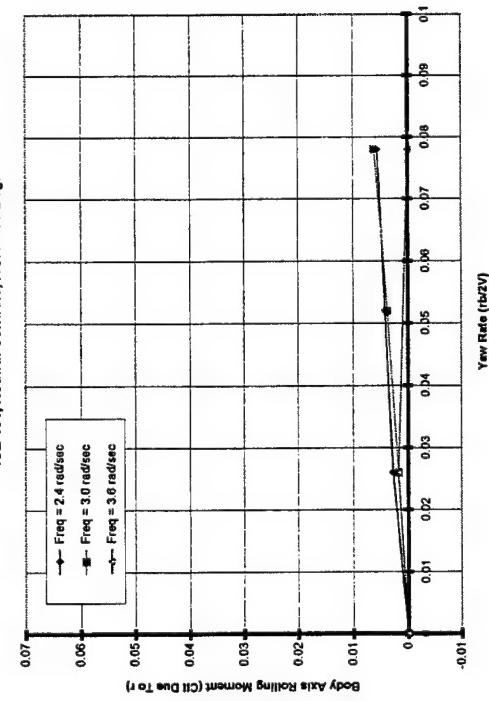
Body Axis Rolling Moment vs $rb/2V$
ICE 101, Neutral Controls, AOA = 85 Deg.

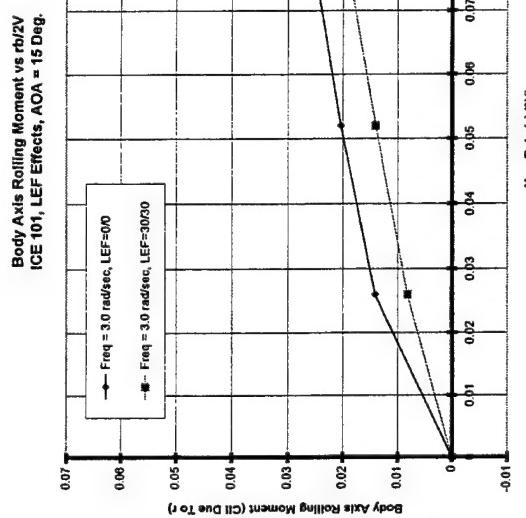
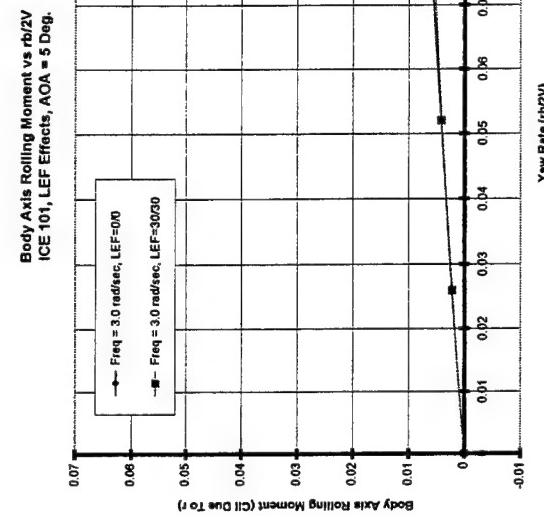
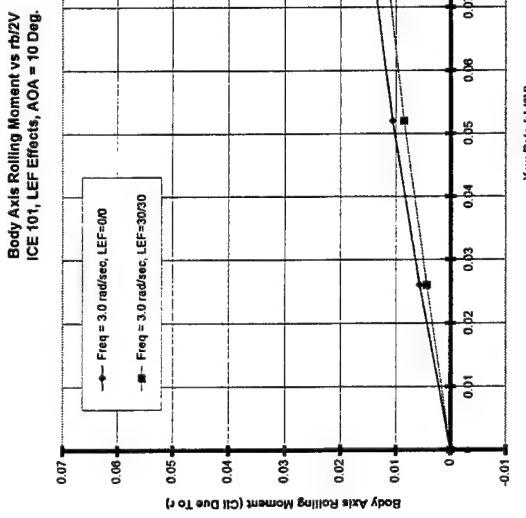
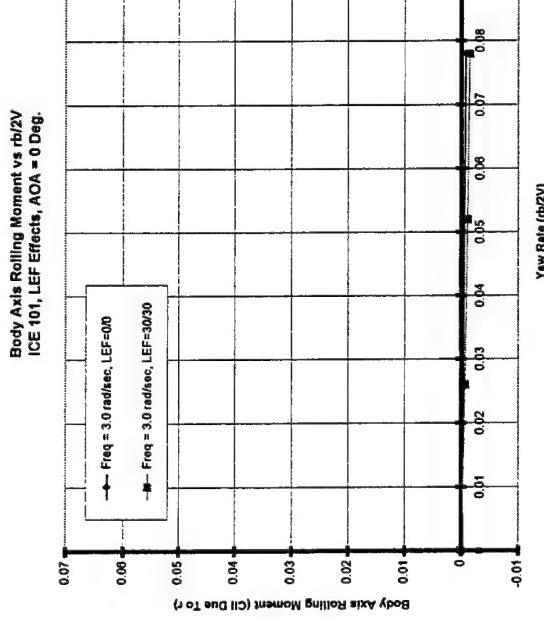


Body Axis Rolling Moment vs $rb/2V$
ICE 101, Neutral Controls, AOA = 80 Deg.

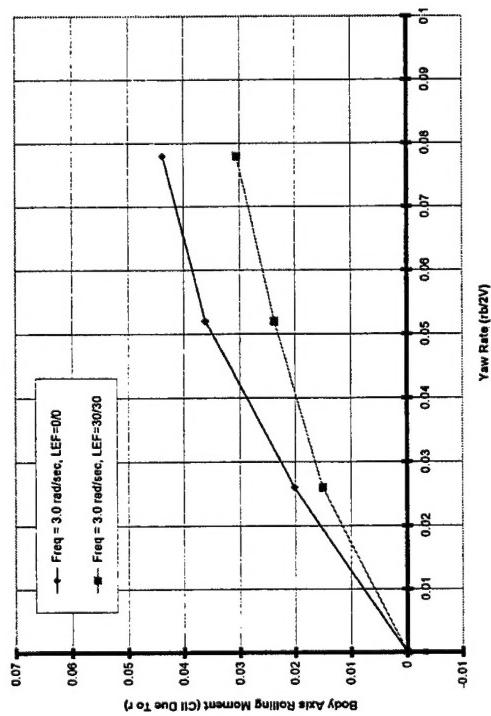


Body Axis Rolling Moment vs $rb/2V$
ICE 101, Neutral Controls, AOA = 90 Deg.

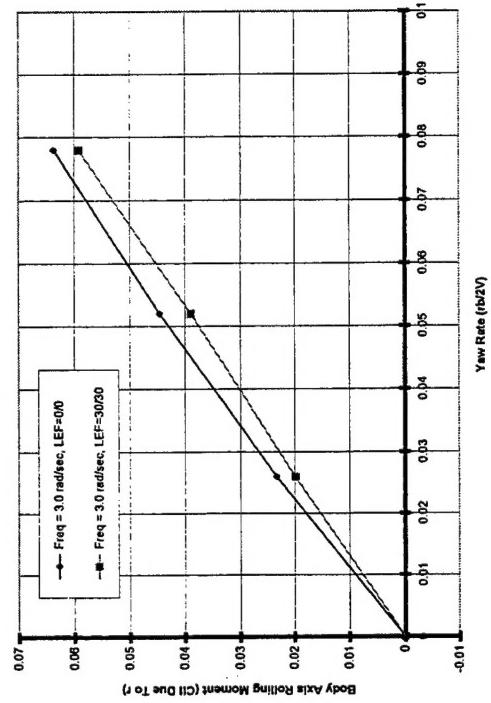




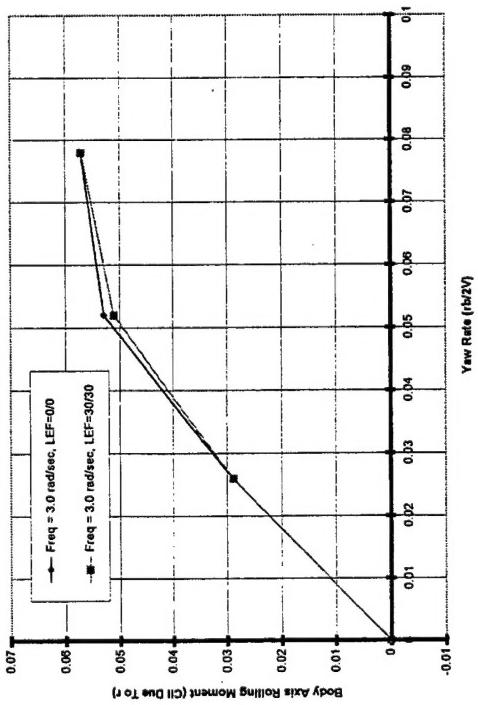
Body Axis Rolling Moment vs $\dot{\theta}/2V$
ICE 101, LEF Effects, AOA = 20 Deg.



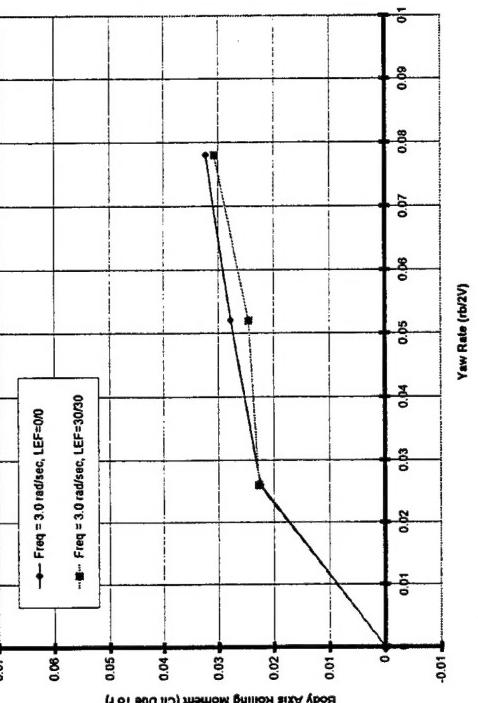
Body Axis Rolling Moment vs $\dot{\theta}/2V$
ICE 101, LEF Effects, AOA = 25 Deg.



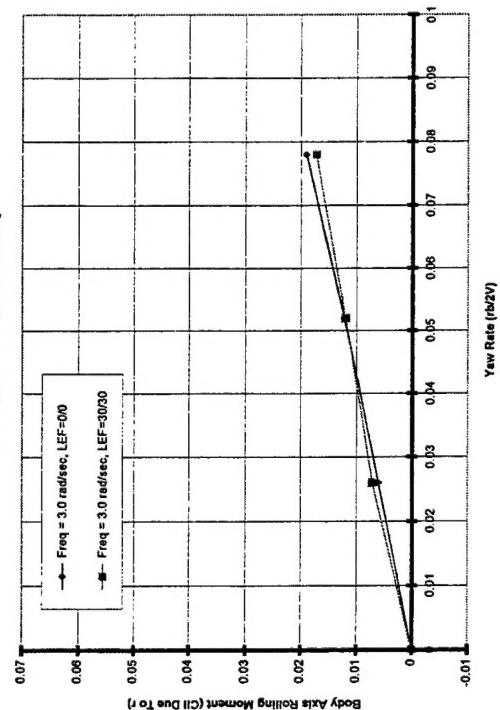
Body Axis Rolling Moment vs $\dot{\theta}/2V$
ICE 101, LEF Effects, AOA = 30 Deg.



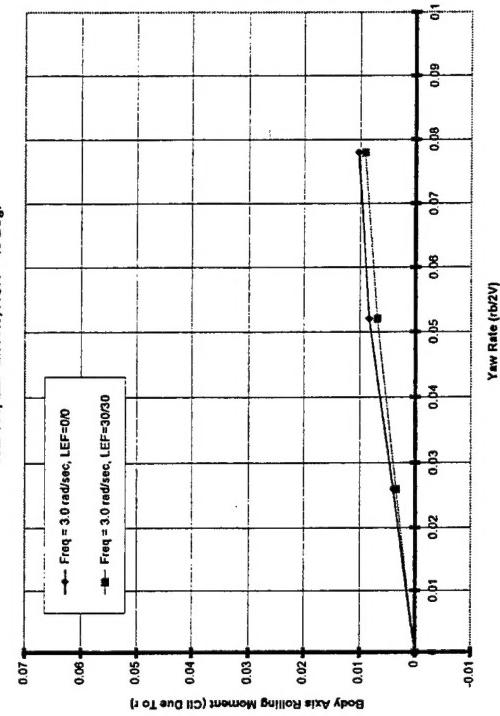
Body Axis Rolling Moment vs $\dot{\theta}/2V$
ICE 101, LEF Effects, AOA = 35 Deg.



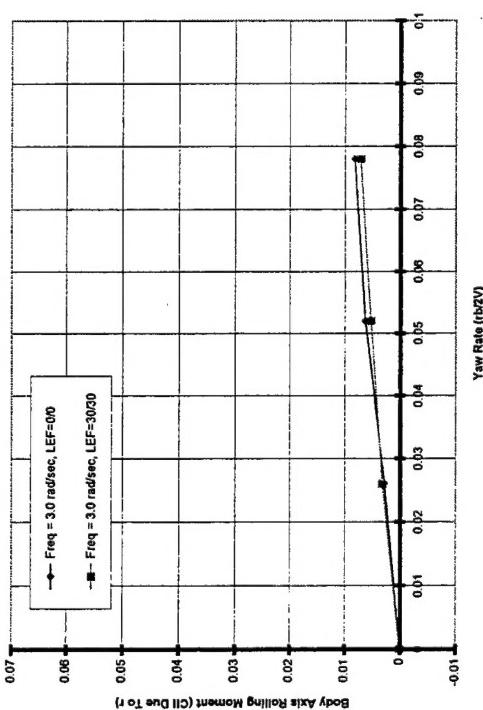
Body Axis Rolling Moment vs $rb/2V$
ICE 101, LEF Effects, AOA = 40 Deg.



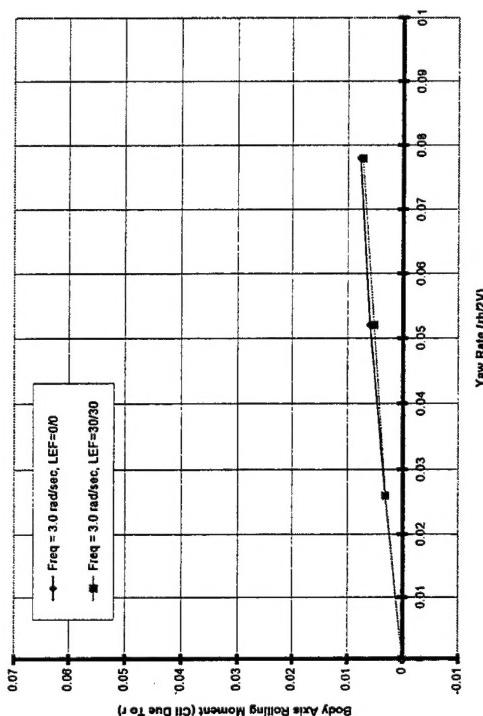
Body Axis Rolling Moment vs $rb/2V$
ICE 101, LEF Effects, AOA = 45 Deg.



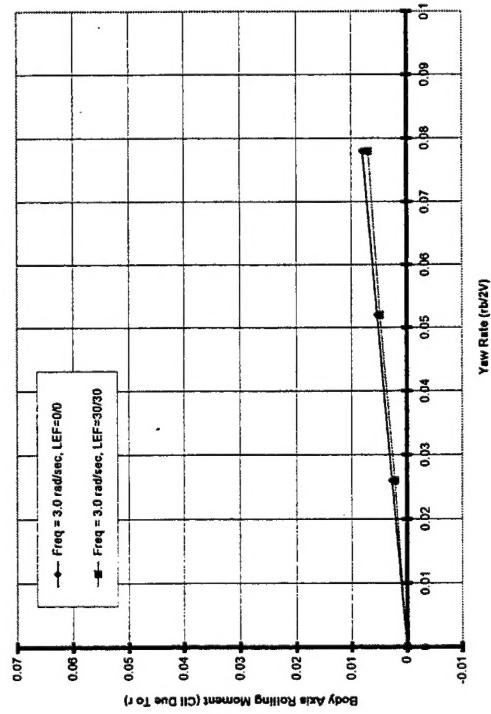
Body Axis Rolling Moment vs $rb/2V$
ICE 101, LEF Effects, AOA = 50 Deg.



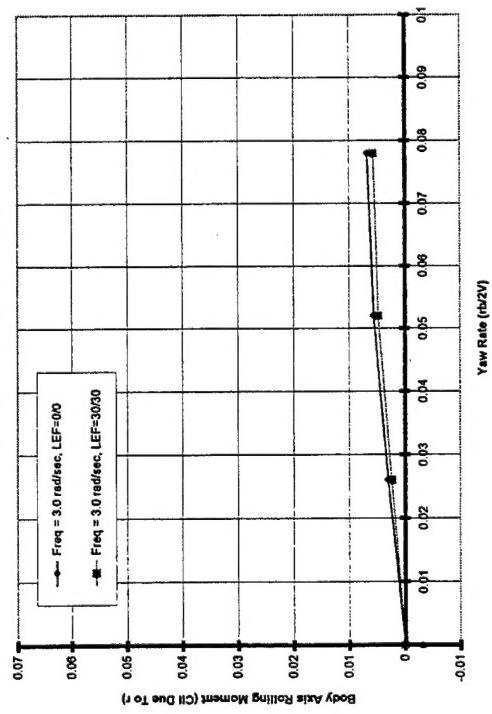
Body Axis Rolling Moment vs $rb/2V$
ICE 101, LEF Effects, AOA = 55 Deg.



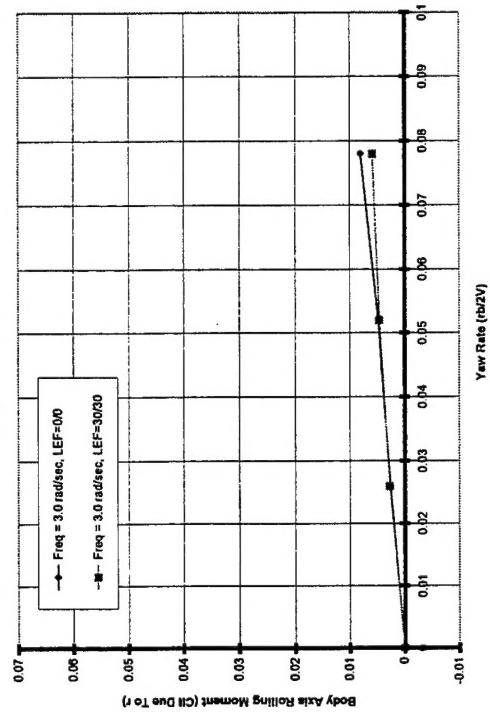
Body Axis Rolling Moment vs $\dot{\theta}/2V$
ICE 101, LEF Effects, AOA = 60 Deg.



Body Axis Rolling Moment vs $\dot{\theta}/2V$
ICE 101, LEF Effects, AOA = 70 Deg.



Body Axis Rolling Moment vs $\dot{\theta}/2V$
ICE 101, LEF Effects, AOA = 65 Deg.



Body Axis Rolling Moment vs $\dot{\theta}/2V$
ICE 101, LEF Effects, AOA = 75 Deg.

